Delayed Neutron & Gamma Measurements of Special Nuclear Materials, their Monte Carlo Simulations, and Applications

Applications et Simulations par Méthode de Monte Carlo de Mesures de Matériaux Nucléaires Spéciaux à l'Aide de Techniques Basées sur les Neutrons Retardés et le Photons Gamma Retardés

A thesis submitted to the
Division of Graduate Studies of the Royal Military College of Canada

By

Madison Andrews

In Partial Fulfillment of the Requirements for the Degree of
Doctor of Philosophy in Nuclear Engineering

January 2015

-This page is intentionally left blank-

Acknowledgements

I would like to thank my supervisors Dr. David Kelly and Dr. Emily Corcoran for their guidance and support throughout my graduate career. David, I appreciate the time you have dedicated to my development as a scientist, I'm very lucky to have you as a supervisor. Emily, thank you for providing so many opportunities, and for your advice as I pursued them. I also appreciate the contributions of Dr. Tim Goorley for mentoring me at Los Alamos National Laboratory and the guidance he has provided throughout my PhD.

The SLOWPOKE-2 Director, Ms. Kathy Nielson and the Radiation Safety Officer, Mr. Dave Ferguson, were incredibly accommodating and supportive of the experimental process (especially when we became an active constructive zone). Technical contributions throughout the project by Mr. John Shaw, Mr. Matthew Mackay, Ms. Kristine Mattson, Mr. Steve White, Mr. Tim Mumby and Mr. Brent Ball are so appreciated. I would be remiss to not point out the wonderful technical work done by Mr. Clarence McEwen on system construction and relocation (twice!). I also appreciate the translation of the abstract by Dr. Hughes Bonin.

I've had the pleasure of meeting many outstanding staff, students, and postdocs, both at RMCC and LANL during my studies. I'm fortunate to have the love and moral support of my father, Norm Sellers, his wife Alison Lewis; and my wonderful in-laws, Toni and Rick Andrews. I greatly appreciate the Canadian Nuclear Safety Commission funded NSERC scholarship.

Finally, thank you to my amazing husband, Stephen Andrews, who has unconditionally supported and encouraged me.

-This page is intentionally left blank-

Abstract

Special nuclear materials (SNMs) are those which contain ^{233}U, ^{235}U and ^{239}Pu. They are safeguarded by the International Atomic Energy Agency (IAEA) in addition to individual governmental organisations. Nuclear forensic analysis (NFA) is concerned with the characterisation and attribution of illicit nuclear materials, especially uranium and plutonium. Physical, chemical, and isotopic characteristics are determined with instrumentation that is ideally rapid, non-destructive, and sensitive. Delayed neutron and gamma emissions from fissioned isotopes have signature yields, energies, and temporal behaviour, their measurement allows the rapid characterisation of SNM content in a variety of matrices.

Previous work developed a delayed neutron counting (DNC) prototype at the Royal Military College of Canada (RMCC). This system sent samples containing ^{235}U content to a SLOWPOKE-2 reactor where they underwent fission. Samples were then sent via pneumatic transfer to the counting arrangement, containing six helium-3 detectors, which recorded the delayed neutron emissions. This undertaking began with the attribution of the time-dependent neutron background present in the SLOWPOKE-2 site used for DNC irradiations; the contribution of this uranium contamination was lowered from a mass equivalent of 120 to 50 *ng* per vial. Subsequent delayed neutron measurements of samples containing mixtures of ^{233}U and ^{235}U were used to determine their relative ratios (in *%*) with an average absolute error of ± 4 *%*. This thesis also included the development of a Delayed Neutron and Gamma Counting (DNGC) system intended to contribute to nuclear forensics instrumentation available to the Canadian Department of National Defence. The delayed gammas emitted from SNM were used in complement with delayed neutron measurements in an example which detected, identified, and quantified ^{233}U content with an average relative error and accuracy of -2.2 and 1.5 *%*, respectively.

Throughout system development detailed measurements of both delayed neutron and delayed gammas from microgram quantities of ^{233}U, ^{235}U, and ^{239}Pu were performed. These were used for comparison to the simulations of delayed particle emissions and detection from the Monte Carlo code MCNP6, in collaboration with Los Alamos National Laboratory. One of the options available in MCNP6 for delayed neutron emissions was found to be discrepant with measurements $\geq$ 100 *s* after fission. These DN comparisons were released as a MCNP6 test suite to all users; the most recent release of MCNP6.1.1β resolves many of the observed discrepancies found by this work. MCNP6 simulations were also used to predict expected delayed gamma signatures useful for NFA, and compared to DNGC system measurements in a final study.

-This page is intentionally left blank-

Résumé

Les matériaux nucléaires spéciaux (MNS) sont ceux qui contiennent les isotopes ^{233}U, ^{235}U et ^{239}Pu. Ils sont réglementés par l'Agence Internationale de l'Énergie Atomique (AIEA) en plus des organisations gouvernementales individuelles. L'analyse nucléaire légale (ANL) se préoccupe de la caractérisation et de l'attribution de matériaux nucléaires illicites, plus particulièrement l'uranium et le plutonium. Les caractéristiques physiques, chimiques et isotopiques sont déterminées par un appareillage qui est idéalement rapide, non-destructif et sensible. Des rendements, énergies et comportements dans le temps caractérisent les neutrons retardés et les émissions gamma des isotopes qui fissionnent, et les mesures de ces particules permettent une caractérisation rapide du contenu de ces MNS dans une variété de matrices.

Une recherche précédente a permis le développement d'un prototype d'un compteur de neutrons retardés (CNR) au Collège militaire royal du Canada. Ce système envoyait des échantillons contenant l'isotope ^{235}U à un réacteur nucléaire SLOWPOKE-2 où ils subissaient des fissions. Les échantillons étaient alors envoyés par un système pneumatique à l'installation de comptage équipé de six détecteurs à l'hélium-3 qui enregistraient les émissions de neutrons retardés. Une première étape dans le développement de cette installation a consisté en la détermination du bruit de fond dépendant du temps au site du réacteur SLOWPOKE-2 utilisé pour les irradiations pour le CNR; la contribution au bruit de fond par la contamination de l'uranium a été réduite de 120 à 50 *ng* en masse équivalente par capsule. On a effectué des mesures subséquentes de neutrons retardés pour des échantillons comprenant des mélanges d'^{233}U et d'^{235}U afin de déterminer leurs rapports relatifs (en %) avec une erreur absolue de ± 4 % en moyenne. La présente thèse inclut aussi le développement d'un système de comptage de neutrons retardés et de photons gamma (SCNRG) pour contribuer à l'instrumentation en méthodes nucléaires légales disponibles au Ministère de la défense nationale du Canada. Les photons gamma retardés émis par les MNS sont utilisés en complément des mesures de neutrons retardés dans un exemple d'application où la teneur en ^{233}U a été détectée, identifiée et quantifiée avec une erreur relative moyenne et une précision de -2.2% et 1.5% respectivement.

Tout au long du développement du système, on a effectué des mesures détaillées des neutrons retardés ainsi que des photons gamma retardés à partir de quantités d'^{233}U, d'^{235}U et de ^{239}Pu de l'ordre du microgramme. Ces mesures ont été utilisées pour les comparer aux résultats de simulations d'émission et de

détection de particules retardées effectuées par le code de Monte Carlo MCNP6 en collaboration avec le Laboratoire National de Los Alamos. On a trouvé qu'une des options disponibles du code MCNP6 pour les émissions de neutrons retardés produisait des résultats différents des mesures pour des temps égaux ou supérieurs à 100 s suivant la fission. Ces comparaisons de neutrons retardés ont été publiées comme une suite de simulations par MCNP6 comme problèmes-tests à l'intention de tous les utilisateurs; la version la plus récente du code, MCNP6.1.1β, élimine plusieurs des erreurs mises en lumière dans le présent travail. On a aussi utilisé des simulations par MCNP6 pour prédire les signatures attendues des photons gamma retardés utilisées en analyse nucléaire légale, et on a comparé les résultats aux mesures par le système SCNRG dans une étude finale.

Co-Authorship Statement

This manuscript thesis encompasses journal papers (5), conference transactions (4), and technical reports (2). In each case the candidate was the principal author, primary researcher and the individual responsible for data analysis. All experimentation was performed by M.T. Andrews (née Sellers), with the exception of ICP-MS measurements in Chapter 4. MCNP6 simulation input decks were written by the candidate (excluding the SLOWPOKE-2 reactor model referenced in Chapter 6 and Chapter 10). In this document, manuscripts appear primarily in the form they were submitted/published with some minor modifications. These modifications include formatting changes to references, nomenclature used, and minor equation alterations to maintain continuity throughout the document. However these changes have no effect on the results or their interpretations.

Although the work of Chapter 3 was completed during M.T. Andrews' MASc, this published manuscript was included as relevant background. Thesis appendices consist of American Nuclear Society Transactions and Los Alamos National Laboratory technical reports, which detail incremental developments of the PhD work primarily concerned with Monte Carlo simulations.

Chapter 3

M.T. Sellers, D.G. Kelly, E.C. Corcoran, "An Automated Delayed Neutron Counting System for the Mass Determination of Special Nuclear Materials" *Journal of Radioanalytical and Nuclear Chemistry*, **291** *2* (2012) pp. 281 – 285.

Chapter 4

M.T. Sellers, E.C. Corcoran, D.G. Kelly, "The Analysis and Attribution of the Time-Dependent Neutron Background Resultant from Sample Irradiation in a SLOWPOKE-2 Reactor" *Journal of Radioanalytical and Nuclear Chemistry,* **295** *2* (2013) pp. 1221 – 1228.

Chapter 5

M.T. Sellers, E.C. Corcoran, D.G. Kelly, "Simultaneous ^{233}U and ^{235}U Characterization through the Assay of Delayed Neutron Temporal Behaviour" *PHYSOR 2012, Advances in Reactor Physics Conference, Knoxville, TN, April 2012.*

Chapter 6

M.T. Andrews, J.T. Goorley, E.C. Corcoran, D.G. Kelly "Modeling the Detection of Delayed Neutron Signatures in MCNP6 and Comparisons with Measurements of ^{233}U, ^{235}U and ^{239}Pu" *Journal of Nuclear Technology,* **187** *3* (2014) pp. 235 - 243.

Chapter 7

M.T. Andrews, T.L. Beames-Canivet, D.G. Kelly, E.C. Corcoran, J.T. Goorley, "MCNP6.1.1 Beta Test Suite Comparisons to Delayed Neutron Measurements of ^{233}U, ^{235}U, and ^{239}Pu at the Royal Military College of Canada" *Los Alamos National Laboratory Report* (2014) LA-UR-14-26521.

Chapter 8

M.T. Andrews, E.C. Corcoran, J.T. Goorley, D.G. Kelly, "A System for the Measurement of Delayed Neutrons and Gammas from Special Nuclear Materials" *Journal of Radioanalytical and Nuclear Chemistry* (2015) DOI:10.1007/s10967-014-3786-6 (in press).

Chapter 9

M.T. Andrews, J.T. Goorley, E.C. Corcoran, D.G. Kelly, "Uranium and Plutonium Fission Product Gamma Intensity Measurements and MCNP6 Simulations" *American Nuclear Society Transactions*, 110 (2014), pp. 490-493.

Chapter 10

M.T. Andrews, J.T. Goorley, E.C. Corcoran, D.G. Kelly "MCNP6 Simulations of Gamma Line Emissions from Fission Products and their Comparisons to Plutonium and Uranium Measurements" *Journal of Progress in Nuclear Energy* (2015) (in press).

Appendix A

M.T. Sellers, J.T. Goorley, E.C. Corcoran, D.G. Kelly "A Preliminary Comparison of MCNP6 Delayed Neutron Emission from ^{235}U and Experimental Measurements" *American Nuclear Society Transactions*, 106 (2012) pp. 813-816, *LA-UR-12-00219.*

Appendix B

M.T. Andrews, J.T. Goorley, E.C. Corcoran, D.G. Kelly, "Fission Product γ-ray Measurements of ^{235}U and MCNP6 Predictions" *American Nuclear Society Transactions*, 109 (2013) pp. 995-998, LA-UR-13-24736.

Appendix C

M.T. Andrews, T.L. Beames-Canivet, D.G. Kelly, E.C. Corcoran, J.T. Goorley, "Updated Delayed Neutron Counting Test Suite Comparisons from RMCC and MCNP6 version 1" *Los Alamos National Laboratory Report*, (2014) LA-UR-14-25702.

Contents

-This page is intentionally left blank-

List of Figures

-This page is intentionally left blank-

List of Tables

Nomenclature

Symbol	Name	Units
Σ_x	Macroscopic Cross Section for Reaction *x*	cm^{-1}
Φ	Neutron Flux	$cm^{-2}s^{-1}$
Ω	Direction	*steradian*
α	Alpha Particle	
α_i	Fraction of total delayed neutrons per fission	
β_i	Fraction of total neutrons per fission	
γ	Gamma Particle	
ε	Detection Efficiency	
ε_i	Intrinsic Efficiency	
ε_g	Geometric Efficiency	
λ	Decay Constant	s^{-1}
λ_{mfp}	Mean Free Path	*cm*
μ_l	Material Linear Mass Attenuation Coefficient	cm^{-1}
ν_d	Total Delayed Neutron Yield per Fission	
ν	Total Neutron Yield per Fission	
ξ	Random Number	
σ	Width Parameter for Gaussian	*MeV*
σ_x	Microscopic Cross Section for Reaction *x*	cm^2
σ_f	Microscopic Fission Cross Section	cm^2
τ	Dead Time Constant	μs
$\psi(\vec{r},\hat{\Omega},E,t)$	Angular Flux	$cm^{-2}sh^{-1}MeV^{-1}steradian^{-1}$
A	Area	
A_o	Initial Activity	s^{-1}
A_B	Time independent neutron background	s^{-1}
$A(t)$	Activity at time *t*	s^{-1}
$B(c)$	Cumulative background	s^{-1}
$B(t)$	Time dependent neutron background	s^{-1}
$C(t)$	Count Rate	s^{-1}
E_γ	Photon Energy	*MeV*
E_b	Electron Binding Energy	*MeV*
E_D	Energy Deposited	*MeV*
E_e	Electron Energy	*MeV*
$E_e(max)$	Maximum Electron Energy	*MeV*
$\frac{I}{I_o}$	Intensity Change	
J	Surface Current	
L	Material Thickness	*cm*
M	Multiplication	

M_L	Leakage Multiplication	
MM	Molar Mass	$g\ mol^{-1}$
N	Number of histories	
N_i	Nuclei per unit volume	cm^{-3}
N_A	Avogadro's Number	mol^{-1}
S	Total Emissions	
$S(t)$	Source Intensity	s^{-1}
S_x	Variance of of variable x	
T_l	Tracklength	cm
V	Volume	cm^3
Z	Atomic Number	
d	Distance	cm
k	Number of delayed neutron groups	
k_{eff}	Multiplication Factor	
m	Mass	g
m_oc^2	Electron Rest Energy	MeV
n	Particle Density	$cm^{-3}MeV^{1}steradian^{-1}$
$\hat{n}$	Surface Normal	
t	Time	s
$t_{1/2}$	Half-life	s
t_c	Count Time	s
t_d	Decay time	s
t_{irr}	Irradiation Time	s
v_n	Velocity of a neutron	$cm\ s^{-1}$
x_i	Individual Contribution to tally	
$\bar{x}$	Mean score of tally	

Acronyms

ACE	A Compact ENDF
ACT	Activation ConTrol
AECL	Atomic Energy of Canada Limited
ANS	American Nuclear Society
ASC	Advanced Simulation & Computing
ASG	Analytical Sciences Group
BNC	Bayonet Neill-Concelman
CI	Confidence Interval
CDF	Cumulative Distribution Function
CNL	Canadian Nuclear Laboratories
CNSC	Canadian Nuclear Safety Commission
CPS	Counts Per Second
CRM	Certified Reference Material
DG	Delayed Gamma
DN	Delayed Neutron
DNC	Delayed Neutron Counting
DND	Department of National Defense
DNGC	Delayed Neutron and Gamma Counting
DGNS	Director General of Nuclear Safety
DU	Depleted Uranium
ENDF	Evaluated Nuclear Data File
FP	Fission Product
FPP	Fission Product Peak
FPY	Fission Product Yield
FWHM	Full Width at Half Max
GEB	Gaussian Energy Broadening
GUI	Graphical User Interface
HEU	High Enriched Uranium
HPGe	High Purity Germanium
IAEA	International Atomic Energy Agency
ICP-MS	Inductively Coupled Plasma Mass Spectroscopy
ISO	International Organization for Standardization
ITDB	Incident and Trafficking Database

ITWG	International Technical Working Group
JNT	Journal of Nuclear Technology
JPNE	Journal of Progress in Nuclear Energy
JRNC	Journal of Radioanalytical and Nuclear Chemistry
LabVIEW	Laboratory Virtual Instrument Engineering Workbench
LANL	Los Alamos National Laboratory
LEU	Low Enriched Uranium
MATLAB	MATrix LABoratory
MC	Monte Carlo
MCNP	Monte Carlo N-Particle
MCPLOT	MCNP Plotter
MG	Multi Group
NDA	Non Destructive Analysis
NF	Nuclear Forensics
NFA	Nuclear Forensics Analysis
NI	National Instruments
NIM	Nuclear Instrumentation Module
NIST	National Institute of Standards and Technology
NNFL	National Nuclear Forensics Library
NPT	Non Proliferation Treaty
NSERC	Natural Sciences and Engineering Research Council
NSS	Nuclear Security Summit
PE	Polyethylene
RDD	Radiological Dispersal Device
RMCC	Royal Military College of Canada
RSICC	Radiation Safety Information Computational Center
SLOWPOKE	Safe LOW POwer (K)critical Experiment
SNM	Special Nuclear Material
SNR	Signal to Noise

Glossary

The following glossary is intended to provide brief descriptions of reoccurring terms in contexts relevant to this thesis. These definitions are therefore not complete, for example all-encompassing descriptions of a code's full capabilities or library's entire contents are not present.

ACE – A compact version of ENDF format used by MCNP.

Attribution – Identification of the source or origin of the material being examined in a nuclear forensics investigation.

Certified Reference Material – Control material used to calibrate and/or validate analytical instrumentation and procedures of defined activity or concentration with established uncertainty.

CINDER'90 – A transmutation code used by MCNP6, it is capable of simulating delayed neutron and gamma particles from fission products.

Characterisation - The determination of the nature of the material being examined in a nuclear forensics investigation.

cinder.dat – A data file called upon by MCNP6 to determine fission product distributions and delayed particle emissions, currently populated with ENDFB/VI data.

cindergl.dat – A nuclear data file called upon by MCNP6 to determine a fission product's gamma line emission energy and its branching ratio, currently populated with ENDB/VI data.

ENDF – Evaluated Nuclear Data Files containing measurements relevant to nuclear engineering applications, the two most recent releases were ENDFB/VI (1990) and ENDFB/VII (2006).

Fissile – Isotopes that can undergo fission with any type of neutron, including neutrons with zero kinetic energy.

Fissionable – Isotopes where fission with neutrons is possible.

ISO 17025 – The accreditation standard a laboratory should hold in order to be established as technically competent.

ITWG – The international technical working group that organizes the nuclear forensics round robin exercises, in which Canada participates.

LabVIEW – A visual programming language from national instruments commonly used for instrumentation control and data acquisition.

Matrix – Non-fissile components of a sample.

MCNP – Monte Carlo N- Particle code developed by Los Alamos National Laboratory. Simulates three-dimensional transport of particles in user-defined geometry. The current production version of the MCNP code is MCNP6.1 and the most recent release is MCNP6.1.1β, which contains several updates relevant to the simulation of delayed particle emissions.

Nuclear Forensic Analysis – The assay of illicit nuclear or radioactive content an associated material with the goal of attribution.

Special Nuclear Materials – A term used to classify the fissile isotopes ^{233}U, ^{235}U, and ^{239}Pu.

Chapter 1

Introduction

Special nuclear materials (SNMs) are those that contain the fissile uranium and plutonium isotopes ^{233}U, ^{235}U, and ^{239}Pu; they are classified as such due their fissile properties, which enable their employment in nuclear weapons. SNMs are safeguarded by the international community and individual governments, however their diversion and theft still occur (IAEA, 2014a). The characterization and attribution of illicit nuclear materials is termed nuclear forensic analysis (NFA); it relies on analytical instrumentation to identify a material's chemical, physical, and isotopic properties. These characteristics are interpreted, with the aim of determining the material's origin, production method, and smuggling route. These analysis techniques should be performed by instrumentation that has been validated with certified reference materials. Additionally, these methods should be accurate, rapid, and sensitive, such that they can contribute to traditional forensic analyses and criminal investigations in a scientifically rigorous and timely manner.

The 2014 Nuclear Security Summit concluded with the Canadian Government stating its commitment to the development of domestic nuclear forensics capabilities; including methods, databases, and instrumentation. Canada is a participatory nation in previous and upcoming international exercises, which serve to evaluate its nuclear forensics capabilities. The Royal Military College of Canada (RMCC) is among those laboratories in Canada involved in domestic nuclear forensics development. RMCC is equipped with the licensing and instrumentation to handle and assay uranium and plutonium content. It also houses a SLOWPOKE-2 reactor, a high intensity neutron interrogation source. Finally, certified reference materials for instrumentation validation and calibration are present at RMCC for ^{233}U, ^{235}U, and ^{239}Pu, in varying environmental and synthetic matrices.

The measurement of delayed neutron and gamma emissions from fissioned SNM has been identified as a valuable NFA technique as it is has many desirable characteristics, *i.e.*, it is rapid, accurate, and non-destructive. In 2010 RMCC designed and built a delayed neutron counting (DNC) system to contribute to its NFA capabilities (Chapter 3). The DNC system facilitated the identification of ^{235}U

content through the assay of the yield and temporal behaviour of the emitted delayed neutrons. As delayed gamma (DG) emissions are also dependent on the isotopic composition of a sample, they can be used in complement to further characterize an unknown nuclear material.

Nuclear simulations play an important role in the design of nuclear instrumentation, including systems at RMCC. Proper simulations can optimize designs, and reduce required project time, and expense. Los Alamos National Laboratory's widely used code MCNP6, which stands for Monte Carlo N-Particle, models three dimensional particle transport in user defined geometries. MCNP6 has the capability to simulate DN and DG emissions, and their detection. With increased interest in the development of instrumentation for the measurement of delayed neutron and gamma emissions, this capability is increasingly important.

This thesis saw the expansion of non-destructive instrumentation at RMCC to include a delayed neutron and gamma counting (DNGC) system for the assay of SNM. The purpose of this thesis was twofold: i) to contribute to NFA instrumentation available to the Canadian Department of National Defense, and ii) to evaluate the capabilities of the Monte Carlo Code, MCNP6, to simulate the measured delayed neutron and gamma emissions, and their detection. Specific thesis objectives were to:

- Attribute and minimize the interference of the observed neutron background arising from the irradiation site used for SNM assay (Chapter 4);

- Demonstrate the application of delayed neutron signatures to characterize mixtures of SNM (Chapter 5);

- Use measured delayed neutron signatures to examine multiple MCNP6 simulation capabilities (Chapter 6, Appendix A), and contribute to MCNP6's delayed particle testing suite (Chapter 7);

- Upgrade the delayed neutron counting system (Chapter 3) to include the concurrent measurement of delayed gamma (Chapter 8);

- Provide a comparison of the relative intensity of fission product pairs useful for nuclear forensics as predicted by MCNP6 and measured in the DNGC system (Chapter 9); and

- Compare measured delayed gamma emissions to the high fidelity gamma line emission capabilities of MCNP6 (Chapter 10, Appendix B).

Chapter 2 provides introductory details on specific topics relevant to the manuscripts contained in the following chapters that comprise this thesis. Several of the sections' relevance to specific manuscript chapters are highlighted. The appendix contains additional papers detailing the incremental progress of the research.

-This page is intentionally left blank-

Chapter 2

Background

2.1 Nuclear Forensic Analysis

Nuclear forensic analysis (NFA) is concerned with the attribution of unidentified nuclear materials (Mayer *et al*., 2005, 2006, 2007). Determination of an illicit material's origin aids both traditional forensics investigations and international efforts concerned with the safeguarding of nuclear materials. These unidentified nuclear materials may be in bulk form, for example the 560 *g* of plutonium and uranium oxide powder intercepted in Munich Airport in 1994 (Wallenius *et al*., 2007), or in trace amounts, perhaps those collected during environmental sampling by safeguards officers (Lee *et al.*, 2009; Usuda *et al.*, 2010). NFA requires a wide-range of analytical instrumentation to identify the physical, chemical and isotopic characteristics of the material (Mayer *et al.*, 2005). It relies on the expertise and experience of scientists interpreting these results to determine a material's origin. In many cases, NF efforts would collaborate with traditional law enforcement to result, when appropriate, in criminal prosecution (Grant *et al.*, 1998). In these cases it is important that the assay of material is accurate, reproducible, and able to withstand scrutiny of the methodology and instruments used (Kristo *et al.*, 2004). Therefore it is valuable if at least some part of the assay of material is non-destructive, whilst at the same time being accurate, with low detection limits and high precision. Additionally, these methods should be validated to the International Organization for Standardization (ISO) standards or the like with Certified Reference Materials (CRMs).

Canada has recognized the importance of nuclear forensics in support of domestic and international nuclear security efforts (NSS, 2014a). The Canadian government is currently expanding its nuclear forensics capabilities through several measures including the development of Canada's National Nuclear Forensics Library (NNFL) led by the Canadian Nuclear Safety Commission (CNSC) (El-Jaby *et al*., 2014). Additionally, Canada is a participant in previous and upcoming nuclear forensics exercises organized by the International Technical Working Group (ITWG) (AECL, 2014; Larsson and Haslip, 2004). These round robin

exercises evaluate the capabilities of Canadian laboratories to perform basic nuclear forensics analyses to support legal investigations and to communicate the results accurately. These exercises focus on the characterisation of special nuclear materials (SNMs), which are often identified via the measurement of their radioactive emissions. The use of both established and novel nuclear forensics methods, for example, the delayed neutron and gamma counting system discussed in this work, are encouraged in the upcoming ITWG exercise.

The Royal Military College of Canada (RMCC) is a valuable contributor to NFA capabilities available to the Canadian government. RMCC houses a SLOWPOKE-2 reactor, discussed in Section 2.7, which enables the active interrogation of nuclear materials. Additional instrumentation available at RMCC includes Inductively Coupled Plasma – Mass Spectroscopy (ICP-MS) and gamma-ray spectroscopy. RMCC's Analytical Sciences Group (ASG) is accredited to the ISO 17025 standard, and the SLOWPOKE-2 Facility at RMCC is a safeguarded facility and can thus hold enriched uranium and plutonium. Finally, the Facility has an array of environmental and synthetic certified reference materials (CRMs) containing ^{233}U, ^{235}U, and ^{239}Pu content.

2.2 Special Nuclear Materials: An Overview

Materials suitable for employment in nuclear weapons include uranium or plutonium enriched in ^{233}U, ^{235}U, or ^{239}Pu, as these can undergo the highly energetic process of fission (Moody *et al.*, 2005). ^{235}U is found in nature as it comprises 0.72 *at*% (atom percent) of natural U (Seyfang and Smales, 1953). ^{235}U content must be increased relative to the predominant ^{238}U in order to become a viable material for nuclear weapons, this process is termed uranium enrichment and may be achieved through several means as detailed by Villani, 1979. ^{233}U and ^{239}Pu are synthetic isotopes produced after the neutron irradiation of ^{232}Th and ^{238}U, respectively; and must be chemically separated from the irradiated feedstock material (Glaser, 2006). Substances that are enriched in ^{233}U or ^{235}U, or contain plutonium are termed as special nuclear materials (SNMs) (US NRC).

The International Atomic Energy Agency (IAEA) monitors SNM production and transport in the Non-Proliferation Treaty (NPT) signatory countries with nuclear instrumentation employed by trained Safeguards Officers (IAEA, 2014b). Even with modern measures and policies in place, SNMs are diverted, or illicitly produced. The IAEA Incident and Trafficking Database (ITDB) records illicit nuclear materials trafficking events, which are self-reported by 125 participating states (IAEA, 2014a). The database includes 16 confirmed incidents between 1993-2013 that involved unauthorized possession of high enriched

uranium (HEU) or plutonium content. Some of these incidents included kilogram quantities, and attempts to sell or traffic materials across state borders. It is therefore important for governmental laboratories to develop and maintain the capability to detect, and secure SNM content in a wide variety of environmental and synthetic matrices.

2.3 Special Nuclear Materials: Their Emissions

Special nuclear materials are often identified according to their particle emissions, which can occur naturally or after the exposure of SNMs to radiation. Those emissions that occur naturally are described as passive signatures, whereas those instigated by interrogating radiation are termed active emissions, and are the focus of this thesis. Neutron and gamma emissions are most commonly measured for SNM detection as they are significantly more penetrating than other emissions, and are therefore most useful for SNM assay. This work concerns the measurement of delayed neutron and gamma signatures, produced after a sample is irradiated in a SLOWPOKE-2 reactor.

2.3.1 Gamma Rays

Radioactive decay results in the transition of an atom into another, the latter often in an excited state. Gamma rays are emitted with the de-excitation of the daughter atomic nuclei (Grover and Gilat, 1967). They lie on the high energy end of the electromagnetic spectrum, with energies ranging from tens of *keV* to about 20 *MeV* (Ramaty *et al.*, 1979). Gamma rays and x-rays vary in their origin, as the latter are released during the rearrangement of electron structure (Compton and Allison, 1935). However, x-rays and low energy gamma rays occupy the same region of the electromagnetic spectrum. Each emission has an associated decay constant, λ [s^{-1}], which is related to the nuclear half-life, $t_{1/2}$ [s] as follows:

$$t_{1/2} = \frac{\ln(2)}{\lambda} \qquad 2\text{-}1$$

Gamma ray emissions will have both a characteristic energy and half-life associated with a particular nuclear transition, making them a useful tool when identifying their precursors (*i.e.*, fission or activation products (De Soete, 1972)).

As photons travel in a medium they are absorbed through various interactions. A simple relationship describing intensity changes of gamma rays I/I_0 with respect to material thickness, L [cm], is as follows (Davisson and Evans, 1952):

$$\frac{I}{I_o} = e^{-\mu_\ell L} \qquad 2\text{-}2$$

Where μ_ℓ is the material's linear attenuation coefficient [cm^{-1}], it is dependent on gamma ray energy, the material's atomic number (Z), and density.

Gamma rays of interest to this work fall in the 100 *keV* to 1.6 *MeV* range and interact via three major processes: photoelectric absorption, Compton scattering, and pair production. In photoelectric absorption the gamma ray interacts with a bound atomic electron such that the entirety of its energy is lost through transfer of energy required to overcome the electron's binding energy, and the kinetic energy of that freed electron. The energy of the photoelectron produced, E_e [*MeV*] is equal to that of the incident photon, E_γ [*MeV*] minus the binding energy of the electron, E_b [*MeV*][i]. Photoelectric absorption is the dominant reaction for low energy gamma rays, and x-rays (Hall, 1936).

$$E_e = E_\gamma - E_b \qquad 2\text{-}3$$

Compton scattering consists of an interaction between a gamma-ray and a free or weakly bound electron, and the partial transfer of the photon's energy to the electron. The maximum energy of the electron produced is related to incident photon energy as follows:

$$E_e(max) = \frac{E_\gamma}{[1 + \frac{m_o c^2}{2E_\gamma}]} \qquad 2\text{-}4$$

Where $m_o c^2$ is the rest energy of an electron (511 *keV*). The final interaction considered, pair production, converts a photon into an electron-positron pair, it can occur if E_γ > 1.022 *MeV* (the minimum energy required to create an electron-positron pair). The photon is eliminated as it transfers all of its energy to the electron-positron pair and the material's nucleus. The positron in turn undergoes annihilation with the surrounding electrons producing two new gamma rays each with energies of 511 *keV*.

2.3.2 **Neutrons**

Neutrons are produced by SNM through a variety of reactions including isotopic decay, (α,*n*) reactions, and most important to this work, fission. The probability that a neutron will undergo a specific reaction *x* is dependent on the neutron's

[i] A very small amount of energy remains with the atom to conserve momentum.

energy and the nucleus it is interacting with, and is termed microscopic cross section, σ_x [cm^2]. Common neutron interactions include elastic (*n,n*), or inelastic (*n,n'*) scattering, photon production (*n,γ*), charged or neutral particle production, and fission (*n,f*). When neutrons are traveling in bulk materials, a macroscopic cross section for reaction *x*, Σ_x [cm^{-1}] is used:

$$\Sigma_x = N_i \sigma_x \tag{2-5}$$

Where N_i is the number of nuclei per unit volume [cm^{-3}]. The total macroscopic cross section, Σ_t, is the superposition of individual reactions and related to a neutron's mean free path, λ_{mfp} [cm] as:

$$\lambda_{mfp} = \frac{1}{\Sigma_t} \tag{2-6}$$

Figure 2.1 depicts microscopic fission cross sections of the fissile isotopes ^{233}U, ^{235}U, and ^{239}Pu, and the fissionable ^{238}U isotope (the most common isotope found in natural uranium). Fissionable isotopes are those for which fission with neutrons is possible and fissile isotopes are those whose fission is possible with any incident neutron energy (DOE Handbook, 1993). In general, the fission probability of SNMs increases with decreasing incident neutron energy. To increase the probability of fission in nuclear instrumentation and reactors, the energy of the neutrons may be decreased through moderation. Good moderating materials are those that remove energy from the neutron in the fewest collisions. They have low atomic mass, A, as neutrons will transfer the largest amount of energy in each interaction as shown below (Rinaldi *et al*., 2009):

$$E'_n = \left(\frac{1-A}{1+A}\right)^2 E_n \tag{2-7}$$

Where E'_n and E_n are the neutron energies before and after collision respectively [*MeV*]. Common moderators include water, beryllium, and as used in this work, paraffin.

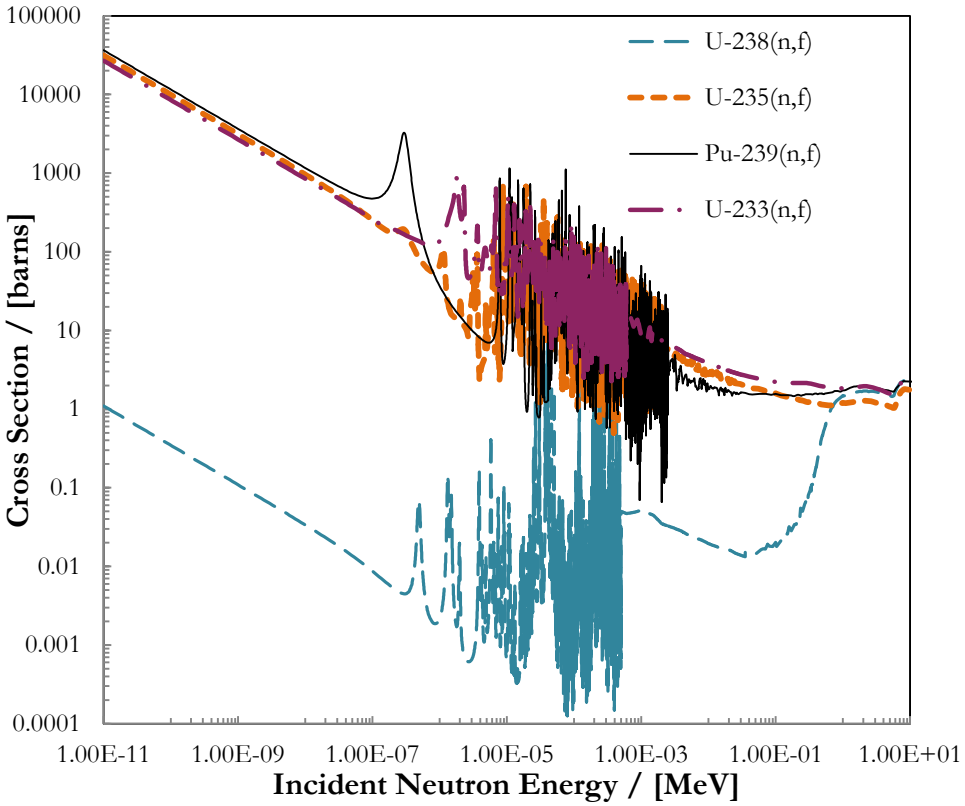

Figure 2.1: Fission cross sections of ^{233}U, ^{235}U, ^{238}U, and ^{239}Pu as a function of incident neutron energy.

Subcritical Multiplication

Instrumentation presented in this work will be used for with the assay of subcritical SNMs, defined as those with a multiplication factor, $k_{eff} < 1$, where (Glasstone and Sesonske, 1967):

$$k_{eff} = \frac{Rate\ of\ neutron\ production}{Rate\ of\ neutron\ absorption + leakage} \qquad 2\text{-}8$$

As implied in Eq. 2-8 neutron population in a subcritical system decreases with time, and approaches zero. Suppose a material has a k_{eff} value of 0.1, and 100 neutrons are introduced into the system. The second generation will have 10 neutrons and the third (and final), one, for a total of 111 neutrons over three generations. The ratio of total neutrons that exist in a sample (111) divided by the

number of those which were started (100) is known as multiplication, *M*. In this example the system has a multiplication of 1.11, in subcritical systems, it is related to the multiplication factor as follows (Reilly *et al*., 1990):

$$M = \frac{1}{1 - k_{eff}} \qquad k_{eff} < 1 \tag{2-9}$$

An understanding of a material's probability of absorbing or producing additional neutrons is very important when measuring particle emissions. When simulating the interrogation of fissile content, it is important that the geometric and material properties are accurately reproduced to avoid systematic errors in multiplication.

2.3.3 Characteristic Neutron and Gamma Emissions from SNM

Fission of a SNM atom creates an average of 2-3 prompt neutrons and typically 2 fission products (Meitner and Frisch, 1939). The exact distribution of the fission product yield is dependent on the incident particle and its energy, and the fissioned isotope (Marrs *et al*., 2008), as demonstrated in Figure 2.2. These fission products are in generally rich in neutrons and as such are susceptible to β^- decay. Particles emitted from fission product decay are termed delayed particles. As these delayed emissions arise from fission product decay, their yields and temporal behaviour are also characteristic of the isotope undergoing fission.

Delayed neutron (DN) precursors, of which 271 have been identified (Kawano *et al*., 2008), are often grouped by their half-lives into 6-8 groups (Keepin *et al*., 1957; Spriggs *et al*., 2002). The ratios of DN emissions to those of all neutrons released, β_i, is shown in Table 2.1 for ^{233}U, ^{235}U and ^{239}Pu. The isotope-dependent differences result in unique temporal characteristics for the DN emissions of each isotope when a sample is removed from a fission source (Myers *et al*., 2006). The DN emissions are used in Chapter 5 to characterise fissile mixtures of ^{233}U and ^{235}U. The concurrent emission of delayed gammas is also dependent on the isotope undergoing fission, resulting in spectra unique to the SNM present and the interrogation source. Delayed gammas are also emitted with unique temporal behaviours and yields dependent on which isotope is fissioned. However, more useful to NFA is the use of the delayed gammas' characteristic energies to identify individual fission products, and their relative intensities, as demonstrated in Chapter 9.

Table 2.1: Delayed Neutron Data for Thermal Fission in ^{233}U, ^{235}U, and ^{239}Pu (Nichols *et al.*, 2008). They are organized into 8 groups with nominal half-lives and associated production ratios. They are discussed in Section 2.5.

Group	$t_{1/2}$ [s]	β_i ^{233}U / [%]	β_i ^{235}U / [%]	β_i ^{239}Pu / [%]
1	55.6	0.0214 ± 0.0015	0.0218 ± 0.0029	0.0072 ± 0.0028
2	24.5	0.0448 ± 0.0024	0.1023 ± 0.0036	0.0533 ± 0.0081
3	16.3	0.0402 ± 0.0022	0.0605 ± 0.0063	0.01859 ± 0.00098
4	5.21	0.054 ± 0.012	0.131± 0.016	0.041 ± 0.012
5	2.37	0.0799 ± 0.0071	0.2200 ± 0.0083	0.0662 ± 0.0073
6	1.04	0.01040 ± 0.00055	0.0600 ± 0.0036	0.01836 ± 0.00097
7	0.424	0.015 ± 0.0068	0.0540 ± 0.0021	0.0162 ± 0.0071
8	0.198	0.00281 ± 0.00015	0.0152 ± 0.0064	0.00416 ± 0.00023
Total		0.268 ± 0.013	0.665 ± 0.021	0.225 ± 0.011

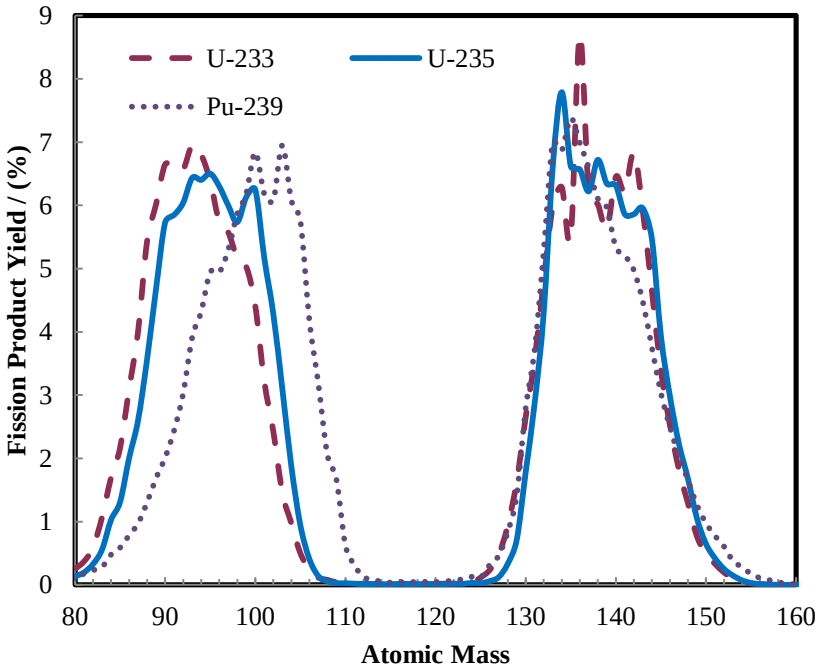

Figure 2.2: Fission product yields of ^{233}U, ^{235}U, and ^{239}Pu thermal neutron fission vs atomic mass of fission product.

2.4 Considerations for the Design of A Delayed Neutron and Gamma Counting System

2.4.1 Detector Performance

The design of nuclear instrumentation for the detection of SNM requires that the equipment is sensitive to particles of interest, and that background contributions are minimized, in order to produce precise results and low detection limits. Overall detection efficiency, ε, is the product of geometric and intrinsic efficiencies (Sher and Untermyer, 1980). It is the probability that a particle emitted from a source will result in a registered count. Detectors are often arranged around a source to maximize the solid angle subtended and increase the probability that the particle will be incident on the detector's surface. Thus, geometric efficiency is increased. However particles may also be attenuated by the intervening medium or the sample itself. Once a particle has reached a detector's active volume, its probability of interaction, intrinsic efficiency, is dependent on the incident particle's energy and the reaction cross section of the material present in the sample.

Energy resolution is important to spectroscopic measurements and is often quantified by a determination of a peak's Full Width at Half Maximum (FWHM). Assuming a peak has a standard Gaussian shape, its FWHM [*MeV*] value is given by (Knoll, 2010):

$$FWHM = 2.35\sigma, \qquad 2\text{-}10$$

where σ is the width parameter for the Gaussian [*MeV*]. Detector resolution is naturally limited by the statistical fluctuations associated with the charge production process. Electronic noise arising from voltage integrity and other instrumentation also contribute to the energy resolution.

Common features of older equipment and gaseous detectors are the contributions of dead time and pulse pile up, which are both present in RMCC's Delayed Neutron and Gamma Counting (DNGC) system. In short, the dead time constant, τ [μs], is the amount of time it takes the system to process an incoming count. If subsequent counts come in during this time, they will not be recorded resulting in a lower than expected count rate, and a distortion to the temporal behaviour measured. Pulse pile up occurs when two separate events are counted as one, often resulting in an energy deposition corresponding to the summation of both counts (Mazed *et al*., 2012). When exposed to high neutron fluence, detector performance will degrade, resulting in decreased efficiency and energy resolution (Kraner *et al*., 1975; Qian *et al*., 1997, 1998).

2.4.2 **Background Contributions & System Calibration**

Of considerable importance to the design of nuclear instrumentation is the reduction of the influence from background signals (Arthur and Reeves, 1992; Peerani *et al*., 2002). Background contributions can be constant and a function of the surrounding environment or an artifact of the experimental process itself that is time-dependent, as will be shown in Chapter 4. Both the background of a system and its variance should be well characterized. Minimization of background eases the collection of statistically valid data at low count rates. This is facilitated by the measurement of background signals made prior to the introduction of samples to be analyzed. Background contributions and their uncertainties can drastically increase the detection limit of a system. The minimum signal that can be used to assert the presence of a radiation source is directly proportional to the uncertainty of the system's background.

The use of certified reference materials can serve to calibrate the energy and efficiency of the detection system, These sources are positioned in the detector arrangement and their spectra recorded for a time sufficient to reduce stochastic uncertainties. The system channels registering expected nuclide peaks are identified and used to determine the relationship between recorded voltage and energy deposition in the detector. Reference sources are additionally used to determine the detection efficiency of the system both in terms of source position and incident particle energy, see Chapter 8. Calibration sources are also employed to determine a system's energy resolution and dead time.

2.4.3 **Gamma Detection**

The main mechanism of gamma detection is ionization, whereby the gamma-ray imparts all or some of its energy within the active volume of the detector, which releases some electrons. These ionized electrons in turn create many more, whose charge is collected. Detectors commonly used for gamma detection include sodium-iodide, NaI, which can be very efficient however offer relatively poor energy resolution. Thus, NaI is unsuitable for high fidelity measurement of complex gamma spectra. Generally, semiconductor detectors, namely high purity germanium (HPGe), are most commonly used for SNM assay due to their high-energy resolution.

Contributions to HPGe spectra are demonstrated in Figure 2.3, which depicts the expected HPGe detector response to the 1.460 *MeV* emission from ^{40}K (which is a common background source). The full energy peak mostly results from photoelectric absorption, as the photoelectrons produced in this process are quickly stopped within the active volume of the detector. This photoelectron is

accompanied by characteristic x-rays with E_b, which are emitted in coincidence, resulting in an output directly proportional to the incident photon energy.

Electrons scattered in Compton processes within a detector are typically stopped in the active volume and produce a pulse proportional to the energy lost by the incident photon, ranging from 0 to $E_e(max)$. This is shown in Figure 2.3 where the Compton edge is found at 1.243 *MeV*, the $E_e(max)$ value dictated by Eq. (2-4). Compton-scattered photons that undergo photoelectric absorption result in backscatter contributions in the detector (shown at 219 *keV*, equal to the minimum photon energy of a Compton scatter). If all annihilation gammas produced via pair production are absorbed in the detector, the reaction contributes to the full energy peak. Single and double escape features appear in gamma spectra when one or two of the annihilation gamma rays escape before they are absorbed, the relative intensity of these peaks is dependent on detector volume. A peak at 511 *keV* occurs when one of the 511 *keV* photons produced by surrounding material is absorbed, it is termed the annihilation peak. Also shown in the spectra are characteristic x-rays of surrounding material.

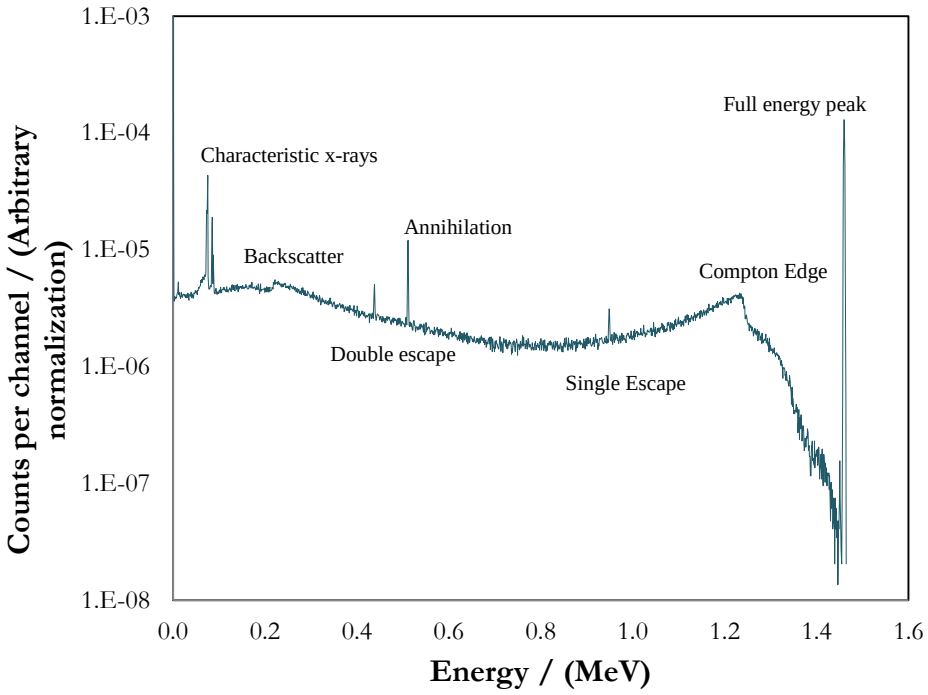

Figure 2.3: MCNP6 Generated HPGe Spectra Resultant from 1.460 *MeV* decay.

2.4.4 **Neutron Detection**

BF_3 and ^{3}He gaseous detectors offer high thermal neutron cross sections and easy gamma discrimination, they are commonly used in SNM assay. Limitations of BF_3 include its toxic nature (Kouzes and Ely, 2010), rendering its pressurization unsafe. ^{3}He proportional counters are one of the most commonly employed neutron detectors for the assay of SNM (*i.e.*, the DNGC system) due to their high thermal neutron cross section. As their name suggests, these detectors are operated in the proportional region where a resulting pulse is directly related to the energy produced by gas ionisation. In the case of thermal neutron interaction in these detectors the triton and hydrogen products are produced with total reaction energy of 0.764 *MeV* (the created proton and triton have energies of 0.573 and 0.191 *MeV* respectively). Often the kinetic energy of these products is dissipated in the sides of the detectors resulting in incomplete charge collection, in the form of a wall effect, Figure 2.4. International ^{3}He supply is limited, leading many to investigate alternative neutron detectors(van Eijk, 2012; Kouzes *et al*., 2010; Peerani *et al*., 2012), however it remains the dominant detector for safeguards applications due to is many advantages.

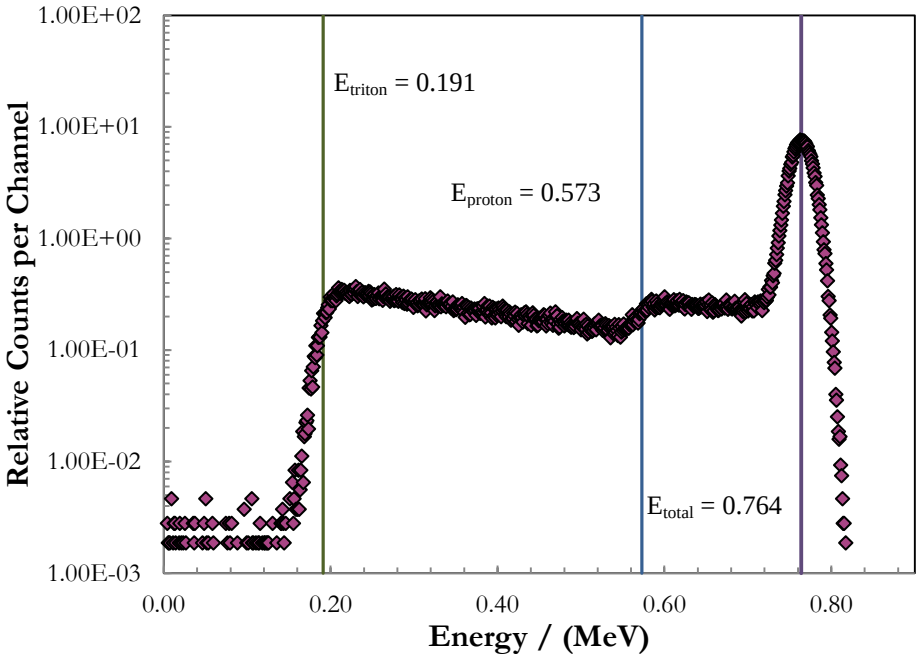

Figure 2.4: MCNP6 simulated energy deposition of neutrons in ^{3}He detectors.

Exposure to high photon fluxes can contribute to background counts in ^{3}He detectors (Spaulding *et al*., 2009) and their degradation (Qian *et al*., 1998). Photons

can be easily discriminated by implementing an energy cut off in the spectra at 0.191 *MeV* (the energy of the triton produced in the $^{3}He(n,p)^{3}He$ reaction). ^{3}He detectors are often embedded in neutron moderators (paraffin, polyethylene, water) in order to thermalize the incident neutron energy, and thus increase the neutron's cross section, as illustrated in Figure 2.5. This figure shows the average initial energy of delayed neutrons emitted from SNM, and the increase of cross section with decreasing neutron energy.

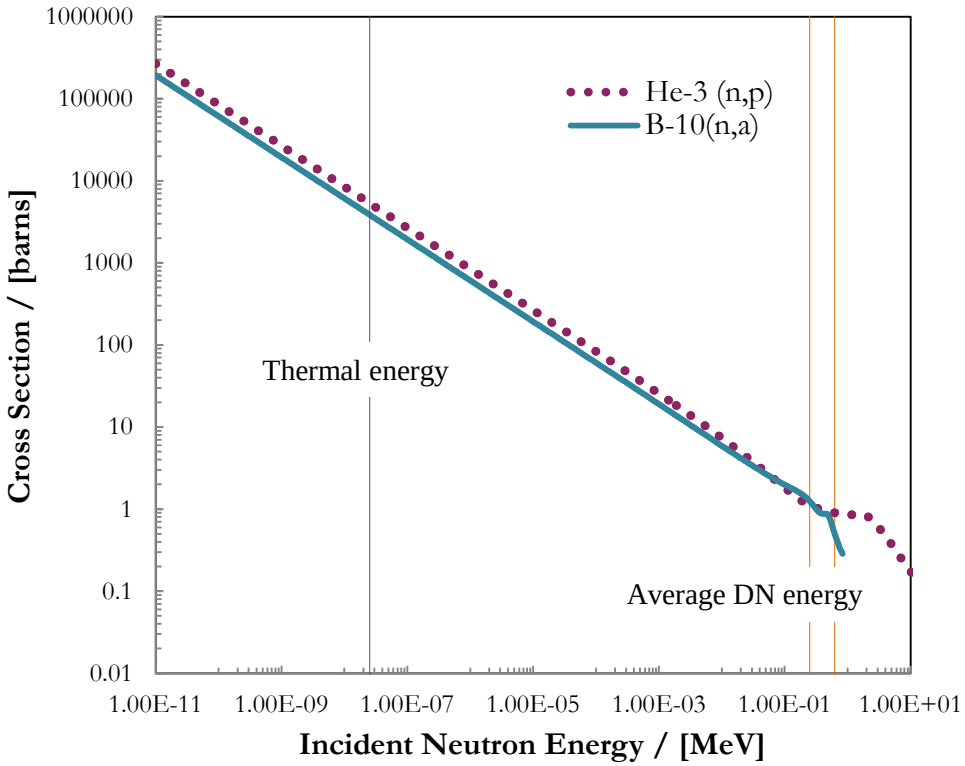

Figure 2.5: Relevant cross sections for ^{3}He and ^{10}B from ENDFV/B VII.1.

2.4.5 **Electronic Instrumentation**

A high voltage bias supply is necessary to provide an electric field for charge collection by both gamma-ray and ^{3}He detectors. Common in non-destructive analysis (NDA) is the use of bias supplies that fit into the frame of a nuclear instrumentation module (NIM). This module provides necessary DC voltages and is often the most reliable unit in a nuclear instrumentation system. A detector's output is typically a low-amplitude, short-duration current pulse, which is converted to a voltage pulse by a pre-amplifier positioned in close proximity to the

detector. The low-voltage pulse is proportional to the initial energy deposited in the detector and is accepted by an amplifier, which converts it to a linear voltage range from 0 – 10 *V*. A multichannel analyzer collects and then sorts the amplifier's pulses to build a digital representation of the pulse height spectrum in the detector.

2.5 Delayed Neutron & Gamma Counting

If the source of counts is delayed neutrons, the total emission, *s* from time t_1 [*s*], to final count t_2 [*s*] can be described as[ii]:

$$s = \int_{t_1}^{t_2} A(t)dt \qquad 2\text{-}11$$

where *A(t)* is the activity of delayed neutrons [s^{-1}], which have been conveniently organized into *k* groups such that:

$$A(t) = \sum_{i=1}^{k} A_{o_i} e^{-\lambda_i t} \qquad 2\text{-}12$$

the initial activity, A_o [s^{-1}] of a particular delayed neutron group *i* (Table 2.1) is dependent on the number of fissile atoms and the flux it is exposed to, and duration of irradiation, t_{irr} [*s*]; it is given by Eq. (2-13) (Binney and Scherpelz, 1978):

$$A_{o_i} = \frac{\beta_i v N_A \sigma_f \Phi m}{MM}(1 - e^{-\lambda_i t_{irr}}) \qquad 2\text{-}13$$

where *MM* is the molar mass of the sample [g mol^{-1}], *m* the fissile mass present [*g*], N_A Avogadro's number [mol^{-1}], and β_i the delayed neutron fraction (Table 2.1). Substituting Eqs. (2-13) and (2-12) into (2-11) and integrating yields:

$$s = \frac{v N_A \sigma_f \Phi m}{MM} \sum_{i=1}^{k} \frac{\beta_i}{\lambda_i}(1 - e^{-\lambda_i t_{irr}})(e^{-\lambda_i t_1} - e^{-\lambda_i t_2}) \qquad 2\text{-}14$$

setting t_c the count time [*s*], equal to $t_2 - t_1$ (t_1 is equivalent to decay time, t_d [*s*]), and rearrangement of the exponentials yields:

$$s = \frac{v N_A \sigma_f \Phi m}{MM} \sum_{i=1}^{k} \frac{\beta_i}{\lambda_i}(1 - e^{-\lambda_i t_{irr}})(1 - e^{-\lambda_i t_c})(e^{-\lambda_i t_d}) \qquad 2\text{-}15$$

[ii] Complete derivation can be found in Appendix E.

The emission rate *S(t)* is the derivative of Eq. 2-15 with respect to t_c:

$$S(t) = \frac{\nu N_A \sigma_f \Phi m}{MM} \sum_{i=1}^{k} \beta_i \left(1 - e^{-\lambda_i t_{irr}}\right)\left(e^{-\lambda_i t_c}\right)\left(e^{-\lambda_i t_d}\right) \quad 2\text{-}16$$

If a sample contains *n* DN producing isotopes, the total emission rate, *S(t)* is the summation of their individual contributions:

$$S(t) = \sum_{j=1}^{n} \frac{\nu_j N_A \sigma_{f_j} \Phi m_j}{MM_j} \sum_{i=1}^{k} \beta_i \left(1 - e^{-\lambda_i t_{irr}}\right)\left(e^{-\lambda_i t_c}\right)\left(e^{-\lambda_i t_d}\right) \quad 2\text{-}17$$

Or simplified:

$$S(t) = \sum_{j=1}^{n} Q(t)_j m_j \quad 2\text{-}18$$

Where

$$Q(t)_j = \frac{\nu_j N_A \sigma_{f_j} \Phi}{MM_j} \sum_{i=1}^{k} \beta_i \left(1 - e^{-\lambda_i t_{irr}}\right)\left(e^{-\lambda_i t_c}\right)\left(e^{-\lambda_i t_d}\right) \quad 2\text{-}19$$

In a thermal neutron irradiation system, knowledge of experimental variables and instrumentation behaviour can allow the determination of the masses of individual fissile isotopes, m_j by recording the magnitude and temporal behaviour of the DN emissions.

Total neutron counting records all pulses resultant from neutron interactions in sensitive volumes of detectors. The total count rate, *C(t)* [s^{-1}], is:

$$C(t) = \varepsilon M S(t) + \mathrm{B(t)} \quad 2\text{-}20$$

Where ε is the detector efficiency, *M* the sample multiplication (Section 2.3.2), and *B(t)* is the neutron background [s^{-1}]. All samples measured and simulated in this work have little absorbing or fissile content and therefore assumed to have a net multiplication of unity. The total neutron count rate recorded by a DNGC system measuring emissions from *n* fissile isotopes is:

$$C(t) = \varepsilon \sum_{j=1}^{n} Q(t)_j m_j + \mathrm{B(t)} \quad 2\text{-}21$$

Delayed neutron counting (DNC) is a well-established technique for the determination of uranium content in a wide variety of matrices (Binney and Scherpelz, 1978). The technique of DNC also lends itself to nuclear safeguard and

nuclear forensics applications (Glasgow, 2008; Lakosi *et al*., 2011; Landsberger *et al*., 2013). More recently the applicability of delayed neutron counting to characterize mixtures of SNM and fissionable isotopes has been demonstrated. Kapsimalis determined ^{235}U and ^{239}Pu content in mixtures prepared by certified reference materials with a typical precision less than 5 % (Kapsimalis, 2013; Kapsimalis *et al*., 2013). Li *et al*., 2004 also examined the intensity-time curve of the delayed neutrons produced from $^{235}U/^{239}Pu$ mixtures to determine their absolute quantities in microgram samples. Myers *et al*., 2006 used a 14 *MeV* neutron generator to induce fission in ^{235}U and ^{238}U contained within bulk samples. The magnitude and temporal behaviour of the DNs were then used to estimate enrichment levels based on the ^{235}U to ^{238}U ratios.

The measurement of delayed gammas provides further information, as their measured energies are characteristic of their fission product precursors (Gmar and Capdevila, 1999; Hollas *et al*., 1987; Johansson, 1965). The ratio of selected gamma line measurements can determine the relative ratio of their fission product precursors, providing further details on a sample's SNM content (Beddingfield and Cecil, 1998; Firestone *et al*., 2005; Marrs *et al*., 2008). Additional work has proposed that delayed neutron and gamma techniques could be combined and have applications in the measurement of fission rates in nuclear fuel (Perret and Jordan, 2011), and the forensic analysis of electrorefining, and pyroprocessing signatures (Durkee, 2012). Delayed gamma assay also lends itself to safeguards and nuclear forensics as it can be employed for the analysis of burn-up of spent nuclear fuel (Mozin *et al*., 2012). Chapter 9 demonstrate the differences in the gamma line intensities from particular fission products with varying fissioned material.

Characterisation of fissile mixtures via DN temporal emissions alone has been demonstrated as achievable, however it requires minimal uncertainties in collected data. Gains in accuracy and a reduction of detection limit can be realised through reductions in background uncertainties and systematic errors. Further characterization of the fissile isotope(s) comprising a sample can be facilitated by a concurrent examination of delayed gamma yields. The net DN counts over a fixed count time can determine mass of an identified fissile isotope with a high degree of accuracy, as will be demonstrated in Chapter 8.

2.6 Monte Carlo Simulations

2.6.1 An Overview of MCNP6

The solution of problems via the simulation of multiple stochastic processes was developed in the 1940s by scientists at Los Alamos National

Laboratory (LANL), and coined the Monte Carlo (MC) technique (Brown, 2005; Metropolis, 1987). The parallel development of scientific computing enabled the automation of MC simulations of particle transport and LANL developed a Monte Carlo Neutron Photon (MCNP) code in 1977 (Brown, 2014). MCNP codes released by LANL are widely used by the nuclear community, and applications include reactor physics, nuclear instrumentation design, and nuclear safeguards (Belian *et al*., 2009; Le Coq, 2013; Henzl *et al*., 2013; Kaplan *et al*., 2014; Lee *et al*., 2011). MCNP6 simulations can be very detailed and accurate; their computational expense is offset by the ease with which they lend themselves to parallelization (Hendricks *et al*., 2000).

MCNP6 simulates the complete history of particles, and their progeny, from their creation to death. Random numbers are used to sample probability density functions created based on possible interactions, often using nuclear data libraries including ENDF, which stands for Evaluated Nuclear Data Files (Chadwick *et al*., 2006). Problems are solved by the use of tallies, which record user specified information about particle interactions in defined regions. A MCNP6.1.1 Beta release in September 2014 contained updates to capabilities of importance to homeland security, non-proliferation applications (Goorley, 2014), and simulations presented in this thesis.

2.6.2 MCNP6 Deck Specification & Particle Transport

Three dimensional volumes are created by specifying their bounding surfaces in MCNP input decks. These volumes are given cell numbers and assigned a corresponding material whose isotopic composition and density are included in the simulation input. In fixed source simulations, which are most relevant to this work, the initial particles to be transported are defined in the input deck. Particle type, energy, location, direction, time, and other important properties, are described by either continuous or discrete probability distributions.

The distance to a particle's next collision, d, is determined using the macroscopic cross sections, Σ_T [cm^{-1}], and a random number, ξ, which is selected from a uniform distribution between 0 and 1:

$$d = -\frac{1}{\Sigma_T}\ln(\xi) \qquad 2\text{-}22$$

If this distance is less than that to an adjacent cell, the reaction type will be determined based on the isotopes in the current cell. The resulting energy, E' [MeV] and direction, Ω' [$steradian$], and production of secondary particles will be determined based on the reaction type. The reaction type that the particle will undergo with a nuclide is determined via the random sampling of a discrete

cumulative distribution function (CDF). If *d* is greater than the distance to the next boundary, the particle is moved to that boundary where a new distance is calculated, and the process continued. MCNP simulations require the simulation of external boundaries which will terminate a particle's history if reached.

2.6.3 **Tallying MCNP6 Results**

In MCNP6 simulations quantities of interest to the user are recorded through the use of tallies. The volume or surface, and the physical parameter to be recorded are selected before a MCNP run is initiated. Relevant tallies to the simulation of delayed particle production and detection in this work include surface current (F1), flux (F4), and pulse height distribution (F8), tallies. Surface current tallies, *J*, record the number of particles passing through a surface (MCNP Team).

$$J = \int dE \int dt \int dA \int d\Omega \left|\hat{\Omega} \cdot \hat{n}\right| \psi(\vec{r}, \hat{\Omega}, E, t) \qquad 2\text{-}23$$

Where *E* is energy [*MeV*], *t* time [*shakes*, *sh*] [iii], *A* surface area [cm^2], Ω a particle's direction vector, $\hat{n}$ the surface normal, and ψ the angular flux [$cm^{-2}sh^{-1}MeV^{-1}steradian^{-1}$] is shown in Eq. 2-24:

$$\psi(\vec{r}, \hat{\Omega}, E, t) = v_n n(\vec{r}, \hat{\Omega}, E, t) \qquad 2\text{-}24$$

Where v_n is neutron velocity [$cm\ sh^{-1}$], and *n* is particle density [$cm^{-3}MeV^{-1}steradian^{-1}$]. In MCNP6 simulations the surface current is determined by tallying the number of particles passing through a surface. Flux tallies, $\bar{\Phi}_v$, [cm^{-2}], which display the average flux in a volume, are determined in MCNP6 by scoring the product of the weight, W [iv], of a particle and its tracklength[v], T_l [*cm*], normalized by a cell's volume, V [cm^3].

$$F4 = W\frac{T_l}{V} \qquad 2\text{-}25$$

Pulse height tallies [*pulses*] record the energy deposition of a single event in a detector volume, E_D [*MeV*]. The particle(s) to be recorded for an individual tally are specified in the input deck, for example, recording hydrogen (*h*) energy depositions in cell 1 would be written as:

F8:h (1)

[iii] A *shake* is 10^{-8} *seconds.*
[iv] In analog simulations, particle weight is 1.
[v] The tracklength is the product of an event's transit time and the particle's velocity.

Furthermore, the energy and temporal information of these energy deposition events are recorded through the use of tally energy and tally time cards, the numbers of which correspond to the type of tally:

F8:h (1)
E8: $e_1 \ldots e_k$
T8: $t_1 \ldots t_k$
FT8: GEB *a b c*

The energy and time bins are specified by their upper bounds in *MeV* and *shakes*, respectively. To account for a detector's resolution, the E_D of an individual event in the detector's volume can be broadened by sampling from a Gaussian distribution by defining the detector's FWHM as a function of incident particle energy, E [*MeV*]:

$$FWHM = a + b\sqrt{E + cE^2} \tag{2-26}$$

Where *a*, *b*, and *c* are constants defined by the user in units of *MeV*, $MeV^{1/2}$, and MeV^{-1}, respectively. This broadening is facilitated by the insertion of a FT (tally modifier card) with the Gaussian Energy Broadening (GEB) specification.

When *N* histories are completed, the mean score of a tally, $\bar{x}$ is determined as:

$$\bar{x} = \frac{1}{N}\sum_{i=1}^{N} x_i \tag{2-27}$$

Where x_i is the value of an individual history's contribution to that tally. The estimated variance on $\bar{x}$, $S_{\bar{x}}$ is determined by the estimated standard deviation of the population of *x* based on those values actually sampled, x_i:

$$S^2 = \frac{\sum_{i=1}^{N}(x_i - \bar{x})^2}{N-1} \tag{2-28}$$

$$S_{\bar{x}}^2 = \frac{S^2}{N} \tag{2-29}$$

Eq. 2-29 depicts that the value of $S_{\bar{x}}$ decreases with $1/\sqrt{N}$ indicating that to decrease the estimated variance by a factor of two the number of histories run must increase by a factor of four. This drawback of Monte Carlo simulations can be reduced through the use of variance reduction and parallel computing.

2.6.4 **Delayed Neutron and Photon Emission Simulations**

Production of delayed particles in MCNP6 (Goorley *et al*., 2012) is facilitated through the use of the Activation Control (ACT) card. This card contains several options for the production of delayed neutron and gamma emissions from fission and non-fission events (Durkee *et al*., 2012).

This thesis examined in detail two MCNP6 options for DN production: library and model. The library option uses ACE (A Compact ENDF) data and sorts the emissions into six time groups. This method of production is only available for delayed neutron production. If delayed gammas are simulated, it must be completed using the model option, which is available for both delayed neutron and gamma production. The model option is more complex, and uses a sub-routine, CINDER'90 (Wilson *et al*., 1995), to simulate the production of fission and activation products. If a fission or activation event occurs, the residual nuclides produced are determined for individual events. In the case of thermal fission, the fission product yield curve is sampled for DN and DG production. Once a nuclide is selected, its identity is sent into the CINDER'90 transmutation code, which generates the decay data for all of its daughter products. Delayed neutron emissions are then determined using *cinder.dat* which was created with ENDF/B-VI data (released in 1990). DN emission energies are determined by pre-integrated emissions probabilities for each of the 271 DN precursors (delay_library_v3.dat). This process is slower than the use of the library option however, should result in more accurate simulations.

Up to ten DNs can be produced during an interaction (only for fixed source simulations) through use of the DNBIAS option. This feature is incredibly useful when simulating low rates of DN emissions, as it increases the number of histories contributing to relevant tallies, N, in turn lowering the estimated variance, Eq. 2-29.

Delayed gamma emissions require the use of the CINDER'90 transmutation code to calculate the residual nuclide's decay products. As with the DN=model option, the total number of DGs produced is calculated using atom densities, decay constants, and emission probabilities. Finally, cumulative distribution functions are sampled to determine the yield, energy, time, and direction of the DGs produced. There are two options available to calculate the DG CDFs, DG=multigroup (MG) and DG=lines. Multigroup is the fastest option for DG simulations as it samples emissions from 25 energy bins for 3400 radionuclides (in *cinder.dat*). Although convergence is considerably more rapid than the line emission option, it lacks detail and cannot reproduce results with high fidelity, Figure 2.6 (top).

An identical simulation using the line emission option is also shown in Figure 2.6 (bottom), it reads the data file *cindergl.dat*, which contains gamma line branching ratios for 979 isotopes. Conveniently, these 979 isotopes were selected to correspond to those common in the thermal fission of ^{235}U and ^{239}Pu. The line emission data was obtained from LANL's Nuclear Information Service, which was extracted from ENDF/B-VI evaluations. There have been recent efforts to update the data contained within *cinder.dat* and *cindergl.dat* to reflect the more recent ENDFVII data (Wilcox *et al*.), however this has not yet been implemented into production releases of MCNP6. As with neutrons, the gamma emissions are sampled from a histogram time bin structure shown in Figure 2.7[vi]. MCNP6.1.1β, released in September 2014, contains a more refined time bin structure for delayed particle emissions, Figure 2.7, its effect on DNGC system simulations are discussed in this work.

[vi] Figure 2.7 was provided by M. James at LANL.

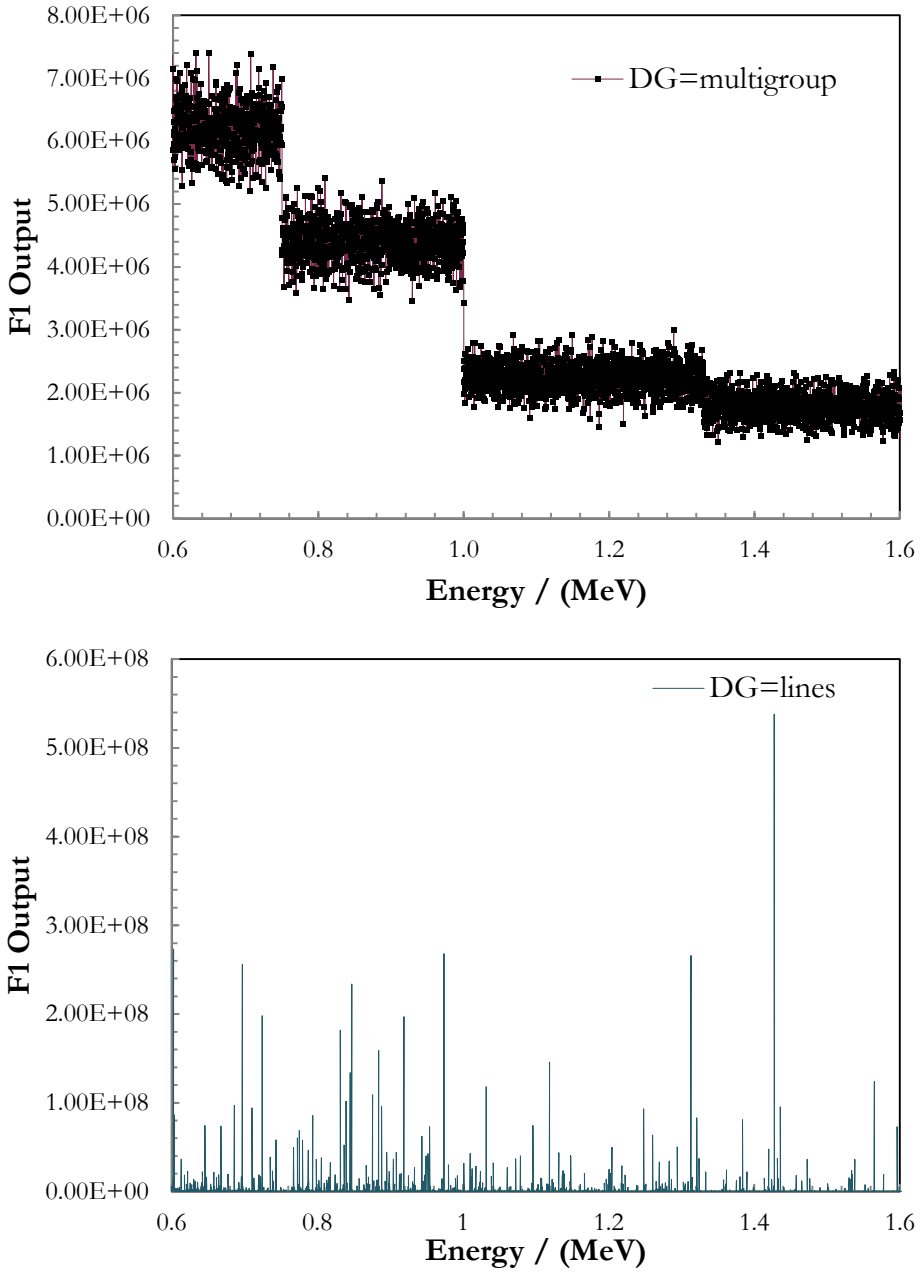

Figure 2.6: A comparison of the simulation of a photon emissions from irradiated LEU using the DG=multigroup (top) and DG=lines (bottom) options.

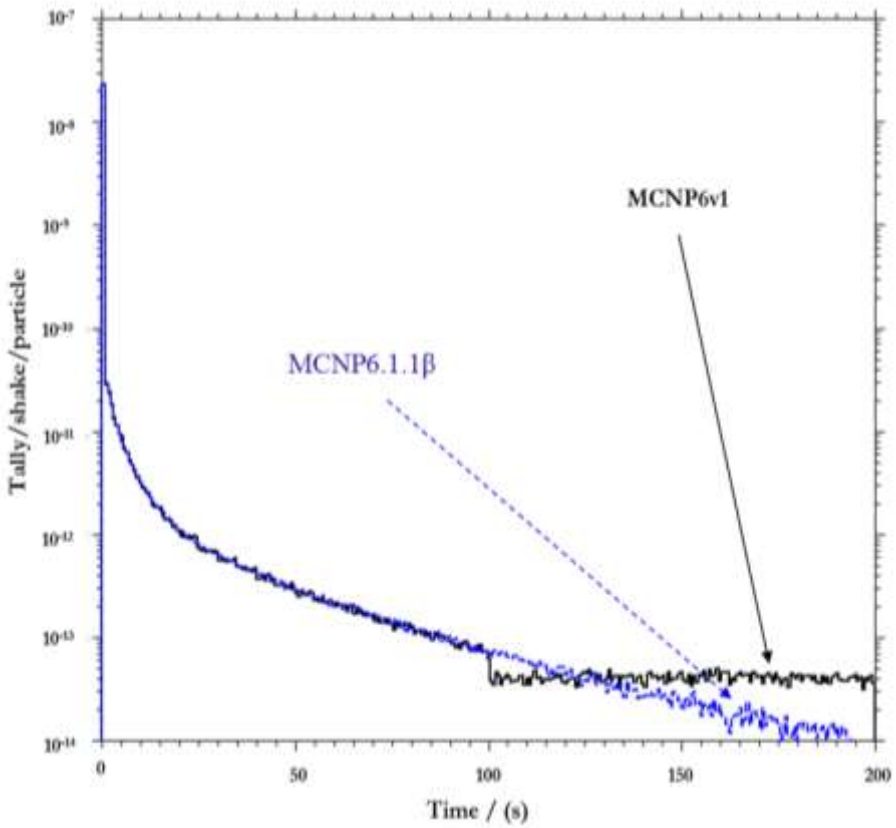

Figure 2.7: Time bin structure differences in MCNP6v1 and MCNP6.1.1β for delayed particle emissions.

2.7 Nuclear Facilities at the Royal Military College of Canada

2.7.1 The SLOWPOKE-2 Reactor

The source of neutron interrogation used in this work is a Safe LOW POwer K(c)ritical Experiment (SLOWPOKE)-2 reactor (Hilborn and Townes, 1987), a 20 *kW* thermal research reactor with nine irradiation sites. The core of the SLOWPOKE-2 reactor, shown in Figure 2.8 has 198 zircaloy fuel pins containing uranium-dioxide (19.89 *wt* % ^{235}U), submerged below 4.4 *m* of water (Pierre, 1996). Five inner irradiation sites are contained within the beryllium reflector of

the SLOWPOKE-2 where samples are exposed to a predominately thermal neutron flux, with a thermal to fast flux ratio of 4.0 ± 0.1. Four outer irradiation sites are just outside the reflector, where an even higher thermal to fast neutron flux of 17.3 ± 0.5 is present (Kennedy *et al*., 2000). Samples can be sent via pneumatic tubing to the individual sites for variable irradiation periods. Atomic Energy of Canada Limited (AECL) designed and installed this low enriched uranium (LEU) SLOWPOKE-2 in 1985. AECL has recently created a MCNP simulation of a LEU SLOWPOKE-2 (Nguyen *et al*., 2012), this file was used in this work to obtain a high fidelity simulation of the neutron flux energy distribution inside irradiation sites.

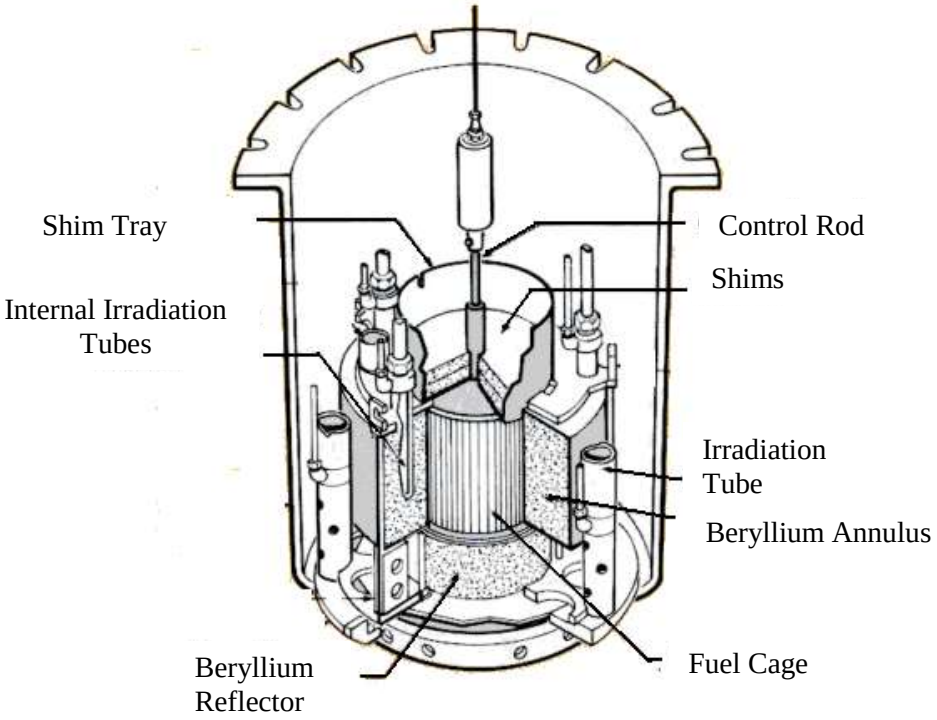

Figure 2.8: The SLOWPOKE-2 Reactor Schematic (Pierre, 1996).

Chapter 3

An Automated Delayed Neutron Counting System for Mass Determinations of Special Nuclear Materials

M.T. Sellers, D.G. Kelly, & E.C. Corcoran

Department of Chemistry and Chemical Engineering,
SLOWPOKE-2 Facility and Analytical Science Group,
Royal Military College of Canada
PO Box 17000 Stn Forces, Kingston, Ontario K7K 7B4, Canada[vii]

[vii] **M.T. Sellers**, D.G. Kelly, E.C. Corcoran, "An automated delayed neutron counting system for mass determinations of special nuclear materials" *Journal of Radioanalytical and Nuclear Chemistry* **291** *2* (2012) pp. 281-285.

3.1 Abstract

An automated delayed neutron counting (DNC) system has been developed at the Royal Military College of Canada (RMCC) to enhance nuclear forensics capabilities pertaining to special nuclear material analysis. The system utilises the SLOWPOKE-2 Facility at RMCC as a neutron source and ^{3}He detectors. System control and data acquisition occur through a LabVIEW platform. The time dependent count rate of the delayed neutron production has been examined for ^{235}U, using certified reference materials. Experimental validation according to ISO 17025 protocols suggests typical errors and precision of 3.6 *%* and 3.1 *%*, respectively, and a detection limit of 0.26 μg ^{235}U.

Keywords: Delayed neutron counting, nuclear forensics

3.2 Introduction

The past decade has seen an increased awareness of global terrorism and the asymmetric nature of many terrorist threats. The contribution of radioactive materials, and particularly fissile special nuclear materials (SNMs) such as ^{233}U, ^{235}U, and ^{239}Pu, to such threats has been widely recognised. Recent exercises (Larsson and Haslip, 2004; Larsson and Hinton, 2006) have highlighted the need for Canada to establish nuclear forensics protocols and analytical procedures to aid in first response, post-event recovery, criminal prosecution and other law enforcement requirements. Whilst the use of SNMs in a fissile device constitutes their primary terrorist risk, the ability of SNMs to undergo fission can also be employed analytically. Upon interaction with thermal neutrons SNMs will immediately release prompt neutrons and fission fragments. Some fission fragments undergo β^- decay and produce delayed neutrons with half-lives of <1 *s* to *ca.* 1 *min* (Keepin *et al*., 1957; Nichols *et al*., 2008). These delayed neutrons can be described by eight distinct groups with well tabulated half lives and production ratios (Nichols *et al*., 2008). The number of detected neutrons can be used for the quantitative determination of fissile mass content in a calibrated system (Li *et al*., 2004).

Delayed neutron counting (DNC) lends itself to nuclear forensics and is complementary to other analytical techniques, such as inductively coupled plasma-mass spectrometry, high resolution gamma–ray spectrometry and alpha spectrometry. DNC is a non-destructive rapid technique, capable of analyzing fissile samples over a large range of concentrations (Papadopoulos and Tsagas, 1994). Irradiation of calibration standards and unknowns containing ^{235}U, ^{233}U or ^{239}Pu by a neutron source and the subsequent detection of delayed neutrons facilitates the determination of fissile mass. Cumulative delayed neutron counts are

sufficient to determine the fissile content of a single known fissile isotope. However, the assumption of one fissile isotope is unattractive in the context of nuclear forensics, and recent work (Li *et al*., 2004) has shown that the time dependent delayed neutron count may be used to determine the concurrent fissile content of two SNM isotopes.

The present work describes two aspects of the development of an automated DNC system at the Royal Military College of Canada (RMC) *viz.*; (i) the *hardware/software* associated with the implemented system and its functionality are examined, and (ii) steps associated with system *validation* for the analysis of ^{235}U, such as efficiency, linearity, reproducibility, robustness (orientation and geometry), accuracy and precision are also described. The latter are consistent with the ISO 17025 standard 'General Requirements for the Competence of Calibration and Testing Laboratories' (ISO, 2005). The DNC system is intended to complement existing radioanalytical techniques available at RMCC and to contribute to Canadian nuclear forensic capabilities.

3.3 Experimental

3.3.1 Hardware/Software.

The DNC system hardware consists of a sample loader, irradiation site, neutron counter and disposal site. Loading is achieved manually via a feed tube. The design currently allows up to eight samples to be placed in the loading chamber; although in its final form a much larger capacity will be desirable. Irradiations occur at an inner site of the SLOWPOKE-2 Facility, RMCC at an operational thermal neutron flux of 5.5×10^{11} $cm^{-2}s^{-1}$ (± 5%) at half power (10kW) (Andrews, 1989). Detection utilises six ^{3}He proportional counters (RS-P4-0406-212, GE Energy, Twinsburg, OH) spaced at the corners of a regular hexagon. Paraffin wax in cylindrical form surrounds detectors, with a central void space for sample analysis. Spacing between detector centres and the void centre is 8.0 ± 0.2 *cm*. Detectors are connected in parallel to a preamplifier (ORTEC 142, Oak Ridge, TN), voltage supply (ORTEC 556), amplifier (ORTEC 575A) and a multichannel buffer (ORTEC 919E). Samples are sent to a padded disposal bin located 5 *m* from the detectors. Transfer between sites is accomplished via polyethylene tubing and is driven by a pneumatic system using dry compressed air. Bimba (University Park, IL) pistons were used to make a custom loader and diverter which are controlled by Norgren pneumatic valves (Littleton, CO).

The hardware is controlled by a LabVIEW (Version 2009, National Instruments, Austin, TX) control and data acquisition executable. The in-house code controls pneumatic valves and is capable of user-defined control of experimental parameters, such as irradiation/decay/count time, analysis repetition or cycling, and the delay time between each repetition or cycle. A data acquisition device (USB 6525, National Instruments) provides input/output signals to the mechanical valves. Output of the LabVIEW executable is a MS Excel^{TM} file which can be analyzed by a fissile analysis code written in MATLAB (R2008b, Mathworks, Natick, MA). The code is capable of data corrections for the time dependent background, detector and MCB dead-time and detector arrangement efficiency. Corrected counts may be output or referenced to count per microgram ^{235}U obtained from an eight point detector calibration. The latter ratios sample to calibration response in 1 *s* increments to obtain a fissile mass. These time-segmented data are used to obtain a mean fissile mass and uncertainty.

3.3.2 **Validation.**

Consumable items were sourced as follows; natural uranium (CRM 4321C, NIST, Gaithersburg, MD), depleted uranium (CRM U005A 0.5064 ± 0.0003 atom *%* ^{235}U, New Brunswick Laboratory, Argonne, IL), Optima nitric acid and sucrose (Optima, ThermoFisher Scientific, Ottawa, ON), 1.5 and 7.0 *ml* polyethylene vials (LA Packaging, Yorba Linda, CA). De-ionised ultra filtered water was prepared in-house (E-pure, Barnstead, Dubuque, IA). A NIST-traceable multi-element radionuclide source (37 *kBq*) containing ^{210}Pb, ^{241}Am, ^{109}Cd, ^{57}Co, ^{139}Ce, ^{203}Hg, ^{113}Sn, ^{85}Sr, ^{137}Cs, ^{88}Y, ^{60}Co, and ^{88}Y was obtained from Eckert and Ziegler (Valencia, CA). A 7.32 ppm ^{235}U calibration stock was prepared from solution 4321C by dilution with 2 % nitric acid (Kelly *et al*., 2008). The CRM U005A control sample was digested in *aqua regia* and diluted with 2 *%* nitric acid to a 5.34 *ppm* stock solution. Further dilutions of both solutions were performed in the same medium. Samples of 1 *ml* nominal volume, unless specified, were heat sealed in polyethylene vials prior to analysis. Vials were contained in secondary 7.0 *ml* vials during irradiation and analysis.

3.4 Results & Discussion

3.4.1 **Hardware/Software.**

The basic functionality of the DNC system consists of the sequential selection of samples from a loader, followed by irradiation, subsequent delayed neutron counting and finally disposal. Each transfer is achieved using a pneumatic transfer

system. Residence times in each location are user defined and controlled using a graphical user interface, Figure 3.1. Additional capacities to re-analyse repeatedly a single sample, after appropriate delay (cycle), or to re-analyse sequentially a complete series of samples (repetition) are incorporated into the system. Furthermore, a troubleshooting mode, which allows the manual activation of individual valves, is available. Extensive studies were performed using sucrose-filled vials to confirm system integrity with respect to the reliability of automated control and data collection. The physical robustness of sample vials to withstand at least eight cycles or repetitions through the pneumatic system was confirmed.

Trials using calibration solutions of ^{235}U content between 1.5 and 7.3 μg were conducted as a function of neutron flux, irradiation time, decay time, count time and number of operational detectors. The counting rate was used to determine that the operational dependence on these parameters. Such trials suggested typical irradiation and post-irradiation decay times of 60 *s* and 25 *s* respectively, with the SLOWPOKE-2 operating at half power. These times negate the uncertainties associated with irradiation time and decay time. Also minimised is the possible interference from the fast neutron interaction $^{17}O(n,p)^{17}N$, which produces delayed neutrons with a half life of 4.174 *s* (Amiel and Peisach, 1963). Analyses of samples of mass > 10 μg ^{235}U could be conducted by a combination of reduced neutron flux, reduced sample size, increased decay time and the operation of fewer detectors.

3.4.2 **Validation.**

Initial experiments were conducted to examine the neutron selectivity of detection and background response of the sample container and matrix. Other institutions with DNC systems have incorporated lead shielding into their systems to reduce gamma-ray background (Li *et al*., 2004). Our experiments using a 37 *kBq* multiple radionuclide gamma-ray spectrometry source (46-1836 *keV*) in direct contact with a ^{3}He detector afforded counts that could not be distinguish from the background obtained in the absence of the source, 4.7 $\pm$ 0.3 and 4.9 $\pm$ 0.5 counts per second respectively. Multiple analyses of empty polyethylene vials, and vials containing 2 *%* nitric acid solution or sucrose displayed a small time-dependent background response in each case. This background has been determined to be independent of total mass of polyethylene and is isolated to the specific site used for DNC irradiations. Whilst, analyses have not been conducted to determine the presence of uranium, the time dependence associated with background response is consistent with the theoretical behaviour of ^{235}U. The general profile of the latter may be expressed as equation (3-1) based on eight delayed neutron forming groups:

$$S(t)_j = \frac{v_j N_A \sigma_{f\,j} \Phi m_j}{MM_j} \sum_{i=1}^{k} \beta_i \left(1 - e^{-\lambda_i t_{irr}}\right)\left(e^{-\lambda_i t_c}\right)\left(e^{-\lambda_i t_d}\right) \qquad 3\text{-}1$$

where ν_j is the average number of delayed neutrons emitted per fission, σ_{fj} is the fission cross section [b], Φ is neutron flux [$cm^{-2}s^{-1}$], N_A is Avogadro's number [mol^{-1}], MM_j is the atomic mass number [$g\ mol^{-1}$], k is the total number of delayed neutron groups, β_{ij} is the fraction of total delayed neutrons for group i, λ_i is the decay constant for group i [s^{-1}], t_{irr} is the irradiation time [s], t_d is the decay time [s], t_c is the time post decay [s], and m_j is the fissile mass [g].

The relationship between, $S(t)_j$, and total recorded counts, $C(t)_j$, may expressed by considering a background contribution and sample fissile dependent terms, equation (3-2);

$$C(t)_j = \varepsilon \cdot S(t)_j + B(t) \qquad 3\text{-}2$$

Where $B(t)$ is the time dependent background correction, [s^{-1}], and ε is the detector arrangement efficiency. The $B(t)$ was determined by an empirical fit to experimental data obtained from the irradiation of eight blank vials. Figure 3.2, is a plot of the recorded counts as a function of time.

Equation (3-3) is the numerical fit obtained from Figure 3.2 using a standard R^2 regression analysis. The cited uncertainty range for equation (3-3) was obtained for the 95% confidence interval.

$$C(t)_j = (114 \pm 8)e^{(-(0.19\pm0.02)t)} + (98 \pm 9)e^{(-(0.032\pm0.004)t)} \qquad 3\text{-}3$$

The theoretical relationship between delayed neutron counts and time can be obtained from equations (3-1) and (3-2) for given experimental conditions and fissile mass, assuming the efficiency term (ε) is unity and the absence of detector dead-time. In practice the size, number and location of detectors, as well as their inherent efficiency and dead-time, reduce this value. In the present work, the dead time was determined by the two source method (Knoll, 2010) and the efficiency by comparing the experimental count rates for eight samples ranging from 0.1 to 0.5 μg of ^{235}U to models using equations (3-1) and (3-2). Small amounts of ^{235}U were used for efficiency calculations as dead time effects are negligible at these low count rates. Data fitting determined an efficiency of 0.29 ± 0.03. No correlation was observed between either parameter and the mass of fissile material.

Figure 3.1: Delayed Neutron Counting System Graphic User Interface enables the selection of experimental parameters including irradiation, decay, count time, and number of cycles. Also includes a troubleshooting mode..

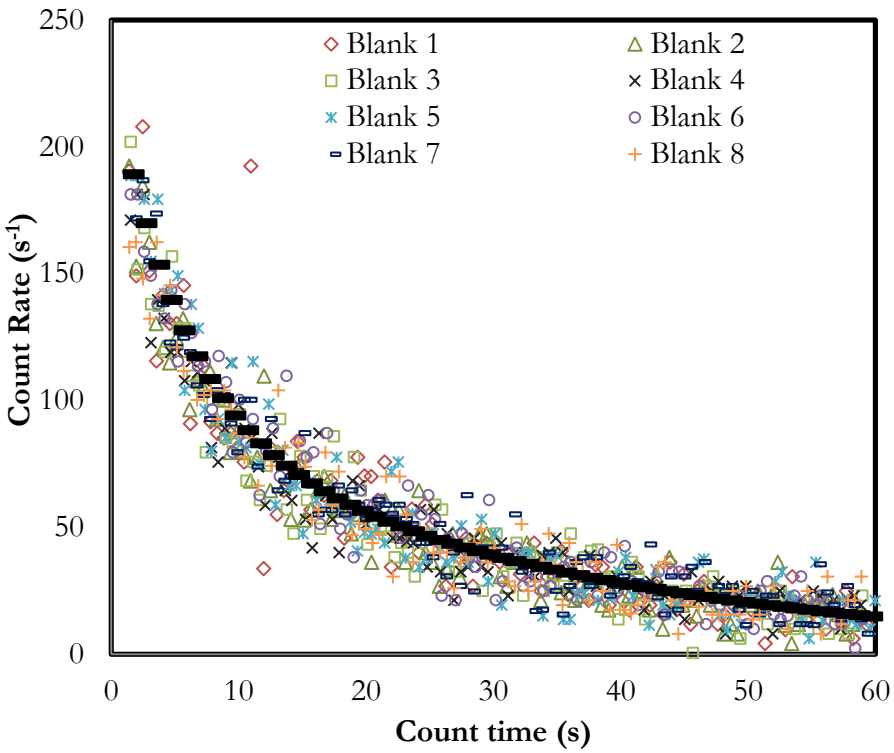

Figure 3.2: Numerical Fit to Experimental Background from Vial irradiation, B(t) Data.

Using the parameters described, eight calibration sets (each containing eight samples with ^{235}U content over a range of 1.5 to 7.5 μg) were prepared by independent dilution of the stock solution and analyzed over a period of several weeks. The relationship between the experimental fissile mass output was plotted against actual mass of ^{235}U. The slope and intercept of each calibration is presented in Table 3.1. Each calibration slope is close to unity with a zero intercept. Thus, linearity and stability are confirmed. The determination of accuracy, precision, linearity and detection limit to the ISO 17025 standard require analysis of samples obtained from a distinct source material. In the present work eight replicate samples were prepared and analysed of fissile mass 5.5-5.6 μg using depleted uranium CRM 005A, Table 3.2. The mean accuracy (% relative error), precision (based on student t-weight 95% confidence) and detection limit (based on student t-weight 95% confidence) were -3.6 %, 3.1 % and 0.26 μg, respectively. Relative errors were consistent for a further eight samples with ^{235}U masses of 1.56-5.6 μg, Table 3.2. Linearity of analysis was confirmed for these analyses by a plot of

experimental fissile mass versus expected mass that yielded a slope, intercept and R^2 value of 0.9406, 0.1246 and 0.9975, respectively.

The robustness of the analytical system, *i.e.*, its sensitivity to small changes in size, geometry or location within the detector are an important feature of nuclear forensic analyses in which such parameters may be driven by field sampling rather than laboratory requirements. Two series of experiments were conducted in which sample location in the detector was modified in a controlled manner, and in which small volume (and therefore size and geometry) were varied for a constant mass of fissile ^{235}U, Table 3.2. The former experiments utilized the standard practice of encapsulating pairs of 1.5 *ml* vials within an outer 7 *ml* vial. Habitual practice dictates the use of the lower vial for analysis. In this study, duplicate analysed were conducted with samples contained in lower and upper locations. Data, obtained from 4.4 μg ^{235}U, CRM 4321C samples failed to detect statistical difference between the two locations. Seven samples of mass ranging from 1.48 – 1.60 μg ^{235}U were also analysed in total sample volume ranging from 0.30 *ml* to 0.94 *mL*. The change in total sample volume shown for samples 17 – 23 in Table 3.2 did not effect the relative error of the DNC ^{235}U mass determination.

Table 3.1: Repetitive ^{235}U calibration using NIST 4321C, slope and intercept with 95 % confidence uncertainties.

Set	**Slope**	**Intercept / [μg]**
A	1.0 ± 0.1	-0.1 ± 0.4
B	1.02 ± 0.04	-0.1 ± 0.2
C	1.014 ± 0.008	0.00 ± 0.04
D	0.97 ± 0.04	0.2 ± 0.2
E	0.99 ± 0.02	0.06 ± 0.08
F	1.01± 0.02	-0.08 ± 0.08
G	1.01 ± 0.01	-0.02 ± 0.04
H	1.008 ± 0.008	-0.03 ± 0.04

Table 3.2: Validation data, accuracy, precision, detection limit, linearity and robustness using CRM005A with 95 % confidence uncertainties.

Sample	Total Volume / [mL]	Mass ^{235}U / [μg]		Relative Error / [%]
		Expected	Experimental	
1	1.03 ± 0.01	5.5 ± 0.2	5.3 ± 0.1	-3.1
2	1.04 ± 0.01	5.6 ± 0.2	5.4 ± 0.1	-3.5
3	1.03 ± 0.01	5.5 ± 0.2	5.4 ± 0.1	-2.5
4	1.04 ± 0.01	5.6 ± 0.2	5.3 ± 0.1	-4.1
5	1.03 ± 0.01	5.5 ± 0.2	5.4 ± 0.1	-2.8
6	1.05 ± 0.01	5.6 ± 0.2	5.4 ± 0.1	-3.8
7	1.05 ± 0.01	5.6 ± 0.2	5.4 ± 0.1	-3.2
8	1.03 ± 0.01	5.5 ± 0.2	5.4 ± 0.1	-2.1
9	1.04 ± 0.01	5.5 ± 0.2	5.3 ± 0.1	-4.6
10	1.25 ± 0.01	4.9 ± 0.1	4.8 ± 0.1	-1.7
11	1.21 ± 0.01	4.3 ± 0.1	4.2 ± 0.1	-4.0
12	1.23 ± 0.01	3.7 ± 0.1	3.6 ± 0.1	-2.3
13	0.97 ± 0.01	3.1 ± 0.1	3.1 ± 0.1	-2.4
14	0.93 ± 0.01	2.49 ± 0.08	2.6 ± 0.1	3.2
15	0.96 ± 0.01	2.13 ± 0.06	2.1 ± 0.1	-1.3
16	0.94 ± 0.01	1.54 ± 0.04	1.5 ± 0.1	-2.6
17	0.29 ± 0.01	1.56 ± 0.04	1.5 ± 0.1	-3.2
18	0.38 ± 0.01	1.56 ± 0.04	1.5 ± 0.1	-3.2
19	0.57 ± 0.01	1.56 ± 0.04	1.5 ± 0.1	-2.6
20	0.66 ± 0.01	1.56 ± 0.04	1.6 ± 0.1	-0.6
21	0.81 ± 0.01	1.54 ± 0.04	1.5 ± 0.1	-3.9
22	0.74 ± 0.01	1.48 ± 0.04	1.5 ± 0.1	-1.4
23	0.94 ± 0.01	1.60 ± 0.04	1.5 ± 0.1	-3.8

3.5 Conclusions

A DNC system had been established at RMCC to enhance nuclear forensic analysis capabilties. The system, which uses the neutron flux of the SLOWPOKE-2 Facility at RMC, includes automated hardware control and sample analysis, as well as automated data collection. The LabVIEW software platform exports data which is read by a MATLAB programme. The latter utilizes a time dependent background correction to report a ^{235}U fissile mass based on segmented time dependent analysis. The system has been validated using certified reference materials in a manner that is consistent with ISO 17025 accreditation. The accuracy, precision and detection limit of analysis complement those of existing techniques, whilst the rapid non-destructive analysis offer distinct benefits to the nulcear forensic capability. It is intended that the time dependent DNC analysis will be extended to ^{233}U and ^{239}Pu using certified reference materials. The capability of the system to

distinguish these fissile isotopes from ^{235}U will established and capacity and limitations of mixed fissile isotope analysis will be explored.

3.6 Acknowledgements

Financial support has been provided by the Director General of Nuclear Safety, the Analytical Sciences Group and the SLOWPOKE-2 Facility at the Royal Military College of Canada. The authors would like to thank Dave Ferguson, John Shaw, Matthew Mackay, Kathy Nielsen and Kristine Mattson for their assistance.

-This page is intentionally left blank-

Chapter 4

The Analysis and Attribution of the Time-Dependent Neutron Background Resultant from Sample Irradiation in a SLOWPOKE-2 Reactor

M.T. Sellers, E.C. Corcoran, D.G. Kelly

Department of Chemistry & Chemical Engineering,
SLOWPOKE-2 Facility, Royal Military College of Canada,
PO Box 17000 Stn Forces, Kingston, Canada[viii]

[viii] **M.T. Sellers**, E.C. Corcoran, D.G. Kelly, "The analysis and attribution of the time-dependent neutron background resultant from sample irradiation in a SLOWPOKE-2 reactor" *Journal of Radioanalytical and Nuclear Chemistry* **295** *2* (2013) pp. 1221-1228.

4.1 Abstract

The Royal Military College of Canada (RMCC) has commissioned a Delayed Neutron Counting (DNC) system for the analysis of the special nuclear materials. A significant, time-dependent neutron background with an initial maximum count rate, more than 50 times that of the time-independent background, was characterised during the validation of this system. This time-dependent background was found to be dependent on the presence of the polyethylene (PE) vials used to transport the fissile samples, yet was not an activation product of vial impurities. The magnitude of the time-dependent background was found to be irradiation site specific and independent of the mass of PE mass. The capability of RMCC's DNC system to analyze the neutron count rates in time intervals < 1 *s* facilitated a more detailed data analysis than that obtained in previous DNC systems recording cumulative neutron counts. An analysis of the time-dependent background behaviour suggested that an equivalent of 120 *ng* of ^{235}U contamination was present on each irradiated vial. However, Inductively Coupled Plasma – Mass Spectroscopy measurements of material leached from the outer vial surfaces after their irradiations found only trace amounts of uranium, 0.118 ± 0.048 *ng* of ^{235}U derived from natural uranium. These quantities are insufficient to account for the time-dependent background, and in fact could not be discriminated from the noise associated with time-independent background. It is suggested that delayed neutron emitters are deposited in the vial surface following fission recoil, leaving the main body of uranium within the irradiation site. This hypothesis is supported by the physical cleaning of the site with materials soaked in distilled water and HNO_3, which lowered the background from a nominal ^{235}U mass equivalent of 120 *ng* to 50 *ng* per vial.

Keywords: delayed neutron counting, neutron background attribution, uranium, nuclear forensics

4.2 Introduction

Delayed Neutron Counting (DNC) is an efficient and non-destructive analytical technique which, for several decades, has found primary applications in the determination of natural uranium content in geological samples through the assay of ^{235}U (Benzing *et al*., 2000; Duke *et al*., 2000; Musilek *et al*., 1996) and the analysis of fissile materials. In the former application, DNC complements a number of alternative analytical techniques. Whilst these techniques do not require access to a neutron flux, destructive digestion methods are required. In contrast, DNC represents a technique that is capable of the non-destructive analysis of uranium in environmental and other complex matrices with little modification for

the specific matrix of interest. Typically, acceptable data can be obtained for natural uranium determinations using the cumulative delayed neutron counts recorded for durations $\geq$ 60 *s* (Minor *et al*., 1982; Moon *et al*., 2009; Rosenberg *et al*., 1977). The facility to detect synthetic fissile isotopes, including ^{233}U and ^{239}Pu, by DNC is of considerable relevance to the nuclear forensics community. The recent international focus on nuclear forensic analysis and the attribution of special nuclear materials (SNM) through DNC does however require sophisticated instrumentation that is capable of discerning and discriminating isotopic signatures through the assay of delayed neutron temporal behaviour (Li *et al*., 2004). A renewed focus on environmental uranium and uranium extraction, as well as developments in SNM detection have led to the development of new DNC systems using research reactors and accelerators (Ni *et al*., 2012; Rosenberg *et al*., 1977).

The Royal Military College of Canada (RMCC) has recently developed a DNC system (Sellers *et al*., 2012a) for the analysis of the SNM isotopes ^{233}U, ^{235}U and ^{239}Pu. This DNC system records the count rate of the delayed neutrons produced by the thermal neutron induced fission of SNM in 0.5 *s* intervals. Analysis of the temporal behaviour of these neutrons facilitates the characterization of the fissile isotopes present in each sample. During this development process a background contribution has been observed in the time-dependent DNC response. Other workers have observed background responses from DNC systems and a detailed examination of potential sources has been reported (Benzing *et al*., 2000). The present paper discusses the analysis of the neutron background contribution observed during the commissioning of the DNC system at RMCC. The contributions of time dependent and independent background are considered, and the relationship between these data and contamination sources is examined.

4.3 Theory

When SNM isotopes undergo fission they release prompt neutrons and fission products. Some of these fission products will undergo β^- decay and emit delayed neutrons with half-lives ranging from less than a second to almost a minute after the fission process (Keepin *et al*., 1957). The many delayed neutron precursors are often organized by the half-life of their delayed neutron emission into eight groups, each with an associated production ratio (Nichols *et al*., 2008). The eight groups for each fissile isotope (^{233}U, ^{235}U and ^{239}Pu) may have the same half-life, however the production ratio of each group of isotope *j*, β_{ij}, will vary due to differences in the fission product yields of each SNM. The delayed neutron emission rate, *S(t)* [s^{-1}], for a fissile isotope, *j*, is described by Eq. 4-1 below:

$$S(t)_j = \frac{v_j N_A \sigma_{f\,j} \Phi m_j}{MM_j} \sum_{i=1}^{k} \beta_i \left(1 - e^{-\lambda_i t_{irr}}\right)\left(e^{-\lambda_i t_c}\right)\left(e^{-\lambda_i t_d}\right) \quad 4\text{-}1$$

Where m_j is the mass of the fissile isotope [g], v_j is the number of neutrons released in the thermal neutron induced fission of isotope j, N_A is Avogadro's number [mol^{-1}], ϕ is the thermal neutron flux [$cm^{-2}s^{-1}$], σ_{fj} is the thermal neutron fission cross section of isotope j [b], MM_j is the molar mass of isotope j [$g\ mol^{-1}$], λ_i is the decay constant for group i [s^{-1}], t_{irr} is the irradiation time [s], t_d is the decay time [s], and t_c is the counting time, which commences immediately after decay time [s].

The total count rate, $C(t)$ [s^{-1}], recorded by the DNC system will be a summation of both a time-independent background, A_B [s^{-1}], and time-dependent background, $B(t)$ [s^{-1}], ε is the neutron detection efficiency of the system, and the delayed neutron production from the fissile isotope j, $S(t)_j$ [s^{-1}], as shown in Eq. (4-2).

$$C(t)_j = \varepsilon \cdot S(t)_j + B(t) + A_B \quad 4\text{-}2$$

Differences between the production ratios of each group for fissile isotopes, β_{ij}, are small. Thus, the successful attribution of SNM through the analysis of the delayed neutron temporal behaviour requires the analysis, attribution and minimization of background contributions as these can distort the time-dependent behaviour of the recorded data. Moreover, appropriate numerical correction of both backgrounds, A_B and $B(t)$ is essential to the application of the overall delayed neutron count rate.

4.4 Experimental

4.4.1 Delayed Neutron Counting

The process of sample preparation and operation of the DNC system have been discussed in detail elsewhere (Sellers *et al*., 2012a). In brief, samples for DNC analysis are heat sealed in 1.5 *ml* polyethylene (PE) vials (LA Packaging, Yorba Linda, CA). To provide secondary containment, the 1.5 *ml* vials are subsequently encapsulated into larger, 7.0 *mL*, PE vials. To minimise internal void space within this secondary container, a second 1.5 *ml* vial is normally also enclosed within this container. Uranium samples were prepared from natural uranium (CRM 4321C, NIST, Gaithersburg, MD) dissolved in dilute nitric acid (Optima, ThermoFisher

Scientific, Ottawa, ON). Depleted uranium (CRM U005A 0.5064 ± 0.0003 atom % ^{235}U, and U0002 0.01755 ± 0.0005 atom % ^{235}U) was obtained from New Brunswick Laboratory, Argonne, IL. The DNC system uses the Facility's SLOWPOKE-2 Reactor (which has a 19.89 % enriched uranium core) as a source of neutron flux. Samples are sent via pneumatic tubing into the an irradiation site where they are exposed to a predominately thermal neutron flux ranging from 10^{11} to 10^{12} cm^{-2} s^{-1} for a pre-designated time period of (1 – 600) *s*. A 3 *s* delay time in the system allows the sample time to travel from the irradiation site to the neutron counting arrangement and is accounted for in Eq. 4-1 by setting t_d = 3 *s*. The neutron counter consists of an array of six ^{3}He detectors embedded in a paraffin moderator. The system records the neutrons detected by the counting apparatus time intervals as small as 0.5 *s*.

4.4.2 Uranium Analysis by Microwave Leaching/Inductively Coupled Plasma - Mass Spectrometry (ICP-MS)

Optima concentrated nitric acid and distilled deionised water (18 MΩ) were used to prepare 2 % nitric acid solutions. Selected PE vials were initially swiped using a glass fibre filter paper (Whatman 934AH, Fisher Scientific, Ottawa, ON, Canada) dampened with 2 % nitric acid. Swipes were made over base and cylindrical sections. This swipe was transferred to an ICP-MS autosampler tube containing 10 *ml* of the same solution and allowed to stand for 5 *min*, after which the acid solution was decanted for analysis. Irrespective of the use of swiping, the exterior surfaces of the polyethylene vials were leached with 2 % nitric acid, 80 ^{o}C for a period of 3 *h*. A MARS 5 Xpress microwave system (CEM Corporation, Matthews, NC) was used for leaching. The dimensions of microwave vessels and PE vials were such that 3 *ml* of 2 % nitric acid was sufficient to leach the base and cylindrical vial surfaces. Telfon plugs were used to keep PE vials immersed in the leachate solution. Leachate solutions made up to 10 *ml* with further 2 % nitric acid prior to ICP-MS analysis. Control samples were prepared by spiking depleted uranium (CRM U005A 0.5064 ± 0.0003 atom % ^{235}U, New Brunswick Laboratory, Argonne, IL, USA) directly into the leachate of an experiment using an unirradiated vial, and by allowing a similar spike to dry on a vial surface prior to leaching. ICP-MS was performed using an ELAN DRC II quadrupole ICP-MS (Perkin-Elmer, Concord, ON, Canada). The instrument was fitted with a perfluoroalkoxy (PFA) cyclonic spray chamber (ESI, Omaha, NE, USA). Uranium determinations were made monitoring m/z = 235 and 238 in dynamic reaction cell mode with argon gas (0.2 *mL*, RPq = 0.25). Data were collected using 4 replicates each consisting of 10 sweeps with 300 *ms* dwell time. Internal standard response was corrected using ^{165}Ho. Calibration was achieved using natural uranium CRM 4321, whilst CRM U005A and CRM U0002 were used for control analyses.

4.5 Results & Discussion

4.5.1 Analysis of the Time-Independent Background

Initial measurements of background response were made by the completion of irradiation cycles in the standard DNC reactor site (site 5). Replicate test cycles (n = 8) were performed in the absence of polyethylene (PE) vials using 60 *s* t_{irr} and 3 *s* t_d. Analysis of the data obtained in 0.5 *s* time intervals suggested that the slope of the response observed was 0.00 ± 0.04 (95 % confidence), implying a time independent response. The time-independent background response for count times of one minute in duration was found to be 3.8 ± 0.8 s^{-1} (95 % confidence). This background response was determined to be independent of SLOWPOKE-2 operating power, producing data for which statistical equivalence could not be rejected (α95 % confidence) for SLOWPOKE-2 neutron flux settings of 1 x 10^{12} and 5 x 10^{11} cm^{-2} s^{-1}. Thus, it may be concluded that background is not of function of either extraneous neutrons produced by the SLOWPOKE-2 reactor or of processes related to irradiation. Although the SLOWPOKE-2 flux is predominantly thermal, fast neutron interactions with oxygen present in air and water could contribute to background (Amiel and Peisach, 1963). The $^{17}O(n,p)^{17}N$ and $^{18}O(n,d)^{17}N$ neutron reactions which will produce delayed neutrons from ^{17}N decay, with a half-life of 4.14 *s*, are clear candidates. However, diversion of the pneumatic air supply used for vial transport failed to reduce background response, suggesting that the contribution of these reactions is negligible, at least in the context of pneumatic transport. A comparison of the energy spectrum recorded as background counts, *A*, was similar to the spectrum obtained from the delayed neutrons produced by fissile materials. Neutron sources are stored in the immediate vicinity of the DNC system and these likely provide this neutron-based background.

4.5.2 Analysis of the Time-Dependent Background

Having established a time independent background, similar irradiations were performed using empty PE vials. It is immediately evident, Figure 4.1, that a time-dependent background, where $B(t) >> A_B$, is observed. Replicate $B(t)$ data for eight 60 s irradiations of empty PE vials, with the contribution of A_B subtracted, were obtained in close succession using a flux setpoint of 5.0 x 10^{11} cm^{-2} s^{-1}. Paired t-tests performed between paired experiments showed no statistically significant difference between any of the paired replicate data ($\alpha = 0.05$). The time-dependent background, $B(t)$, is therefore reproducible for multiple PE vials, at least within a single batch. Thus, the time-dependent background was investigated as a function of experimental parameters, including vial mass, irradiation time, neutron flux and reactor site.

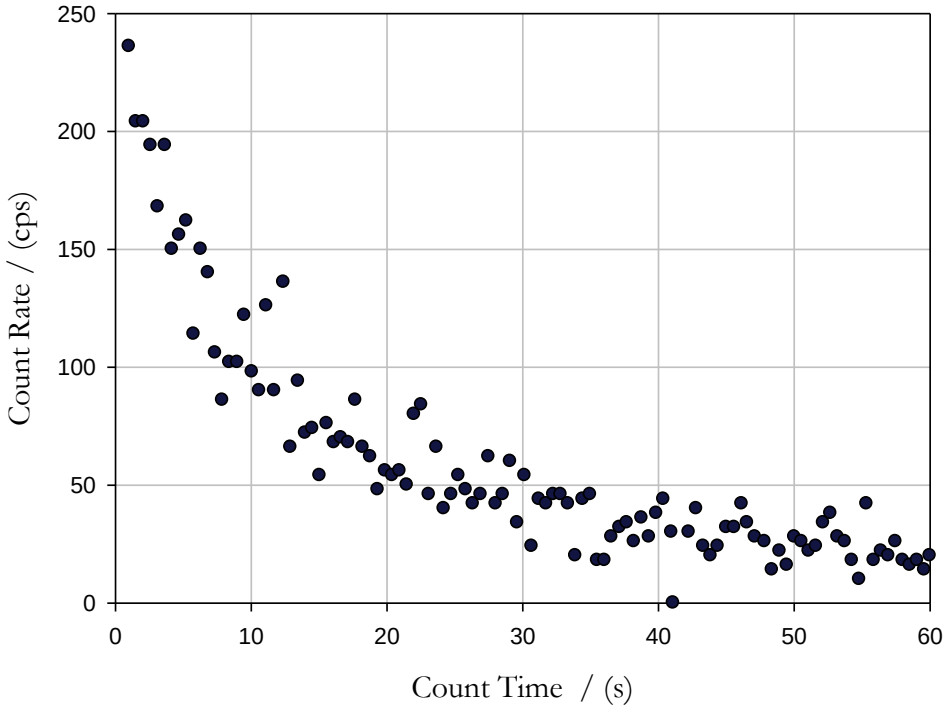

Figure 4.1: Time-Dependent DNC Counts Obtained from the Irradiation of an Empty PE Vial.

The presence of fissile material impurities in the vials, mostly likely natural uranium, was examined by the addition of vial fragments inside the 1.5 *ml* PE vials. Experiments were performed using 3.3, 5.7 and 6.6 *g* of total PE material. Paired t-tests once again found that no statistically significant difference could be observed between *B(t)* for the varying PE masses ($\alpha = 0.05$). *B(t)* was also determined for a series of empty PE vials with irradiation times of (5 – 600) *s*. A simplified comparison was achieved using the cumulative counts, *B(c)*, obtained as the sum of *B(t)* from t = 0 *s* to t = 60 *s*, Table 4.1. A non-linear relationship is observed, Figure 4.2. The influence of neutron flux (ϕ) on *B(c)* was also examined by the analysis of PE vial analyses at 10 %, 50 %, 75 % and 100 % of reactor full power (flux setting 1.0 x 10^{12} $cm^{-2}s^{-1}$), Table 4.2. In this case a linear relationship (slope 4.64 x 10^{-9} cm^{-2} s^{-1}, intercept -43 and R^2 0.9985) was observed, Figure 4.3. To determine if the source of *B(t)* was dependent on the irradiation site used for DNC (site 5) the pneumatic tubing to the SLOWPOKE-2 was temporarily changed to a site that has similar neutron flux properties (site 3) (Andrews, 1989). The time-

independent background rate, A_B, recorded at sites 3 and 5 were identical, 3.7 ± 0.6 and 3.8 ± 0.8 counts s^{-1}, respectively. Analyses conducted using equal ^{235}U masses also confirmed the consistent function of irradiation control and detection in the two sites. Subsequently, twenty-four vials of varying PE mass were irradiated in site 3 and were found to have a count rate of 3.8 ± 0.8 counts s^{-1}, an equivalent rate to that measured in the absence of vials. Figure 4.4 shows a comparison of data collected in sites 3 and 5 for PE vials and background counts in the absence of the PE irradiation vials.

Table 4.1: Background DNC Response *B(c)* for Empty Vial Irradiation as a Function of Irradiation Time, t_{irr}

Irrad. Time t_{irr} /s	**Cumulative Counts, *B(c)***
5	705
10	1040
30	1855
45	2327
60	2400
120	2852
300	3118
600	2906

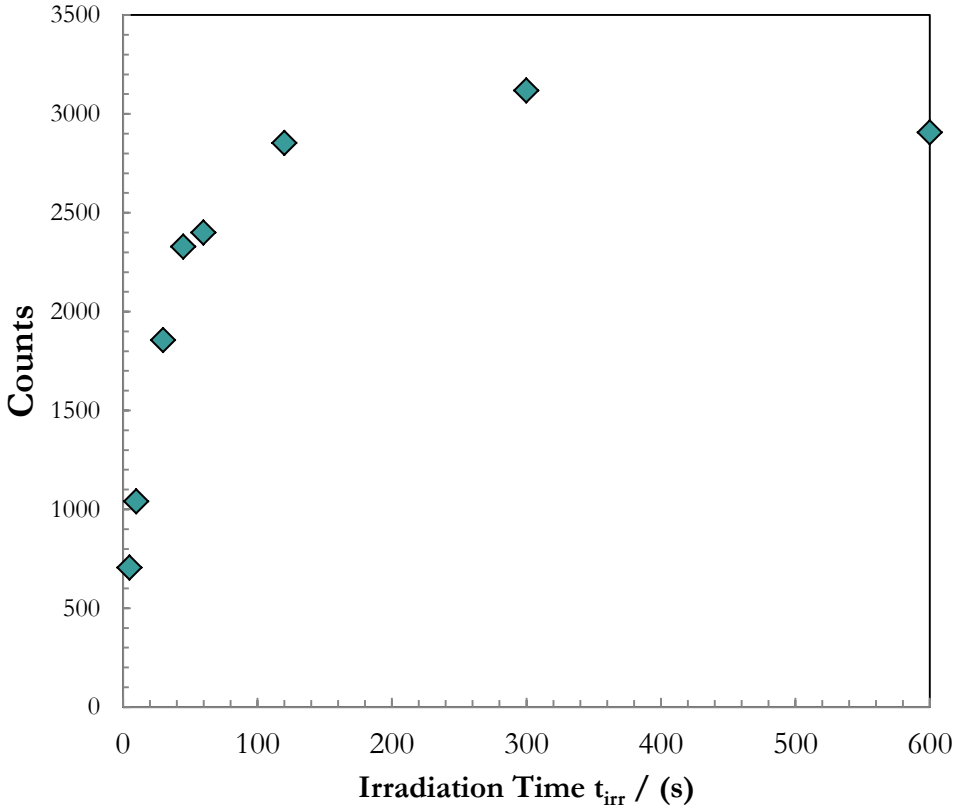

Figure 4.2: Cumulative Background Counts, *B(c)*, Obtained as a Function of Irradiation Time, t_{irr}

Table 4.2**:** Background DNC Response *B(c)* for Empty Vial Irradiation as a Function of Neutron Flux Setting.

Neutron Flux /10^{12} cm^{-2}s^{-1}	**Cumulative Counts, *B(c)***
0.10	449
0.10	437
0.50	2279
0.50	2259
0.50	2269
0.75	3413
0.75	3325
1.0	4715
1.0	4571

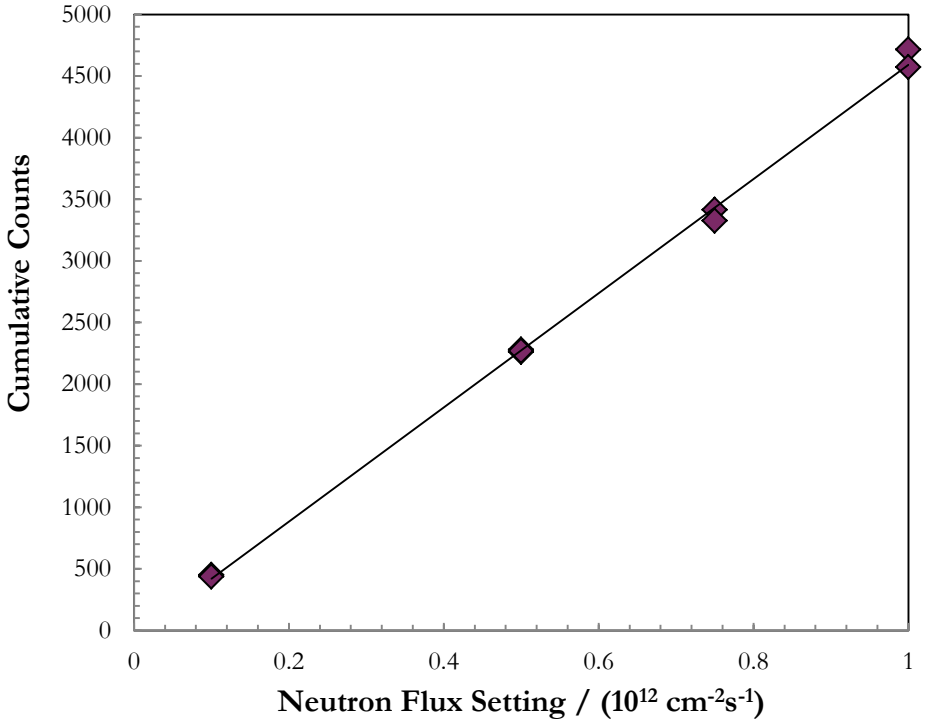

Figure 4.3: Cumulative Background Counts, *B(c)*, Obtained as a Function of Neutron Flux.

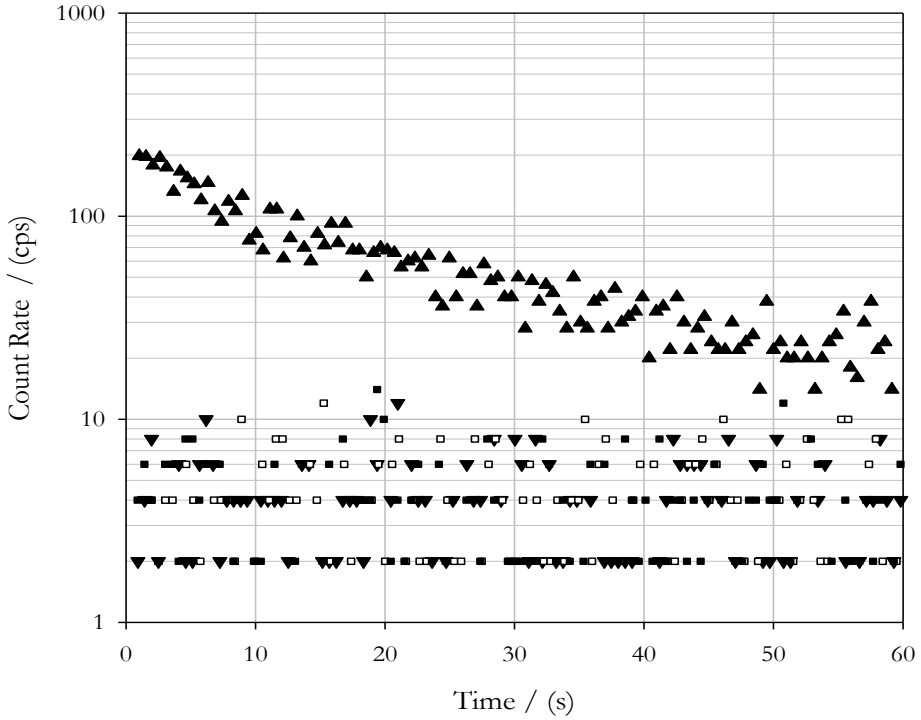

Figure 4.4: A Comparison of Background DNC Responses Observed With PE Vials (Site 3 ▼, Site 5 ▲) and no PE Vial Irradiation (Site 3 □, Site 5 ■).

It was noted that the shape of *B(t)* in site 5 was similar to the measured delayed neutron response obtained from the irradiation of small amounts of ^{235}U, once *A* and *B(t)* had been subtracted from the recorded count rate *C(t)*. As such, following the determination of system efficiency (ε), the time-dependent background *B(t)* could be quantified as a ^{235}U contribution using Eq. (4-1). System efficiency was obtained using a known concentration of uranium that provided $S(t)_j >> B(t)$. Following the subtraction of *B(t)* and *A*, substitution of $S(t)_j$ in Eq. (4-2) afforded ε. The data obtained from empty PE vials under default conditions (t_{irr} 60 *s*, t_d 3 s, flux setting 5.0 x 10^{11} cm^{-2} s^{-1}, site 5) were analysed using Eq. (4-1). DNC software, developed to quantify ^{235}U, found *B(t)* to be equivalent to 120 ± 8 *ng* of ^{235}U based on eight replicate analyses. The hypothesis that *B(t)* is derived from a ^{235}U fission is supported by all experiment data. The relationship between flux and *B(t)* is linear, as predicted using Eq. (4-1). The more complex relationship between t_{irr} and *B(t)*, Figure 4.2, is also predicted using Eq. (4-1). Assuming a 120 *ng* ^{235}U background contribution, [experimental ^{235}U/expected ^{235}U] has been calculated at various t_{irr}. A plot of [experimental ^{235}U/expected ^{235}U] versus t_{irr}

displays the consistent experimental determination of ^{235}U, Figure 4.5. The slope and intercept of this plot are effectively zero ($2 \times 10^{-5} \pm 4 \times 10^{-4}\ s^{-1}$) and one ($1.02 \pm 0.10$), respectively; supporting adherence to Eq. (4-1). Similarly, the absence of correlation between [experimental ^{235}U/expected ^{235}U] and t_{irr} ($R^2 = 0.012$) is consistent with a time-dependent background that can be modelled by ^{235}U fission. That the source of uranium is located within the irradiation system is supported by the independence of *B(t)* to PE vial mass and dependence on irradiation site. Since there had been no history of ^{233}U or ^{239}Pu use in the system before or during the background characterisation, detailed examinations of these potential contaminants were not made. However, comparisons of DNC profiles for ^{235}U, ^{233}U and ^{239}Pu supported the attribution of *B(t)* to ^{235}U. Clearly, the capability of RMCC's DNC system to discern temporal as well as cumulative response has allowed comparisons to be made between the theoretical behaviour of ^{235}U and experimental results for *B(t)*.

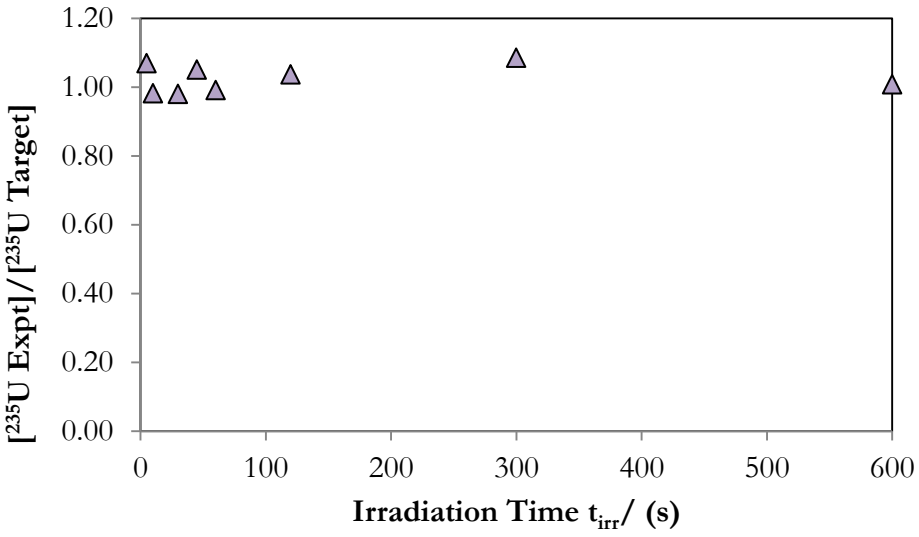

Figure 4.5: Expected/Nominal ^{235}U Background Obtained as a Function of Irradiation Time, t_{irr}.

Two possible mechanisms for the origin of the extraneous ^{235}U counts were considered and investigated: i) the deposition of U contaminant on the vials at, or during transport to, the irradiation site or ii) the recoil of fission product daughters as PE vials sit in the irradiation site. In the first hypothesis uranium masses consistent with *B(t)* would be deposited on the vial surface. Moreover, an increase in *B(t)* as a function of repeated irradiation and counting cycles should occur. Uranium would be incrementally deposited on the vial surface with each cycle,

although some partial loss of loosely adhered uranium might also occur during subsequent irradiation cycles. In a second hypothesis, uranium accumulation on vial surfaces would not occur, and increases in *B(t)* would not be observed if a sufficient decay period was incorporated into the cyclic analysis. DNC studies considered 4 cycles of irradiation and counting under default conditions. An inter-cycle decay time of 600 *s* was used to allow the neutron activity to reach background levels. Analysis of the cumulative neutron counts recorded for each irradiation cycle found no dependence of *B(c)* on number of irradiation cycles. The obtained slope (-20 ± 60 counts per irradiation cycle at 95% confidence) could not be statistically distinguished from zero, and given that a mean *B(c)* for these cycles of 2250 counts was obtained, the accumulation of uranium may be considered to be at best negligible. Further chemical analysis of the post-uranium surface content of PE vials will be discussed in detail.

4.5.3 The Reduction of the Time-Dependent Background

The attribution of the time-dependent background allowed for its reduction through the cleaning of the SLOWPOKE-2 irradiation site with distilled water and HNO_3. The ^{235}U containment equivalent per vial was reduced by more the half, to 50 *ng* of ^{235}U. Having identified the source and location of background contamination, it is hoped that a more physically and chemically specific decontamination will facilitate the further reductions in *B(t)* to reduce detection limits below 5 *ng* of ^{235}U.

4.5.4 Surface Uranium Contamination Measurement

A series of experiments were conducted in which the uranium surface contamination of empty PE vials was determined following irradiation under variable conditions, Table 4.3. These results are expressed as total uranium content, rather than ^{235}U. In general, a surface leaching procedure using 2 % nitric acid was employed; although for a limited number of vials the presence of loose contamination was assessed by a swipe with an acid dampened glass fibre swipe prior to leaching. Experiments were conducted in conjunction with appropriate controls. Thus, blank analyses of surface swipes and leachate experiments afforded uranium masses < 0.10 *ng* and < 0.05 *ng*, respectively. Control samples prepared from NIST CRM 4321C, natural uranium, were spiked into a leachate solution and alternatively allowed to dry onto a PE vial surface before leaching. The nominal mass used, 0.5 *ng*, was obtained with 74 % and 68 % recovery, respectively.

Table 4.3: PE Vial Experimental Conditions and Measured Uranium (^{235}U + ^{238}U) Mass

Sample #	Experimental Variable	Vial Uranium Mass[a] /*ng*
1	Default Conditions[b]	10.4
2	Irradiation Time (1 *s*)	10.9
3	Irradiation Time (5 *s*)	17.1 (10.8 + 6.3)
4	Irradiation Time (10 *s*)	12.3
5	Irradiation Time (30 *s*)	15.1
6	Irradiation Time (45 *s*)	12
7	Irradiation Time (120 *s*)	12.5
8	Irradiation Time (300 *s*)	22
9	Irradiation Time (600 *s*)	18.4 (8.9 + 9.5)
10-12	Flux (1.0 x 10^{11} cm^{-2} s^{-1})	16.2, 15.4, 18.7
13,14	Flux (7.5 x 10^{11} cm^{-2} s^{-1})	24.7, 14.0
15,16	Flux (10 x 10^{11} cm^{-2} s^{-1})	27.1, 13 (5.5 + 7.5)
17,18	Irradiation Cycles (2)	17.8 (8.8 + 9.0), 25.4 (8.2 + 17.2)
19	Irradiation Cycles (3)	27.0 (12.8 + 14.2)
20	Irradiation Cycles (4)	31.6 (16.2 + 15.4)
21-30	Default – after cleaning	9.4, 11.8. 11.8. 9.7, 8.9, 12.5, 9.1. 9.2, 15.4, 38.1
31	Site 3 Irradiation Time (1 *s*)	19.3
32	Site 3 Irradiation Time (5 *s*)	9.4
33	Site 3 Irradiation Time (10 *s*)	14.6
34	Site 3 Irradiation Time (30 *s*)	9.9
35	Site 3 Irradiation Time (45 *s*)	23.7
36	Site 3 Irradiation Time (60 *s*)	12.3 (5.2 + 7.1)
37	Site 3 Irradiation Time (120 *s*)	18.6
38	Site 3 Irradiation Time (300 *s*)	16.7

a) Figures in parenthesis correspond to swipe and leachate contributions;
b) t_{irr} = 60 *s*, t_d = 3 *s*, flux setting = 5.0 x 10^{11} cm^{-2} s^{-1}, site = 5

A series of experiments were conducted under various experimental conditions, with data being compared to the uranium surface contamination obtained under default condition (t_{irr}, 60 *s*; site 5; neutron flux setting, 5.0 x 10^{11} cm^{-2} s^{-1}). Surface uranium masses obtained under default and other conditions are identified in Table 4.3. Samples 1 (default) and samples 2-9 demonstrate an independence of surface uranium mass with respect to irradiation time, whilst independence from flux, samples (1, 10-16), is also evident. Regression analyses for these conditions afford slopes of 0.012 (± 0.014) *ng* s^{-1} and 0.40 (± 1.4) *ng* cm^2 *s*, respectively, at 95 % confidence. Some dependence with respect to the number of irradiation cycles was observed, 6.7 (± 5.4) *ng* $cycle^{-1}$, (samples 1, 17-20). However, this relationship implies an increase in uranium per additional cycle that is less than the mass associated with a single irradiation cycle. Thus, although some additional uranium may accumulate during repeated cycles, this either represents a process of accumulation and loss, or the accumulation of lower masses during subsequent irradiation cycles. The former mechanism appears

more likely, given that, for the four PE vials which were initially surface swiped in site 5, almost half of the uranium detected (45 % ± 8 %) was removed by surface swiping. Experiments were also performed using replicate irradiations to determine the surface uranium mass of PE vials following cleaning of the site 5 location (samples 21-30), and by performing irradiations in an alternative (site 3) reactor location (samples 31-38). The latter used the same transfer pneumatics, which were physically disconnected from site 5 and reconnected to site 3. Irradiations performed in site 5 under default conditions after cleaning, samples 21-30, were not statistically different from those obtained prior to cleaning (13.6 ± 8.9 *ng*), whilst those samples obtained using varying irradiation times in site 3 could not be determined to be statistically different from the equivalent experiments performed in the uncleaned site 5 using a paired *t*-test at 95 % confidence [$t(7) = -0.31$, $t_{critical} = 2.36$, $p = 0.76$].

A number of experiments were conducted in which PE vials were initially swiped, then leached. These experiments include examples from wider datasets in which no dependence between uranium mass and experimental variable could be determined at 95 % confidence, including samples 3 and 9 (varied irradiation time), sample 16 (varied flux) and sample 32 (varied irradiation time, site 5). In each case, a Grubbs test failed to demonstrate that the sum of swiped and leached uranium represented an outlier from the wider leached-only dataset. *Z* scores of 0.68 (2.21), 0.98 (2.21), 1.00 (2.02) and 0.67 (1.00) were obtained, respectively, with $Z_{critical}$ values in parentheses. It is clear from the experiments described that a reasonably consistent mass of uranium can be obtained irrespective of irradiation time, flux, reactor site and site cleaning. Moreover, much of this uranium is loosely adhered to the vial, such that it can be removed by surface swiping and repeated cycles of irradiation appear to result in uranium loss and accumulation. The consistent transfer of uranium to PE vials is particularly notable because; (i) a negligible time dependent DNC response is observed in site 3, and (ii) a significant post-cleaning reduction was recorded in site 5.

Consideration of the relationship between DNC background (expressed as ^{235}U) and surface detection of total uranium (^{235}U + ^{238}U) requires the determination of the isotopic composition of the surface uranium. The integrity of isotope ratio analysis was established by the analysis of CRM U0002 and U005A containing 0.02 % atom and 0.5 % atom nominal ^{235}U depletion. Data are consistent with these CRMs using quadruple ICP-MS, with ^{235}U % atom values and expected values in parentheses of 0.021 % atom (0.01755 % atom) and 0.049 % atom (0.05064 % atom), respectively. The relatively poor accuracy obtained for the former CRM is a reflection of the relative low ^{235}U counts per second recorded for this highly depleted material. Isotope ratios measured for all uranium swiped or leached from PE vials are consistent with natural uranium; ^{235}U being 0.70 ± 0.2 % atom compared with an expected value of 0.72 % atom. Hence,

the unlikely possibility of uranium loss from the 19.89 % enriched SLOWPOKE-2 core can be immediately eliminated. The mean total uranium mass obtained across all irradiated vial analyses was 16.6 ± 6.7 *ng*. Assuming a natural uranium isotope ratio, this corresponds to 0.118 ± 0.048 *ng* ^{235}U. Two conclusions are immediately evident; (i) if adhered uranium were present during irradiation, this uranium would contribute ca. 0.1 *%* to the total time dependent background observed by DNC in the uncleaned site 5, (ii) assuming an approximate initial ^{235}U DNC response of 2 counts s^{-1} ng^{-1}, the DNC contribution from adhered uranium is negligible, ca. 0.2 *counts* s^{-1}, and would be lost within the uncertainty associated with time independent background A_B (3.8 ± 0.8 *cps*) even in the uranium-free site 3. Given these conclusions, it can be suggested that the presence or absence of vial uranium, and its possible presence during irradiation cannot be established by DNC. The magnitude of this ^{235}U contribution clearly indicates that the adherence and transfer of uranium to the DNC cannot be the source of time dependent background. Moreover, the absence of correlation between site changes and cleaning further suggest that the reactor site is not the location in which this adherence occurs. Clearly, some locations within the pneumatic system impart trace levels of uranium to PE vials, but the magnitude of mass transfer is extremely small and this process is not relevant to the time-dependent DNC response.

4.6 Conclusions

The origin of the time-dependent neutron background in the SLOWPOKE-2 reactor at RMCC has been established as resulting from uranium contamination within the irradiation site used for DNC analysis. Analysis of PE vials from nominally decontaminated and clean irradiation sites demonstrates the presence of surface uranium of natural isotope ratio. However, the mass of uranium present is *ca.* 0.1 % of that associated with the time dependent background and provides a maximum response that cannot be distinguished from the noise associated with time independent response. Thus it may be concluded that the uranium associated with time-dependent contamination is not directly transferred to PE vials. Instead uranium contamination produces fission products daughters, which as a consequence of recoil, become embedded in the PE vials as they are irradiated in the SLOWPOKE-2 reactor. The delayed neutron behaviour of these fission product daughters is entirely consistent with that derived from the transfer of irradiated uranium. The daughters subsequently produce delayed neutrons, which account for the time-dependent background observed in the SLOWPOKE-2 reactor. This background was significantly reduced through the removal of contamination from the irradiation site.

4.7 Acknowledgements

The thoughtful input from Dr. Gregory Kennedy from École Polytechnique on the source of contamination in the SLOWPOKE-2 irradiation site is appreciated. The authors would also like to thank Dave Ferguson, Kristine Mattson, Kathy Nielsen and Steve White for their assistance in experimentation. Funding for this project was provided by the Director General of Nuclear Safety and the Natural Sciences and Engineering Research Council of Canada.

-This page is intentionally left blank-

Chapter 5

Simultaneous ^{233}U and ^{235}U Characterization Through the Assay of Delayed Neutron Temporal Behaviour

M.T. Sellers, E.C. Corcoran, D.G. Kelly

Department of Chemistry and Chemical Engineering,
Royal Military College of Canada
P.O. Box 17000 Stn. Forces
Kingston, Ontario, Canada K7K 7B4[ix]

[ix] **M.T. Sellers**, E.C. Corcoran, D.G. Kelly, "Simultaneous ^{233}U and ^{235}U Characterization Through the Assay of Delayed Neutron Temporal Behavior" *PHYSOR 2012 – Advances in Reactor Physics*, Knoxville, TN, April 15 (2012).

5.1 Abstract

Aqueous solutions containing dissolved ^{233}U and ^{235}U were irradiated for 60 *s* in the SLOWPOKE-2 reactor at the Royal Military College of Canada. The temporal behavior of the delayed neutrons produced was recorded by the Facility's Delayed Neutron Counting (DNC) system. The percentage of ^{233}U as a function of total fissile mass present in each sample ranged from 0 to 100 *%* and was predicted by the DNC system with average absolute errors of ± 4 *%*. Future work will upgrade the system electronics and software to reduce both uncertainties in timings and electrical noise. Mixture analysis will also be expanded to include ^{239}Pu and fissile materials contained in non-aqueous matrices.

Keywords: delayed neutron, special nuclear materials, nuclear forensics

5.2 Introduction

The attribution and characterization of special nuclear materials (SNM) is dependent on the establishment of comprehensive and rigorous nuclear forensics analysis (NFA) instrumentation and protocols. The Nuclear Research Group at the Royal Military College of Canada (RMCC) aims to strengthen Canada's NFA capabilities through the development of both NFA protocols and instrumentation capable of analyzing SNM. Current research is focused on evaluating existing analytical instrumentation and enhancing analytical capabilities pertinent to the analysis of SNM at RMCC.

RMCC has recently commissioned a delayed neutron counting (DNC) system and validated it for the analysis of ^{235}U (Sellers *et al*., 2012a). The DNC system complements existing instrumentation used for the assay of SNM as it is a non-destructive and rapid method for the determination of fissile mass present in a sample. Previous work by (Li *et al*., 2004; Myers *et al*., 2006) and Myers *et al.* have examined the delayed neutron signatures from the mixtures containing $^{235}U/^{239}Pu$ and $^{235}U/^{238}U$, respectively, and characterized the individual isotope contributions to the overall count rate in this work. A series of DNC measurements were made at the RMCC with samples containing both ^{233}U and ^{235}U to examine the capability of the instrument to attribute the delayed neutron signals produced from each fissile isotope.

5.3 Theory

Induced fission of the isotopes ^{233}U and ^{235}U results in the production of both prompt neutrons and fission products. Some of these fission products undergo β^- decay and release delayed neutrons. These particular fission products are denoted as delayed neutron precursors and are organized by the half-life of their associated delayed neutron emissions. Table 5.1 shows the relative yield, α, of the eight delayed neutron groups, i, for each isotope examined in this study, the total number of delayed neutrons produced per thermal fission of ^{233}U and ^{235}U is 0.0067 and 0.0162, respectively (Nichols *et al*., 2008). The temporal behavior of the delayed neutron groups is dependent on the isotope undergoing fission due to the difference in fission product yields (and therefore delayed neutron precursors produced).

The count rate recorded from fissile isotope j after the irradiation of n fissile isotopes, $C(t)$, is a superposition of the delayed neutron production, $Q(t)_j$, and the system background signal, $B(t)$ (Myers *et al*., 2006):

$$C(t) = \sum_{j=1}^{n} Q(t)_j m_j \varepsilon + B(t) \qquad 5\text{-}1$$

Where m_j is the mass of the fissile isotope j [g] and

$$Q(t)_j = \frac{\sigma_{f_j} \nu_d \Phi N_A}{MM_j} \sum_{i=1}^{8} \alpha_{i_j} \left(1 - e^{-\lambda_i t_{irr}}\right)\left(e^{-\lambda_i t_d}\right)\left(e^{-\lambda_i t}\right) \qquad 5\text{-}2$$

ε is the detection efficiency of the instrumentation, σ_{f_j} is the thermal fission cross section of isotope j [b], ν_d is the number of delayed neutrons produced in that isotope, Φ is the thermal neutron flux [$cm^{-2}\,s^{-1}$], N_A is Avogadro's number [mol^{-1}], MM_j its molecular mass [$g\ mol^{-1}$], λ_i is the decay constant for group i [s^{-1}], t_{irr} the irradiation duration of the sample [s], t_d the decay time of the sample before the commencement of counting [s], and t the count time [s] (formerly denoted as t_c in this thesis). Therefore in the analysis of fissile mixtures in a fully characterized system, the only unknowns in Eq. (5-1) are the masses of the fissile isotopes, m_j.

Table 5.1: Delayed Neutron Group Fraction, α_i, ^{233}U and ^{235}U ($\pm 1\sigma$) (Nichols *et al*., 2008).

Half-Life / [s]	**α_i ^{233}U / [%]**	**α_i ^{235}U / [%]**
55.6	7.97 ± 0.36	3.28 ± 0.42
24.5	16.70 ± 0.35	15.39 ± 0.68
16.3	15.00 ± 0.30	9.1 ± 0.9
5.21	20.0 ± 4.0	19.7 ± 2.3
2.37	29.8 ± 2.2	33.08 ± 0.66
1.04	3.88 ± 0.08	9.02 ± 0.45
0.424	5.6 ± 2.5	8.12 ± 0.16
0.195	1.05 ± 0.02	2.29 ± 0.95
$\sum \boldsymbol{\alpha_i}$	100.0 ± 5.3	100.0 ± 2.9

The experimentally observed differences in temporal behavior of solutions containing only ^{233}U and ^{235}U fissile material are shown in Figure 5.1. As expected, ^{235}U delayed neutrons have a rapid die-away time, when compared to ^{233}U, because of the lesser relative yields of the longer lived delayed neutron groups described in Table 5.1.

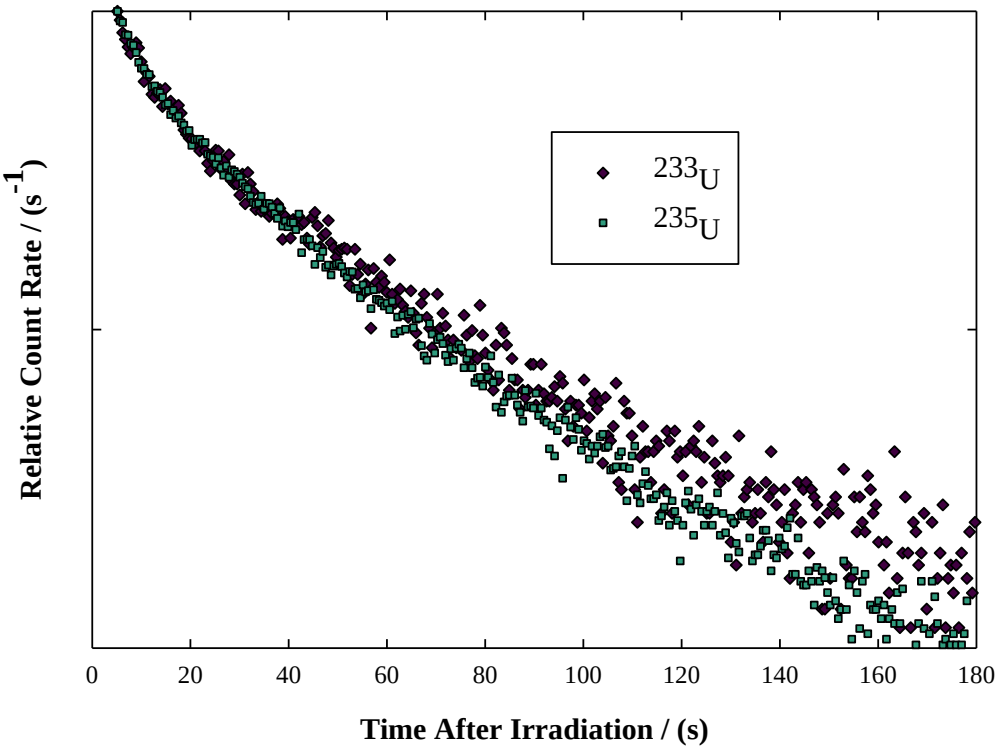

Figure 5.1: A comparison of measured temporal behavior of U-233 and U-235. The first count rate data point has been normalized to the same initial value, emphasizing the temporal differences.

5.4 Experimental

Samples were prepared from natural uranium (CRM 4321C, NIST, Gaithersburg, MD) and 99 % atom percent ^{233}U (CRM 111-A, 99.49 atom % ^{233}U, New Brunswick Laboratory, Argonne, IL) dissolved in nitric acid (Optima, ThermoFisher Scientific, Ottawa, ON). Each fissile solution was prepared with nominal volumes ranging from 0.2 to 1.0 *ml* and heat-sealed in a 1.5 *ml* polyethylene vial (LA Packaging, Yorba, Linda, CA). Two 1.5 *ml* vials (one containing ^{233}U solution and the other ^{235}U) were then encapsulated in a 7 *ml* polyethylene vial (LA Packaging, Yorba, Linda, CA). Previous experimentation

(Sellers *et al*., 2012a) has found that the position of the fissile material within the larger vial has no effect on the counts recorded by the apparatus. The aqueous solutions containing nitric acid and distilled water were also found not to contribute to the delayed neutron production recorded by the apparatus. The total fissile mass of each sample ranged from 1.7 to 9.4 μg. The fissile content ratio of ^{233}U:^{235}U was varied from 0:100 to 100:0 %. The system's detection efficiency was calibrated with eight samples containing depleted U (CRM U005A, New Brunswick Laboratory, Argonne, IL) containing ^{235}U amounts from 1.5 to 5.5 μg.

The DNC system at RMCC uses the SLOWPOKE-2 reactor onsite to provide a predominately thermal neutron flux (Andrews, 1989). These samples were irradiated in the SLOWPOKE-2 for 60 *s* at two thermal neutron flux settings, 4.5 x 10^{11} and 1.0 x 10^{12} $cm^{-2}s^{-1}$ (± 5 %). After the samples were irradiated, they were sent to the delayed neutron counting array which consists of six helium-3 detectors embedded in a paraffin moderator via pneumatic tubing. The system recorded the number of neutrons detected by the apparatus in half-second intervals for a duration of three minutes following irradiation. These data were imported into fissile isotope analysis software written on the Matlab™ platform (R2011a, Mathworks, Natick, MA), which corrected for system background and electrical dead time effects. The software also used Eq. (5-2) to generate the expected behavior of ^{233}U and ^{235}U delayed neutron count rates using the experimental parameters of the apparatus. The fissile isotope analysis software then performed least squares regression on the experimental data to determine the amounts of ^{233}U and ^{235}U present. Additional information on the DNC system, hardware and software components is described in (Sellers *et al*., 2012a).

5.5 Results & Discussion

Two independent experiments were conducted on the samples prepared for this study. Section 5.5.1 discusses the capability of the system to determine the amount of ^{233}U as a percentage of total fissile material present or the ratio of ^{233}U:^{235}U. Section 5.5.2 discusses the accuracy and precision of the system when characterizing the amount of each isotope (^{233}U and ^{235}U, respectively) and therefore total fissile mass contained in the samples.

5.5.1 ^{233}U as a Function of Total Fissile Mass

As previously mentioned the nitric acid and distilled water solution, which contain the fissile material, does not contribute to the count rate recorded by the apparatus (Sellers *et al*., 2012a). There was a small system background, *B(t)*, which has been extensively characterized (Sellers *et al*., 2013), and was automatically

subtracted when the raw data was analyzed by the fissile isotope analysis software. Therefore, the only delayed neutron counts recorded from the irradiation of these samples results from the fission of ^{233}U and ^{235}U.

To examine if the DNC system could determine the contribution of ^{233}U to the overall delayed neutron count rate, a series of 15 samples were analyzed. Each sample was prepared with varying ratios of fissile isotopes content (*i.e.*, the ^{233}U:^{235}U ratio was varied from 0:100 to 100:0). Table 5.2 shows a comparison of the actual fissile isotope ratio and the experimentally determined ratio of ^{233}U: ^{235}U. Each measurement represents the mean of duplicate measurements. The average absolute error in these measurements was found to be ± 4 %.

Table 5.2: The Determination of ^{233}U Content in Total Fissile Mass (± 1s)

	Actual Ratio of ^{233}U:^{235}U of Total Fissile Mass / [%]		**Experimentally Determined Ratio of ^{233}U:^{235}U of Total Fissile Mass / [%]**		**Absolute Error / [%]**
1	0 : 100		4 : 96	(± 3)	4
2	13.1 : 86.9	(± 0.3)	11 : 89	(± 4)	-2
3	14.4 : 85.6	(± 0.3)	13 : 87	(± 5)	-1
4	17.7 : 82.3	(± 0.3)	19 : 81	(± 5)	1
5	31.3 : 68.7	(± 0.6)	27 : 73	(± 4)	-4
6	32 : 68	(± 1)	36 : 64	(± 3)	4
7	36 : 64	(± 1)	44 : 56	(± 4)	8
8	37 : 63	(± 1)	45 : 55	(± 8)	8
9	39.9 : 61.1	(± 0.7)	36 : 64	(± 7)	-4
10	46 : 54	(± 2)	46 : 54	(± 6)	0
11	51 : 49	(± 2)	50 : 50	(± 6)	-1
12	54 : 46	(± 1)	59 : 41	(± 5)	4
13	71 : 29	(± 1)	78 : 22	(± 6)	7
14	96 : 4	(± 4)	92 : 8	(± 2)	-4
15	100 : 0		97 : 3	(± 2)	-3

5.5.2 Individual and Total Fissile Mass Determinations

The determination of individual and total fissile masses present in several samples is presented in Table 5.3 and Table 5.4, respectively. The system was able to discern the amounts of both ^{233}U and ^{235}U in mixtures with average absolute errors

of 0.3 μg and 0.2 μg, respectively. These results mirror the absolute errors of the system when determining the amount of fissile content in samples containing only ^{235}U. The results of the previous, with only ^{235}U, study are listed in Table 5.5 for comparison purposes. In addition, changes in volume and geometry demonstrated that the system is insensitive to changes in geometry and that uncertainties result from those associated with CRMs, solution preparation and data analysis.

Table 5.3: Mass Determinations of ^{233}U and ^{235}U (±1s)

	^{233}U Actual Amount /[μg]	**^{233}U Experimental /[μg]**	**^{235}U Actual Amount /[μg]**	**^{235}U Experimental /[μg]**
A	3.0 ± 0.1	3.2 ± 0.5	6.5 ± 0.3	6.4 ± 0.3
B	3.0 ± 0.1	2.8 ± 0.5	5.0 ± 0.3	5.3 ± 0.3
C	3.0 ± 0.1	3.1 ± 0.8	3.4 ± 0.2	3.8 ± 0.5
D	3.0± 0.1	3.54 ± 0.03	5.4 ± 0.3	4.09 ± 0.06
E	2.9 ± 0.1	3.04 ± 0.07	0.14 ± 0.007	0.07 ± 0.05
F	3.0 ± 0.1	3.1 ± 0.5	2.9 ± 0.1	2.9 ± 0.3
G	0.49 ± 0.02	0.3 ± 0.1	3.2 ± 0.2	3.19 ± 0.07
H	0.48 ± 0.02	0.3 ± 0.3	2.9 ± 0.1	2.8 ± 0.1
I	0.45 ± 0.02	0.5 ± 0.4	2.1 ± 0.1	2.0 ± 0.3
J	1.0 ± 0.05	0.6 ± 0.5	2.1 ± 0.1	2.3 ± 0.3
K	1.2 ± 0.06	0.9 ± 0.5	1.80 ± 0.09	1.9 ± 0.2
L	1.2 ± 0.06	1.4 ± 0.2	1.06 ± 0.05	0.9 ± 0.1
M	1.2 ± 0.06	1.3 ± 0.2	0.69 ± 0.03	0.7 ± 0.1
N	1.2 ± 0.06	1.40 ± 0.07	0.50 ± 0.02	0.42 ± 0.03

Table 5.4: Total Fissile Mass Determination (±1s)

	Total Fissile Mass /[μg]	Total Mass Experimental /[μg]	Absolute Error /[μg]
Sample I	1.74 ± 0.07	1.82 ± 0.04	0.08
Sample II	1.93 ± 0.07	1.98 ± 0.06	0.05
Sample III	2.28 ± 0.08	2.33 ± 0.08	0.05
Sample IV	2.6 ± 0.1	2.5 ± 0.1	-0.1
Sample V	3.00 ± 0.1	2.8 ± 0.2	-0.2
Sample VI	3.00 ± 0.1	2.9 ± 0.2	-0.1
Sample VII	3.1 ± 0.1	3.42 ± 0.02	0.3
Sample VIII	3.3 ± 0.1	3.2 ± 0.1	-0.1
Sample IIX	3.7 ± 0.2	3.49 ± 0.03	-0.2
Sample IX	5.8 ± 0.2	5.9 ± 0.2	0.1
Sample X	6.4 ± 0.2	7.0 ± 0.3	0.6
Sample XI	8.0 ± 0.3	8.1 ± 0.2	0.1
Sample XII	8.4 ± 0.3	7.63 ± 0.03	-0.8
Sample XIII	9.4 ± 0.4	9.6 ± 0.1	0.2

Table 5.5: Previous Mass Determinations for One Fissile Isotope (±1s) (Sellers *et al*., 2012a)

	Total Fissile Mass / [μg ^{235}U]	Total Mass Experimental /[μg]	Absolute Error / [μg]
Sample i	5.6 ± 0.2	5.3 ± 0.1	-0.3
Sample ii	4.3 ± 0.1	4.2 ± 0.1	-0.1
Sample iii	2.49 ± 0.08	2.6 ± 0.1	0.11
Sample iv	1.54 ± 0.04	1.5 ± 0.1	-0.04

5.6 Future Work

Further experimentation will be conducted to expand the data set to provide a complete evaluation of associated uncertainties for duplicate measurements. A DNC system upgrade is underway at the Royal Military College of Canada, which will replace several electrical components in the system to reduce electrical noise, dead time and pulse pile up effects. It is hoped that a reduction in noise will positively affect the capability of the fissile isotope analysis software to discriminate between delayed neutrons produced from the individual isotopes in samples containing mixtures of fissile isotopes. Finally, additional curve fitting techniques will be explored in an attempt to provide improved fissile analysis

capabilities. Analysis will be expanded to include mixtures containing ^{239}Pu and fissile content in non-aqueous matrices.

5.7 Conclusions

This paper describes the initial steps of the delayed neutron counting facility at the Royal Military College of Canada to differentiate between delayed neutrons produced by ^{233}U and those of ^{235}U through the analysis of their temporal behavior. The system measured accurately the total fissile mass ratio of ^{233}U:^{235}U with average absolute errors of ± 4 %. The masses of the isotopes ^{233}U and ^{235}U were found in mixtures containing 1.7 to 9.4 μg of fissile materials with average absolute errors of 0.3 μg and 0.2 μg, respectively. Further experimentation will include the analysis of ^{239}Pu with the DNC system.

5.8 Acknowledgements

The authors wish to acknowledge the Director General of Nuclear Safety and the Natural Sciences and Engineering Research Council of Canada for providing financial support of this project. Also, the assistance of S. White, K. Nielsen and D. Ferguson is appreciated. The authors also acknowledge the support and guidance of T. Goorley and the XCP-3 Group of Los Alamos National Laboratory.

Chapter 6

Modeling the Detection of Delayed Neutron Signatures in MCNP6 and Comparisons with Measurements of ^{233}U, ^{235}U and ^{239}Pu

M.T. Andrews[1], J.T. Goorley[2], E.C. Corcoran[1], D.G. Kelly[1]

[1]Royal Military College of Canada
P.O. Box 17000 Stn Forces
Kingston, ON K7K 7B4

[2]Monte Carlo Codes, MS: A143
Los Alamos National Laboratory
Los Alamos, NM, 87545[x]

[x] **M.T. Andrews**, J.T. Goorley, E.C. Corcoran, D.G. Kelly, "Modeling the Detection of Delayed Neutron Signatures in MCNP6 and Comparisons with Measurements of ^{233}U, ^{235}U and ^{239}Pu" *Journal of Nuclear Technology* **187** *3* (2014) pp. 235-242

6.1 Abstract

Study of the magnitude and temporal behavior of delayed neutrons (DNs) enables the identification of fissile isotopes and a determination of their relative quantities. Thus, the ability to model accurately these neutrons and the methods of their detection is of relevance to nuclear forensics and counter terrorism. The capability of MCNP6 to model these emissions was examined and compared to measurements of the DNs produced by ^{233}U, ^{235}U and ^{239}Pu after neutron induced fission. Fissile samples were irradiated in a SLOWPOKE-2 research reactor for 60 *s* and were then conveyed via pneumatic tubing to an array of six ^{3}He detectors embedded in a paraffin moderator. Several MCNP6 input files were created to reproduce irradiation conditions, temporal DN emission, and the detection arrangement. Nuclear reactions and other effects within the ^{3}He detectors were reproduced by MCNP6, and detection efficiencies of this modeled arrangement determined by MCNP6 were in agreement with experimental measurements. Finally, the library and model DN emission options in the MCNP6v1 release were evaluated and compared to the measured magnitudes and temporal behavior of ^{233}U, ^{235}U, and ^{239}Pu. Significant discrepancies observed between the DN model option and measurements for count times > 100 *s* are discussed.

Keywords: MCNP6; delayed neutron; nuclear instrumentation

6.2 Introduction

Fission results in the release of prompt neutrons and fission products, many of which will undergo β^- decay and subsequently release additional delayed neutrons (DNs). These DN precursors are often organized into several groups with half-lives ranging from < 1 *s* to almost a minute (Keepin *et al*., 1957; Li *et al*., 2004). The magnitude and temporal behavior of DN emission is dependent on the isotopes undergoing fission (Li *et al*., 2004). Thus, the assay of DNs can enable the rapid and non-destructive characterization of fissile isotopes and a determination of their relative quantities (Li *et al*., 2004; Myers *et al*., 2006). The ability to simulate these neutron emissions and their detection has valuable nuclear forensics applications (Durkee *et al*., 2012). Los Alamos National Laboratory has developed MCNP™ (Goorley *et al*., 2012; MCNP, 5; Pelowitz and others, 2005)[xi], a Monte Carlo computer code capable of modeling particle transport in user-specified three-dimensional geometries. MCNP6v1, the newest release of this software, includes

[xi] MCNP, MCNP5, MCNPX and MCNP6 are trademarks of Los Alamos National Security, LLC, Los Alamos National Laboratory.

the merging of MCNP5 and MCNPX capabilities. MCNP6 includes the ability to simulate DN emissions (Durkee *et al*., 2012) and the other nuclear interactions pertinent to their detection.

A delayed neutron counting (DNC) system has been designed and validated for the analysis of the aqueous solutions containing ^{233}U, ^{235}U and ^{239}Pu content at the SLOWPOKE-2 nuclear reactor facility within the Royal Military College of Canada (RMCC). This system (Sellers *et al*., 2012a) aims to discern between fissile isotopes by recording the temporal behavior of their DN emissions in half second time intervals. The acquisition of these measurements has afforded an opportunity to evaluate the capability of MCNP6 to predict measured DN emissions from special nuclear materials (SNMs). In the present work, three measured results are compared to MCNP6 simulations. The delayed neutron detection efficiency of the system is determined by MCNP6 and compared to measurements. Wall effects and other nuclear interactions within the ^{3}He detectors were examined in modeling and experimentation. Finally, the magnitude and temporal behavior of DNs produced from SNM after a 60 *s* irradiation were modeled in MCNP6 and compared to measurements. The library-technique and physics-model DN emission options available in MCNP6 were each compared to experimental measurements for ^{233}U, ^{235}U and ^{239}Pu.

6.3 Experimental

Natural and depleted uranium samples were prepared as acidified aqueous solutions from certified reference standard material (CRM 4321C, NIST, Gaithersburg, MD and CRM U005A 0.5064 ± 0.0003 atom% ^{235}U, New Brunswick Laboratory, Argonne, IL). Samples containing ^{233}U were in provided in nitrate form (CRM 111-A, 99.4911 ± 0.0006 atom% ^{233}U, New Brunswick Laboratory) and plutonium solutions, also in nitrate form, were obtained from Eckert & Ziegler (Isotope Products Laboratories Lot #1195.20, 97.937 at% ^{239}Pu, 2.0542 at% ^{240}Pu, 0.0061% ^{241}Pu, 0.0014 at% ^{238}Pu and 0.0010 at% ^{242}Pu, Eckert & Ziegler, Valencia, CA). All standards were further diluted with distilled water and nitric acid (Optima, ThermoFisher Scientific, Ottawa, ON) such that each vial contained between 54 *ng* and 3.79 μg of fissile content. Samples containing 54 – 534 *ng* of ^{235}U were used to examine energy depositions within the detectors and solutions containing between 0.353 and 3.79 μg of fissile content provided large signal to noise ratios (SNRs) for temporal measurements. The irradiation and counting of each fissile isotope was performed in triplicate to decrease stochastic uncertainty contributions to the measurements. Each solution was encapsulated in a 1.5 *ml* polyethylene vial and heat sealed before being placed in a larger 7 *ml* polyethylene vial (LA Packaging, Yorba Linda, CA).

System hardware and software have been described in detail elsewhere (Sellers *et al*., 2012a). Once the fissile samples were prepared they were sent via pneumatic tubing to an inner irradiation site within the SLOWPOKE-2 reactor. Previous studies of neutron flux spectra within SLOWPOKE-2 reactors have found inner irradiation site *thermal:epithermal* and *thermal:fast* flux ratios of 19.8 ± 0.4 and 4.0 ± 0.1, respectively (Kennedy *et al*., 2000). Measurements of thermal neutron flux magnitude in the DNC system irradiation site were performed with 5 hour irradiations of ^{59}Co flux wires (ESPI Metals, Ashland, Oregon) which were counted for 18 hours with a HPGe detector (GMX4094-70-S, Ortec, TN). A 2 hour delay before the commencement of counting minimized ^{60m}Co contributions ($t_{1/2}$ = 10.5 *min*). Detector effects were examined while the SLOWPOKE-2 reactor was operating at half power (the typical operational state for this reactor) with a measured thermal neutron flux of 5.5 x 10^{11} $cm^{-2}s^{-1}$ (± 5 %) in the DNC irradiation site. Temporal measurements were performed to maximize the signal to neutron background ratios, thus a higher setting with a corresponding measured thermal flux of 8.8 x 10^{11} $cm^{-2}s^{-1}$ (± 5 %) was employed. After a 60 *s* irradiation, the samples were sent to the DN counting apparatus. This counter consisted of six ^{3}He detectors (RS-P4-1613-202, GE Energy, Twinsburg, OH) embedded in a paraffin moderator. There was up to a 5 *s* delay between the expiration of the irradiation and commencement of neutron recording.

The total neutron count rate, $C(t)_j$ [s^{-1}], recorded by the apparatus after the irradiation of one fissile isotope, *j*, will be a function of DNs emitted from 1 *g* that isotope, $Q(t)$ [$g^{-1}s^{-1}$], the mass [*g*] of the fissile isotope *j*, m_j, the detection efficiency of the system, ε, and any neutron background in the system $B(t)$ [s^{-1}], as shown in Eq. (6.1). $C(t)$ is the total number of DNs recorded over the set measurement interval, which in the case of this work was 0.5 *s*.

$$C(t)_j = Q(t)_j m_j \varepsilon + B(t) \tag{6.1}$$

The many DN precursors are often organized according to their half-life into several groups, each with an associated production ratio, $\alpha_{i\,j}$. This production ratio is the fraction of all DNs emitted from group *i* and dictates the temporal behavior of the DNs emitted from fissile isotope *j*. Grouping the DN precursors allows $Q(t)_j$ to be expressed as follows:

$$Q(t)_j = \frac{\sigma_{f\,j}\nu_{d\,j}\Phi N_A}{MM_j}\sum_{i=1}^{k}\alpha_{i\,j}\left(1-e^{-\lambda_i t_{irr}}\right)\left(e^{-\lambda_i t_d}\right)\left(e^{-\lambda_i t}\right) \tag{6.2}$$

In Eq. (6.2), σ_{f_j} is the thermal fission cross section [b], v_{d_j} is the average number of DNs produced per fission, Φ is the thermal neutron flux [$cm^{-2}\ s^{-1}$], N_A is Avogadro's number [mol^{-1}], MM_j is isotope j's molecular mass [$g\ mol^{-1}$], λ_i is the decay constant for delayed neutron group i [s^{-1}], k is the total number of DN groups used, t_{irr} is irradiation duration [s], t_d is the decay time of the sample before counting initiation [s], and t is the count time [s].

The detection efficiency of the system is the product of geometric efficiency, ε_g, and intrinsic efficiency, ε_{int}, as expressed in Eq. (6.3) (Sher and Untermyer, 1980).

$$\varepsilon = \varepsilon_g \varepsilon_{int} \tag{6.3}$$

Geometric efficiency is the probability that an emitted neutron will penetrate the sensitive part of the ^{3}He fill. It is dependent on the solid angle between the source and detectors and the separating medium. The intrinsic efficiency is the likelihood that a neutron will produce a count once in the active fill and it is dependent on the energy of the incident neutron and the pressure of the fill gas. In ^{3}He detectors the incident neutron reacts with the helium fill and produces a triton (^3_1H) and proton (^1_1H) through the following process (Knoll, 2010):

$$^3_2He + {}^1_0n \rightarrow {}^3_1H + {}^1_1H \qquad\qquad Q = 0.764\ MeV$$

In the case of thermal neutron interactions the total energy produced in the above reaction is 0.764 *MeV*, with the triton and protons having energies of 0.191 and 0.573 *MeV*, respectively. Many reaction products will come into contact with the detector walls and therefore not all of the kinetic energy produced will be recorded by the active fill gas. Thus, the net charge deposited after each triton-proton reaction will range from 0.191 *MeV* (the kinetic energy of a triton) to 0.764 *MeV* and is often referred to as the wall effect. Furthermore, recorded energy is broadened by effects that include variation in gas amplification and recombination (Mazed *et al*., 2012). Also, the measured ^{3}He energy spectra may include low energy contributions from γ-rays (Spaulding *et al*., 2009). In the presence of a high γ-ray background, several of these γ-ray pulses may be recorded at one time, resulting in significant pulse pile up effects and an increase in observed energy (Mazed *et al*., 2012). If pulse pile up effects are severe, they may exceed the energy threshold for neutron events in the detectors (0.191 *MeV*). These pulse pile up effects may also affect the high energy depositions as neutrons and γ-rays may be recorded simultaneously, these would result in a broadening of the energies recorded by the detector. ^{3}He recoils produced by the scattering of an energetic neutron and the partial transfer of its energy to the ^{3}He nucleus are also possible,

however experimental observations showed they are negligible in spectra produced by this experiment.

The characteristics of the DNC system have been previously investigated (Sellers, 2011) with regard to a number of parameters critical to MCNP6 modeling and experimental/model comparisons. The DN detection efficiency of this system was previously determined by irradiating small quantities of natural uranium for 60 *s* (at a measured thermal neutron flux of 5.5e11 $cm^{-2}s^{-1}$) and recording the DNs produced 3 to 63 *s* after the elapse of irradiation. Eqs. (6.1) and (6.2) were then used during the system's commissioning to determine a maximum experimental detection efficiency, ε, of 34 ± 5 % (95% confidence) (Sellers, 2011). This ε value confidence interval was determined via the propagation of flux magnitude measurement, sample preparation, background contributions, and dead time correction uncertainties.

Energy discrimination was used for temporal measurements to reduce the contribution of γ-ray pulse pile ups to the recorded neutron counts and minimize the distortion of measured DN temporal behavior. Inevitably, the employment of energy discrimination also eliminated some of the lower neutron energy depositions, resulting in an operational efficiency, which is lower than the maximum experimental detection efficiency. This change in operational efficiency and its effect on the comparisons are addressed in the results section.

Dead time contributions were accounted for with an empirical correction (Sellers, 2011) to the measured count rates before comparison to MCNP6 simulations. Finally, a time dependent background, *B(t),* was believed to arise from small amounts of uranium content in the irradiation site (Sellers *et al*., 2013). The characteristics of this background were determined by multiple irradiations and the counting of polyethylene vials in the absence of fissile content. This background was removed from the total measured count rate, C*(t),* so that a direct comparison of measured DN emissions and those predicted by MCNP6 could be achieved.

6.4 MCNP6 Modeling

6.4.1 Overview

The MCNP6 modeling was split into three separate parts: a) The irradiation of a vial in a SLOWPOKE-2 reactor to determine the flux energy distribution b) the reproduction of the irradiation flux in a vial containing the SNM solution, and the recording of the time and energy of neutrons emitted from the surface of the

solution vial, and c) the transport and detection of source neutrons with previously tallied energy distributions in the counting apparatus geometry.

6.4.2 Flux in the SLOWPOKE-2 Reactor Irradiation Site

A MCNP model of a SLOWPOKE-2 reactor was provided by Atomic Energy of Canada Limited (AECL) (Nguyen *et al*., 2012). The AECL model was modified to include the PE vial containing water and HNO_3 in an inner irradiation site, to correspond to RMCC measurements. The neutron beam tube unique to RMCC's SLOWPOKE-2 reactor was not included in this model, and the control rod was in a completely withdrawn position. A f4 tally with the WIMS Library Update Project 69 group energy structure recorded the flux energy distributions within the PE vial.

6.4.3 Reproduction of SLOWPOKE-2 Irradiation Conditions and DN emissions

Irradiation conditions were recreated for 60 *s* in a solution containing SNM by using the flux energy distribution recorded from the SLOWPOKE-2 model, and flux magnitude was reproduced with the *wgt* option on the source definition card. Only the solution was included in this model, once a flux or fission neutron left any surface its time and energy was recorded with a F1 tally; and then this neutron was killed to prevent the distortion of SLOWPOKE-2 spectra. A F4 tally confirmed the SLOWPOKE model flux energy distribution was reproduced and *thermal:epithermal* and *thermal:fast* ratios agreed with measurements.

Tallying the temporal behavior of DNs at count times up to three minutes was computationally expensive due to: i) The low fissile content present in the experiments resulting in low probabilities of a source neutron inducing fission, ii) the low probability of a DN emission once a fission process has occurred and iii) the short half-lives of most DN precursors, leading to very few emissions at count times > 60 *s*. Two deviations from the experiment were used in the MCNP6 model to decrease the relative errors associated with tallying DN temporal behavior. These were; *i)* fissile material increases (1000x) in the model relative to experiments[xii], and *ii*) DN biasing options to produce up to 10 DNs per interaction (DNBIAS=10 on the activation (ACT) card (Pelowitz, 2013)).

[xii] This large increase in fissile content (relative to the non-fissile solution) resulted in no significant increase in the net multiplication of solution due to the very subcritical initial amount of fissile material. The density of the simulated solution remained that of the experimental value.

6.4.4 **Counting Geometry and DN Detection**

The DN counting geometry and materials were reproduced in MCNP6 with the physical dimensions measured during apparatus commissioning and material properties provided by manufacturers. Neutrons with MCNP6 DN emission energy distributions were recreated on the solution's surface and interacted with the surrounding polyethylene, paraffin and ^{3}He detectors, Figure 6.1. Each detector had a defined active and inactive zone as described in the manufacturer's specifications. The number of proton/triton pairs that deposit energy in the active zone of the detector was used to determine the DN detection efficiency. This process was repeated for all three isotopes and DN emission options to observe any efficiency dependence on energy spectra changes. The energy distribution used in the previous *sdef* card was also used to examine wall effects and γ-ray background within the helium fill via a pulse height tally, (*F8* [*pulses*]). A Gaussian Energy Broadening (GEB) card (Pelowitz, 2013) was included in each F8 tally with energy bins, to approximate the energy resolution of the ^{3}He detectors. This treatment selects the energy recorded by the detector via sampling from a Gaussian distribution with that full width at half max (FWHM).

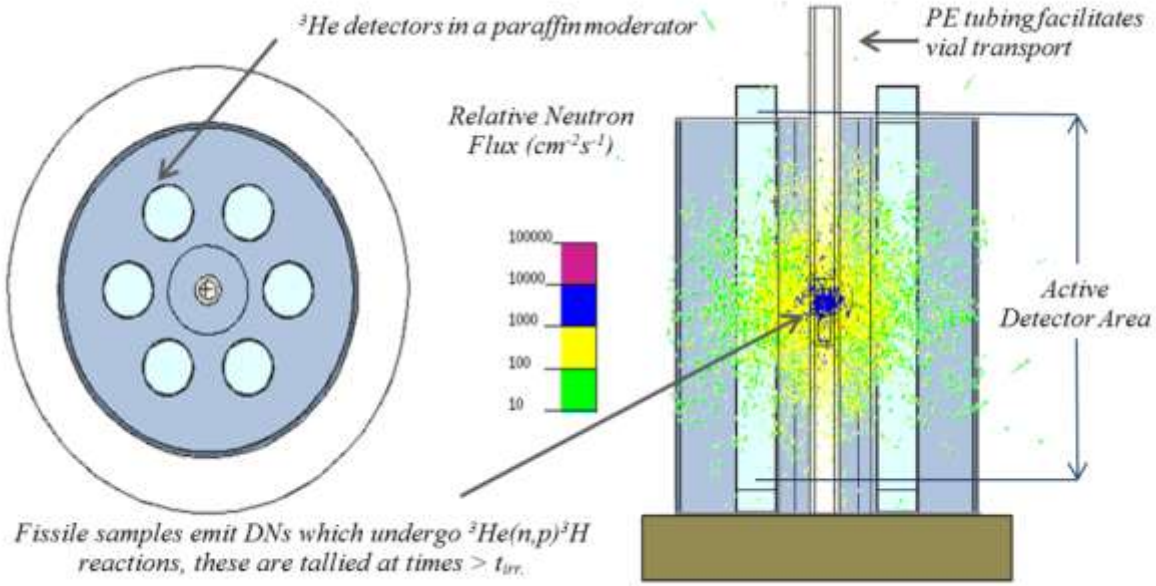

Figure 6.1: An example of MCNP6 counting geometry and DN emission, detector height 36 *cm*.

6.4.5 **Delayed Neutron Emission Options in MCNP6**

Two DN options within MCNP6 were examined: the library-data technique and the physics-model, both of which are described in detail by Durkee *et al.* 2012a. The library-data technique uses ACE data (A Compact ENDF) and is available in the event of neutron induced fission of ^{233}U, ^{235}U and ^{239}Pu examined in this work. The physics-model option uses CINDER'90, a transmutation code (Wilson *et al*., 1995), to calculate the total isotopic concentrations resultant from the radioactive decay of residual nuclides produced by activation or fission events. DN emission probabilities and energies are sampled from DN precursors contained in delay_library_v2.dat (Pelowitz, 2013). The comparison between each output was facilitated by the creation of input files with identical geometry, materials and physics; the only difference between these files being the DN option selected on the ACT card. The physics-model technique was examined by setting DN=model and the library-data technique with DN=library. A third option, DN=both uses physics-models only when library data is unavailable for DN emission (Pelowitz and *et al*., 2005). The ability to account for neutrons produced by non-fission events can also be added by setting the nonfiss=n parameter on the ACT card (by default nonfiss=none in MCNP6). For the following simulations, MCNP6v1 was used (load date:05/08/13).

6.5 Results & Discussion

6.5.1 **Delayed Neutron Detection Efficiency, ε**

Detailed energy spectra from ^{235}U were obtained from DN emissions after a 60 *s* irradiation, 3 *s* decay and 60 *s* count (for both DN=library and DN=model). Neutron energy distributions emitted from the solution surface during the count times were recreated on the surface of the solution within a simulation containing counting geometry and materials. Efficiency was determined by comparing the number of triton/proton pairs that deposited energy in the active portions of the detectors with the number of source particles produced. The energy distributions obtained using DN=library and DN=model each had an ε_{MCNP} value of 35.8 (± 0.2) %, where uncertainties arise from differences in MCNP energy spectra for various DN options and the relative error associated with the MCNP6 tally. Slight variations arose with different isotopes and DN emission option energy spectra but each had an ε_{MCNP} value of 36 %. The SLOWPOKE-2 model flux distribution was used to determine the expected fission rate of ^{235}U provided a new maximum $\varepsilon_{experimental}$ of 35 ± 5 %.

6.5.2 ^{3}He Detector Effects

The energy distribution of the photons and proton/triton pairs produced within the active fill of the ^{3}He detectors was experimentally measured and determined in MCNP6, Figure 6.2. To facilitate a direct comparison, the measured waveform was normalized by equating the counts in energy range of 0.175 – 0.900 *MeV* to that predicted by MCNP6. MCNP6 predicted the general trend of the observed wall effect (an energy independent FWHM value of 0.05 *MeV* was used in simulations); however, there were two discrepancies between experiments and the model; recombination effects, and the energies of the recorded γ-ray backgrounds. The discrepancy between the model and measurements at the higher energies is believed to result from the recombination of ion-electron pairs in the detector.

γ-ray and background contributions to the waveforms are dominant at energies less than 0.175 *MeV* and there are evident differences between MCNP6 simulations and measurements. It is believed that the experimental waveform has higher peak energy when compared to MCNP6 due to pulse pile up effects. It is probable that multiple photons are being recorded simultaneously by the apparatus as one pulse with a total energy that is the summation of individual photons. This hypothesis was proved correct when the γ-ray peak energy for different amounts of fissile material (and therefore different photon production amounts) were examined in the experimental system. As the number of photons incident on the detectors decreased, as did the recorded energy at which the maximum number of γ-ray counts occur. For example, counting of samples containing 534 and 54 *ng* of irradiated ^{235}U had observed γ-ray maxima of 0.062 and 0.029 *MeV*, respectively. This indicates that there were significant pulse pile effects, whose severity was dependent on photon emission rates.

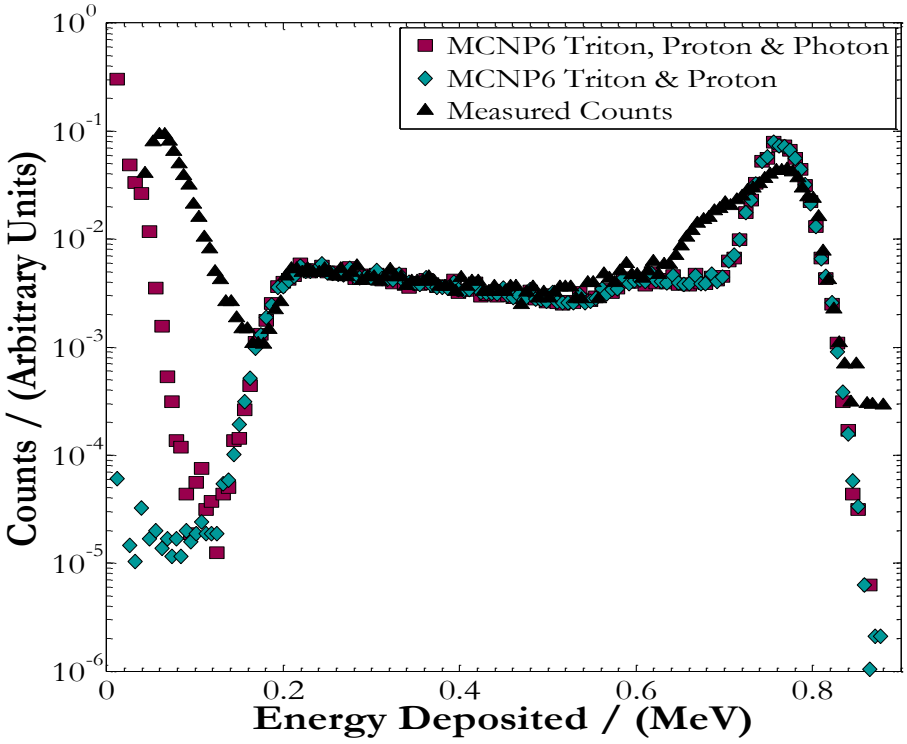

Figure 6.2: MCNP6 and measured ^{3}He spectra, emphasizing photon contributions.

Although there are differences arising from pulse pile up and recombination modeling, the waveform confirmed the assumption that when energy discrimination is employed during typical DNC operation conditions the contributions from photons are negligible.

6.5.3 DN Signatures from ^{233}U, ^{235}U and ^{239}Pu

Energy discrimination bins were used to limit the contributions of photons to the recorded count rates of DN temporal measurements. A comparison of cumulative counts at both maximum detection and operational energy discriminator levels determined a $\varepsilon_{operational}$ value of 33 ± 5 %. Uncertainties arising from experimental flux, sample preparation, background contributions and dead time correction have been incorporated into expressed efficiency. Count rates recorded by the apparatus had the neutron background, *B(t)*, subtracted and were then normalized by $\varepsilon_{operational}$ to determine experimental *Q(t)*. The count time uncertainties are ± 0.5 *s* (95 % confidence).

Figure 6.3 shows a comparison of ^{233}U *Q(t)* measurements and two MCNP6 outputs, (DN=model and DN=library from MCNP6). The final DN option (DN=both) was also examined, and in all cases (^{233}U, ^{235}U and ^{239}Pu) the results for this option did not deviate significantly from DN=library. The original DN=model output deviated significantly from both measurements and library simulations at $t >$ 100 *s*, for all three isotopes examined. The MCNP6 development team confirmed this to be a bug arising from the time bin structure used by DN=model option (Goorley, 2013) to sample delayed neutron emission. Most ^{233}U measurements are in agreement for both the physics-model (excluding > 100 *s* counts) and the library option, Figure 6.3 and 6.4. Normalized ^{239}Pu measurements also agreed well with simulations, Figure 6.5 and 6.6.

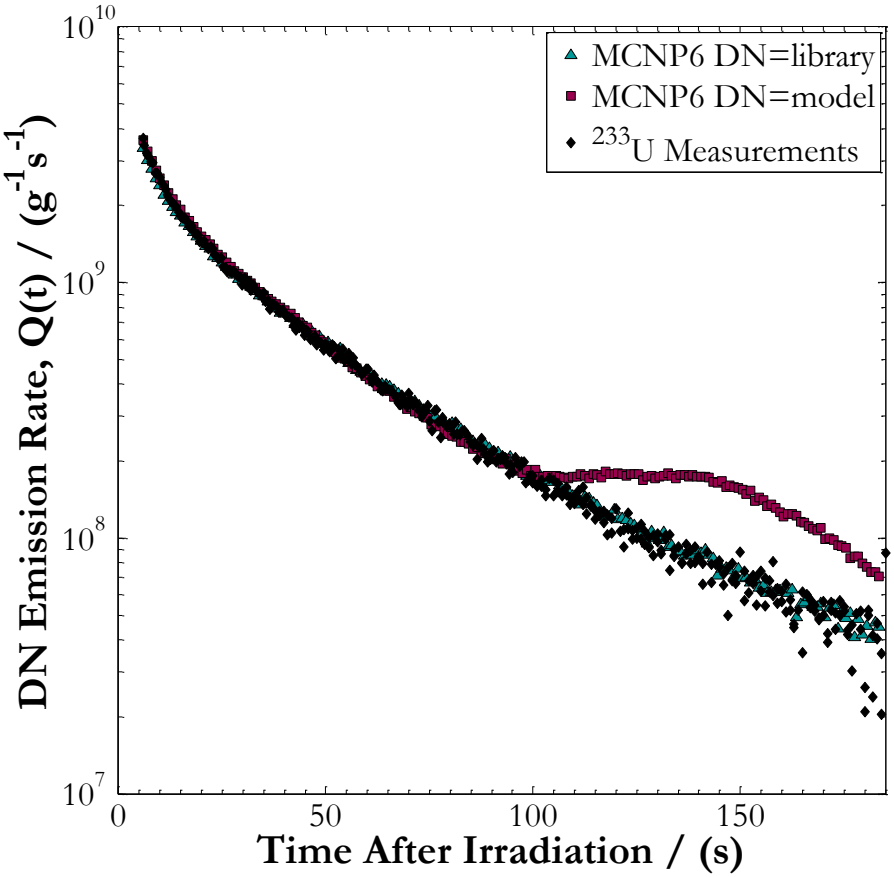

Figure 6.3: Experimental, MCNP6v1 Library and Model DN Emission Rates for ^{233}U.

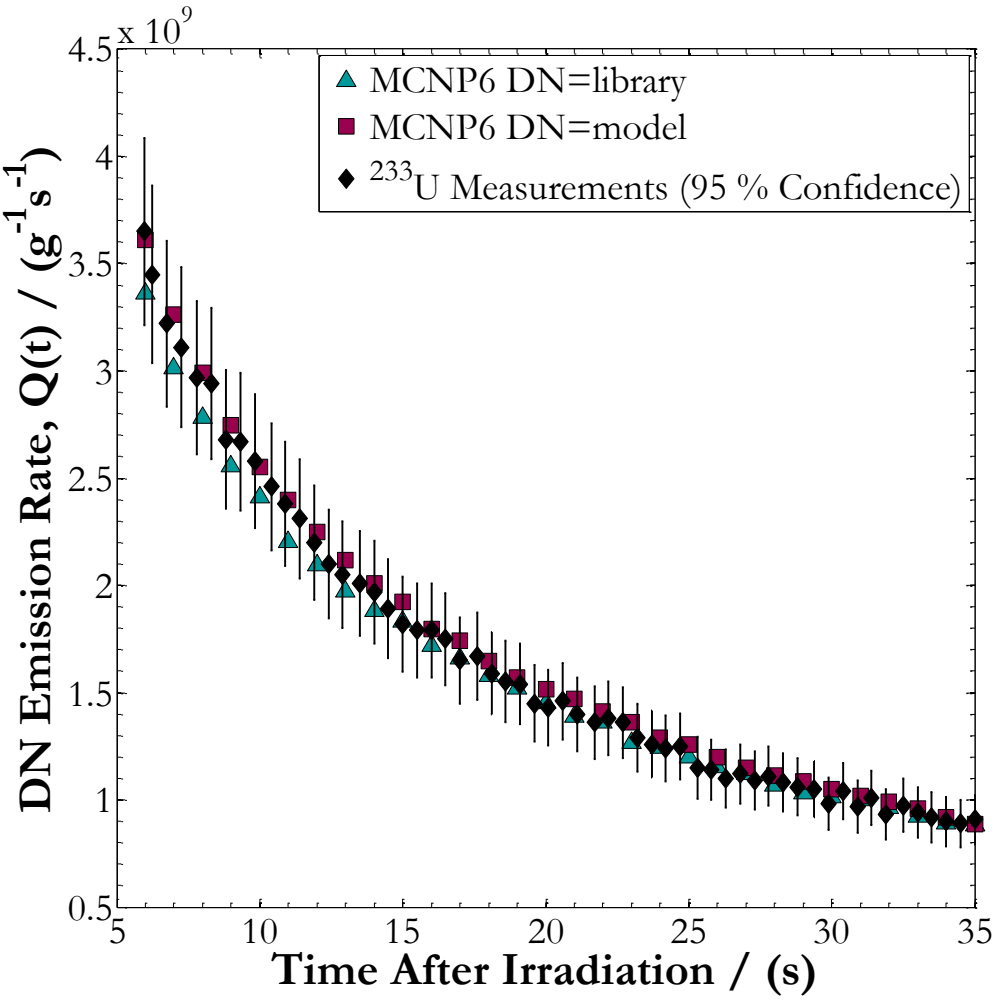

Figure 6.4: Measured DN Emission Rates and MCNP6 Simulations for ^{233}U.

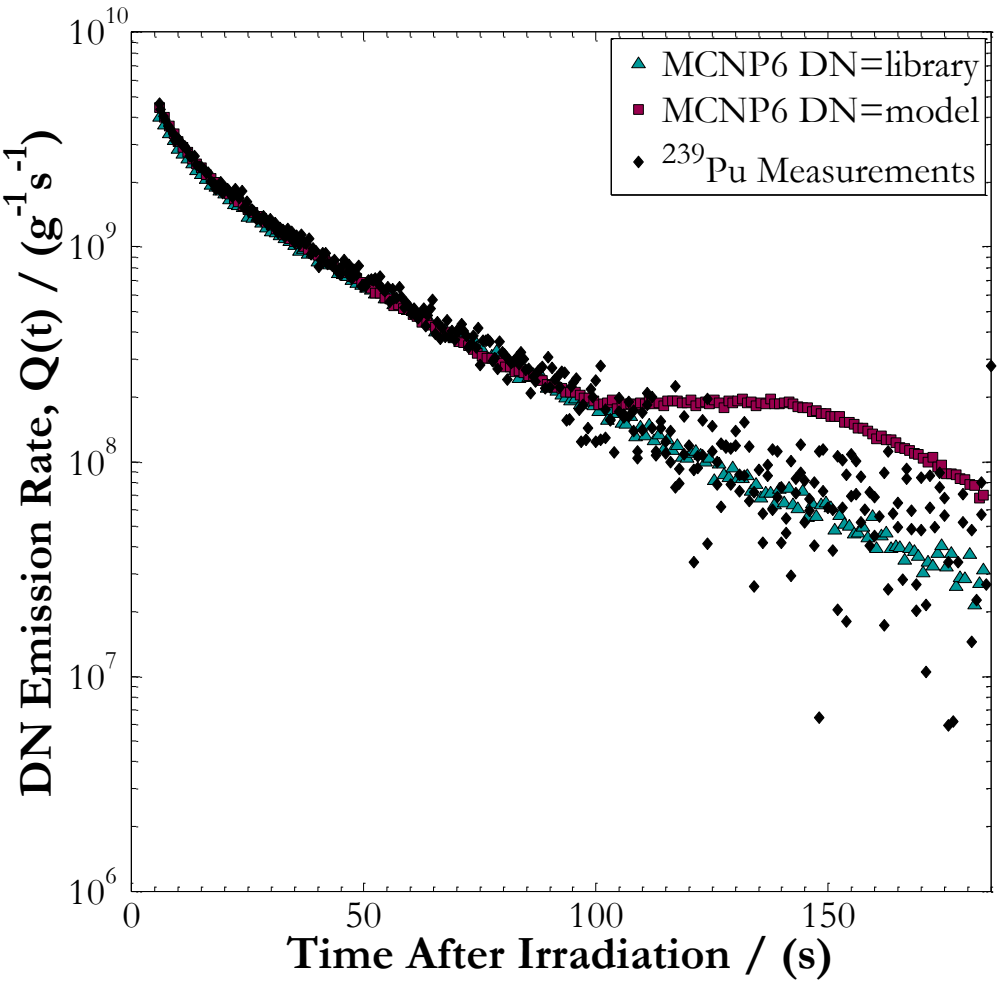

Figure 6.5: DN Emission Rates for ^{239}Pu.

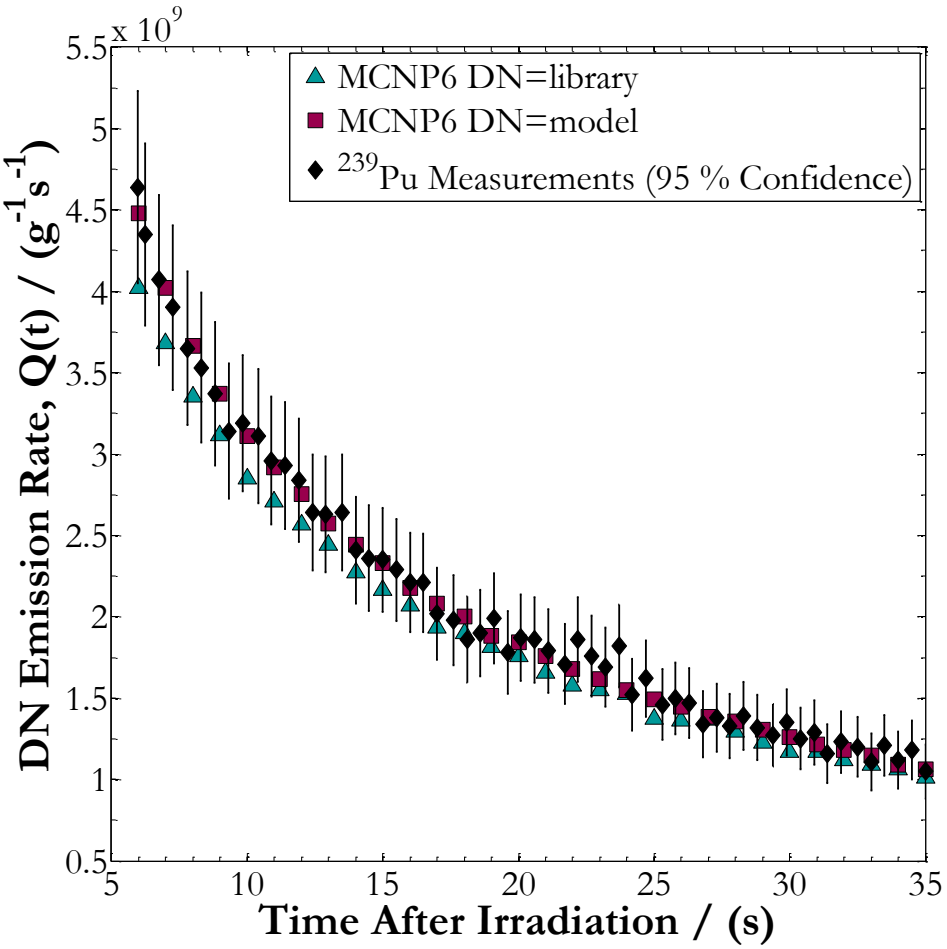

Figure 6.6: Measured DN Emission Rates and MCNP6 Simulations for ^{239}Pu.

The final comparison depicts differences between library, physics-model and measured natural U DN behavior, Figure 6.7 and 6.8. Separate decks were generated to account for ^{238}U fission contributions. ^{238}U DN emission outputs were then normalized to recreate ^{235}U and ^{238}U isotopic abundances in natural U before being added to ^{235}U simulation outputs. The total number of DNs produced was examined for each isotope with nonfission events turned on and off for neutron interactions, the inclusion of these events in the input files found no significant difference in DN yields.

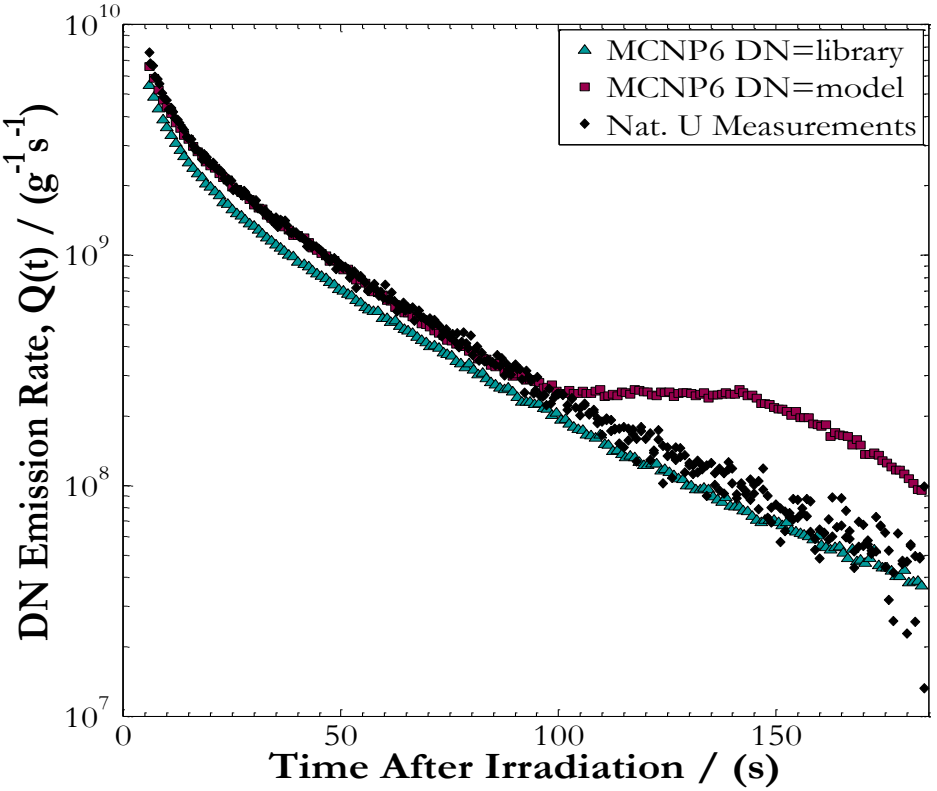

Figure 6.7: Experimental, Library and Model DN Emission Rates for Natural Uranium.

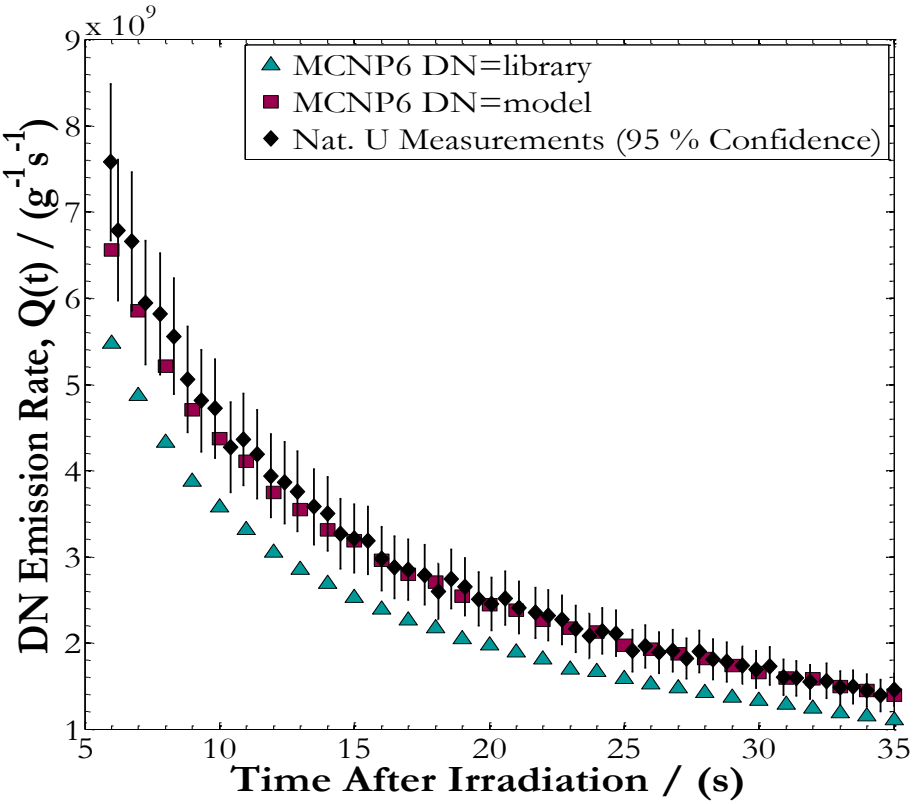

Figure 6.8: Measured Nat. U DN Emission Rates Compared to MCNP6 Simulations.

Differences in DN yield from ^{235}U were found upon the comparison of the DN model and library options, the library-data option in MCNP6 systematically under-predicted observed magnitude. When uncertainties arising from measured flux, fissile content concentration, neutron background and dead time corrections are accounted for, library-data yields were not within experimental uncertainty (95 % confidence) for natural U.

6.6 Conclusions & Future Work

Overall MCNP6 was successful in simulating many aspects of measured DN emissions from irradiated SNM. MCNP6 predicted maximum neutron detection efficiency was in agreement with measurements, 36 % and 35 ± 5 %, respectively. DN emission from the model and library options were compared to measurements from irradiation ^{233}U, ^{235}U and ^{239}Pu and were found to have significant temporal differences for the physics-model DN option in MCNP6. This discrepancy has been acknowledged by MCNP developers as a moderate priority bug (Goorley, 2013) to be addressed in future public releases of MCNP6. Data comparisons between the relatively simple experimental system and simulation have served to validate and improve MCNP6. Similarly, experimental artifacts are readily identified by comparisons between experimental and simulated data. As a consequence, steps to reduce measured recombination and pulse pile up effects have been incorporated into an experimental apparatus upgrade, which also includes the capability to simultaneously record delayed neutrons and gamma-rays from SNM. The success of these upgrades and comparisons to MCNP6 will form part of future studies.

6.7 Acknowledgements

Funding was provided by the Advanced Simulation and Computing program at Los Alamos National Laboratory, the Director General Environment and Nuclear Safety and the Natural Sciences and Engineering Research Council of Canada. Also, the authors would like to Kathy Nielsen and Dave Ferguson for assisting in experimentation for this project. Finally, the technical work of Steve White, John Shaw, Matthew Mackay, and Clarence McEwen is greatly appreciated.

-This page is intentionally left blank-

Chapter 7

MCNP6.1.1 Beta Test Suite Comparisons to Delayed Neutron Measurements of ^{233}U, ^{235}U, and ^{239}Pu at the Royal Military College of Canada

M.T. Andrews[1,2], T.L. Beames-Canivet[1], D.G. Kelly[1], E.C. Corcoran[1], J.T. Goorley[2]

[1]Department of Chemistry and Chemical Engineering,
Royal Military College of Canada
P.O. Box 17000 Stn. Forces
Kingston, Ontario, Canada K7K 7B4

[2]XCP-3 Monte Carlo Codes
Los Alamos National Laboratory[xiii]

[xiii] **M.T. Andrews**, T.L. Beames-Canivet, D.G. Kelly, E.C. Corcoran, J.T. Goorley, "MCNP6.1.1 Beta Test Suite Comparisons to Delayed Neutron Measurements of ^{233}U, ^{235}U, and ^{239}Pu at the Royal Military College of Canada" *Los Alamos National Laboratory Technical Report,* LA-UR-14-26251 (2014).

Title: MCNP6.1.1 Beta Test Suite Comparisons to Delayed Neutron Measurements of ^{233}U, ^{235}U, and ^{239}Pu at the Royal Military College of Canada.

Author(s): M.T. Andrews[1,2], T.L. Beames-Canivet[1], D.G. Kelly[1], E.C. Corcoran[1], J.T. Goorley[2]

[1] *Royal Military College of Canada, P.O. Box 17000 Stn Forces, Kingston, ON, K7K 7B4,*
[2] *Los Alamos National Laboratory, Los Alamos, NM, 87545*

Intended for:

- An update to LA-UR-14-25702, which compared the MCNP6.1 simulations to measurements.
- Inclusion in M.T. Andrew's RMCC PhD dissertation.

Accompanying Materials:

- 6 updated MCNP input decks simulating delayed neutron emissions from SNM.

Date: August 2014

7.1 Overview

This brief report contains updated delayed neutron (DN) test suite comparisons of MCNP6.1.1Beta to measurements from ^{233}U, ^{235}U, and ^{239}Pu. MCNP simulations recreate the irradiation of milligram quantities of special nuclear materials (SNMs) in aqueous solutions for 60 *s*. DN magnitudes and temporal behaviors are recorded with F1 tallies and compared to measurements performed at the Royal Military College of Canada. DN emissions of ^{233}U, ^{235}U (contained in Nat. U) and ^{239}Pu were examined up to 3 minutes after the elapse of irradiation, using the three DN options available in MCNP6.1.1 Beta (DN=model, DN=library, and DN=both). This report also demonstrates the improved agreement between measurements and DN=model simulations in MCNP6.1.1 Beta when compared to MCNP6.1 outputs (Andrews *et al*., 2014a).

7.2 Experimentation

Solutions containing ^{233}U, ^{239}Pu and natural uranium were prepared from certified reference material standards and further diluted with nitric acid and distilled water. Samples were placed in polyethylene vials before pneumatic transport to an inner SLOWPOKE-2 research reactor irradiation site where they were exposed to a predominately thermal neutron flux for 60 *s*. After irradiation the samples were sent to an array of ^{3}He detectors, which recorded the DN emissions as a function of count time for up to 3 minutes. Further details regarding the delayed neutron counting system and these measurements can be found in (Sellers *et al*., 2012a). Experimental data has been corrected for dead time effects and neutron background contributions (Sellers *et al*., 2013). **Measurements have been normalized by fissile mass [*g*] and detection efficiency (33 *%*) to obtain DN emission rate, *Q(t)* [$s^{-1}g^{-1}$].** Each isotope (^{233}U, ^{235}U, and ^{239}Pu) was irradiated and counted in triplicate; the provided measurements represent their average *Q(t).* Plots with error bars included represent the 95 *%* confidence interval on measurements.

7.3 MCNP Simulations

Atomic Energy of Canada Limited has provided a MCNP input deck containing LEU SLOWPOKE-2 dimension and material specifications, the contents of which are detailed in (Nguyen *et al*., 2012). This input deck was modified to include a polyethylene vial within an inner irradiation site to determine a higher fidelity neutron flux spectrum. This flux was recreated within the vial solution of a second

input deck, which includes the irradiation of a fissile solution for 60 *s* and the recording of subsequent DN emissions from the vial. The DN emission rate, *Q(t)* [$s^{-1}g^{-1}$], for each MCNP6 simulation was compared to the normalized measurements described in the previous section. Further details on MCNP simulations are included in (Andrews *et al*., 2014b). An example of an input deck is shown in Section 0.

7.4 Comparisons

7.4.1 MCNP6.1.1 β DN=model, library, and both.

Figure 7.1 compares the measurements of DN emissions for ^{233}U and MCNP6.1.1 beta simulations using the three DN emission options. The DN=both option is omitted in subsequent comparisons because it is indistinguishable from the DN=library option. Figure 7.2 - 7.4 compare the DN emission rate for ^{233}U, ^{235}U (in Nat. U), and ^{239}Pu, using the DN=model and DN=library options in MCNP6.1.1 beta.

7.4.2 MCNP6.1.1 β comparisons to MCNP6.1

Simulations using MCNP6.1 and the DN=model option resulted in deviations from measurements at approximately 100 *s* because of the time-bin structure used to sample delayed particle emissions (Goorley, 2013). MCNP6.1.1 beta contains updates to the delayed particle time-bin structure (Goorley, 2014), which eliminates the 100 *s* anomaly, shown in Figure 7.5 - 7.7. Figure 7.9 - 7.10 compare DN emission rates using the DN=library option with MCNP6v1 and MCNP6.1.1 beta, which remained the same between versions. Figures 7.11 – 7.13 depict measurements with 95 % confidence intervals.

7.5 Summary

DN emissions from ^{233}U, ^{235}U, and ^{239}Pu were compared to MCNP61.1 Beta simulations using the DN=model, both, and library options. Significant improvements in the agreement with measurements and the MCNP6.1.1 Beta DN=model option are noted when compared to MCNP6.1 simulations.

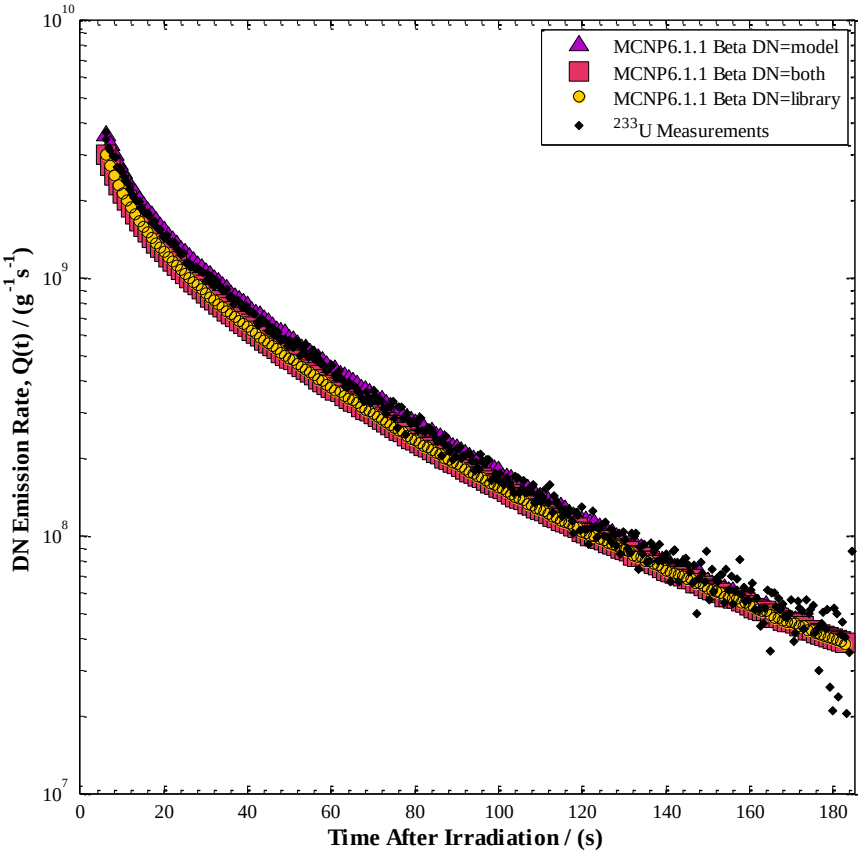

Figure 7.1: Delayed neutron emission rates from ^{233}U measurements and three DN options in MCNP6.1.1 Beta simulations.

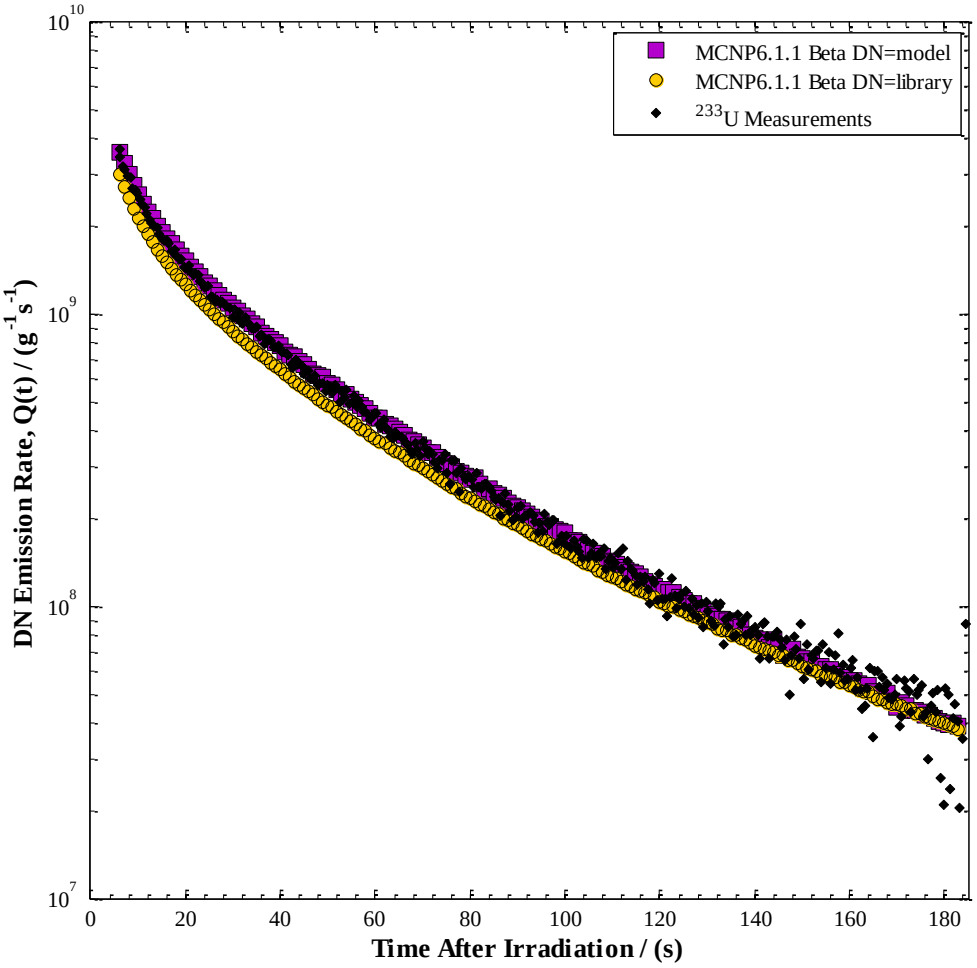

Figure 7.2: Delayed neutron emission rates from ^{233}U measurements, model and library DN options in MCNP6.1.1 Beta simulations.

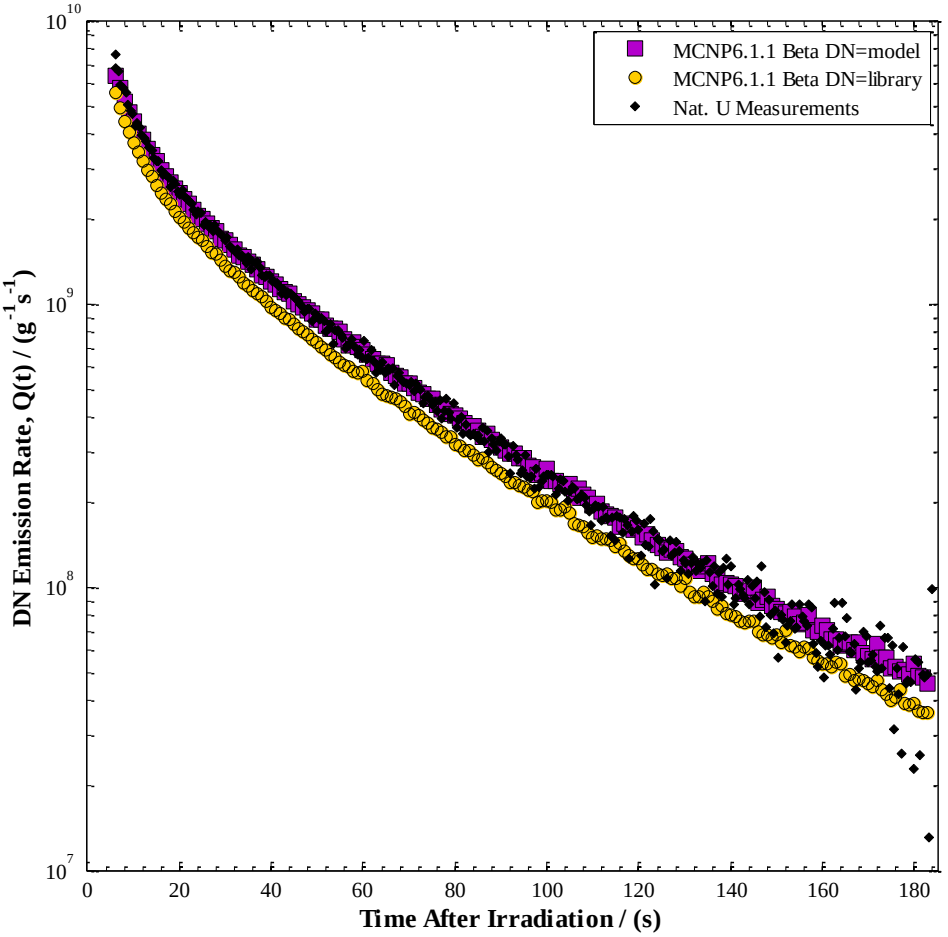

Figure 7.3: Delayed neutron emission rates from nat. U measurements, model and library DN options in MCNP6.1.1 Beta simulations.

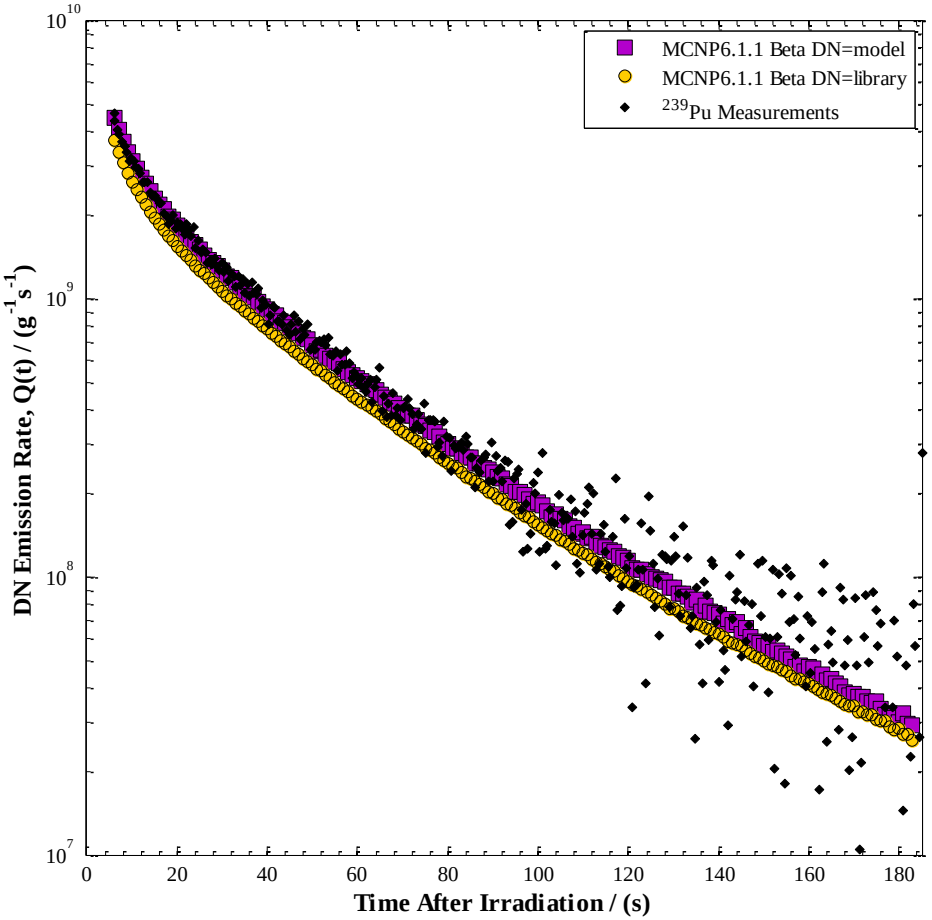

Figure 7.4: Delayed neutron emission rates from ^{239}Pu measurements, model and library DN options in MCNP6.1.1 Beta simulations.

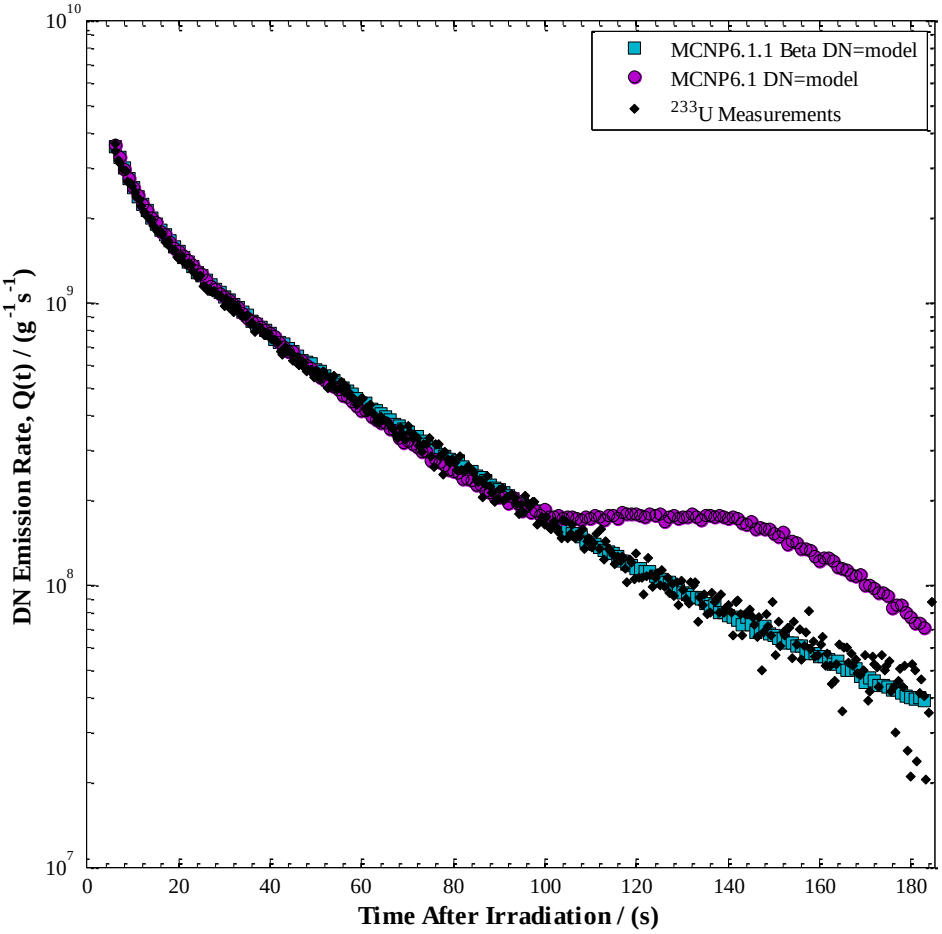

Figure 7.5: Delayed neutron emission rates from ^{223}U measurements, DN=model simulations with MCNP6.1 and MCNP6.1.1 Beta.

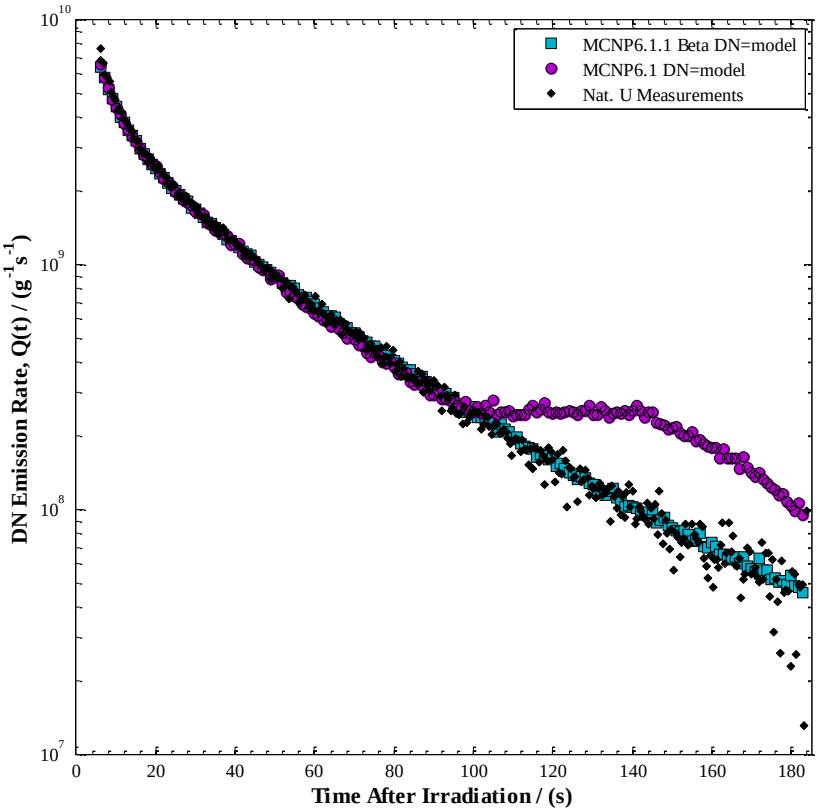

Figure 7.6: Delayed neutron emission rates from nat. U measurements, DN=model simulations with MCNP6.1 and MCNP6.1.1 Beta.

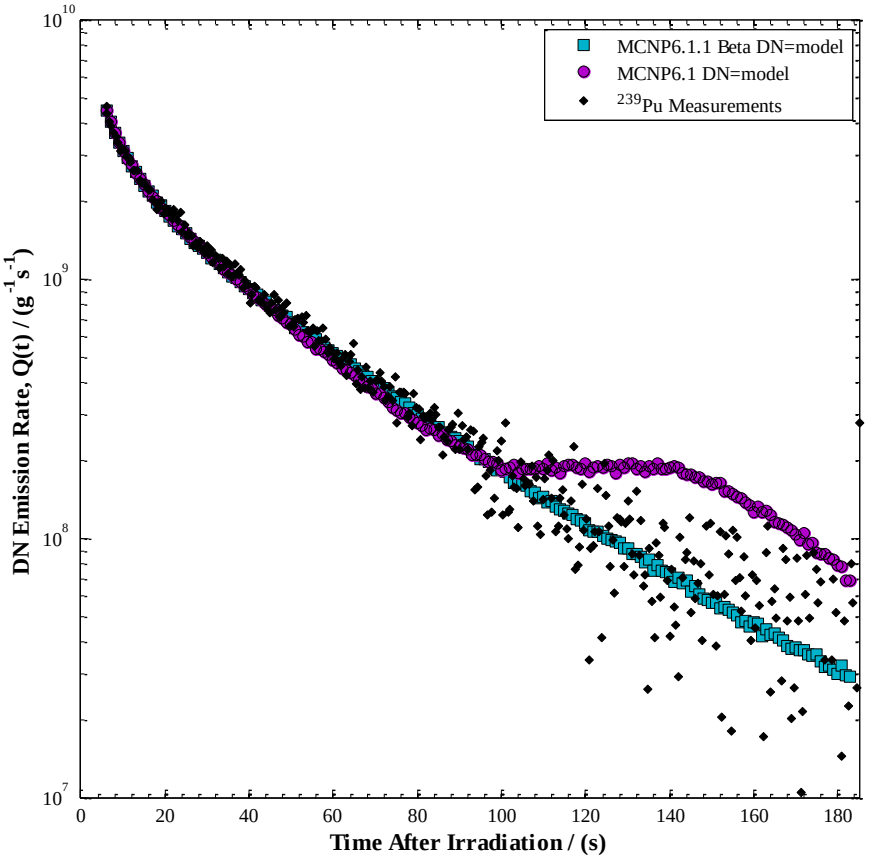

Figure 7.7: Delayed neutron emission rates from ^{239}Pu measurements, DN=model simulations with MCNP6.1 and MCNP6.1.1 Beta.

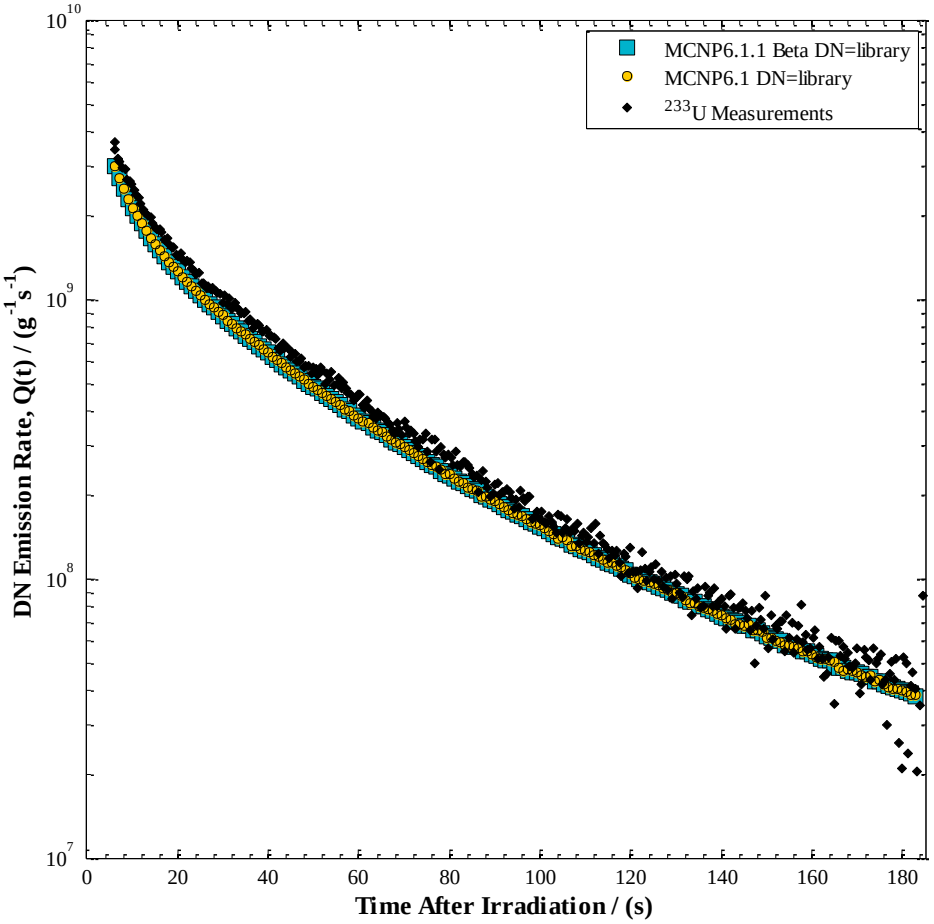

Figure 7.8: Delayed neutron emission rates from ^{223}U measurements, DN=library simulations with MCNP6.1 and MCNP6.1.1 Beta.

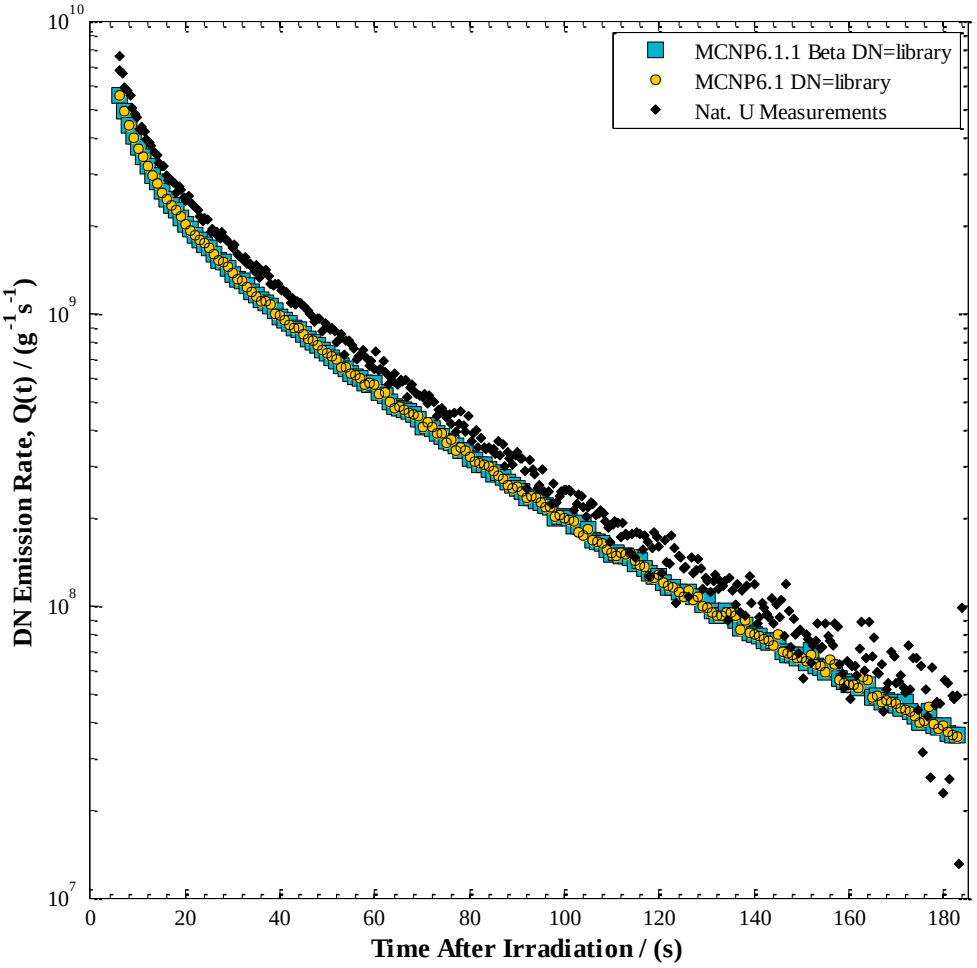

Figure 7.9: Delayed neutron emission rates from nat. U measurements, DN=library simulations with MCNP6.1 and MCNP6.1.1 Beta.

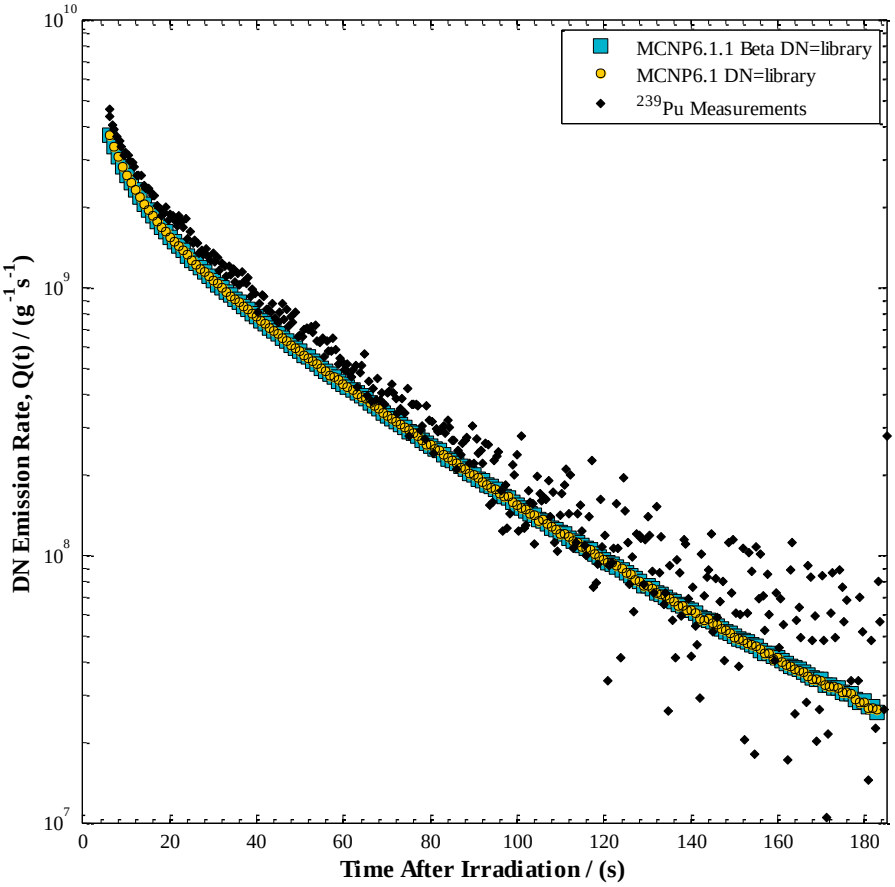

Figure 7.10: Delayed neutron emission rates from ^{239}Pu measurements, DN=library simulations with MCNP6.1 and MCNP6.1.1 Beta.

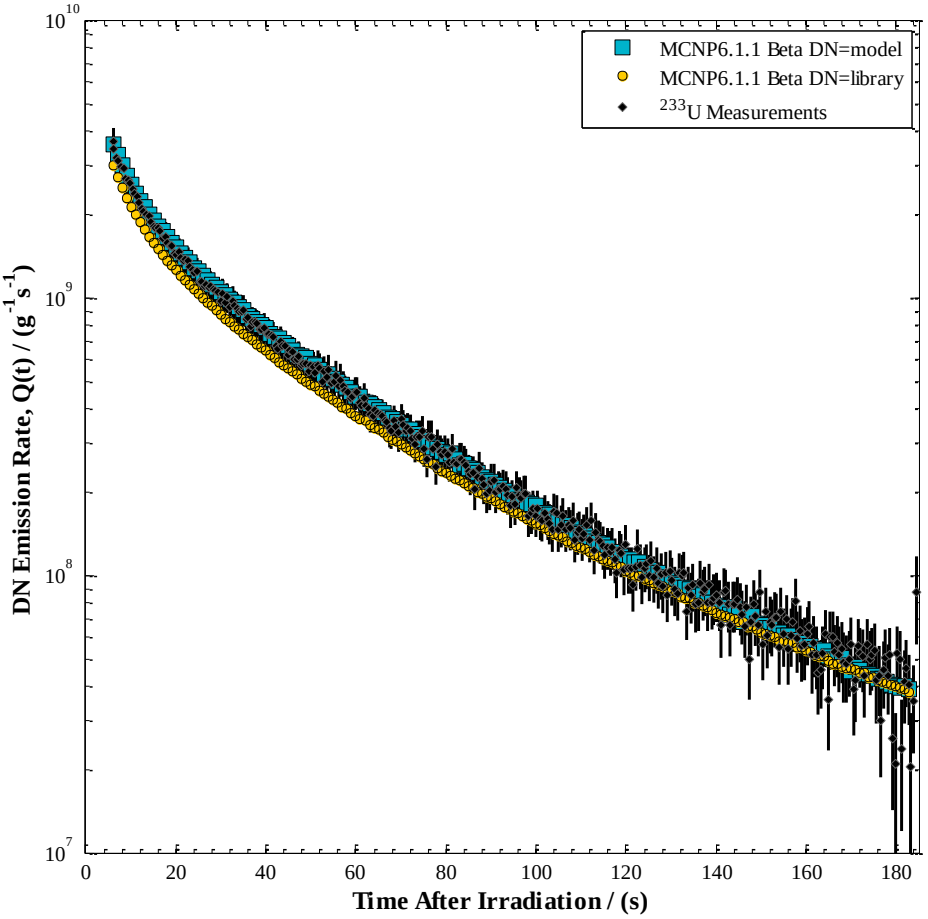

Figure 7.11: Delayed neutron emission rates from ^{233}U measurements, model and library DN options in MCNP6.1.1 Beta simulations. Error bars represent 95 % confidence intervals.

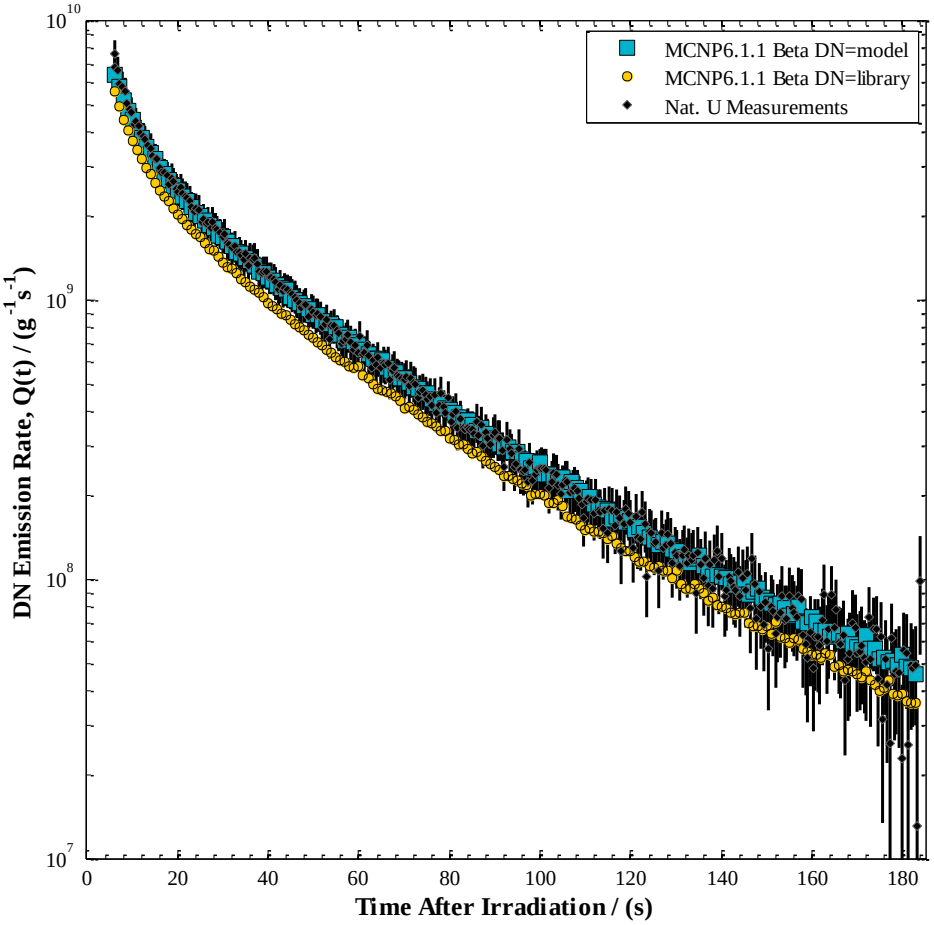

Figure 7.12: Delayed neutron emission rates from nat. U measurements, model and library DN options in MCNP6.1.1 Beta simulations. Error bars represent 95 % confidence intervals.

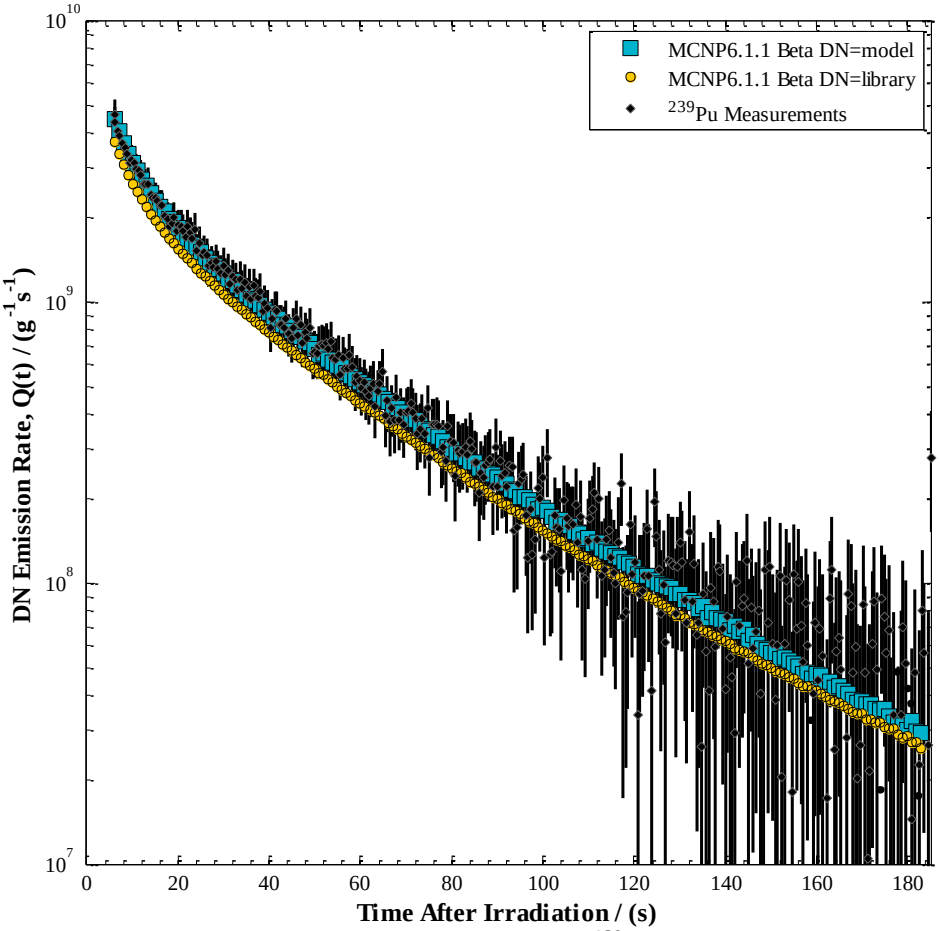

Figure 7.13: Delayed neutron emission rates from ^{239}Pu measurements, model and library DN options in MCNP6.1.1 Beta simulations. Error bars represent 95 % confidence intervals.

7.6 Example of an Input Deck

```
Modeling Delayed Neutron Emissions in RMCC's DNC System
c
c ----------------------------GEOMETRY-------------------------------------
c
  27  5000   -0.9977    -509   $ top smaller vial solution
      imp:n=1
c
  30     0              509   $ geometry void
      imp:n=0
c

c ----------------------SURFACE CARDS-------------------------------------------------------
c
 509       rcc 0 0 17.3            0 0 1.38       0.4826   $ top small vial solution
c

c --------------------------MATERIAL AND SOURCE CARDS-----------------------------------
c
mode  n
c
 ACT
      DN=both   $ change between DN=model, DN=both and DN=library
      DNBIas=10   $ biases the # of DNs produced
c
c ------------------------------MATERIAL DEFINITIONS-----------------------------------
c
m5000
       94239      -2.14e-3   $ 94239 for Pu239, 92233 for U233, 92235 for U235
       1001       -0.10531
       8016       -0.87777
       7014       -0.01478
mt5000  lwtr.10t
c
c ------------------------SOURCE DEFINITION-----------------------------------------
c
sdef pos=0 0 18.0 par=n cel=27
    Rad=D2 Ext=D3 AXS 0 1 0
c To be used when reproducing flux magnitude
    erg=d4 tme=d1   wgt=1.92e14   $ accounts for flux and mass norms
c
c                    Irradiation Time (shakes)
si1 H 0 60e8
sp1 D 0 1
c
si2 H 0 0.4826
sp2 -21 1
si3 -0.7 0.7
c                   Particle Time, Weight and Energy Cut-Offs
cut:n 243e8 j 0 0
```

```
c
F1:n (509.1 509.2 509.3)
T1: 63e8 179i 243e8
c
F44:n 27   $ checking the flux distribution
E44: 0.625e-6 0.5 10
T44: 1e8 243e8
c
c si4 & sp4 reproduce the 69 energy group neutron flux of the SLOWPOKE-2 (omitted from report).
```

-This page is intentionally left blank-

Chapter 8

A System for the Measurement of Delayed Neutrons and Gammas from Special Nuclear Materials

M.T. Andrews[1,2], E.C. Corcoran[1], J.T. Goorley[2], D.G. Kelly[1]

[1]Royal Military College of Canada
P.O. Box 17000 Stn Forces
Kingston, ON, K7K 7B4[xiv]

[2]Monte Carlo Codes and Radiation Transport Applications
Los Alamos National Laboratory
Los Alamos, NM, 87545.

[xiv] **M.T. Andrews**, E.C. Corcoran, J.T. Goorley, and D.G. Kelly, "A System for the Measurement of Delayed Neutrons and Gammas from Special Nuclear Materials" *Journal of Radioanalytical and Nuclear Chemistry (2015)* in press. DOI: 10.1007/s10967-014-3786-6.

8.1 Abstract

The delayed neutron counting (DNC) system at the Royal Military College of Canada has been upgraded to accommodate concurrent delayed neutron and gamma measurements. This delayed neutron and gamma counting (DNGC) system uses a SLOWPOKE-2 reactor to irradiate fissile materials before their transfer to a counting arrangement consisting of six ^{3}He and one HPGe detector. The application of this system is demonstrated in an example where delayed neutron and gamma emissions are used in complement to examine ^{233}U content and determine fissile mass with an average relative error and accuracy of -2.2 and 1.5 %, respectively.

Keywords: delayed neutron, delayed gamma, nuclear forensics, MCNP.

8.2 Introduction

Nuclear forensics relies on the use of analytical techniques to identify properties of illicit nuclear materials, which may include, their origin, intended use, production method, previous owners, and smuggling routes (Mayer *et al*., 2005). These measurements should be performed by validated analytical methods, with ISO or similar protocols, and in conjunction with the analysis of certified reference material (Leggitt *et al*., 2009). Ideal nuclear forensic analysis methods would be accurate, rapid, and sensitive (Grogan and O'Kelly, 2014). The conclusion of the 2014 Nuclear Security Summit saw both the international community and the Canadian government reiterate their commitment to the development of nuclear forensics methods and tools (NSS, 2014a, 2014b). Canada continues to evaluate its nuclear forensics capabilities through participation in exercises organized by the International Technical Working Group (AECL, 2014; Larsson and Haslip, 2004). The Royal Military College of Canada (RMCC) supports Canadian nuclear forensics efforts through the provision of analytical instrumentation for SNM assay. The nuclear laboratory at RMCC is licenced to handle SNM and has a SLOWPOKE-2 nuclear reactor for neutron interrogation. This site also has microgram quantities of ^{233}U, natural and depleted uranium, and ^{239}Pu certified reference materials for instrumentation calibration and validation.

The measurement of DN emissions from fissioned SNM has been identified as a valuable nuclear forensics tool as it is a non-destructive, rapid, and an accurate form of assay (Durkee *et al*., 2012; Eriksson *et al*., 2013; Grogan and O'Kelly, 2014; Kapsimalis *et al*., 2013). The yield and temporal behaviour of DN emissions are dependent on the fissioned material (Keepin *et al*., 1957), and these have been used to characterize mixtures of U and Pu content (Kapsimalis *et al*.,

2013; Li *et al*., 2004; Myers *et al*., 2006; Sellers *et al*., 2012b). The Royal Military College of Canada designed a delayed neutron counting (DNC) system to support nuclear forensics capabilities available to the Canadian government (Sellers *et al*., 2012a). Samples were irradiated, and then transferred to a ^{3}He detector arrangement, which recorded the resulting DN emissions and their temporal behaviour. This system was shown to be a non-destructive and rapid means of identifying and characterizing SNM (Sellers *et al*., 2012b). Furthermore, it was used to examine DN emission simulation capabilities of the widely-used Monte Carlo code, MCNP6 (Goorley *et al*., 2012). Measurements by the DNC system were used to identify discrepancies in MCNP6 simulated DN yields at count times greater than 100 *s* (Andrews *et al*., 2014b). These discrepancies were addressed in the newest version of MCNP6, MCNP6.1.1beta (Goorley, 2014).

As research efforts at RMCC have been expanded to include the non-destructive assay of fissionable content, an expansion of analytical capabilities was required. Delayed gamma (DG) emissions from fission products can be examined to further characterize unknown SNMs (Beddingfield and Cecil, 1998; Marrs *et al*., 2008; Norman *et al*., 2004). In addition, the neutron capture of ^{238}U yields a prominent 75 *keV* emission from ^{239}U decay (Haciyakupoglu and Gencay, 1999). DN emissions from ^{238}U were limited in the DNC system due to the highly thermalized reactor flux used for neutron interrogation. System detection capabilities have been expanded to accommodate concurrent delayed gamma (DG) and DN measurements from SNM. This paper describes these system upgrades, which have culminated in a replacement delayed neutron and gamma counting (DNGC) system capable of providing extensive SNM characterisation. MCNP6 simulations of the irradiation and counting processes were used to design and characterize the system, and confirm experimental measurements. System capabilities are demonstrated via the analyses of ^{233}U solutions.

8.3 Experimental and Simulations

8.3.1 Sample Preparation, Irradiation and Counting Process

Fissile samples were prepared from certified reference material (natural U CRM 4321C, NIST, Gaithersburg, MD, CRM 111-A, 99.4911 ± 0.0006 atom% ^{233}U, New Brunswick Laboratory, Argonne IL) and placed in 1.5 *ml* polyethylene vials (LA Packaging, Yorba Linda, CA). They were diluted with a 2 % nitric acid solution before double encapsulation in a 7.0 *ml* transport vial. Samples were placed in the system loader before being sent to a SLOWPOKE-2 irradiation site with a nominal thermal neutron flux of 2.6 x 10^{11} $cm^{-2}s^{-1}$, from which they were

transported to the counting arrangement, positioned within the reactor room. Transfer to and from the SLOWPOKE-2 is facilitated by pneumatic tubing running along the wall and underneath the reactor room flooring. There is a programmed 3 *s* delay between irradiation and the initiation of counting; during which the sample has enough time to reach the counting arrangement. The low enriched uranium SLOWPOKE-2 reactor (Hilborn and Townes, 1987) at RMCC has 9 irradiation sites, 4 inside the beryllium reflector, and 5 outside. Inner sites have a maximum thermal neutron flux of 10^{12} $cm^{-2}s^{-1}$ and SLOWPOKE-2 thermal to fast ratios, f_F, have been measured to range from of 4.0 ± 0.1 to 17.3 ± 0.5 (Kennedy *et al*., 2000) for inner and outer sites, respectively. Upon the elapse of count time, samples were sent to the storage site where they were retrieved for further experimentation, stored for future use, or disposed of.

8.3.2 System Hardware Control

A custom LabVIEW™ program written at RMCC controlled the original DNC system hardware. Users were able to select irradiation, decay, and count times before a sample's transport became automated. The DNGC system upgrade featured several improvements to the LabVIEW™ capabilities and interface, Figure 8.1. Experimental parameters, which may be chosen by the user, were expanded to include irradiation, decay, count, and dwell times for both neutron and gamma detection. In addition, the capability to alter timings on valves that control the pneumatics of the system is now available; a useful option in the event of counter, irradiation site, or storage site relocation. The program also prompts the user to specify experimental parameters including reactor flux settings, applied detector voltages and any additional experimental notes, which are saved alongside measurements from selected detectors at the end of a run.

8.3.3 The Counting Arrangement

The DNC system had six ^{3}He detectors (RS-P4-1613-202, GE Energy) positioned 8.3 *cm* from the centre of the source location in the counter, embedded in paraffin. ^{3}He detectors are 36 *cm* high and 2.54 *cm* in radius. The sample was surrounded by a PE tube with a wall thickness of 0.45 *cm* and diameter of 2.6 *cm*. The DNGC system has the same ^{3}He detectors, which have been rearranged to accommodate a high purity germanium detector (GMX-1890, Ortec, TN, 18 % relative efficiency); the latter being a minimum of 9.0 *cm* from the source's centre, its distance can be increased if desired. Half a centimetre of lead shields the ^{3}He detectors from the sample's gamma radiation, Figure 8.2. The ^{3}He detectors are surrounded by paraffin and were moved from a previous distance of 8.3 ± 0.2 to 9.0 ± 0.1 *cm* from

the axial centre of the sample. ^{3}He detectors are connected in parallel to a preamplifier (ORTEC 142, Oak Ridge, TN), voltage supply (ORTEC 556), amplifier (ORTEC 575A) and a multichannel analyzer (ORTEC 919E). The HPGe detector is connected to a DSPEC plus (ORTEC) which is a AC-powered, stand-alone unit. The original DNGC system is currently in the reactor room, 3 *m* from the edge of the SLOWPOKE-2 pool.

8.3.4 Efficiency and Waveform Property Determinations

The neutron detection efficiency and waveform properties of the DNGC system were determined after the 60 *s* irradiation and 10 *s* decay of 49 *mg* of nat. U prepared from CRM. Background contributions of empty polyethylene vials were subtracted and dead time corrections applied before the determination of cumulative counts recorded for 50 *s*. Relative detector efficiencies for each ^{3}He detector were examined by counting weak, uncalibrated, ^{252}Cf samples for 5-minute intervals. Each neutron measurement was repeated in the absence of a source to determine appropriate background subtractions. The relative energy-dependent intrinsic detection efficiency of the HPGe detector was determined with the use of a multi-nuclide radioactive decay standard source (source 1423-99-21, Eckert & Ziegler, Valencia, CA) containing 13 isotopes with energies ranging from 47 *keV* to 1.8 *MeV*, placed on the exterior of the detector's endcap.

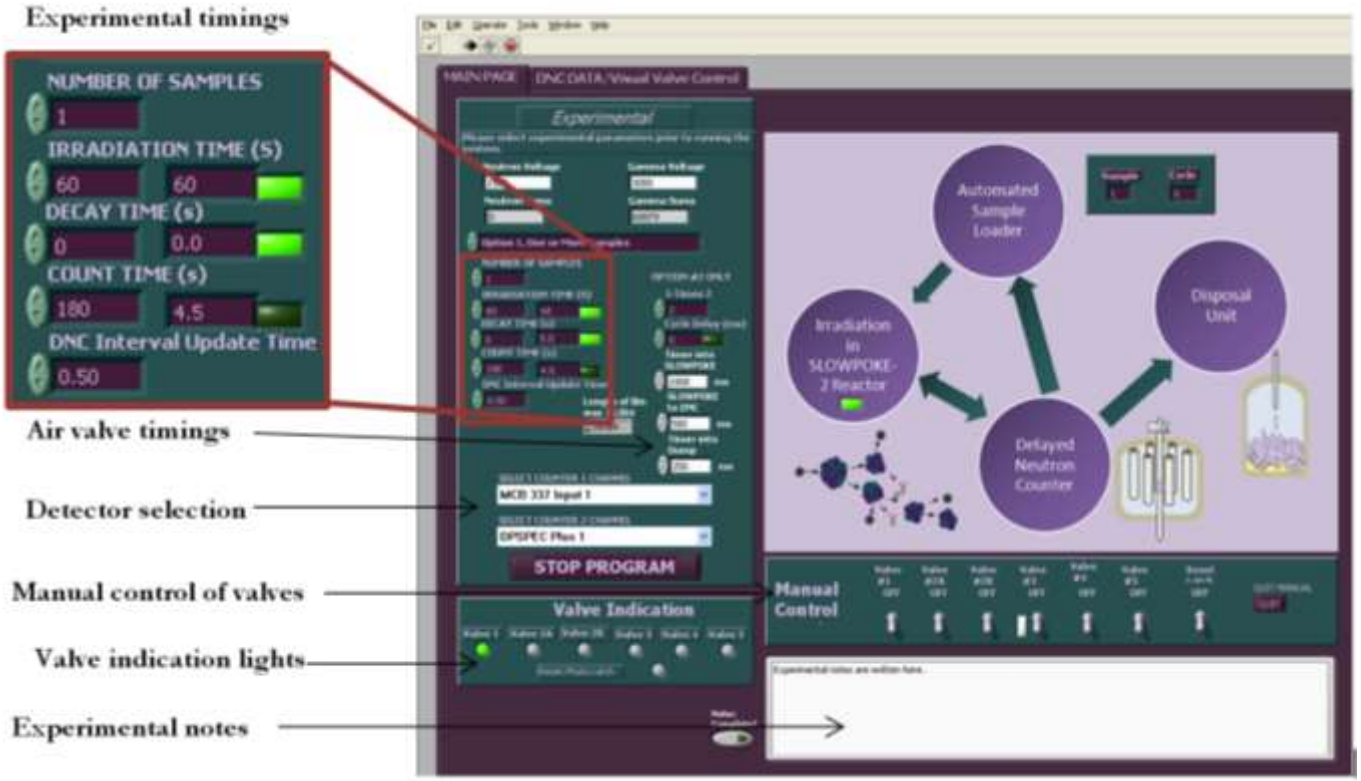

Figure 8.1: Graphic User Interface of DNGC System at the Royal Military College of Canada. User controlled experimental parameters include number of samples to analyze, irradiation, decay, and count timings and the frequency of data sampling

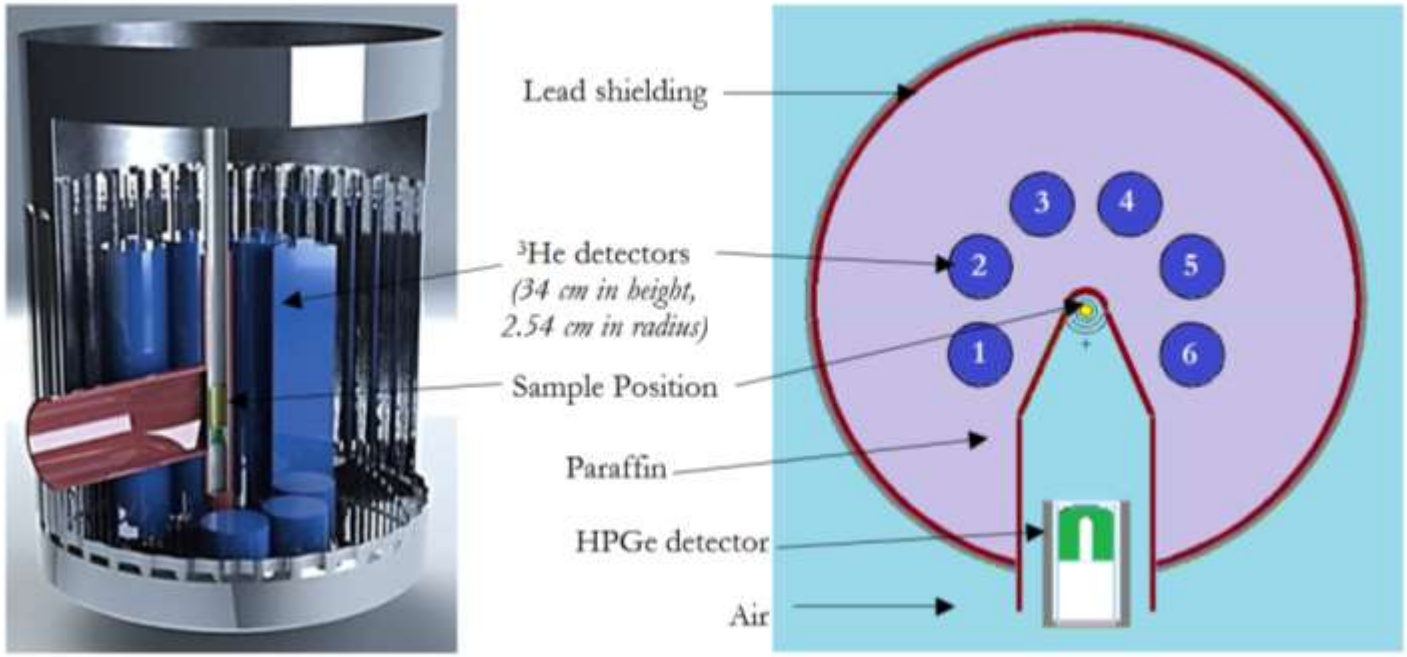

Figure 8.2: The delayed neutron and gamma counting arrangement Computer Aided Drawings (left) and MCNP model (right). The ^{3}He detectors are embedded in paraffin, and the High Purity Germanium detector slides in and out.

8.3.5 **MCNP6 Simulations**

The newest public release of the Monte Carlo code, MCNP6.1 (Goorley *et al*., 2012), has been used to simulate the behaviour of both the DNC and DNGC systems. The irradiation process was also simulated with MCNP using a SLOWPOKE-2 reactor model provided by Atomic Energy of Canada Limited (Nguyen *et al*., 2012). It was modified to include additional beryllium shims added at RMCC and the placement of vials full of water in the irradiation sites positions. A detailed 69-group neutron energy distribution was determined by MCNP6 simulations and found to agree with thermal, epithermal, and fast flux measurements of the DNGC irradiation site (Kennedy *et al*., 2000).

Ratios of DN and DG emissions from varying SNMs were simulated by recreating the SLOWPOKE-2 flux distribution for 60 *s* within a vial containing 2 *mg* of ^{233}U, ^{235}U and ^{239}Pu. Surface (F1) tallies were used to record the delayed neutrons and gammas released after the irradiation process with time and energy bins corresponding to HPGe measurements. Neutrons with energy distributions corresponding to DN emissions were created for neutron detection efficiency comparisons. DNGC geometries were measured during their assembly and were reproduced in MCNP. Pulse height (F8) tallies placed inside each ^{3}He and the HPGe detector recorded the reaction products, and their energy depositions within a detector's active zone. Detailed descriptions of these MCNP6 simulations can be found in (Andrews *et al*., 2014b, 2014c).

8.4 Results & Discussion

8.4.1 **Improvements to Neutron Detection**

The system upgrade provided an opportunity to address noted experimental deficiencies in the original DNC system, namely a significant photon background contribution and the resulting pulse pile up at low energies (Andrews *et al*., 2014b). 0.5 *cm* of lead lining was installed to limit the contributions of samples' photon emissions to ^{3}He recordings, Figure 8.2. Figure 8.3 depicts the energy depositions in the ^{3}He tubes in each system after the 60 *s* irradiation, 3 *s* decay, and 60 *s* counting of a sample containing 3.5 μg of ^{235}U (natural U certified reference material was used). The total counts have been normalized in the 0.2 – 0.9 *MeV* region for comparison purposes. The system upgrade resulted in an 84 *%* decrease in relative photon amounts, from 0 – 0.2 *MeV* (Figure 8.3). Gamma contributions

are removed from DN analysis by eliminating counts less than 0.2 *MeV* in the data processing.

Previous work examined the time-dependent neutron background resulting from irradiation of empty vials in the DNC system (Sellers *et al*., 2013). Analysis found this contribution was equivalent to 50 *ng* of ^{235}U contaminant on each vial, which was acquired while in the SLOWPOKE-2 irradiation site. An outer irradiation site was chosen for DNGC system use, as there was no such contamination. In addition, the significantly higher thermal to fast flux ratio in the outer site limits ^{238}U DN interferences in the assay of natural, depleted, and enriched uranium samples. Empty vials were irradiated for 60 *s*, allowed to decay for 3 *s* and neutron counts recorded for 180 *s* (n=8). The neutron count rate in the detectors was found to be 7.8 ± 0.8 s^{-1} (95 % confidence), it is independent of both count time and the presence of an irradiated vial in the counting arrangement.

8.4.2 Characterization of the Delayed Neutron and Gamma Counting System

MCNP simulations of an outer site's irradiation flux found a f_F ratio of 18.1, within the 95 *%* confidence interval of SLOWPOKE-2 reactor measurements (Kennedy *et al*., 2000). MCNP6 simulations of DN emissions produced by a natural U solution after a 60 *s* irradiation, 10 *s* decay, and 50 *s* count were compared to measurements of 3.5 μg of ^{235}U to determine a DN detection efficiency of 29 ± 4 % (95 *%* confidence), within uncertainty of an efficiency of 32.5 *%* predicted by MCNP6. The inclusion of a HPGe detector necessitated the re-arrangement of the ^{3}He detectors, to concentric but non-symmetric conditions, Figure 8.2. In the event of high-count rates exceeding 7000 counts s^{-1}, the full array of ^{3}He detectors may not be used as dead times will approach 30 *%*, the prescribed cut off for measurements (Knoll, 2010). It is therefore important to understand their individual contributions to the total count rate. MCNP6 simulations predicted a higher relative efficiency for the ^{3}He tubes adjacent to the HPGe (labelled 1 and 6 in Figure 8.2), due their increased distance from adjacent ^{3}He tubes, this was confirmed experimentally Figure 8.4[xv]. Measured uncertainties include intrinsic efficiency detector uncertainties and counting statistics.

[xv] Simulation uncertainty was determined by stochastically varying the axial positioning of the detectors by ± 0.1 *cm* (n=8), the quoted tolerance of their displacement during arrangement manufacture.

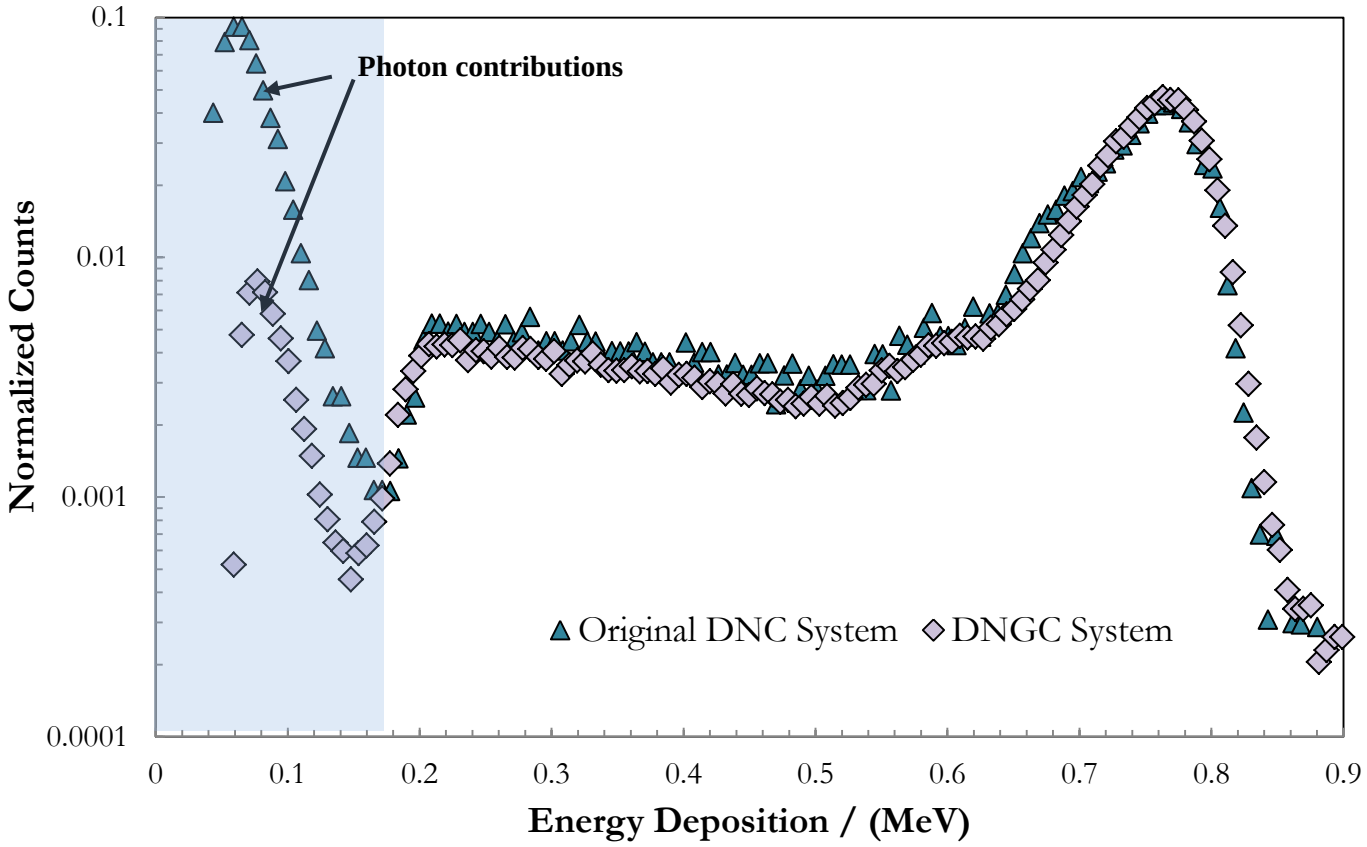

Figure 8.3: ^{3}He Energy Deposition Comparisons in DNC and DNGC Systems

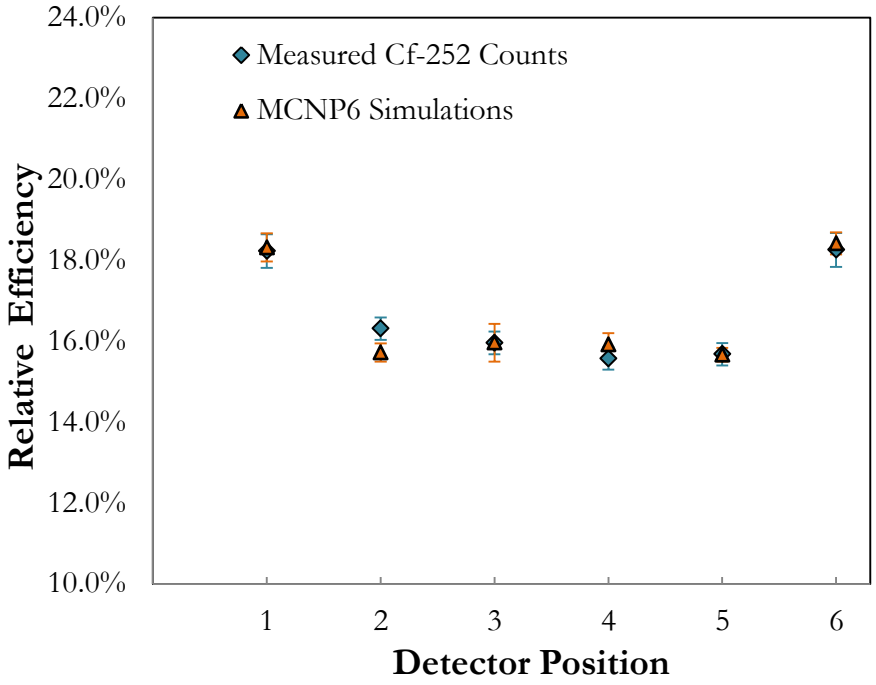

Figure 8.4: Relative efficiencies and neutron backgrounds of detector positions. 95 % confidence intervals displayed. The position of detectors 1 to 6 are pictured in Figure 8.2.

Figure 8.5 depicts the measured efficiencies of the HPGe detector after a 10 *min* count of the aforementioned multi-nuclide source decay placed on the endcap of the detector, the associated MCNP simulations, and their relative ratios. MCNP6 over-predicted measured detection efficiencies by 142 ± 9 % with no observed energy dependence over the range examined. It is believed that dead layer growth in this aging detector, accompanied by a decrease in active detector area (Quang Huy, 2010), and geometric assumptions in simulations has contributed to differences in efficiencies, as has been observed in other work (Boson *et al*., 2008; Padilla Cabal *et al*., 2010). MCNP6 simulations with increased dead layer growth did not account for the systematic overprediction, which remained consistent when additional geometries, including that shown in Figure 8.2, were simulated.

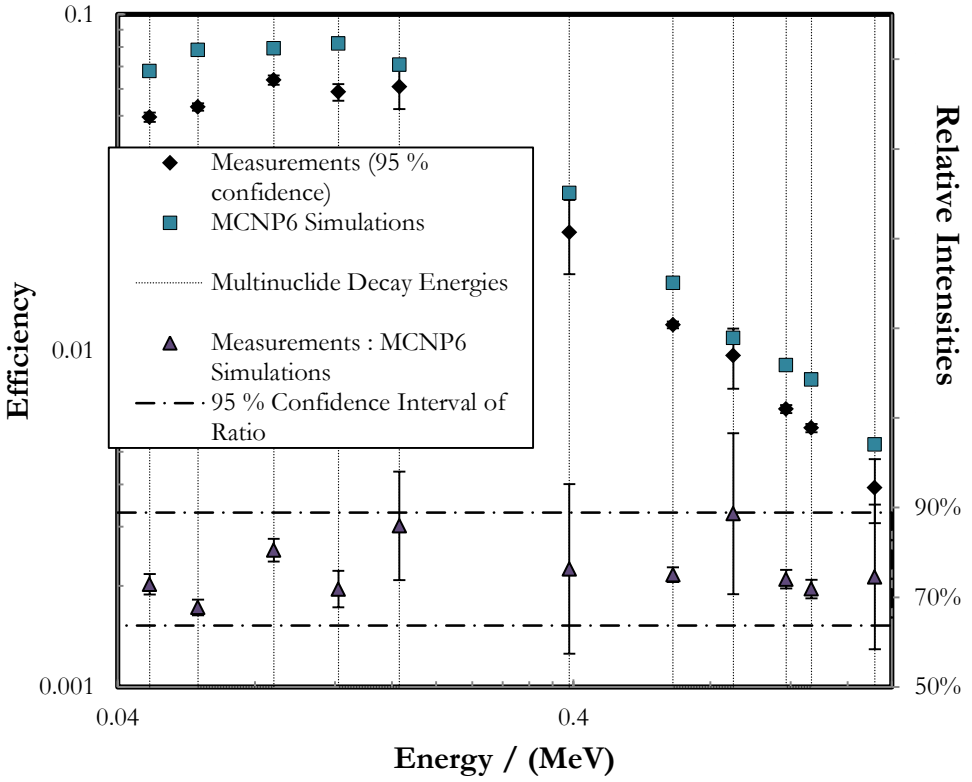

Figure 8.5: Gamma efficiency measurements, MCNP6 simulations, and their relative intensities.

8.4.3 **Processing of the DNGC System Data**

A Matlab™ algorithm has been developed to assay delayed gamma data. It imports the energy and time spectra from the data collection file and determines decay and count times. In addition to spectra of fission products, background spectra of empty vials irradiated and counted under the same experimental conditions are saved. The user specifies the count intervals to be examined and the algorithm will search through the saved spectra to find the appropriate background to subtract. Peaks in a low signal to noise ratio area are resolved by the optional application of a Savitzky-Golay filter (Savitzky and Golay, 1964) to the spectra. Count rates are used to determine and correct for the dead time effects and overflow error for each interval, and background contributions are subtracted. Final count spectra are normalized by the measured energy-dependent detection efficiency and the Compton edge is subtracted, to allow a direct comparison of gamma line

intensities. Figure 8.6 shows the 10 *min* cumulative, unprocessed, count of a nat. U solution irradiated for 60 *s*. Gamma line growth with respect to time and energy for the post-processed data is demonstrated in Figure 8.7, plot color is used to depict cumulative counts.

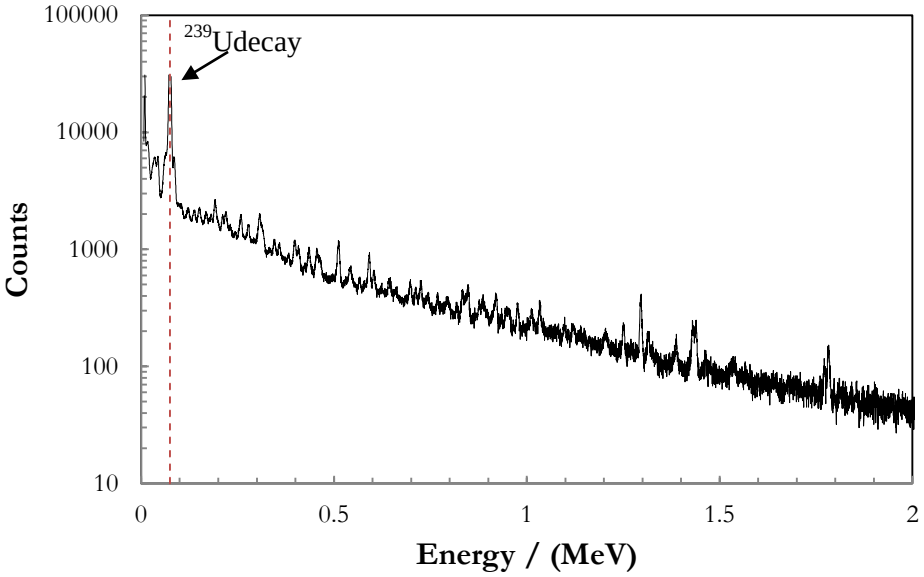

Figure 8.6: Pre-Processed Gamma Spectra Recorded by DNGC System

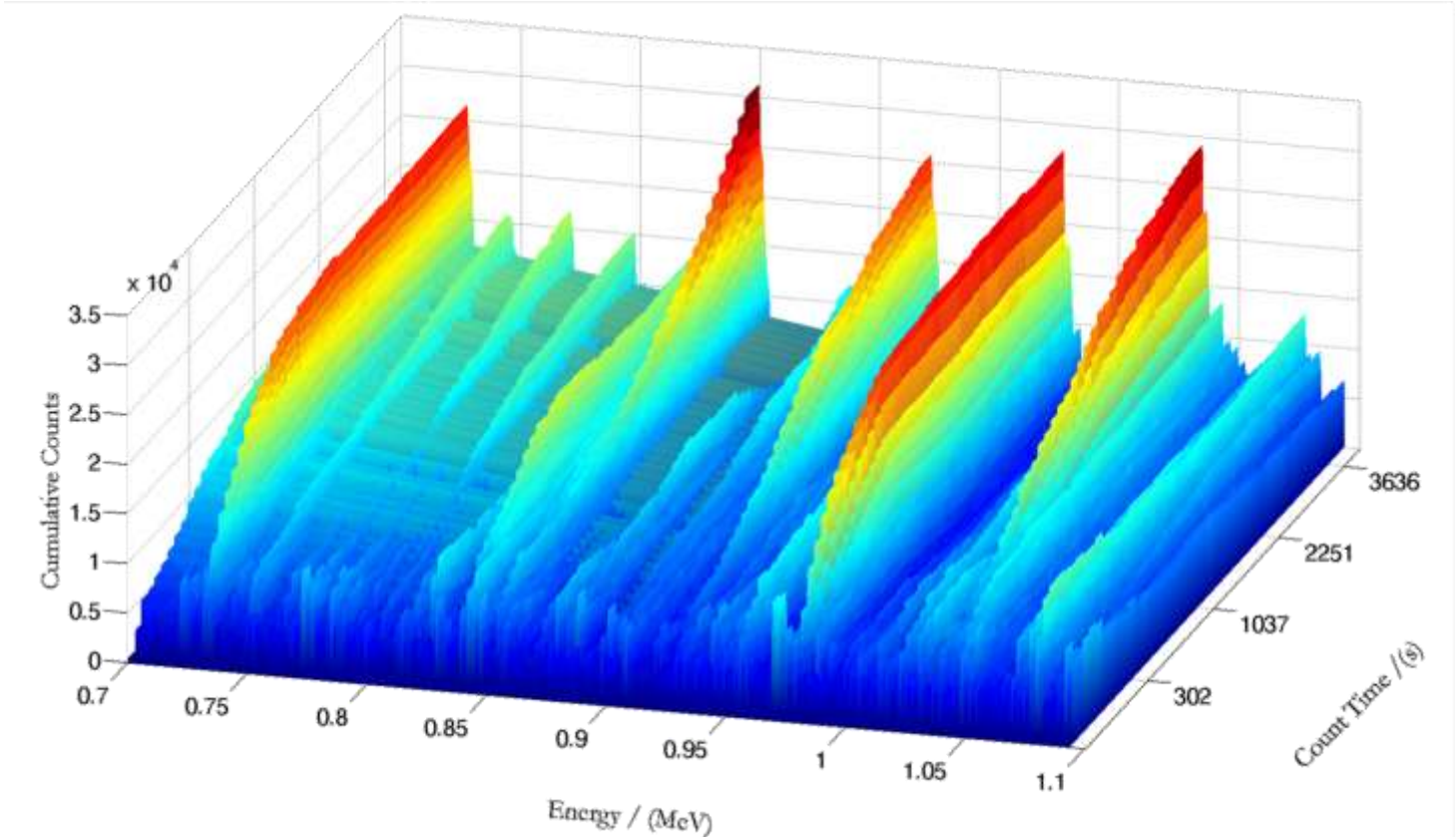

Figure 8.7: An example of measured natural U fission product gamma line growth.

8.4.4 Expected DN and DG Signatures from SNM in the DNGC System

The routine use of ^{233}U and ^{239}Pu calibration materials is undesirable due to their expense and handling limitations. However, the combined use of DN and DG signatures can afford SNM assignment and quantitation using only natural uranium calibration. The presence of delayed neutron emissions is indicative of fissile content, and DG emissions from fission products can be used to further characterize samples. ^{238}U presence in a sample will lead to the capture of neutrons and the production of gamma rays with energies of 75 *keV* from ^{239}U, Figure 8.6 (Marrs *et al*., 2008) identified additional useful delayed gamma lines for comparisons and determinations of fissile content in unknown solutions for varying count times. For example, during the counting range of 18 – 33 *min* after the elapse of irradiation, the ratio of ^{89}Rb (1032 *keV*) and ^{138}Cs (1010 *keV*) can be used to distinguish between fissioned content. MCNP6 simulations using the delayed gamma capability (Durkee *et al*., 2012) of ^{233}U, ^{235}U, and ^{239}Pu irradiations were used to simulate expected values for ^{89}Rb:^{138}Cs gamma line ratios at these energies in the DNGC system.

The flux distribution determined by MCNP6 was used to evaluate the relative ratios of total DN emissions for nat. U, ^{233}U, ^{235}U, and ^{239}Pu after a 60 *s* irradiation, 10 *s* decay and 50 *s* count. Therefore, if the presence of a specific SNM in a solution is established, its quantity can be determined through the use of a nat. U standard and the below relationship. A summary of DN and DG makers relevant to this discussion is found in Table 8.1.

$$m_{identified\ SNM} = m_{Nat\ U} \cdot \left(\frac{DN\ \ Counts_{identified\ SNM}}{DN\ \ Counts_{Nat\ U\ standard}}\right) \cdot (Relative\ DN\ Emissions \cdot \left(\frac{Nat.U\ standard}{identified\ SNM}\right))$$

Table 8.1: Expected Delayed Neutron and Gamma Signatures in the DNGC System

Marker	^{233}U	^{235}U	^{239}Pu
^{89}Rb:^{138}Cs (1032:1010 *keV*) Gamma Line Ratio 60 *s* – 18 *m* – 15 *m* irradiation-decay-count	2.5 ± 0.2	1.45 ± 0.06	0.62 ± 0.04
Cumulative DN Emissions (relative to nat. U) 60 *s* – 10 *s* - 50 *s* irradiation-decay-count	0.64	0.99	0.71

8.4.5 An Example of ^{233}U Characterisation using the DNGC System

The application of expected DN and DG signatures for SNM characterization was challenged via the examination of eight samples containing ^{233}U. One of the samples was irradiated and counted for 1 hour; the lack of a substantial 75 *keV* peak indicated an absence of ^{238}U content. ^{89}Rb and ^{138}Cs DG emission lines in the 18 – 33 *min* counting range were compared for the sample and a natural U standard. The natural U standard used for system calibration had a ^{89}Rb:^{138}Cs value of 1.55 ± 0.02 and the ^{233}U sample was also in agreement with theoretical values (Table 8.1), at 2.45 ± 0.04. Once the presence of ^{233}U was confirmed through an examination of the relative gamma line ratios, the cumulative delayed neutron counts were compared to that of a nat. U standard to determine the total ^{233}U content. Table 8.2 shows the expected and experimental mass determinations of 8 solutions; ^{233}U content was determined with an average relative error of -2.2 *%* and precision of 1.5 *%*. An average blank background of 593 (± 4 *%*) counts in typical DNGC system operating procedure yields detection limits of 0.008, 0.012, and 0.013 μg for ^{235}U, ^{233}U, and ^{239}Pu respectively.

Table 8.2: ^{233}U mass determination, accuracy, precision, with 95 % confidence intervals.

Sample	Mass ^{233}U / (µg)		Relative error / (%)
	Expected	Experimental	
1	*4.25 ± 0.03*	4.2 *± 0.1*	*-2*
2	*3.21 ± 0.03*	3.08 *± 0.08*	*-4*
3	*2.85 ± 0.03*	*2.76 ± 0.08*	*-3*
4	*2.36 ± 0.02*	*2.32 ± 0.07*	*-2*
5	*1.88 ± 0.02*	*1.81 ± 0.05*	*-4*
6	*1.46 ± 0.02*	*1.46 ± 0.04*	*-0*
7	*1.41 ± 0.02*	*1.41 ± 0.04*	*-0*
8	*0.93 ± 0.02*	*0.90 ± 0.03*	*-3*

8.5 Conclusions & Future Work

This paper describes the Delayed Neutron and Gamma Counting (DNGC) system at the Royal Military College of Canada and its characterization. The system is improved by changes in hardware and software, by increased specificity of neutron detection and by the concurrent detection of neutrons and gammas. Delayed gamma line emission ratios of ^{89}Rb and ^{138}Cs were used to confirm the presence of ^{233}U in aqueous solutions, and excluded assignment to other SNMs. DN cumulative counts were then used to quantify ^{233}U content with average relative errors and accuracies of -2.2 and 1.5 %, respectively. Planned future work includes the examination of fissile content in a variety of synthetic and environmental matrices. The capability of MCNP6 to simulate additional fission product delayed gamma emissions from SNM will also be compared to measurements obtained from the DNGC system.

8.6 Acknowledgements

Project funding has been provided by a Canadian Nuclear Safety Commission Doctoral Award, and Natural Sciences and Engineering Research Council of Canada. The technical work and assistance of J. Shaw, C. McEwen, K. Nielsen, K. Mattson, and D. Ferguson is much appreciated.

-This page is intentionally left blank-

Chapter 9

Uranium and Plutonium Fission Product Gamma Intensity Measurements and MCNP6 Simulations

M.T. Andrews[1,2], J.T. Goorley[2], E.C. Corcoran[1], D.G. Kelly[1]

[1]Department of Chemistry and Chemical Engineering,
Royal Military College of Canada
P.O. Box 17000 Stn. Forces
Kingston, Ontario, Canada K7K 7B4[xvi]

[2]XCP-3: Monte Carlo Codes
Los Alamos National Laboratory
MS A143, Los Alamos, New Mexico, US 87545.

[xvi] **M.T. Andrews**, J.T. Goorley, E.C. Corcoran, D.G. Kelly "Uranium and Plutonium Fission Product Gamma Intensity Measurements and MCNP6 Simulations" *Transactions of the American Nuclear Society* **110** (2014) pp. 490-493.

9.1 Introduction

The fission product gamma ray spectra of irradiated thin HEU and plutonium disks (93.15 at% ^{235}U and 98.97 at% ^{239}Pu, respectively) has been previously measured by Beddingfield and Cecil, 1998. They evaluated the intensities of prominent fission product peaks (FPPs) and examined the variation in their intensity ratios arising from ^{235}U vs. ^{239}Pu content. Those experiments were recently simulated by (Durkee *et al*., 2012) when demonstrating the delayed gamma (DG) capability in MCNP6. This summary discusses additional comparisons in the same energy range (0.8 – 1.6 *MeV*) between MCNP6v1 and FPP measurements of solutions containing ^{233}U, ^{235}U and ^{239}Pu after a 60 *s* irradiation, 15 *s* decay and 180 *s* count.

9.2 Description of Actual Work

9.2.1 A Description of the Experiment

Samples containing between 1.32 and 4.27 μg of fissile content were prepared from certified reference materials (Nat U. CRM421C, NIST, Gaithersburg, MD, CRM 111-A 99.4911 at% ^{233}U, New Brunswick Laboratory, and Isotope Products Laboratories Lot #1195.20, 97.937 at% ^{239}Pu, Eckert & Ziegler, Valencia, CA) in aqueous form. Solutions were doubly encapsulated in polyethylene vials before their 60 *s* irradiation in a predominately thermal SLOWPOKE-2 reactor. A counting arrangement consisting of a HPGe detector (GMX 18190, SH-GMX CFG:S/N 26-N1476A) and six ^{3}He detectors records both gamma and neutron energy depositions as a function of count time. Measurement procedures and the counting arrangement have been described in detail in Andrews *et al*. 2014a. The HPGe detector was calibrated with a multi-nuclide standard source containing 13 isotopes with energies ranging from 47 *keV* to 1.836 *MeV* (Source 1423-99-21, Eckert & Ziegler, Valencia, CA).

9.2.2 MCNP6 Simulations

Irradiation conditions were simulated using an input deck provided by Atomic Energy of Canada Limited containing SLOWPOKE-2 geometry and material specifications (Nguyen *et al*., 2012). This model was modified to include a vial containing an aqueous solution in an inner irradiation site. A flux (F4) tally was placed in the vial to determine the neutron energy group distributions. This flux profile was then recreated in a second deck with only a PE vial containing a fissile solution. The *DG=lines* option in MCNP6 simulated DG emissions; the energy and time of emissions were recorded by a surface current (F1) tally placed

on the exterior of the vial. Time and energy binning parameters were chosen to correspond to experimental irradiation, decay and count times, and channel width. Gamma emissions up to 4 *MeV* were recorded.

DG detection was simulated by modeling the counting arrangement and recreating gamma energy distributions (obtained from the aforementioned F1 tally), from the vial position within the counting geometry. A pulse height (F8) tally was placed in the active zone of the detector, which recorded photon energy depositions. Energy resolution effects were recreated via use of the *Gaussian Energy Broadening (GEB)* card in MCNP6. Current simplifications in the simulations include the omission of ^{238}U content contributions in the simulations containing natural U.

MCNP6 DG production is explained in detail in (Durkee *et al*., 2012). DG options available in MCNP consist of multigroup (MG) and line data, which are based on ENDF/B-VI evaluations. When *DG=lines* option is selected (as is the case in this work) the resulting DG emission will be comprised of discrete lines (currently available for 979 radionuclides in the gamma line data file *cindergl.dat* released with MCNP6v1) and continuous data evaluated at 10 *keV* intervals. Current efforts at Los Alamos National Laboratory include the development of a code ENDF2CINDER, which updates these files with ENDFVII data (Wilcox *et al*.). Gamma line emission files containing ENDFVII.1 library data were provided by T. Wilcox at LANL and were also used in this comparison.

9.3 Results

9.3.1 Post Processing of MCNP Output and Measurements

Measurements and their associated MCNP pulse height tally outputs were imported into a Matlab™ script, which corrects for both dead time effects and background spectra contributions in the former. A Savitzky-Golay filter is applied to smooth the datasets before the algorithm identifies peaks in both spectra, and selects the most prominent experimental peaks for further comparison. An example of spectra analyzed in this work is shown in Figure 9.1. Cumulative counts are normalized by total fissile mass in both measurements and simulations.

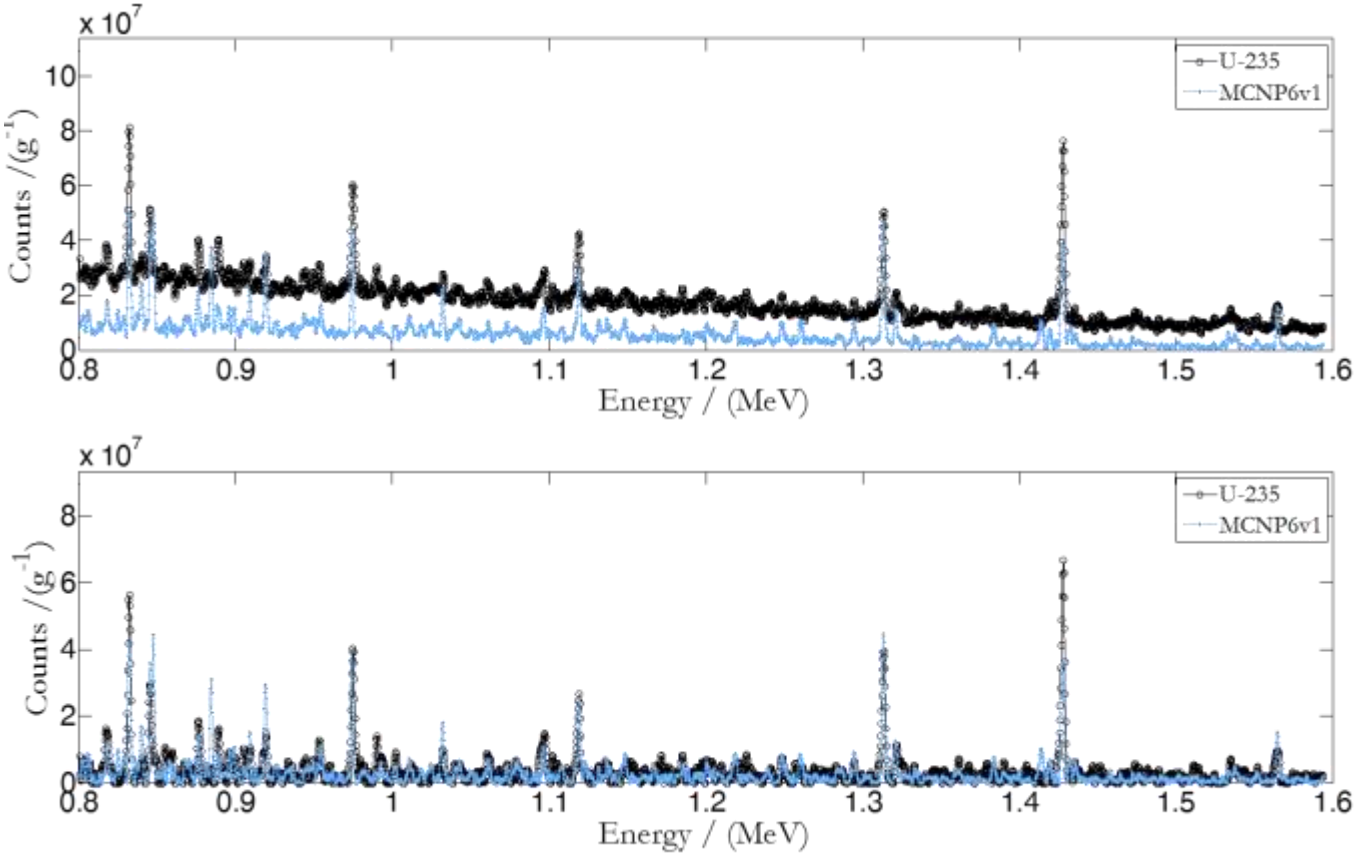

Figure 9.1: ^{235}U Measurements and MCNP6v1 Predictions without (top) and with (bottom) Compton continuum subtraction.

9.3.2 **HPGe Detector Properties**

MCNP6 simulations and measured waveform spectra after a 10 *min* count of the multi-nuclide standard provided a comparison of intrinsic efficiencies. MCNP6 simulations were found to over predict measured intrinsic efficiencies by 132 ± 10 *%,* with no observed energy dependence from 47 *keV* to 1.836 *MeV.* It is likely that dead layer growth in this older detector has contributed to a decrease in observed intrinsic efficiency (Quang Huy, 2010). Examination of the measured waveform also allowed for a determination of energy resolution broadening effects which were simulated in MCNP6 with a *GEB* card.

All MCNP6 outputs were normalized by the difference in intrinsic efficiencies and simulated fissile mass. Preliminary comparisons of FPPs from irradiated fissile material showed a considerable difference in observed spectra and MCNP6v1 output, Figure 9.1 (top). This is possibly due to the omission of > 4 *MeV* gamma reproduction in the counting MCNP6 deck. These energetic gamma rays would have a considerable Compton continuum contribution to energy deposition. A more direct comparison of fission product peak intensities was facilitated by the subtraction of local minima counts from both spectra, Figure 9.1 (bottom).

9.3.3 **A Comparison of Fission Product Peak Intensities**

Significant differences between MCNP6v1 and measurement FPP magnitudes, namely $^{90/90m}$Rb and $^{132/132m}$Sb, have been previously noted (Andrews *et al*., 2013). Several of these discrepancies could be attributed to the older ENDFVI data called upon in MCNP6v1 for delayed gamma emission simulations. Therefore updated gamma line files with ENDFVII.1 data were also used in simulations.

Figure 9.2 shows MCNP6 and measured cumulative counts for three samples, a ^{233}U solution (top), a mixture with the fissile content comprised of 40 wt *%* ^{239}Pu and 60 *%* ^{235}U (contained in Nat. U), and a natural uranium solution (bottom). Figure 9.2 depicts the MCNP6 simulation results, which used updated gamma line (GL) files, however identical runs using default files provided with the current MCNP6v1 release were also examined. Table 9.1 summarizes observed peak magnitudes and those predicted by MCNP6v1 (with and without updated gamma line data files) for the 10 most prominent peaks in each spectrum. The peak intensities in each case were determined by summing the peak channel and the 4 adjacent channel counts, in both simulations and experiments. 68 % confidence

intervals were calculated via the propagation of flux magnitude, counting statistics and intrinsic efficiency correction uncertainties. Results within the 95 % confidence interval have been shaded.

MCNP6 predicted the presence of all but one prominent peak for each spectrum. This peak, at 1.145 *MeV,* was observed during several fissile irradiations (but not all). It is not believed to be a fission product peak. FPPs whose cumulative channel counts were less than 400 had high absolute errors, 38 ± 19 %. Updates to the cinder gamma line data files resulted in improved agreement for the previously noted discrepancies $^{90/90m}$Rb and $^{132/132m}$Sb.

A final comparison examined the intensity ratios of the three most prominent peaks in measured spectra: ^{94}Sr (1.428 *MeV*), $^{90/90m}$Rb (0.832 *MeV*) and $^{132/132m}$Sb (0.975 *MeV*). These ratios for each solution and the corresponding MCNP6 output are shown in Table 9.1. In each of the 9 cases the update to the gamma line files resulted in a lower absolute error between MCNP6 simulations and measurements. MCNP6v1 (with modifications to the gamma line data files) was able to predict these ratios within the 95 % confidence interval in 7 of the 9 comparisons, Table 9.2. There is no dependence of relative error on peak energy (in this 0.8 - 1.6 *MeV*) range, however a notable dependence on total cumulative counts is evident.

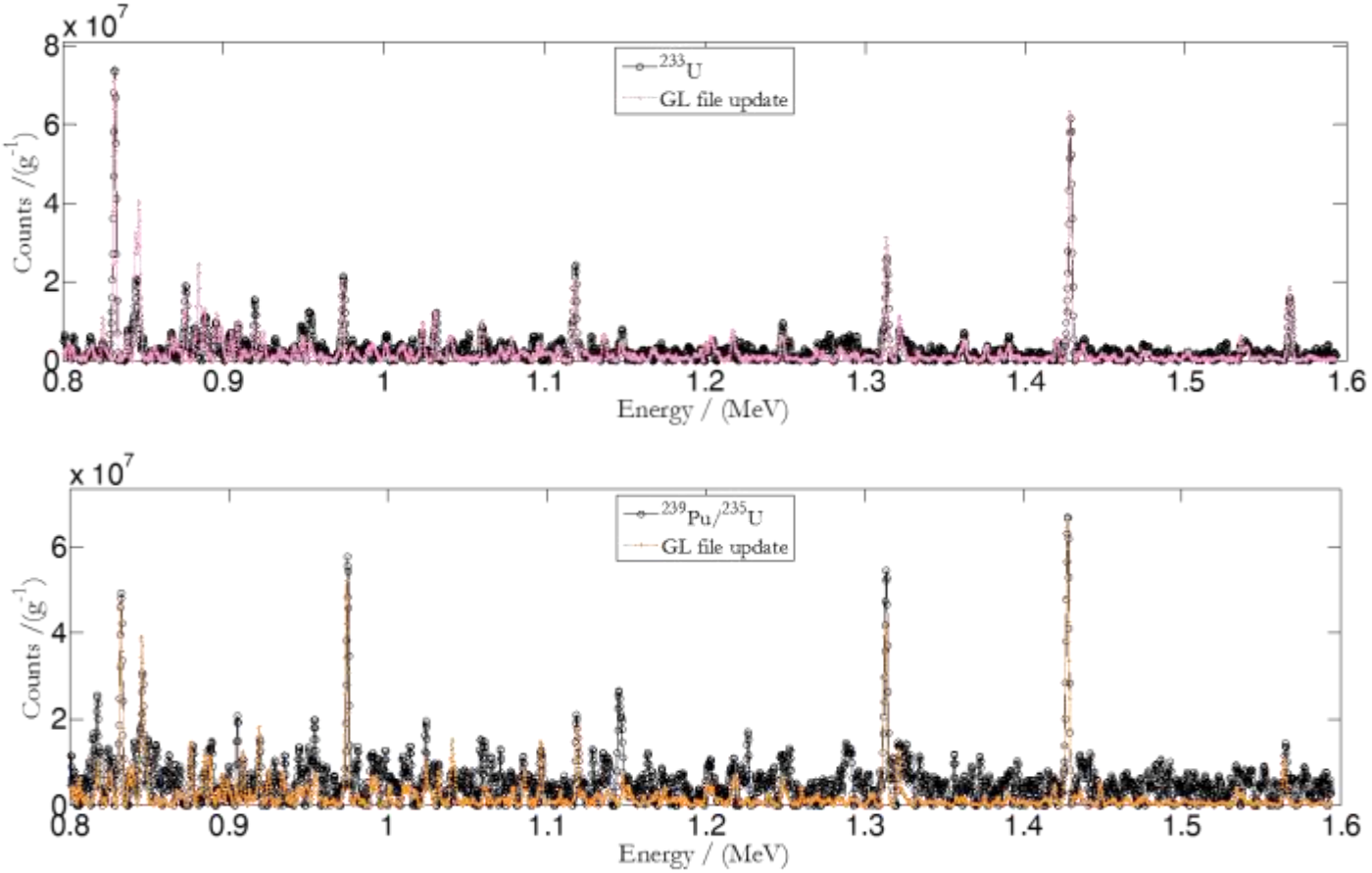

Figure 9.2 i: MCNP6 Predictions & Measured Spectra for ^{233}U (top), $^{239}Pu/^{235}U$ (middle) and ^{235}U (bottom) solutions.

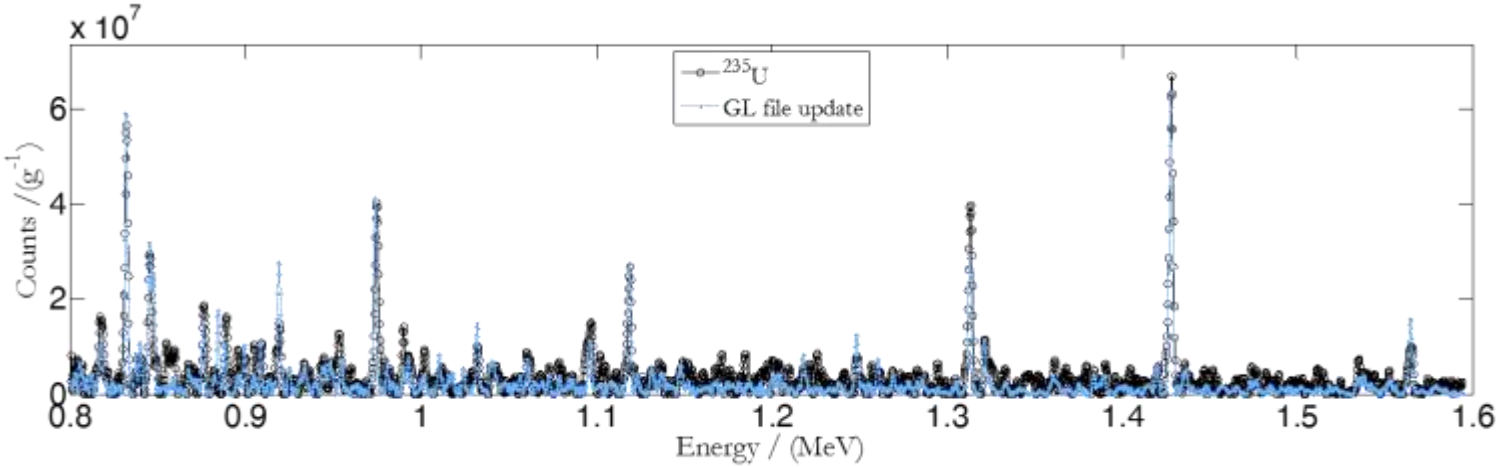

Figure 9.3 ii: MCNP6 Predictions & Measured Spectra for ^{233}U (top), $^{239}Pu/^{235}U$ (middle) and ^{235}U (bottom) solutions.

Table 9.1: MCNP : Measured Ratios of Prominent Peaks (± 68 % Confidence Intervals). Results within the 95 % confidence interval have been shaded. FPPs with experimental cumulative counts exceeding 400 have been bolded.

^{235}U Sample			^{233}U Sample			^{239}Pu/^{235}U Mixed Sample		
Energy / (MeV)	**MCNP6v1**	**Updated *GL* files**	**Energy / (MeV)**	**MCNP6v1**	**Updated *GL* files**	**Energy / (MeV)**	**MCNP6v1**	**Updated *GL* files**
1.428	**0.89 ± 0.06**	**0.95 ± 0.07**	0.832	**0.51 ± 0.04**	**0.95 ± 0.07**	1.428	**0.93 ± 0.07**	**0.99 ± 0.08**
0.832	**0.49 ± 0.04**	**1.03 ± 0.07**	1.428	**1.01 ± 0.07**	**1.03 ± 0.07**	0.975	**0.68 ± 0.05**	**0.93 ± 0.07**
0.975	**0.83 ± 0.06**	**1.00 ± 0.07**	1.314	**1.36 ± 0.10**	**1.20 ± 0.09**	1.314	**0.87 ± 0.07**	**0.79 ± 0.06**
1.314	**0.90 ± 0.07**	**0.70 ± 0.05**	1.119	**0.87 ± 0.07**	**0.87 ± 0.07**	0.832	0.51 ± 0.04	0.94 ± 0.07
0.846	**1.11 ± 0.08**	**1.05 ± 0.08**	0.975	**0.71 ± 0.05**	**0.92 ± 0.07**	0.846	1.16 ± 0.10	1.31 ± 0.11
1.119	**0.87 ± 0.07**	**1.01 ± 0.08**	0.846	**1.26 ± 0.10**	**1.52 ± 0.12**	1.145	-	-
0.876	**0.64 ± 0.05**	**0.82 ± 0.06**	0.876	**0.68 ± 0.05**	**0.87 ± 0.07**	0.817	0.35 ± 0.03	0.41 ± 0.03
0.817	0.62 ± 0.05	0.71 ± 0.06	1.565	**1.13 ± 0.09**	**1.14 ± 0.09**	1.119	0.66 ± 0.06	0.90 ± 0.07
0.889	0.84 ± 0.06	0.63 ± 0.05	0.919	0.65 ± 0.05	0.61 ± 0.05	0.954	0.40 ± 0.03	0.40 ± 0.03
1.097	0.77 ± 0.06	0.76 ± 0.06	0.953	0.65 ± 0.05	0.35 ± 0.03	0.905	0.33 ± 0.03	0.28 ± 0.02

Table 9.2: Ratios of ^{94}Sr, $^{90/90m}$Rb and $^{132/132m}$Sb Intensities: Measurements & MCNP6 (± 68 % CI).

	^{235}U Sample			^{233}U Sample			^{239}Pu/^{235}U Mixed Sample		
Ratio	**Exp.**	**MCNP6**	**Updated *GL* files**	**Exp.**	**MCNP6**	**Updated *GL* files**	**Exp.**	**MCNP6**	**Updated *GL* files**
^{94}Sr:^{90}Rb	1.20±0.09	1.66	1.12	0.85±0.06	0.70	0.92	1.40±0.12	1.83	1.56
^{94}Sr:^{132}Sb	1.65±0.13	1.76	1.57	2.91± 0.23	1.54	2.05	1.20±0.10	1.33	1.28
^{90}Rb:^{132}Sb	1.36±0.10	1.06	1.40	3.41± 0.26	2.19	2.22	0.86±0.08	0.73	0.82

9.4 Conclusions & Future Work

This summary discusses comparisons between MCNP6v1 and the measurement of fission product gamma intensities in the 0.8 – 1.6 *MeV* range. Several discrepancies in FPP measured intensities and MCNP6v1 predictions were resolved with the use of gamma line data files populated with ENDFVII.1 library data. For example, ^{235}U $^{90/90m}$Rb and $^{132/132m}$Sb MCNP to measured peak intensity ratios increased from 0.51 ± 0.04 to 1.03 ± 0.07, and 0.71 ± 0.05 to 0.92 ± 0.07, respectively.

Future work will see the continuation of these comparisons with varying irradiation, decay, and count times. Sample irradiations and counting will be performed in triplicate to reduce stochastic uncertainties in measured spectra. Also, FPP intensity comparisons with energies ranging from 10 *keV* to 2 *MeV* will be examined.

9.5 Acknowledgements

The authors would like to thank T. Wilcox for providing updated cinder data files. Funding for this work was provided LANL's Advanced Simulation and Computing program, the Canadian Nuclear Safety Commission, and NSERC.

Chapter 10

MCNP6 Simulations of Gamma Line Emissions from Fission Products and Their Comparisons to Plutonium and Uranium Measurements

M.T. Andrews[1,2], J.T. Goorley[2], E.C. Corcoran[1], D.G. Kelly[1]

[1]Department of Chemistry and Chemical Engineering,
Royal Military College of Canada
P.O. Box 17000 Stn. Forces
Kingston, Ontario, Canada K7K 7B4[xvii]

[2]XCP-3: Monte Carlo Codes
Los Alamos National Laboratory
MS A143, Los Alamos, New Mexico, US 87545.

[xvii] **M.T. Andrews**, D.G. Kelly, E.C. Corcoran, J.T. Goorley, "Fission Product Gamma Line Measurements and MCNP6 Simulations" *Journal of Progress in Nuclear Energy, (2015), in press.*

10.1 Abstract

Aqueous solutions containing microgram quantities of special nuclear materials (SNMs) were irradiated for 60 *s* using a SLOWPOKE-2 reactor, and their delayed gamma (DG) emissions were recorded as a function of count time up to three minutes after irradiation. The irradiation and counting processes were simulated using the production release of MCNP6.1 and the more recent MCNP6.1.1β version, and the line emission option was used to create DGs. In every simulation MCNP6 successfully predicted the 25 most prominent measured fission product peaks for each SNM solution in the 0.1 – 1.6 *MeV* energy range. Fission products with gamma emissions greater than 0.6 *MeV* were selected for a detailed comparison of their relative measured and simulated magnitudes. There were significant fission product peak outliers, several of which were attributed to the outdated ENDF/B VI gamma line data used by MCNP6 for DG emissions. The updated time-bin structure used by MCNP6.1.1β for DG production and its effect on time-dependent measurements are also discussed. Discrepancies between measurements and simulations were further resolved in a final comparison which used MCNP6.1.1β alongside updated gamma line data files.

Keywords: MCNP6, delayed gamma, special nuclear materials.

10.2 Introduction

The detection of delayed gamma (DG) emissions has widespread applications including the assay of special nuclear materials (Beddingfield and Cecil, 1998; Haciyakupoglu and Gencay, 1999; Marrs *et al*., 2008), and nuclear forensic analysis (Durkee *et al*., 2012). DG magnitudes and relative intensities can provide information about the identity of the fissioned isotope, its quantity, and the energy of the neutrons inducing fission (Marrs *et al*., 2008). The measurement of the spectral and temporal dependence of DGs produced by fission can be employed to interrogate sea cargo (Norman *et al*., 2004), examine unexpected fission events (Marrs *et al*., 2008), and to assay nuclear fuel (Campbell *et al*., 2011).

The ability to simulate the production of DG emissions and their behaviour is an important tool when designing complex nuclear detection systems (Durkee *et al*., 2012). A detailed simulation can optimize these designs (Bronson *et al*., 2009), and reduce experimental expenses and project time required for their completion. MCNP6 (Goorley *et al*., 2012), developed by Los Alamos National Laboratory, is a Monte Carlo code that is capable of 3D simulations of radiation transport in user-defined geometries and is commonly used by the nuclear community for the design of nuclear instrumentation (Bronson *et al*., 2009). MCNP6 includes a delayed

particle feature consisting of two structures for DG emission: multigroup and line data (Durkee *et al*., 2012), the latter enables the simulation of fission product gamma line emissions from interrogated SNM. Previous MCNP simulations of such measurements include those performed by Beddingfield and Cecil, who exposed thin disks of highly enriched uranium and plutonium to a moderated ^{252}Cf source and measured the resulting gamma line emissions (Beddingfield and Cecil, 1998). MCNP simulations reproduced the prominence of the measured experimental peaks observed at times > 1000 *s* after the fission process (Durkee *et al*., 2009; Goorley *et al*., 2012). However, a direct comparison of fission product peak (FPP) magnitudes was not possible as experimental arrangement and detector details not documented/retained and therefore had to be approximated in MCNP simulations.

The present work compares MCNP6 simulations to measurements of DGs collected by the Royal Military College of Canada's (RMCC's) delayed neutron and gamma counting system. This system (Andrews *et al*., 2015b) characterizes special nuclear materials (SNMs) by irradiation using a SLOWPOKE-2 reactor and by the subsequent recording of the temporal behaviour of delayed neutron (DN) and delayed gamma (DG) emissions. It contributes to the analytical capabilities available to the Canadian Department of National Defense for the assay of SNM. MCNP6 is used at RMCC to predict both delayed neutron and gamma line emissions useful for the characterisation of SNM. The irradiation process, DG emissions, and counting geometry of the system have been simulated in MCNP6. These measurements provided an opportunity to examine the capabilities of MCNP6 to predict DG emissions behaviour from SNM. This paper discusses comparisons of simulated and measured DG fission product energies and magnitudes of prominent peaks from 0.1 – 1.6 *MeV*. These DG measurements and simulations are intended to complement previous work (Andrews *et al*., 2014b), which compared MCNP6 delayed neutron emissions and measurements from SNM (Sellers *et al*., 2012a).

10.3 Experimental & Data Processing

Four aqueous solutions were prepared containing 3.51 μg of ^{235}U (in nat. U), 2.13 and 4.27 μg of ^{233}U, and a mixture containing both ^{235}U (comprising 60 % of SNM content by mass) and ^{239}Pu (40 %) for a total fissile mass of 1.32 μg. Certified reference materials used included nat U. CRM421C, (NIST, Gaithersburg, MD), CRM 111-A 99.4911 % ^{233}U, (New Brunswick Laboratory, Argonne, IL), and Isotope Products Laboratories Lot #1195.20, 97.937 at % ^{239}Pu (Eckert & Ziegler, Valencia, CA). Samples were diluted with distilled water and 2 % nitric acid before they were sealed in polyethylene vials (LA Packaging, Yorba Linda, CA). These

solutions were irradiated for 60 *s* in a SLOWPOKE-2 reactor (Hilborn and Townes, 1987). Cumulative gamma spectra were recorded by a high purity germanium detector (HPGe) (Ortec, GMC 18190, SH-GMX CFG-S/N 26-N1476A) as a function of count time up to 180 *s* after irradiation, including a 15 *s* delay. Background contributions to the spectra were determined by the irradiation and counting of an empty polyethylene vial. Cumulative spectra 15 - 180 *s* after the elapse of irradiation were selected for detailed comparisons. These measurements were facilitated by the delayed neutron and gamma counting (DNGC) system, which is described in detail by Andrews *et al*., 2015b.

Measured gamma spectra were imported into a Matlab™ script, which corrected for dead time effects and subtracted background contributions. These measurements were performed with the HPGe detector front located 15 *cm* from centre of the sample to reduce dead time. This distance resulted in a 30 % reduction in geometric detection efficiency relative to earlier studies (Andrews *et al*., 2015b). Local minima were subtracted from the overall photon spectra to eliminate Compton continuum contributions to total counts, Figure 10.1.

10.4 MCNP6 Simulations

Irradiation neutron flux distribution was determined in MCNP using a SLOWPOKE-2 model developed by Atomic Energy of Canada Limited (Nguyen *et al*., 2012) as described in reference (Andrews *et al*., 2014b). This flux distribution was reproduced in a second deck, which simulated a 60 *s* irradiation of 50 *mg* of fissile content[xviii] inside an aqueous solution. The DG=lines option on MCNP6's activation control card (ACT) was used to simulate the high fidelity gamma ray emissions from the activation and fission products produced (Pelowitz, 2013).

A surface current (F1) tally was placed on the surface of the solution, which recorded the time and energy distribution of the emitted gamma rays. Time and energy bins on the surface current tally were chosen to correspond to experimental parameters. The magnitude and energy distribution of gamma emissions were reproduced in a separate counting geometry deck containing the HPGe detector configuration. A pulse height (F8) tally was used alongside a Gaussian energy broadening (GEB) card to simulate the energy-dependent resolution of the HPGe detector. As with experimental measurements, the local minima were detected and

[xviii] The minor contributions of ^{238}U fission to the overall DG emission from Nat. U were not included in MCNP6 simulations. The density of the vial's solution was held constant to 1.00 $g\ cm^{-3}$.

their counts subtracted from MCNP outputs to facilitate a direct comparison of fission product peak intensities. This also removed the contributions of continuous energy depositions arising from DG emissions from FPs without associated gamma line data. Energy depositions from the elastic scattering of delayed neutrons emitted from the fissile content and Ge nuclei are prominent a < 0.1 *MeV* energies (Krmar *et al*., 2013). However, because neutron transport was not included in detection simulations, < 0.1 *MeV* comparisons are not performed. The MCNP simulations were normalized by differences in experimental and MCNP6 fissile masses, neutron flux magnitudes, and by observed differences in simulated and measured HPGe detection efficiencies (Andrews *et al*., 2015b).

Relevant to this work is the bin structure used to sample delayed particle intensities with respect to time. It had been previously noted that the time-bin structure used to create delayed particle emission in MCNP6.1 resulted in anomalous time-dependent results (Andrews *et al*., 2014b; Goorley, 2013). MCNP6.1.1β contains many updates and code fixes. Most pertinent to this work is the resolution of anomalous time-dependent results via an update to the delayed particle time-bin structure (Goorley, 2014). To examine the effects of this change, gamma measurements from 0.1 to 1.6 *MeV* were compared to MCNP6.1 (load date = 06/13/2013) and MCNP6.1.1β (load date = 07/23/14).

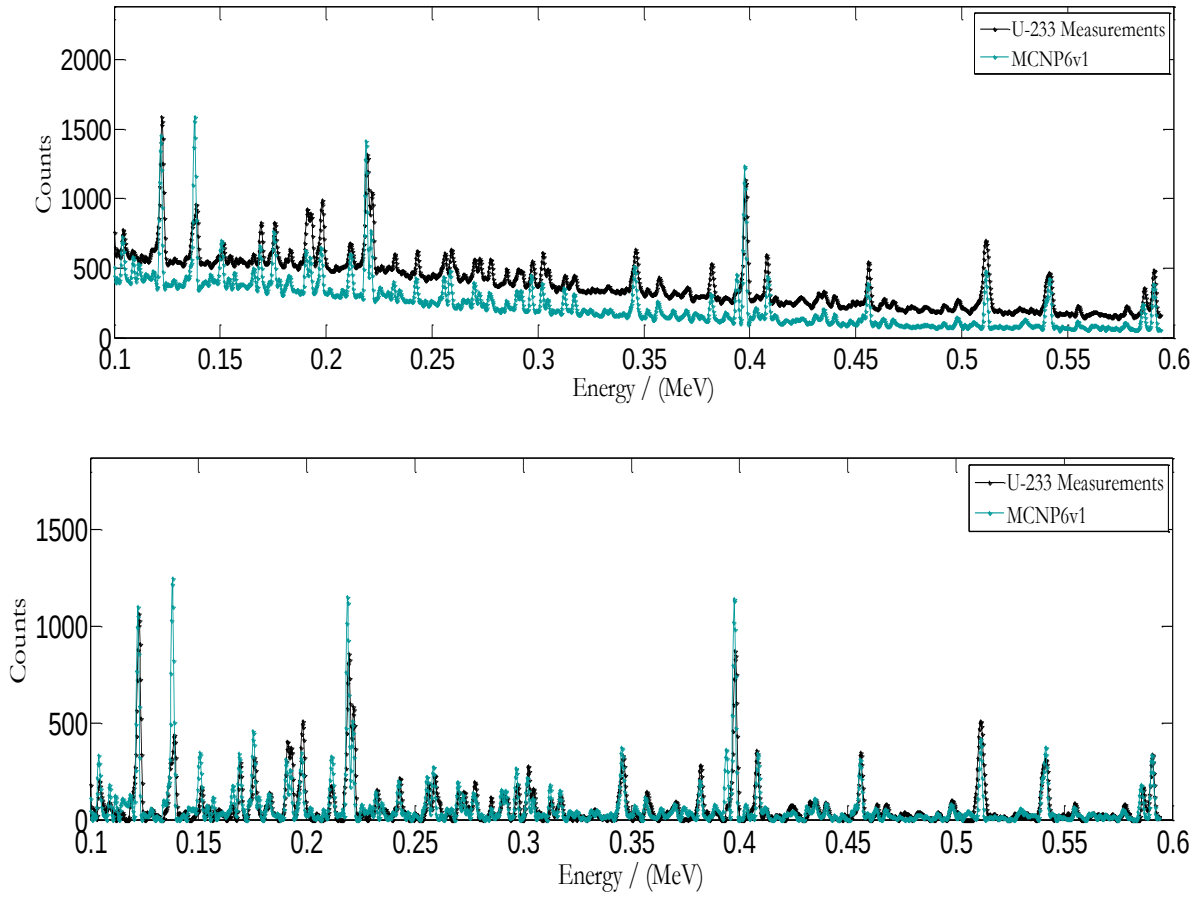

Figure 10.1: ^{233}U Measurements and MCNP6v1 without (top) and with (bottom) local minima subtraction.

10.5 Results & Discussion

Simulations are compared to experimental measurements of three SNM-containing materials to evaluate the capability of MCNP6.1 and MCNP6.1.1β to: i) simulate observed prominent fission product peaks, ii) reproduce measured peak magnitudes, and iii) to examine the effects of the use of updated gamma line data files.

10.5.1 MCNP6 Peak Predictions

Using the processing described in Section 3, measured delayed gamma spectra were generated, along with their corresponding MCNP6 simulation for three solutions containing; (i) natural uranium, (ii) ^{233}U, and (iii) a mixture of nat. U and ^{239}Pu. These comparisons were performed with both MCNP6.1 and MCNP6.1.1β. For clarity measured and simulated data are presented as separate spectra, with data appearing for the energy ranges 0.1-0.8 and 0.8-1.6 *MeV* on separate plots. MCNP6.1 simulations and their comparisons to nat. U measurements are depicted in Figure 10.2 and Figure 10.3. MCNP6.1.1β simulations of the ^{233}U and the ^{235}U/^{239}Pu samples, and their corresponding measurements are shown in Figure 10.4 through Figure 10.7. Both measured spectra and their corresponding MCNP6 simulations are those afforded by typical irradiation and analysis parameters used for the DGNC system at RMCC; *viz. 60 s* irradiation, 15 *s* decay, and the subsequent collection of cumulative counts recorded up to 180 *s* after the elapse of irradiation. It is evident that there is, in general, an excellent correspondence between measured and simulated data. However, interesting features are identified by consideration of the peaks observed and by a systemic comparison of data. MCNP simulations are assessed qualitatively against the presence/absence of the 25 most prominent measured peaks in the 0.1 – 1.6 *MeV* energy range for each of the three SNM solutions experimental peaks. An analysis algorithm is employed to identify the apex energies of Gaussian peaks found in both measured and simulated spectra. If the energies of the measured and simulated peaks are within 0.0015 *MeV*, the algorithm identifies the peaks as paired and makes these pairs available for further analysis. In practice, the majority of prominent peaks are paired, and many are readily identified as being derived from specific radionuclides. The most intense measured fission products were unsurprisingly those with high fission product yields (FPYs) (either cumulative or individual), prominent gamma branching ratios, gamma line emission energies with high detection efficiency, and half-lives within the counting range of the experiment, Table 10.1.

Table 10.1: Prominent Measured Fission Product Peaks, their emission energies, branching ratios, half-lives, independent, and cumulative fission product yields for ^{233}U thermal fission (England and Rider, 1994).

Isotope	Gamma Energy(s) / MeV	Branching Ratio from ENDFB/ VII.1 / %	Isotope Half-life /s	^{233}U Thermal Fission				
				Individual FPY /%	Cumulative FPY / %	Fission Parent /(s)	Fission Parent Yield /%	Parent Half-life /s
^{90}Kr	0.122 1.119	36 % 39 %	32 *s*	3.95	4.13	^{90}Br	0.23	2 s
^{139}Xe	0.219	56 %	39.7 s	2.9	3.1	^{139}Xe	0.22	2.3 s
^{144}La	0.398 0.541	94% 39 %	40.7 s	1.29	4.57	^{144}Ba	3.28	11.4 s
^{140}Cs	0.602	53 %	66 s	2.89	4.48	^{140}Xe	1.59	13.6 *s*

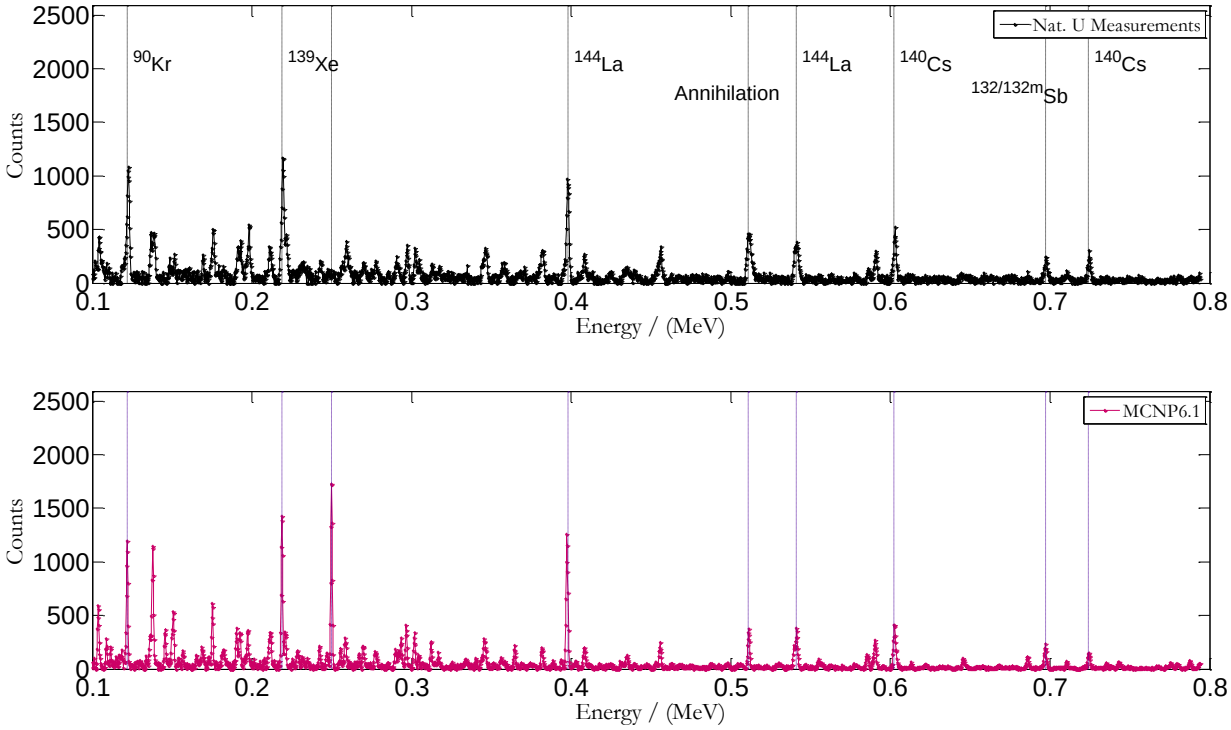

Figure 10.2: Nat. U Measurements (top) and MCNP6.1 Simulations (bottom): 0.1 – 0.8 *MeV*.

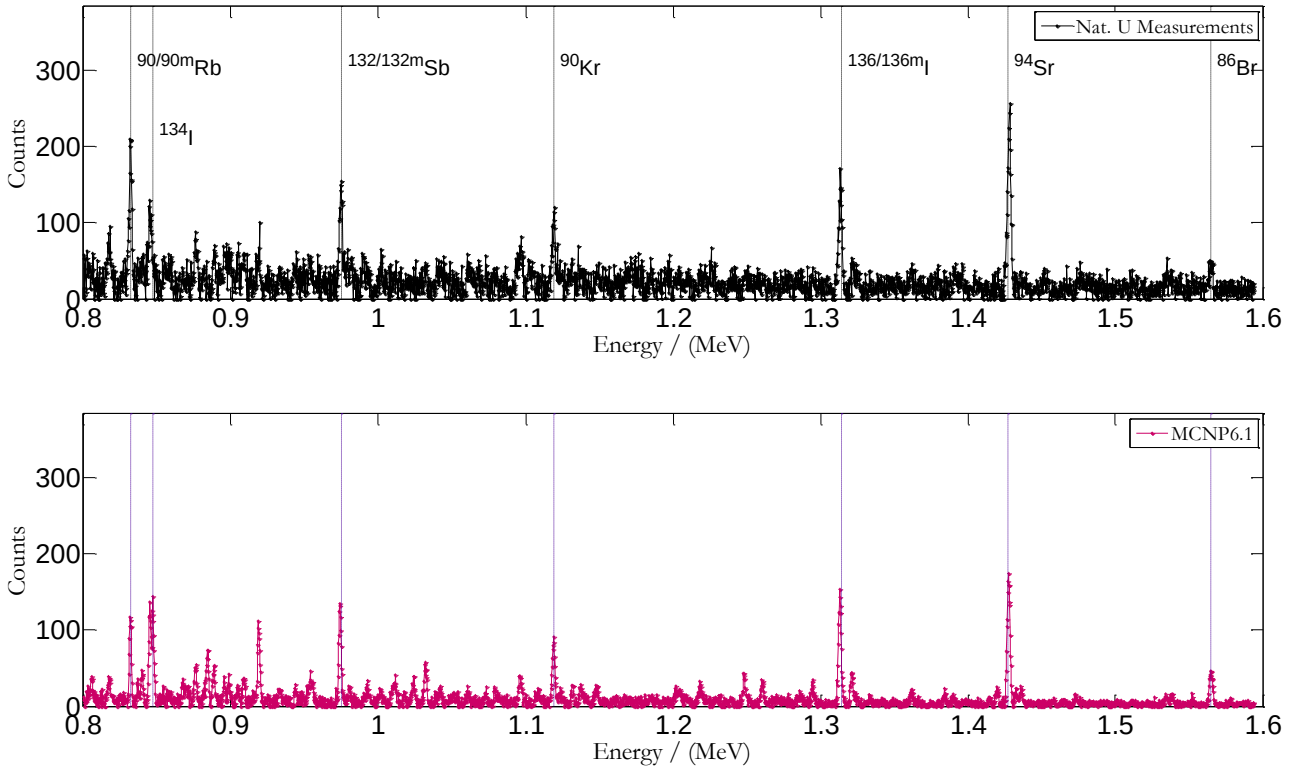

Figure 10.3: Nat. U Measurements (top) and MCNP6.1 Simulations (bottom): 0.8 – 1.6 *MeV*.

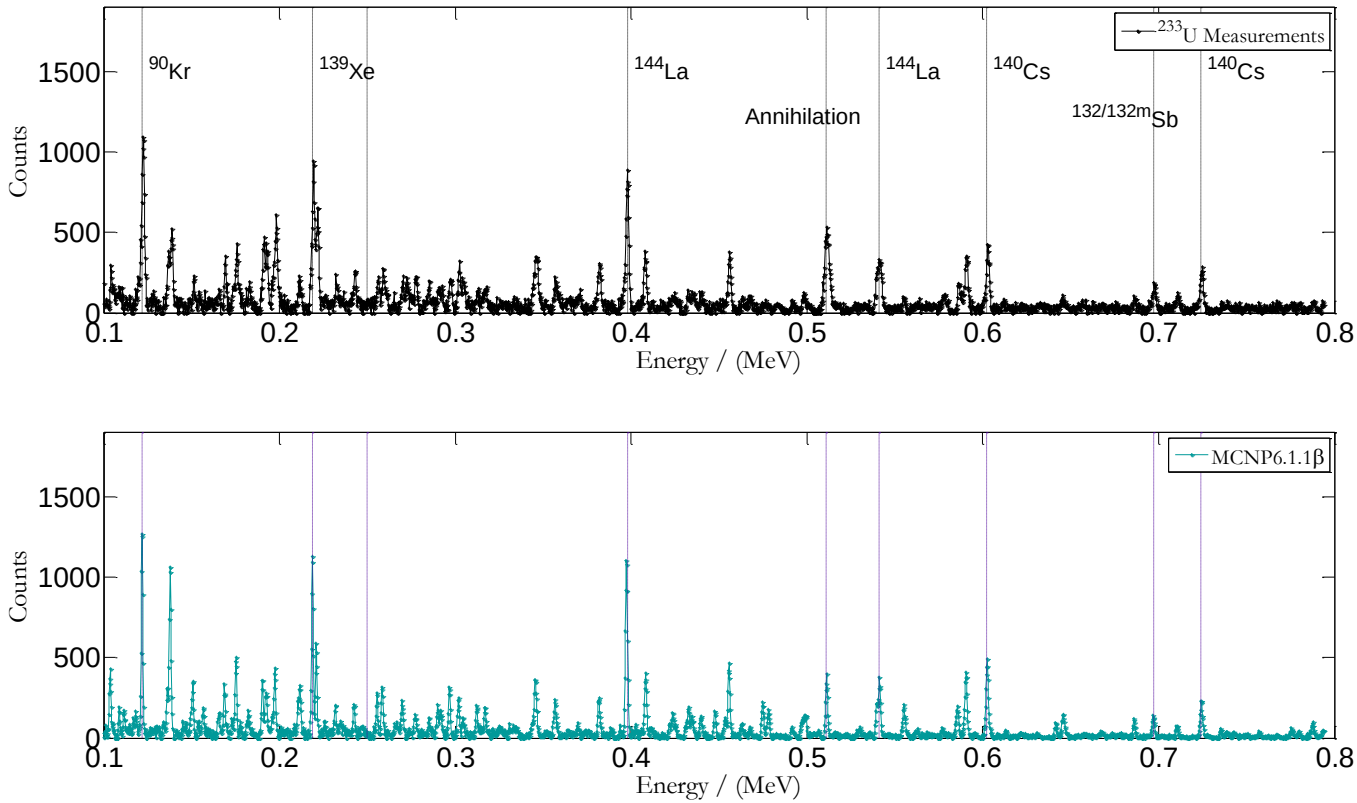

Figure 10.4: ^{233}U Measurements (top) and MCNP6.1.1β Simulations (bottom): 0.1 – 0.8 *MeV*.

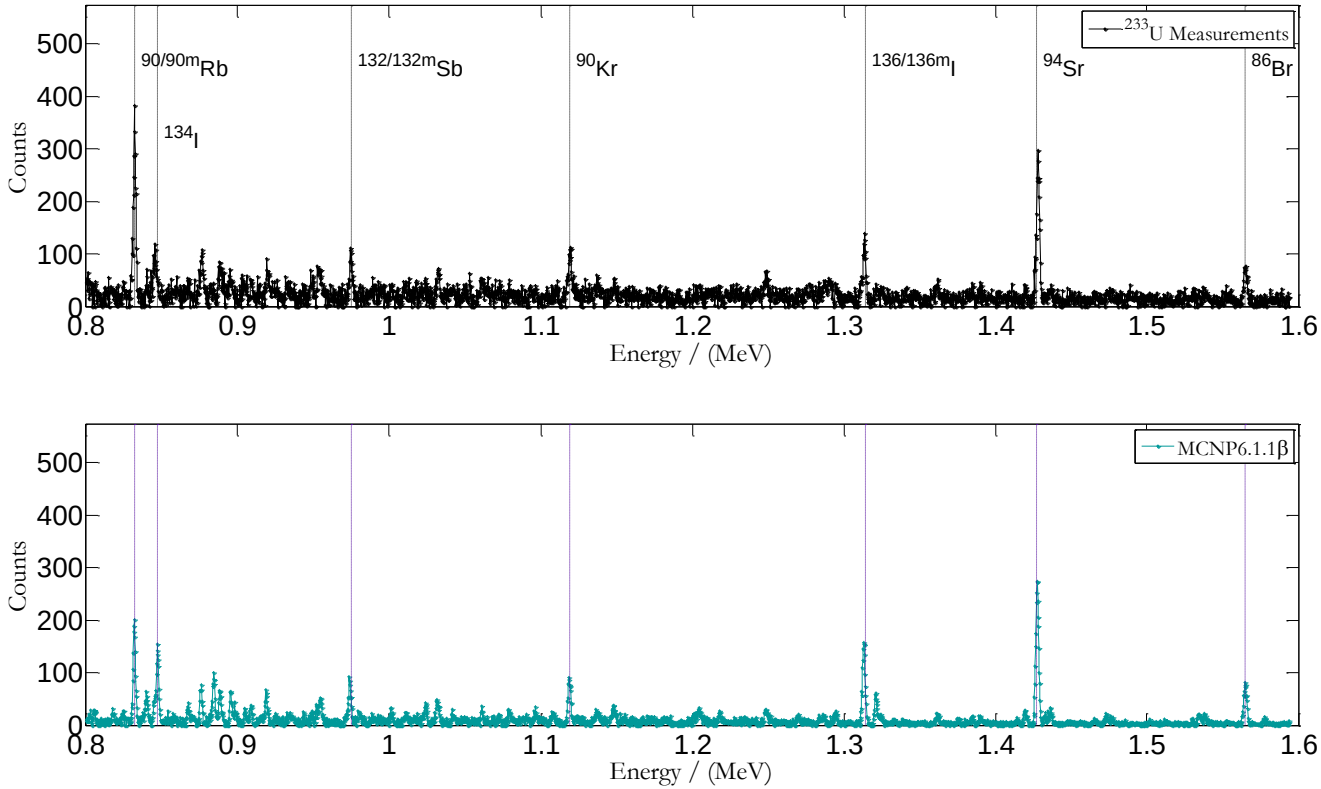

Figure 10.5: ^{233}U Measurements (top) and MCNP6.1.1β Simulations (bottom): 0.8 – 1.6 *MeV*.

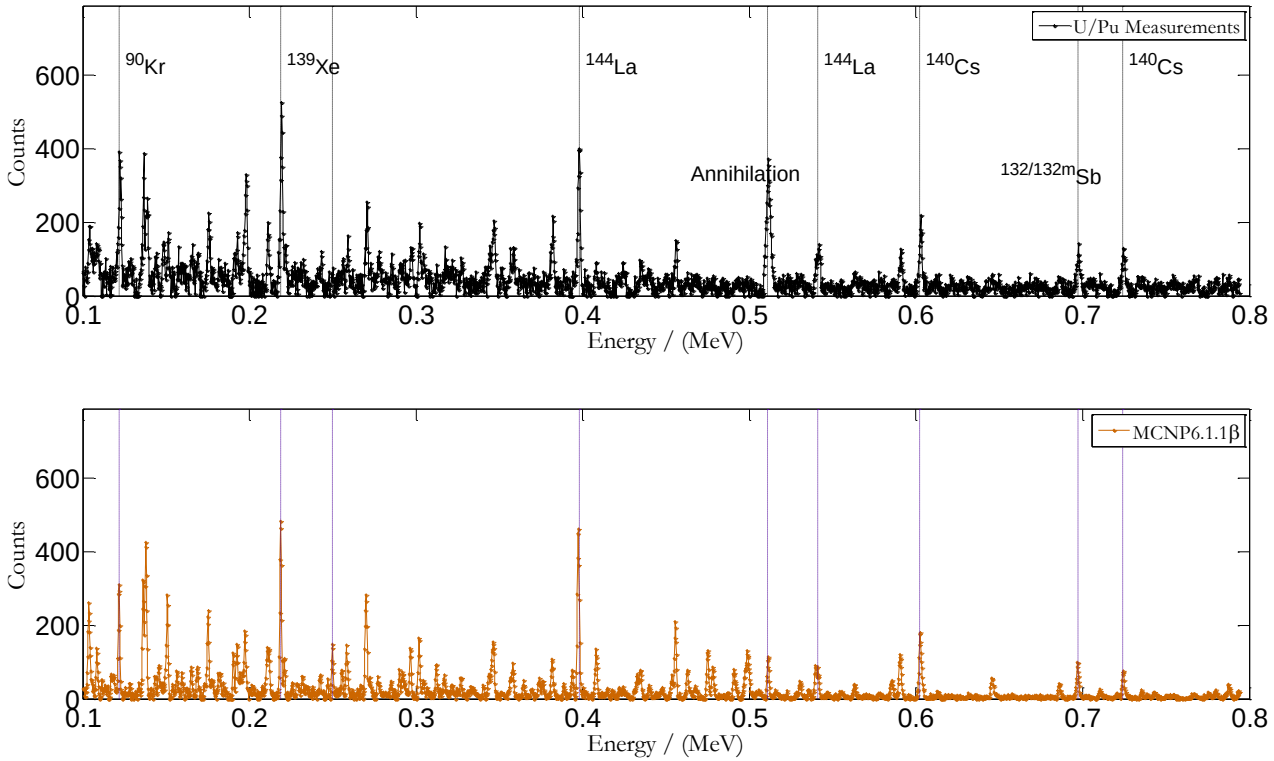

Figure 10.6: U/Pu Measurements (top) and MCNP6.1.1β Simulations (bottom): 0.1 – 0.8 *MeV*.

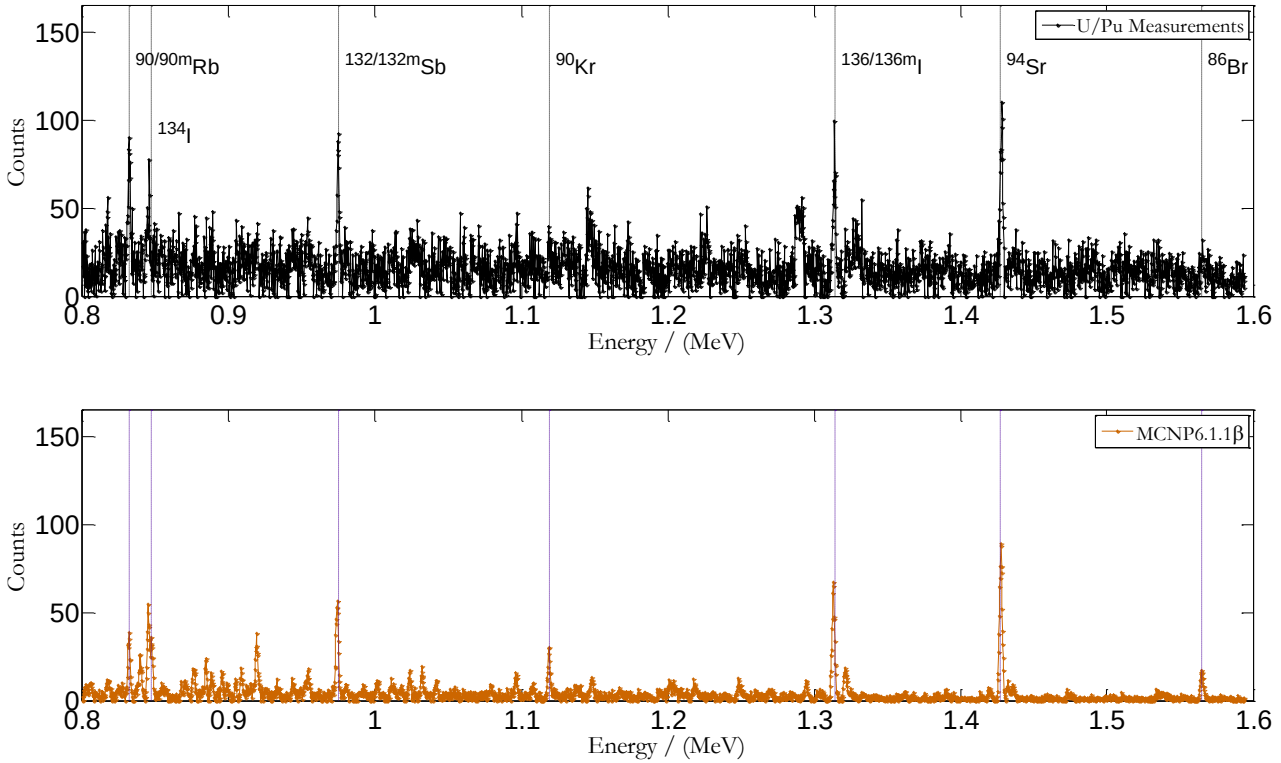

Figure 10.7: U/Pu Measurements (top) and MCNP6.1.1β Simulations (bottom): 0.8 – 1.6 *MeV*.

Two sources of anomalies in simulation and measurement comparisons were observed: i) those which could be attributed to HPGe detector activation, and most interesting ii) simulated peaks in MCNP output, not present in measurements. First, although gammas originating from activation and fission processes are modeled, delayed neutrons created by these interactions are not included in simulations. Thus, they are not transported in the detection simulation and their activation and energy depositions in the HPGe detector are not examined in this work. The most intensive gamma lines resultant from neutron capture in HPGe detectors, 0.139 and 0.198 *MeV* (Krmar *et al*., 2013), were present in measurements and expectantly discrepant from simulations. In addition, two prominent simulated peaks were not observed in measurements; 0.250 MeV (in simulations containing ^{235}U content) and 0.847 *MeV* (in all SNM comparisons), Figure 10.8. These energies correspond to intense gamma emissions from ^{135}Xe and ^{134}I with half-lives of 9 *hours* and 53 *min*, respectively, which are unexpected in simulations due to their long half-lives. To confirm the origin of the peaks, gamma line data for ^{135}Xe and ^{134}I found in the data file used for GL simulations in MCNP6 were removed and the simulations repeated. The absence of these emissions with ^{135}Xe and ^{134}I data removed confirmed these data to be the origin of this discrepancy. These anomalies were present in both MCNP6.1 and MCNP6.1.1β simulations, although with lesser prominence in the later. Also shown in Figure 10.8 is the large difference between simulated and measured ^{90}Rb magnitudes at 0.832 *MeV*, which is discussed in the subsequent section. Both MCNP6.1 and MCNP6.1.1β predicted the presence of the 25 most prominent measured fission product peaks, shown for the nat. U and ^{233}U comparisons.

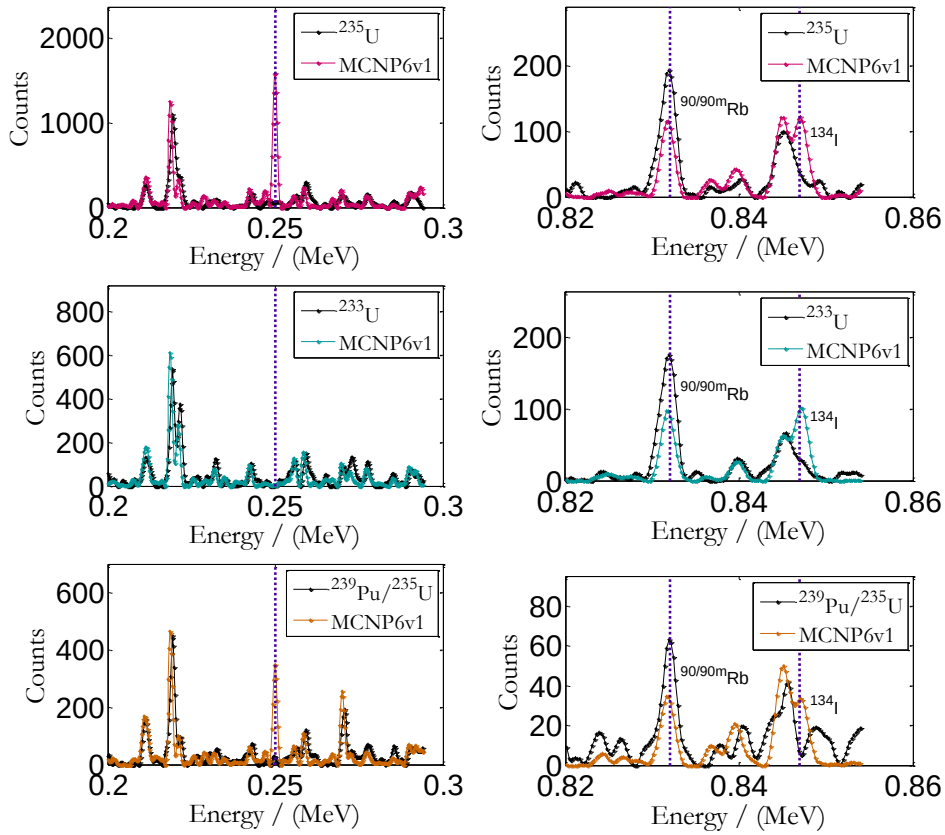

Figure 10.8: Some of the largest discrepancies between MCNP6.1 simulations and measurements include ^{135}Xe (0.250 *MeV*), $^{90/90m}$Rb (0.832 *MeV*), and ^{134}I (0.847 *MeV*). Discrepant energies are noted with vertical dashed lines.

10.5.2 **A Comparison of Peak Absolute Magnitudes**

MCNP6.1

Peaks with energies from 0.6 – 1.6 *MeV* were selected for detailed comparisons as these gamma emissions are associated with lower background contributions, less complex spectra (Marrs *et al.*, 2008), and encompass previous MCNP and measurement comparisons by (Durkee *et alet al.*, 2009). Net counts were determined by identifying the apex of each peak and summing the adjacent 10 channels (for a total energy range of 0.0025 *MeV*). The ratios displayed in Table 10.2 are those of MCNP6.1 simulations to measurements. Flux magnitude

uncertainties, the stochastic nature of DG emission, and uncertainties in efficiency corrections to MCNP simulations were included in calculations of confidence intervals. Several decay energies, corresponding to ^{140}Cs, ^{90}Kr, $^{136/136m}$I, and ^{86}Br were in good agreement with measurements; within the 95 % confidence intervals for all three materials examined. However, other isotopes, such as, ^{93}Sr, ^{145}Ce, and $^{90/90m}$Rb were well outside the quoted uncertainties of the measurements. The causes of these differences are not immediately apparent based on the comparison of simulation and experimental data.

Table 10.2: Prominent Observed Peaks and MCNP6:Measured Ratios 15-180 *s* after irradiation. 95 % Confidence Intervals (CIs) Included. Shaded ratios indicate they are within 2s of unity.

Energy / (MeV)	**Possible Origin and Half-Life**	**Ratio of MCNP6v1 to Measured Counts**		
		Nat. U (3.51 *ug* ^{235}U)	**U-233 (4.27 *ug*)**	**U/Pu Mix (1.32 *ug* fissile content)**
0.603	^{140}Cs (64 *s*)	0.85 ± 0.13	1.04 ± 0.15	0.96 ± 0.15
0.697	$^{132/132m}$Sb (2.8, 4 *min*)	0.93 ± 0.14	0.77 ± 0.12	0.85 ± 0.13
0.711	^{93}Sr (7.4 *min*)	0.59 ± 0.09	0.71 ± 0.11	0.68 ± 0.11
0.725	^{145}Ce (3.0 *min*)	0.56 ± 0.08	0.77 ± 0.12	0.56 ± 0.09
0.832	$^{90/90m}$Rb (158, 258 *s*)	0.55 ± 0.08	0.53 ± 0.08	0.54 ± 0.09
0.975	$^{132/132m}$Sb (2.8, 4 *min*)	0.79 ± 0.12	0.69 ± 0.11	0.79 ± 0.13
1.119	^{90}Kr (32 *s*)	0.76 ± 0.12	0.92 ± 0.14	0.93 ± 0.16
1.314	$^{136/136m}$I (47, 83 *s*)	0.96 ± 0.15	1.32 ± 0.21	0.85 ± 0.14
1.427	^{94}Sr (75 *s*)	0.71 ± 0.11	1.02 ± 0.15	0.85 ± 0.13
1.565	^{86}Br (66 *s*)	1.09 ± 0.18	1.11 ± 0.18	0.91 ± 0.16

Two samples containing ^{233}U content (2.3 and 4.27 μg) were prepared, irradiated, and counted under the same experimental conditions to examine mass dependencies and to evaluate the validity of the expressed uncertainties against experimental data. The former is particularly important in the present work, since gamma counts and consequent detector dead times occur as a function of fissile mass. The application of accurate dead time corrections result in consistent in MCNP6:measured ratios regardless of fissile mass. For none of the gamma lines considered was it possible to reject the null hypothesis that the observed ratios were statistically equivalent at a 95% confidence interval, Table 10.3.

Table 10.3: Examination of the Reproducibility of Ratios for Two Samples of ^{233}U. 95 % Confidence Intervals (CIs) Included.

Energy / (MeV)	Possible Origin	Ratio of MCNP6 to Measured Counts	
		U-233 (2.3 *ug*)	U-233 (4.27 *ug*)
0.603	^{140}Cs (64 *s*)	0.92 ± 0.14	1.04 ± 0.15
0.697	$^{132/132m}$Sb (2.8, 4 *min*)	0.73 ± 0.11	0.77 ± 0.12
0.711	^{93}Sr (7.4 *min*)	0.58 ± 0.09	0.71 ± 0.11
0.725	^{145}Ce (3.0 *min*)	0.70 ± 0.11	0.77 ± 0.12
0.832	$^{90/90m}$Rb (158, 258 *s*)	0.50 ± 0.08	0.53 ± 0.08
0.975	$^{132/132m}$Sb (2.8, 4 *min*)	0.76 ± 0.12	0.69 ± 0.11
1.119	^{90}Kr (32 *s*)	0.84 ± 0.13	0.92 ± 0.14
1.314	$^{136/136m}$I (47, 83 *s*)	1.14 ± 0.18	1.32 ± 0.21
1.427	^{94}Sr (75 *s*)	0.92 ± 0.14	1.02 ± 0.15
1.565	^{86}Br (66 *s*)	1.04 ± 0.18	1.11 ± 0.18

MCNP6.1.1β

The relative intensities of prominent emissions at energies marked were tallied as a function of time to examine the effects of the new time bin structure used for delayed particle production and further changes included in MCNP6.1.1β. The time-dependent emission of the most prominent peaks, denoted with vertical lines in Figure 10.2 through Figure 10.7 were tallied and compared. Though most showed minimal change, 4 of the isotopes tabulated, ^{135}Xe (0.250 *MeV*), ^{144}La (0.541 *MeV*), ^{134}I (0.847 *MeV*), and ^{94}Sr (1.427 *MeV*) showed significant differences in emission magnitude and temporal behaviour. ^{144}La and ^{135}Xe energies depict the temporal discrepancy at 100 *s* after the elapse of irradiation in MCNP6.1, which was previously noted in delayed neutron comparisons (Andrews *et al*., 2014b). These temporal anomalies at 100 *s* were indeed removed in MCNP6.1.1β simulations. Additionally, the prominence of the anomalies corresponding to ^{135}Xe and ^{134}I decay is reduced in MCNP6.1.1β simulations.

The same 10 decays selected for detailed MCNP6.1 comparison, Table 10.2, were also selected for comparison to MCNP6.1.1β simulations, Table 10.4. Overall there were no significant changes in ratios of MCNP6 to measured counts between the two executables with the exception of ^{94}Sr which increased from 0.71 ± 0.05 to 0.89 ± 0.07 (1*s*) for the nat. U comparison. MCNP6.1.1β simulations of $^{90/90m}$Rb, ^{93}Sr, and ^{145}Ce comparisons remained in poor agreement with measurements.

Updates to Gamma Line Emission Data

Although MCNP6 uses ENDF/B- VII data for the majority of its activities, when creating delayed gammas MCNP6 utilises *cindergl.dat* and *cinder.dat*, both of which are populated with ENDF/B-VI data. Although many lines produced acceptable ratios, including ^{140}Cs, ^{90}Kr, $^{136/136m}$I, and ^{86}Br, Table 10.2, a number of lines diverged significantly from unity for all of the comparisons, or for specific SNMs. Several of these discrepancies can be attributed to a number of cases where the branching ratios of ENDF/B-VI differ from the more current ENDF/B-VII decay library. Therefore a final comparison using updated *cindergl.dat* and *cinder.dat* files (populated with ENDF/B-VII data[xix]) with MCNP6.1.1β was performed. This final simulation resolved the 0.250 and 0.847 *MeV* anomalies, shown for Figure 10.9 and Figure 10.10, respectively. Furthermore, when the energies from Table 10.2 were examined there was significant improvement for many of the ratios, most notable ^{90}Rb, Figure 10.10. ^{145}Ce (0.725 *MeV*) simulations remain well below measured values. The branching ratios, half-life, and fission product yields used by MCNP6 simulations were compared to other nuclear data libraries, no discrepancies were found that could explain the large difference intensities.

[xix] Preliminary simulations found the MCNP6 executable did not read the entirety of the 3329 radionuclides in the updated *cindergl.dat*. Therefore this file was further modified to a final version which contained updated data for the original 979 isotopes.

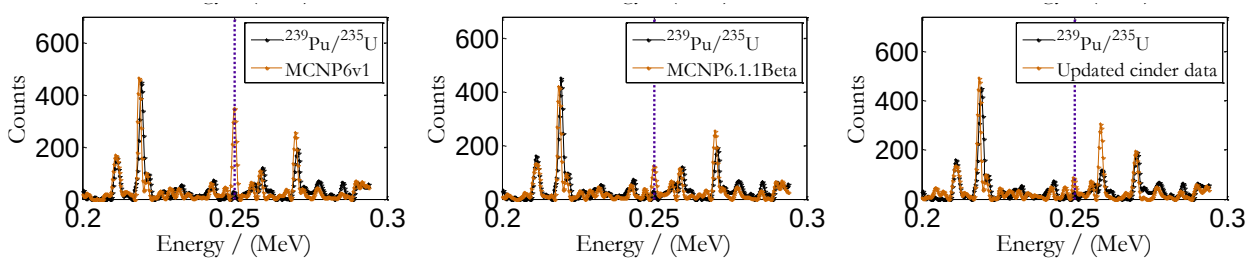

Figure 10.9: Measured cumulative counts from ^{239}Pu/^{235}U mixture in 0.2 – 0.3 *MeV* energy range and corresponding MCNP6.1 (left column), MCNP6.1.1β (middle), and MCNP6.1.1β with updated cinder data (right), simulations. The presence 0.250 *MeV* anomaly, corresponding to ^{135}Xe decay is reduced with the use of MCNP6.1.1 β and eliminated when updated *cinder.dat* and *cindergl.dat* files are used.

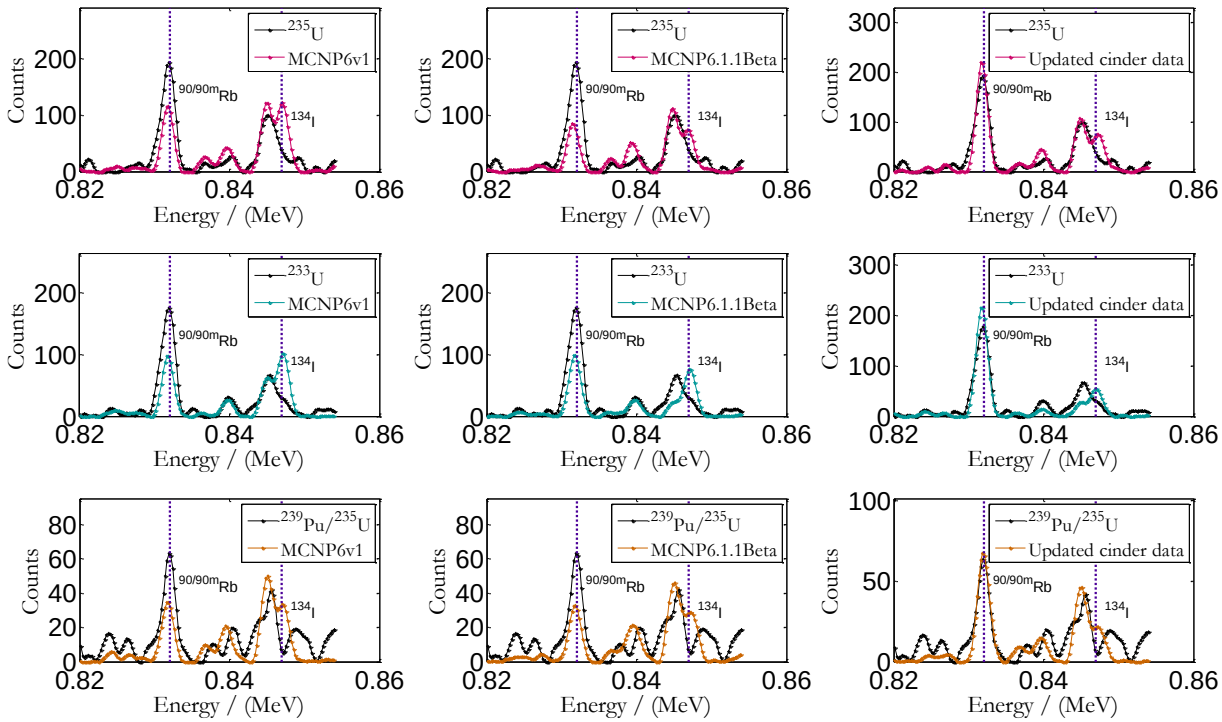

Figure 10.10: Measured cumulative counts in 0.82 – 0.86 *MeV* energy range and corresponding MCNP6.1 (left column), MCNP6.1.1β (middle), and MCNP6.1.1β with updated *cinder.dat* and *cindergl.dat* files (right), simulations. The presence 0.847 *MeV* anomaly, corresponding to ^{134}I decay is reduced with the use of MCNP6.1.1 β and further decreased when more recent cinder data files are used. Additionally, the discrepancy between measured counts at 0.832 *MeV* ($^{90/90m}$Rb decay) is resolved when an update to the cinder data files used.

Table 10.4: Prominent Observed Peaks and MCNP6.1.1 β with updated *cindergl.dat* and *cinder.dat* files : Measured Ratios 15-180 *s* after irradiation. 95 % Confidence Intervals (CIs) Included.

Energy / (MeV)	**Possible Origin and Half-Life**	**Ratio of MCNP6.1.1β with updated *cindergl.dat* and *cinder.dat* files to Measured Counts**		
		Nat. U (3.51 *ug* ^{235}U)	**U-233 (4.27 *ug*)**	**U/Pu Mix (1.32 *ug* fissile content)**
0.603	^{140}Cs (64 *s*)	0.81 ± 0.12	1.00 ± 0.15	0.97 ± 0.15
0.697	$^{132/132m}$Sb (2.8, 4 *min*)	1.03 ± 0.16	0.81 ± 0.12	0.93 ± 0.15
0.711	^{93}Sr (7.4 *min*)	0.70 ± 0.11	0.86 ± 0.13	0.96 ± 0.15
0.725	^{145}Ce (3.0 *min*)	0.59 ± 0.09	0.78 ± 0.12	0.63 ± 0.10
0.832	$^{90/90m}$Rb (158, 258 *s*)	1.03 ± 0.16	1.19 ± 0.18	1.06 ± 0.17
0.975	$^{132/132m}$Sb (2.8, 4 *min*)	0.93 ± 0.14	0.99 ± 0.15	0.95 ± 0.15
1.119	^{90}Kr (32 *s*)	0.85 ± 0.13	0.86 ± 0.13	0.89 ± 0.15
1.314	$^{136/136m}$I (47, 83 *s*)	0.87 ± 0.13	1.24 ± 0.19	0.80 ± 0.13
1.427	^{94}Sr (75 *s*)	0.62 ± 0.09	1.00 ± 0.15	0.84 ± 0.13
1.565	^{86}Br (66 *s*)	1.14 ± 0.19	1.07 ± 0.17	0.79 ± 0.14

10.6 Conclusions & Future Work

Comparisons of measurements and MCNP6 simulations of microgram quantities of SNM were performed from 0.1-1.6 M*eV*. MCNP6 predicted the presence of the 25 most prominent fission product peaks observed in measurements for each SNM with varying degrees of accuracy. Ten DG emissions with energies from 0.6 – 1.6 *MeV* were selected for detailed comparisons of relative intensities for ^{233}U, nat. U, and ^{235}U/^{239}Pu samples, for a total of 30 cases. MCNP6.1 simulations of those fission product peak intensities were in agreement with measurements for 19/30 cases examined. This number increased to 26/30 pairs in agreement when MCNP6.1.1β was used with updated *cindergl.dat* and *cinder.dat* files. Additionally, the anomalous 0.250 and 0.847 *MeV* peaks predicted by MCNP6.1 were resolved. The present work demonstrates the value of experimental and simulation comparisons in identifying experimental artifacts and simulation discrepancies. Future work includes the expansion of comparisons to include longer irradiation and count times. Additionally, MCNP6 simulations of those isotopes in good agreement with measurements will be used to identify gamma line

pairs useful for special nuclear materials identification and characterisation in an upcoming nuclear forensic exercise at RMCC. In regard to such exercises, MCNP6 simulations allow advanced preparation to determine appropriate irradiation, decay, and count timing in a significantly more efficient and inexpensive manner that can be achieved by preparatory experimental studies.

10.7 Acknowledgements

Funding for this work was provided by the Advanced Simulations and Computing Program at LANL, a CNSC sponsored doctoral award, and NSERC. The technical assistance of K. Mattson, K. Nielson, T. Mumby, and D. Ferguson is appreciated. The authors appreciate the updated files *cindergl.dat* and *cinder.dat* provided by T. Wilcox.

-This page is intentionally left blank-

Chapter 11

Summary, Conclusions, & Recommendations

11.1 Summary

11.1.1 Delayed Neutron and Gamma Measurements from Special Nuclear Materials

This thesis describes the use of delayed neutron and gamma measurements at the Royal Military College of Canada (RMCC) to detect, identify, and quantify Special Nuclear Materials (SNMs). A prototype-delayed neutron counting (DNC) was created at the RMCC (Chapter 3). The origin of the time-dependent neutron background in the prototype-delayed neutron counting (DNC) system was attributed to uranium contamination within the irradiation site (Chapter 4). Analysis of the vials used for irradiation concluded the site was contaminated and that fission products became embedded in the vials as the sample underwent irradiation. Many of these fission products were themselves delayed neutron precursors, which were responsible for the time-dependent neutron count rate. The effects of the fission product depositions on the vial surfaces were reduced 58 % when the site was cleaned.

The DNC was then used to examine samples containing mixtures of ^{233}U and ^{235}U content, which range from 0 to 100 % ^{233}U as a function of total fissile mass (Chapter 5). By examining the differences in temporal delayed neutron (DN) emissions as a function of count time, the relative ratio of ^{233}U to that of ^{235}U (in %) was determined with average absolute errors of ± 4 %. Samples contained between 1.7 and 9.4 μg of total fissile mass, the DNC system found the absolute mass of ^{233}U and ^{235}U with average absolute errors of 0.3 and 0.2 μg, respectively.

The prototype DNC system was updated to the Delayed Neutron and Gamma Counting (DNGC) system (Chapter 8). Delayed gamma measurements were facilitated by a re-arrangement of the existing ^{3}He detectors and the inclusion of a High Purity Germanium (HPGe) detector. Parallel updates to the hardware and software were included, and system characterisation was confirmed with MCNP simulations. The applicability of the system to nuclear forensic studies was

demonstrated when delayed gamma line measurements from ^{89}Rb and ^{138}Cs were used to confirm the presence of ^{233}U in aqueous solutions. The measured delayed neutron measurements facilitated the determination of ^{233}U content with an average relative error and accuracy of -2.2 and 1.5 *%*, respectively.

11.1.2 Monte Carlo Simulations

Delayed neutron and gamma measurements of ^{233}U, ^{235}U, and ^{239}Pu, were used to examine the capability of MCNP6 to model these emissions and their detection. The irradiation of vials in a SLOWPOKE-2 reactor, and the subsequent detection of the delayed neutron and gamma emissions by the DNC and DNGC system were simulated in MCNP6 so that direct comparisons could be facilitated. The DNC neutron detection efficiencies were successfully predicted by MCNP6 (Chapter 6) and library and model options for DN emissions were compared to measured magnitudes and temporal behaviour. Significant discrepancies between the DN model option and measurements for count times > 100 *s* were observed, and eliminated in the following release of MCNP6.1.1β (Chapter 7). A preliminary version of a DN test suite created using these simulations and measurements was released with MCNP6.1, it has since been updated (Chapter 7).

Delayed gamma measurements from SNM irradiation in DNGC system were also compared to the production release version of MCNP6.1 and the more recent MCNP6.1.1β version (Chapter 9, Chapter 10). MCNP6 simulations successfully predicted the presence of the 25 most prominent measured fission product peaks in the 0.1 – 1.6 *MeV* observed during a 3 *min* count following the termination of irradiation. A detailed comparison of > 0.6 *MeV* gamma lines found several discrepancies in MCNP6.1 comparison, many of which were resolved using the updated time-bin probability function used to sample delayed particle time of emission in MCNP6.1.1β. Finally, the benefit of updating the gamma line data files used in simulations, to more current libraries is demonstrated as 26/30 gamma lines selected for comparison would then be in agreement, compared to the original 19/30.

11.1.3 Applications

This work has demonstrated the applicability of delayed neutron and gamma measurements to detect, identify, and quantify trace amounts of SNM content, non-destructively, and rapidly. These measurements also afforded the opportunity to examine the capabilities of MCNP6 to simulate detection systems, which measure delayed neutron and gamma emissions. MCNP6 simulations identified avenues of improvement in the detection apparatus, demonstrated in the simulation and reduction of photon pulse pile-ups in the ^{3}He detector arrangement. The MCNP6 simulations of the DNGC system also provide the opportunity to

predict expected delayed neutron and photon signatures from nuclear forensic samples. These simulations will be used in preparation for an upcoming NFA exercise.

11.2 Conclusions

In conclusion:

- The source of time-dependent neutron counts in RMCC's delayed neutron counting system was determined and minimized.
- Monte Carlo simulations were used to identify and improve experimental deficiencies in the DNC system, resulting in a Delayed Neutron and Gamma Counting system which is able to detect and quantify special nuclear material content.
- Many successful experiments have been performed with the DNC and DNGC systems. The results of these experiments have been used to identify contamination, validate computer models, and quantify the isotopic composition of SNM.
- Both the DNC and DNGC system measurements have been compared to MCNP6 simulations of delayed particle emissions and detections. MCNP6 simulation capabilities and deficiencies were identified and addressed.
- The DNGC system will remain operational at the RMCC. The system and the models developed by this thesis will be utilized in upcoming NFA exercises and isotopic identification on suspected SNM, if required.

11.3 Recommendations

11.3.1 Hardware & Software Suggestions

Data acquisition of the DNGC system could be improved through the update to software and hardware currently used. Specific and relatively inexpensive examples include the shortening of the cable length between the ^{3}He detectors and their preamplifier. Decreases in neutron and photon background in the system could be facilitated by the inclusion of borated polyethylene and lead shielding, respectively. Finally, directly connecting each ^{3}He detector to an individual preamplifer and multichannel analyzer could decrease dead-time effects.

11.3.2 **Delayed Neutron Temporal Measurements**

This thesis examined the delayed neutron emissions recorded for 3 *mins* following a 60 *s* irradiation and 3 *s* decay. It is recommended that other experimental timings for irradiation, decay, and counting, and their effect on the accuracy and precision of results are examined. For example, an irradiation time of 120 *s* for samples containing small amounts of fissile content (and therefore low dead time contributions) could increase the signal to noise ratio. Whereas samples containing substantial SNM content would benefit from short irradiation times that would decrease the effects of dead time on the distortion of the signal. The capability of the DNGC system to characterise mixtures should be expanded to include those from ^{239}Pu and ^{235}U as these are significantly more likely to be found together in a sample.

11.3.3 **Additional MCNP6 Comparisons**

The use of longer lived fission products (those with half-lives ~10 *mins* – 1 *hour)* and their delayed gamma emissions as a useful NFA signature should be examined both experimentally and with MCNP6. Furthermore, a delayed gamma test suite, similar to the one discussed in Chapter 7 should be created using these simulations and measurements.

Chapter 12

References

AECL (2014). Canadian National Nuclear Forensic Capability Project Stream 1: NF Lab Network, Nuclear Forensics International Technical Working Group (ITWG) 4th Collaborative Materials Exercise (CMX-4).

Amiel, S., and Peisach, M. (1963). Oxygen-18 Determination by Counting Delayed Neutrons of Nitrogen-17. Analytical Chemistry *35*, 323–327.

Andrews, W.S. (1989). Thermal Neutron Flux Mapping around the Reactor Core of the SLOWPOKE-2 at RMC, M. Eng. Thesis, RMC, Kingston, Canada.

Andrews, M.T., Corcoran, E.C., Kelly, D.G., and Goorley, J.T. (2013). Fission Product γ-ray Measurements of 235U and MCNP6 Predictions. Transactions of the American Nuclear Society *109*, 995–998.

Andrews, M.T., Beames-Canivet, T.L., Kelly, D.G., Corcoran, E.C., and Goorley, J.T. (2014a). Updated Delayed Neutron Counting Test Suite Comparisons from RMCC and MCNP6 Version 1 Release (Los Alamos National Laboratory).

Andrews, M.T., Goorley, J.T., Corcoran, E.C., and Kelly, D.G. (2014b). Modeling the Detection of Delayed Neutron Signatures in MCNP6 and Comparisons with Measurements of 233 U, 235U, and 239Pu. Nuclear Technology *187*, 235–242.

Andrews, M.T., Goorley, J.T., Corcoran, E.C., and Kelly, D.G. (2014c). Uranium and Plutonium Fission Product Gamma Intensity Measurements and MCNP6 Simulations. Transactions of the American Nuclear Society *110*, 490–493.

Andrews, M.T., Goorley, J.T., Corcoran, E.C., and Kelly, D.G. (2015a). MCNP6 Simulations of Gamma Line Emissions from Fission Products and their Comparisons to Plutonium and Uranium Measurements. Progress in Nuclear Energy.

Andrews, M.T., Corcoran, E.C., Goorley, J.T., and Kelly, D.G. (2015b). A System for the Measurement of Delayed Neutrons and Gammas from Special Nuclear Materials. Journal of Radioanalytical and Nuclear Chemistry.

Arthur, R.J., and Reeves, J.H. (1992). Methods for achieving ultra-low backgrounds in above-ground germanium detector systems. Journal of Radioanalytical and Nuclear Chemistry, Articles *160*, 297–304.

Beddingfield, D.H., and Cecil, F.E. (1998). Identification of fissile materials from fission product gamma-ray spectra. Nuclear Instruments and Methods in Physics Research Section A: Accelerators, Spectrometers, Detectors and Associated Equipment *417*, 405–412.

Belian, A.P., Bourva, L.C., Kane, S.C., and Lebrun, A.R. (2009). The Use of Monte Carlo techniques for the calibration of IAEA safeguards instrumentation. In 2009 First International Conference on Advancements in Nuclear Instrumentation Measurement Methods and Their Applications (ANIMMA), pp. 1–6.

Benzing, R., Baghini, N.M., Bennett, B.A., and Parry, S.J. (2000). Apparent neutron emissions from polyethylene capsules during neutron activation and delayed neutron counting. Journal of Radioanalytical and Nuclear Chemistry *244*, 447–451.

Binney, S.E., and Scherpelz, R.I. (1978). A review of the delayed fission neutron technique. Nuclear Instruments and Methods *154*, 413–431.

Boson, J., Agren, G., and Johansson, L. (2008). A detailed investigation of HPGe detector response for improved Monte Carlo efficiency calculations. Nuclear Instruments and Methods in Physics Research Section A: Accelerators, Spectrometers, Detectors and Associated Equipment *587*, 304–314.

Bronson, F.L., McElroy, R., Philips, S., Russ, W., and Croft, S. (2009). The application of mathematical modeling for commercial nuclear instrument design, development, and calibration. In Advancements in Nuclear Instrumentation Measurement Methods and Their Applications (ANIMMA), (IEEE), pp. 1–8.

Brown, F.B. (2005). Fundamentals of monte carlo particle transport. Los Alamos National Laboratory, LA-UR-05-4983.

Brown, F.B. (2014). Nuclear Fission in Monte Carlo Particle Transport Simulations (FIESTA 2014, Fission School and Workshop).

Chadwick, M.B., Obložinský, P., Herman, M., Greene, N.M., McKnight, R.D., Smith, D.L., Young, P.G., MacFarlane, R.E., Hale, G.M., Frankle, S.C., *et al.* (2006). ENDF/B-VII.0: Next Generation Evaluated Nuclear Data Library for Nuclear Science and Technology. Nuclear Data Sheets *107*, 2931–3060.

Compton, A.H., and Allison, S.K. (1935). X-rays in Theory and Experiment.

Le Coq, A.G. (2013). Design of a Safeguards Instrument for Plutonium Quantification in an Electrochemical Refining System. Master's Thesis, Texas A & M University. Available Electronically from Http://hdl. Handle. net/1969 *1*, 151148.

Davisson, C.M., and Evans, R.D. (1952). Gamma-ray absorption coefficients. Reviews of Modern Physics *24*, 79.

DOE Handbook. (1993). Nuclear Physics and Reactor Theory. Washington DC: Department of Energy.

Duke, M.J.M., Taylor, C.A., and Fernando, A. (2000). Uranium analysis of ores and tailings: a comparison of delayed neutron counting, natural gamma-ray spectrometry, INAA and XRF. In 3rd International Conference on Isotopes: Isotope Production and Applications in the 21st Century., (World Scientific), p. 1142.

Durkee, J.W. (2012). Characterization of Delayed-Neutron and Delayed-Gamma Pyroprocessing Emission Signatures Using MCNP6 (Los Alamos National Laboratory (LANL)).

Durkee, J.W., James, M.R., McKinney, G.W., Trellue, H.R., Waters, L.S., and Wilson, W.B. (2009). Delayed-gamma signature calculation for neutron-induced fission and activation using MCNPX. Part II: Simulations. Progress in Nuclear Energy *51*, 828–836.

Durkee, J.W., James, M.R., McKinney, G.W., Waters, L.S., and Goorley, T. (2012). The MCNP6 Delayed-Particle Feature. Nuclear Technology *180*, 336–354.

Van Eijk, C.W. (2012). Inorganic scintillators for thermal neutron detection. Nuclear Science, IEEE Transactions on *59*, 2242–2247.

El-Jaby, A., Kosierb, R., Dimayuga, I., Edwards, G., Barber, D., Wojtaszek, D., and Doucet, F. (2014). Galaxy Serpent Virtual Tabletop Exercise: Canada's Approach, Findings, and Lessons Learned. Nuclear Materials Management *42*.

England, T.R., and Rider, B.F. (1994). ENDF-349 evaluation and compilation of fission product yields. Rep (LA-UR-94-3106).

Eriksson, S.M., Mackey, E.A., Lindstrom, R.M., Lamaze, G.P., Grogan, K.P., and Brady, D.E. (2013). Delayed-neutron activation analysis at NIST. Journal of Radioanalytical and Nuclear Chemistry *298*, 1819–1822.

Firestone, R.B., English, G.A., Reijonen, J., and Gicquel, F. (2005). Analysis of fissile materials by high-energy neutron-induced fission decay gamma-rays. J Radioanal Nucl Chem *265*, 241–245.

Glaser, A. (2006). On the proliferation potential of uranium fuel for research reactors at various enrichment levels. Science and Global Security *14*, 1–24.

Glasgow, D.C. (2008). Delayed neutron activation analysis for safeguards. Journal of Radioanalytical and Nuclear Chemistry *276*, 207–211.

Glasstone, S., and Sesonske, A. (1967). Nuclear reactor engineering, 1967. Reinhold: Van Nostrand.

Gmar, M., and Capdevila, J.M. (1999). Use of delayed gamma spectra for detection of actinides (U, Pu) by photofission. Nuclear Instruments and Methods in Physics Research Section A: Accelerators, Spectrometers, Detectors and Associated Equipment *422*, 841–845.

Goorley, J.T. (2013). MCNP6 Version 1.0 Known Issues. Los Alamos National Laboratory Technical Report.

Goorley, J.T. (2014). MCNP 6.1.1–Beta Release Notes. Los Alamos National Laboratory Technical Report.

Goorley, T., James, M., Booth, T., Brown, F., Bull, J., Cox, L.J., Durkee, J., Elson, J., Fensin, M., Forster, R.A., *et al*. (2012). Initial MCNP6 release overview. Nuclear Technology *180*, 298–315.

Grant, P.M., Moody, K.J., Hutcheon, I.D., Phinney, D.L., Whipple, R.E., Haas, J.S., Alcaraz, A., Andrews, J.E., Klunder, G.L., Russo, R.E., *et al*. (1998). Nuclear forensics in law enforcement applications. Journal of Radioanalytical and Nuclear Chemistry *235*, 129–132.

Grogan, K.P., and O'Kelly, D.J. (2014). Analytical applications of delayed and instrumental neutron activation analysis. Journal of Radioanalytical and Nuclear Chemistry *299*, 543–549.

Grover, J.R., and Gilat, J. (1967). De-Excitation of Highly Excited Nuclei. Physical Review *157*, 802.

Haciyakupoglu, S., and Gencay, S. (1999). Determination of 235 U/238 U ratio by instrumental neutron activation analysis. Journal of Radioanalytical and Nuclear Chemistry *241*, 611–616.

Hall, H. (1936). The theory of photoelectric absorption for X-rays and γ-rays. Reviews of Modern Physics *8*, 358.

Hendricks, J.S., Adams, K.J., Booth, T.E., Briesmeister, J.F., Carter, L.L., Cox, L.J., Favorite, J.A., Forster, R.A., McKinney, G.W., and Prael, R.E. (2000). Present and future capabilities of MCNP. Applied Radiation and Isotopes *53*, 857–861.

Henzl, V., Croft, S., Richard, J., Swinhoe, M.T., and Tobin, S.J. (2013). Determination of the plutonium content in a spent fuel assembly by passive and active interrogation using a differential die-away instrument. Nuclear Instruments and Methods in Physics Research Section A: Accelerators, Spectrometers, Detectors and Associated Equipment *712*, 83–92.

Hilborn, J.W., and Townes, B.M. (1987). Converting the SLOWPOKE reactor to low-enrichment uranium fuel. Journal of Radioanalytical and Nuclear Chemistry *110*, 385–392.

Hollas, C.L., Close, D.A., and Moss, C.E. (1987). Analysis of fissionable material using delayed gamma rays from photofission. Nuclear Instruments and Methods in Physics Research Section B: Beam Interactions with Materials and Atoms *24–25, Part 1*, 503–505.

IAEA (2014a). IAEA Incident and Trafficking Database (ITDB): Incidents of nuclear and other radioactive material out of regulatory control, 2014 fact sheet (International Atomic Energy Agency).

IAEA (2014b). How we implement safeguards. http://www.iaea.org/safeguards/what.html Accessed November 14, 2014.

ISO, B. (2005). IEC 17025: 2005 General requirements for the competence of testing and calibration laboratories. Requisitos Gerais de Competência Para Laboratórios de Ensaio E Calibração.

Johansson, S.A. (1965). Gamma de-excitation of fission fragments:(II). Delayed radiation. Nuclear Physics *64*, 147–160.

Kaplan, A.C., Henzl, V., Menlove, H.O., Swinhoe, M.T., Belian, A.P., Flaska, M., and Pozzi, S.A. (2014). Determination of total plutonium content in spent nuclear

fuel assemblies with the differential die-away self-interrogation instrument. Nuclear Instruments and Methods in Physics Research Section A: Accelerators, Spectrometers, Detectors and Associated Equipment *764*, 347–351.

Kapsimalis, R.J. (2013). The simultaneous quantification of fissile U and Pu nuclides using delayed neutron activation analysis. PhD Dissertation. University of Texas at Austin.

Kapsimalis, R., Glasgow, D., Anderson, B., and Landsberger, S. (2013). The simultaneous determination of 235U and 239Pu using delayed neutron activation analysis. Journal of Radioanalytical and Nuclear Chemistry *298*, 1721–1726.

Kawano, T., Möller, P., and Wilson, W.B. (2008). Calculation of delayed-neutron energy spectra in a quasiparticle random-phase approximation–Hauser-Feshbach model. Physical Review C *78*, 054601.

Keepin, G.R., Wimett, T.F., and Zeigler, R.K. (1957). Delayed neutrons from fissionable isotopes of uranium, plutonium and thorium. Journal of Nuclear Energy (1954) *6*, IN2–IN21.

Kelly, D.G., Bennett, L.G.I., Fill, M.M., Mattson, K.M., Nielsen, K.S., White, S.D., and Allen, J.F. (2008). Analytical methods for the environmental quantification of uranium isotopes: Method of validation and environmental application. Journal of Radioanalytical and Nuclear Chemistry *278*, 807–811.

Kennedy, G., St-Pierre, J., Wang, K., Zhang, Y., Preston, J., Grant, C., and Vutchkov, M. (2000). Activation constants for Slowpoke and MNS reactors calculated from the neutron spectrum and k0 and Q0 values. Journal of Radioanalytical and Nuclear Chemistry *245*, 167–172.

Knoll, G.F. (2010). Radiation detection and measurement (John Wiley & Sons).

Kouzes, R.T., and Ely, J.H. (2010). Status summary of 3He and neutron detection alternatives for homeland security (Pacific Northwest National Laboratory).

Kouzes, R.T., Ely, J.H., Erikson, L.E., Kernan, W.J., Lintereur, A.T., Siciliano, E.R., Stephens, D.L., Stromswold, D.C., Van Ginhoven, R.M., and Woodring, M.L. (2010). Neutron detection alternatives to 3He for national security applications. Nuclear Instruments and Methods in Physics Research Section A: Accelerators, Spectrometers, Detectors and Associated Equipment *623*, 1035–1045.

Kraner, H.W., Pehl, R.H., and Haller, E.E. (1975). Fast Neutron Radiation Damage of High-Purity Germanium Detectors. IEEE Transactions on Nuclear Science *22*, 149–159.

Kristo, M.J., Smith, D.K., Niemeyer, S., and Dudder, G.B. (2004). Model Action Plan for Nuclear Forensics and Nuclear Attribution. Lawrence Livermore National Laboratory.[2004]. URL: Https://ereports-Ext. Llnl. gov/pdf/305453. Pdf (access Date: 15.01. 2010).

Krmar, M., Hansman, J., Jovančević, N., Lalović, N., Slivka, J., Joković, D., and Maletić, D. (2013). A method to estimate a contribution of Ge (n,n′) reaction to the low-energy part of gamma spectra of HPGe detectors. Nuclear Instruments and Methods in Physics Research Section A: Accelerators, Spectrometers, Detectors and Associated Equipment *709*, 8–11.

Lakosi, L., Tam Nguyen, C., and Serf, E. (2011). Neutron interrogation of shielded/unshielded uranium by a 4MeV linac. Applied Radiation and Isotopes *69*, 1251–1254.

Landsberger, S., Biegalski, S., Kapsimalis, R., Pryor, M., and Tamalis, D. (2013). Nuclear forensics education at the University of Texas at Austin. Journal of Radioanalytical and Nuclear Chemistry *296*, 333–337.

Larsson, C.L., and Haslip, D.S. (2004). Consolidated Canadian Results to the HEU Round Robin Exercise (DTIC Document).

Larsson, C.L., and Hinton, A. (2006). Nuclear Forensic Field Exercise# 1 (DTIC Document).

Lee, C.-G., Suzuki, D., Esaka, F., Magara, M., Shinohara, N., and Usuda, S. (2009). Selective detection of particles containing highly enriched uranium for nuclear safeguards environmental samples. Journal of Nuclear Science and Technology *46*, 809–813.

Lee, T.-H., Menlove, H.O., Swinhoe, M.T., and Tobin, S.J. (2011). Monte Carlo simulations of differential die-away instrument for determination of fissile content in spent fuel assemblies. Nuclear Instruments and Methods in Physics Research Section A: Accelerators, Spectrometers, Detectors and Associated Equipment *652*, 103–107.

Leggitt, J., Inn, K., Goldberg, S., Essex, R., LaMont, S., and Chase, S. (2009). Nuclear forensics—metrological basis for legal defensibility. Journal of Radioanalytical and Nuclear Chemistry *282*, 997–1001.

Li, X., Henkelmann, R., and Baumgärtner, F. (2004). Rapid determination of uranium and plutonium content in mixtures through measurement of the intensity–time curve of delayed neutrons. Nuclear Instruments and Methods in Physics Research Section B: Beam Interactions with Materials and Atoms *215*, 246–251.

Marrs, R.E., Norman, E.B., Burke, J.T., Macri, R.A., Shugart, H.A., Browne, E., and Smith, A.R. (2008). Fission-product gamma-ray line pairs sensitive to fissile material and neutron energy. Nuclear Instruments and Methods in Physics Research Section A: Accelerators, Spectrometers, Detectors and Associated Equipment *592*, 463–471.

Mayer, K., Wallenius, M., and Ray, I. (2005). Nuclear forensics—a methodology providing clues on the origin of illicitly trafficked nuclear materials. Analyst *130*, 433–441.

Mayer, K., Wallenius, M., and Ray, I. (2006). Tracing the origin of diverted or stolen nuclear material through nuclear forensic investigations. In Verifying Treaty Compliance, (Springer), pp. 389–408.

Mayer, K., Wallenius, M., and Fanghänel, T. (2007). Nuclear forensic science—from cradle to maturity. Journal of Alloys and Compounds *444*, 50–56.

Mazed, D., Mameri, S., and Ciolini, R. (2012). Design parameters and technology optimization of 3He-filled proportional counters for thermal neutron detection and spectrometry applications. Radiation Measurements *47*, 577–587.

MCNP Team (5). Monte Carlo Team, MCNP–A General Purpose Monte Carlo N-Particle Transport Code, Version 5 (Los Alamos National Laboratory).

Meitner, L., and Frisch, O.R. (1939). Disintegration of uranium by neutrons: a new type of nuclear reaction. Nature *143*, 239–240.

Metropolis, N. (1987). The beginning of the Monte Carlo method. Los Alamos Science *15*, 125–130.

Minor, M.M., Hensley, W.K., Denton, M.M., and Garcia, S.R. (1982). An automated activation analysis system. Journal of Radioanalytical Chemistry *70*, 459–471.

Moody, K.J., Hutcheon, I.D., and Grant, P.M. (2005). Nuclear forensic analysis (CRC Press).

Moon, J.H., Kim, S.H., Chung, Y.S., Lim, J.M., Ahn, G.H., and Koh, M.S. (2009). U determination in environmental samples by delayed neutron activation analysis in Korea. Journal of Radioanalytical and Nuclear Chemistry *282*, 33–35.

Mozin, V., Hunt, A.W., Reedy, E., and Ludewigt, B. (2012). Assessment of Delayed Gamma-Ray Technique Parameters for Spent Nuclear Fuel Assay. In Proceedings of the INMM-2012 Annual Meeting,.

Musilek, A., Buchtela, K., and Grass, F. (1996). Determination of fissionable materials by simultaneous measurement of delayed neutrons and gamma-spectra. Journal of Trace and Microprobe Techniques *14*, 29–36.

Myers, W.L., Goulding, C.A., and Hollas, C.L. (2006). Determination of 235 U Enrichment of Bulk Uranium Samples Using Delayed Neutrons. PHYSOR-2006, Vancouver, BC, Canada.

Nguyen, T.S., Wilkin, G.B., and Atfield, J.E. (2012). Monte Carlo calculations applied to SLOWPOKE full-reactor analysis. AECL Nuclear Review *1*, 43–46.

Ni, B., Xiao, C., Huang, D., Sun, H., Zhang, G., Liu, C., Wang, P., Zhang, H., and Tian, W. (2012). A brief introduction to NAA facilities of China Advance Research Reactor at CIAE. Journal of Radioanalytical and Nuclear Chemistry *291*, 313–319.

Nichols, A.L., Aldama, D.L., and Verpelli, M. (2008). Handbook of nuclear data for safeguards: database extensions, August 2008. IAEA INDC (NDS)-0534.

Norman, E.B., Prussin, S.G., Larimer, R.-M., Shugart, H., Browne, E., Smith, A.R., McDonald, R.J., Nitsche, H., Gupta, P., Frank, M.I., *et al*. (2004). Signatures of fissile materials: high-energy γ rays following fission. Nuclear Instruments and Methods in Physics Research Section A: Accelerators, Spectrometers, Detectors and Associated Equipment *521*, 608–610.

NSS (2014a). Nuclear Security Summit 2014 National Progress Report Canada.

NSS (2014b). The Hague Nuclear Security Summit Communique.

Padilla Cabal, F., Lopez-Pino, N., Luis Bernal-Castillo, J., Martinez-Palenzuela, Y., Aguilar-Mena, J., D'Alessandro, K., Arbelo, Y., Corrales, Y., and Diaz, O. (2010). Monte Carlo based geometrical model for efficiency calculation of an n-type HPGe detector. Applied Radiation and Isotopes *68*, 2403–2408.

Papadopoulos, N.N., and Tsagas, N.F. (1994). Rapid nondestructive isotopic uranium analysis by neutron activation delayed neutron counting. Journal of Radioanalytical and Nuclear Chemistry *179*, 35–43.

Peerani, P., Carbol, P., Hrnecek, E., and Betti, M. (2002). Assessment of a Compton-event suppression γ-spectrometer for the detection of fission products at trace levels. Nuclear Instruments and Methods in Physics Research Section A: Accelerators, Spectrometers, Detectors and Associated Equipment *482*, 42–50.

Peerani, P., Tomanin, A., Pozzi, S., Dolan, J., Miller, E., Flaska, M., Battaglieri, M., De Vita, R., Ficini, L., Ottonello, G., *et al*. (2012). Testing on novel neutron detectors as alternative to 3He for security applications. Nuclear Instruments and Methods in Physics Research Section A: Accelerators, Spectrometers, Detectors and Associated Equipment *696*, 110–120.

Pelowitz, D.B. (2013). MCNP6 User's Manual (Los Alamos National Laboratory).

Pelowitz, D.B., and *et al*. (2005). MCNPX user's manual version 2.5. 0 (Los Alamos, NM: Los Alamos National Laboratory).

Perret, G., and Jordan, K.A. (2011). On the combination of delayed neutron and delayed gamma techniques for fission rate measurement in nuclear fuel. In Advancements in Nuclear Instrumentation Measurement Methods and Their Applications (ANIMMA), (IEEE), pp. 1–7.

Pierre, J.R.M. (1996). Low Enrichment Uranium (LEU)-fueled SLOWPOKE-2 nuclear reactor simulation with the Monte-Carlo based MCNP 4A code. MASc. Royal Military College of Canada.

Qian, T., Tonner, P., Keller, N., and Buyers, W.J.L. (1997). Degradation of boron trifluoride and helium detectors in neutron and gamma fields. In Nuclear Science Symposium, 1997. IEEE, (IEEE), pp. 503–509.

Qian, T., Tonner, P., Keller, N., and Buyers, W.J.L. (1998). A method for comparing degradation of boron trifluoride and helium detectors in neutron and gamma fields. IEEE Transactions on Nuclear Science *45*, 636–642.

Quang Huy, N. (2010). The influence of dead layer thickness increase on efficiency decrease for a coaxial HPGe p-type detector. Nuclear Instruments and Methods in Physics Research Section A: Accelerators, Spectrometers, Detectors and Associated Equipment *621*, 390–394.

Ramaty, R., Kozlovsky, B., and Lingenfelter, R.E. (1979). Nuclear gamma-rays from energetic particle interactions. The Astrophysical Journal Supplement Series *40*, 487–526.

Reilly, D., Ensslin, N., Smith, H., and Kreiner, S. (1990). Passive Nondestructive Assay of Nuclear materials (Los Alamos National Laboratory).

Rinaldi, R., Liang, L., and Schober, H. (2009). Neutron Applications in Earth, Energy, and Environmental Sciences (Springer).

Rosenberg, R.J., Pitkänen, V., and Sorsa, A. (1977). An automatic uranium analyser based on delayed neutron counting. Journal of Radioanalytical and Nuclear Chemistry *37*, 169–179.

Savitzky, A., and Golay, M.J. (1964). Smoothing and differentiation of data by simplified least squares procedures. Analytical Chemistry *36*, 1627–1639.

Sellers, M.T. (2011). A Delayed Neutron Counting System for the Analysis of Special Nuclear Materials. Royal Military College of Canada.

Sellers, M.T., Kelly, D.G., and Corcoran, E.C. (2012a). An automated delayed neutron counting system for mass determinations of special nuclear materials. Journal of Radioanalytical and Nuclear Chemistry *291*, 281–285.

Sellers, M.T., Corcoran, E.C., and Kelly, D.G. (2012b). Simultaneous 233 U and 235 U characterization through the assay of delayed neutron temporal behavior. pp. 1–8.

Sellers, M.T., Corcoran, E.C., and Kelly, D.G. (2013). The analysis and attribution of the time-dependent neutron background resultant from sample irradiation in a SLOWPOKE-2 reactor. Journal of Radioanalytical and Nuclear Chemistry *295*, 1221–1228.

Seyfang, A.P., and Smales, A.A. (1953). The determination of uranium-235 in mixtures of naturally occurring uranium isotopes by radioactivation. Analyst *78*, 394–405.

Sher, R., and Untermyer, S. (1980). The detection of fissionable materials by nondestructive means (American Nuclear Society).

De Soete, D. (1972). Neutron activation analysis (New York: Interscience; Division of Wiley).

Spaulding, R., Morris, C., Greene, S., Makela, M., and Forest, T. (2009). Design Fundamentals for Cost-Optimized Neutron Detectors Based on an Array of Helium-3 Tubes. In APS Four Corners Section Meeting Abstracts, p. 1066.

Spriggs, G.D., Campbell, J.M., and Piksaikin, V.M. (2002). An 8-group delayed neutron model based on a consistent set of half-lives. Progress in Nuclear Energy *41*, 223–251.

US NRC Nuclear Regulatory Legislation. Atomic Energy Act, 1954.

Usuda, S., Magara, M., Esaka, F., Yasuda, K., and Saito-Kokubu, Y. (2010). QA/QC Activities and Estimation of Uncertainty for Ultra-trace Analysis of Uranium and Plutonium in Safeguards Environmental Samples. Journal of Nuclear and Radiochemical Sciences *11*, A5–A9.

Villani, S. (1979). Uranium enrichment (New York, NY: Springer-Verlag).

Wallenius, M., Lützenkirchen, K., Mayer, K., Ray, I., de las Heras, L.A., Betti, M., Cromboom, O., Hild, M., Lynch, B., Nicholl, A., *et al*. (2007). Nuclear forensic investigations with a focus on plutonium. Journal of Alloys and Compounds *444*, 57–62.

Weldon, R.A., Fensin, M.L., and McKinney, G.W. (2014). Testing the Delayed Gamma Capability in MCNP6 (Los Alamos National Laboratory).

Wilcox, T., McKinney, G.W., Fensin, M.L., Durkee, J.W., and James, M.R. A 250 Energy bin Delayed gamma END/B VII.0 Data Library for MCNPX 2.7.0 (Los Alamos National Laboratory).

Wilson, W.B., England, T.R., George, D.C., Muir, D.W., and Young, P.G. (1995). Recent development of the CINDER'90 transmutation code and data library for actinide transmutation studies (Los Alamos National Lab., NM (United States)).

Appendix A

A Preliminary Comparison of MCNP6 Delayed Neutron Emission from ^{235}U and Experimental Measurements

M.T. Sellers[1], J.T. Goorley[2], E.C. Corcoran[1], D.G. Kelly[1]

[1] Royal Military College of Canada,
P.O. Box 17000 Stn Forces, Kingston, ON, K7K 7B4

[2]Monte Carlo Codes, MS: A143,
Los Alamos National Laboratory,
Los Alamos, NM, 87545[xx]

[xx] M.T. Sellers, J.T. Goorley, E.C. Corcoran, D.G. Kelly, "A Preliminary Comparison of MCNP6 Delayed Neutron Emissions from ^{233}U and Experimental Measurements" *American Nuclear Society Transactions,* 106 (2012) pp. 813-816.

A.1 Introduction

A delayed neutron counting (DNC) system has been commissioned at the Royal Military College of Canada (RMCC). This system was modeled in MCNP6 (Goorley *et al*., 2012) and the delayed neutron measured from the fission of ^{235}U were compared to MCNP6 predictions.

A.2 Description of Actual Work

A.2.1 A Description of the Experiment

The DNC system at RMCC uses the SLOWPOKE-2 reactor (Hilborn and Townes, 1987) as a source of neutrons. Samples containing ^{235}U were prepared as acidified aqueous solutions from certified reference standards (natural U standard CRM 4321C, NIST, Gaithersburg, MD, and depleted U standard CRM U005A 0.5064 ± 0.0003 atom% ^{235}U, New Brunswick Laboratory, Argonne, IL). Each solution was contained in heat sealed small polyethylene (PE) vials (LA Packaging, Yorba Linda, CA) with a nominal solution of 1 *mL*. To minimize the potential of solution leakage into the pneumatic tubing of the system, secondary containment was achieved using heat sealed 7 *ml* polyethylene vials (LA Packaging). By irradiating the inner and outer polyethylene vials without any fissile sample, the vials have been found to contain no impurities that contribute to the overall neutron count rate recorded by the DNC system (Sellers *et al*., 2013).

Samples containing the fissile content were sent to an irradiation site inside the SLOWPOKE-2 beryllium reflector where they were exposed to a predominately thermal neutron spectrum of 5.6x 10^{11} $cm^{-2}s^{-1}$ (± 5 %) for durations up to 60 *s*. After the samples were irradiated they were automatically sent, via pneumatic transfer system, to the neutron counting arrangement. This consisted of six 304 Stainless Steel (S.S.); Reuter Stokes ^{3}He detectors (RSP4-1613-202, GE Energy, Twinsburg, OH) embedded in a paraffin moderator. Samples were located at the center of the hexagonal detector array. A delay time of 3 *s* was employed to account for sample travel time from the irradiation site and the commencement of the delayed neutron count. Delayed neutrons were recorded as a function of time, in 0.5 *s* intervals.

A.2.2 The MCNP6 Model

The geometry of the DNC apparatus was modeled using the physical dimensions measured during DNC system commissioning. Figure A-1 shows a 2-D view of MCNP6 input geometry and materials. Experiments and modeling accommodated two smaller vials inside a larger polyethylene vial. In practice, solutions containing fissile content and air were located in the upper and lower vials, respectively, for both experimental runs and the MCNP6 model. The polyethylene capsules were modeled with dimensions provided by the manufacturer and the distances of the sample from the detectors were measured and then duplicated in the MCNP6 input deck. Each ^{3}He detector was modeled with two cells defining each fill gas area; one of which contains the active zone of the detectors as detailed by the provided technical specifications and the other a thin inactive portion surrounding the active cell where charge depositions were not recorded by the detector. Neutrons, tritons, and protons were all explicitly tracked in these calculations.

The temporal behavior of the experiment was modeled in the MCNP6 input deck by a time-dependent *sdef* card. The *sdef* card reproduced the SLOWPOKE-2 neutron flux by specifying both the energies of source neutrons and the duration for which the sample was irradiated. Several variations of neutron flux inputs were examined: one which contained just thermal neutrons, the other which accounted for the epithermal and fast flux measurements made in the specific irradiation site, and the final a 69-group energy spectrum. The thermal neutron spectrum was used, as an examination of the output of the three flux input decks showed no significant differences in the magnitude and behavior of the delayed neutrons produced.

Pulse Height (F8) tallies summed both the number of pulses and energy deposition from proton and triton tracks in the active zones of the six detectors, which started 1 *s* after the end of the irradiation time. The 1 *s* time bins of the F8 tallies recorded count rates for up to 180 *s* after irradiation and were further subdivided by the energy of the pulse. Although using the detector geometry for the irradiation is not physically accurate (because the U samples were actually in the reactor during their irradiation), it is expected that the energy distribution of the neutrons irradiating the sample is not significantly altered. The flux inside the model's polyethylene vial was weighted to match experimental measurements of the thermal flux in that specific irradiation site, by using the *wgt* entry on the *sdef* card, facilitating a direct comparison of the magnitude of DNs produced in the model with those measured at RMCC. Thus, the energy deposition in the ^{3}He tubes and the temporal nature of the delayed neutron emission after the irradiation of the fissile samples could be ascertained.

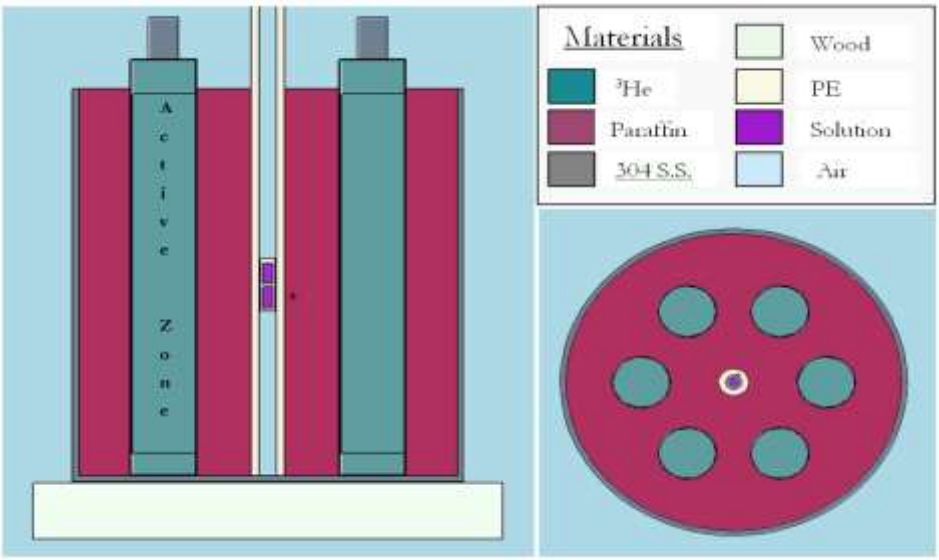

Figure A-1: MCNP6 Representation of Geometry and Materials

A.3 Results

A.3.1 Neutron Detection Efficiency Comparisons

The efficiency of the DNC system was determined by a separate calculation, which tallied proton and triton creation and energy deposition inside the active portion of the detectors. A source was defined inside the detector system geometry that released neutrons with the activities and energies expected of delayed neutrons produced from the fission of ^{235}U. The number of proton/triton pairs that deposited energy above 0.191 *MeV* in the active portions of the detectors during the simulation was compared to the total number of neutrons produced by the U sample, and the efficiency of the system was determined to be 37 %. This value is slightly higher than the experimentally determined efficiency of 34 ± 5 %, but within experimental uncertainty (which is quoted with ±2σ) of the latter. Major sources of uncertainty in the experimentally measured efficiency arise from the precision of the irradiation flux spectrum, energy discrimination levels and solution concentration.

A.3.2 Energy Deposition in ^{3}He Detectors

In ^{3}He detectors the incident neutron reacts with the helium isotope and produces a triton ($^{3}_{1}H$) and proton ($^{1}_{1}p$) through the following process:

$$^{3}_{2}He + {}^{1}_{0}n \rightarrow {}^{3}_{1}H + {}^{1}_{1}p \qquad \text{Q Value} = 0.764 \text{ MeV}$$

In an ideal ^{3}He detector all kinetic energy of the reaction products would be recorded by the detector, resulting in a singular peak at 0.764 *MeV*. However, many of the reaction products will come into contact with the wall of the detector and some of the kinetic energy produced in a neutron-^{3}He reaction will not be recorded by the apparatus. The net charge deposited after each triton-proton reaction will range from 0.191 *MeV* (the kinetic energy of the triton produced in the reaction) to the total reaction energy of 0.764 *MeV*.

Figure **A-2** illustrates the experimentally measured energy deposition in all six detectors for small amounts of ^{235}U delayed neutron production. Also depicted at energies less than 0.191 *MeV*, is the γ-background contribution from the fission process and (n,γ) reactions of non-fissile samples present in the matrix. Although the γ-background was recorded for this particular trial, it is excluded from the recorded count rates in typical DNC system operation. Significant broadening of the peak at 0.764 *MeV* is, in part, a consequence of the modest energy resolution of the apparatus.

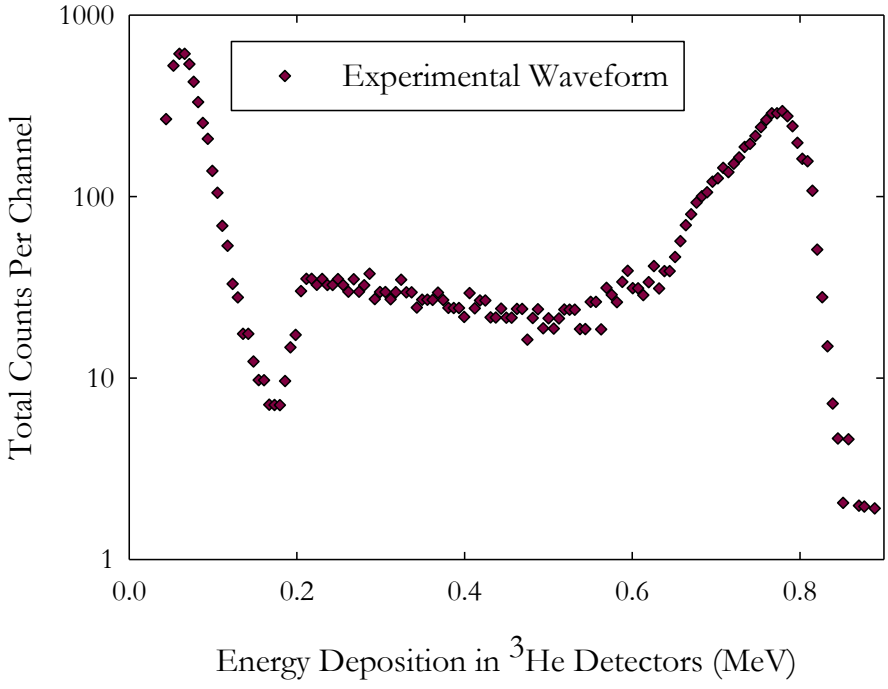

Figure A-2: Measured Experimental Waveform

A Gaussian Energy Broadening, *GEB* tally card was used in MCNP6 to represent the energy broadening resultant from the low energy resolution. Various full widths at half maxima (FWHMs) were defined and assumed to be energy independent. The result for a 50 *keV*, energy independent FWHM modeled in MCNP6 is shown below in Figure A-3. As evident in Fig. 3, the 50 *keV* GEB model does not account for the entire experimental energy spectrum. There are several possible sources of the discrepancies observed, these include; (i) the experimental possibility of an energy dependent FWHM value, (ii) potential recombination effects which were not accounted for in the current MCNP model, and (iii) significant photon pulse pile up in the experimental system, which would result in higher than predicted background energies.

A.3.3 Comparison of ACE and CINDER Delayed Neutron Production

A comparison of two identical input decks with changes in the *dnb* option in the phys:n card identified differences in the ACE (ENDF/B-VII.0) and CINDER (lib00c, Oct 2 2000) *dnb* option outputs (which had *dnb* values of -1001 and -101,

respectively). Table A-1 shows that, whilst the same number of prompt neutrons are produced for each input file, the number of delayed neutrons per source particle differs between the ACE and CINDER outputs. A comparison of the delayed neutron temporal behavior for CINDER and ACE models also had significant variations, as shown in Figure A-4.

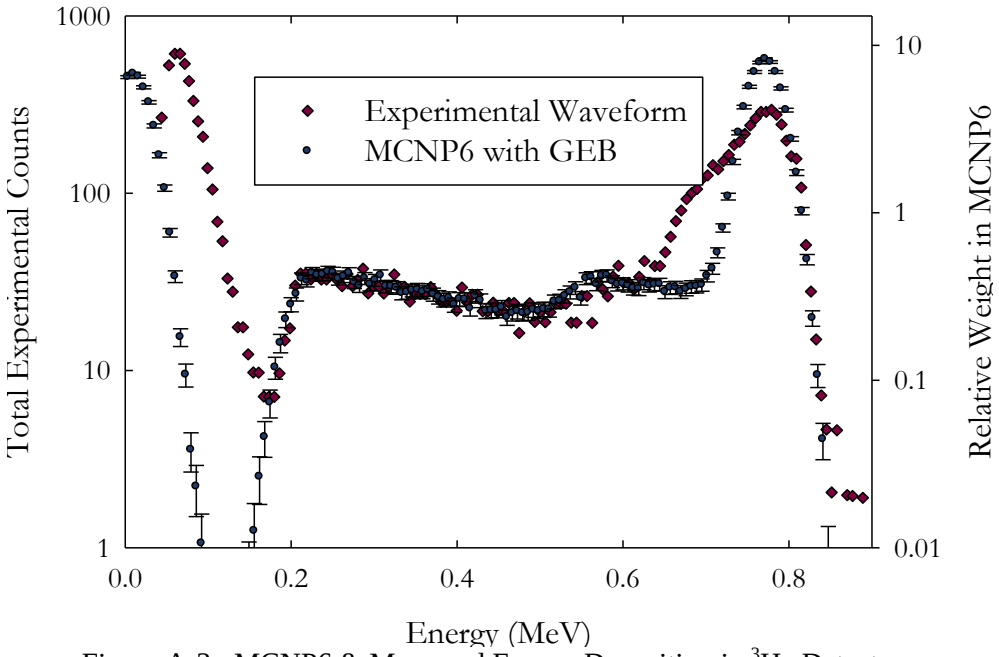

Figure A-3: MCNP6 & Measured Energy Deposition in ^{3}He Detectors

A.3.4 Initial Comparisons of Absolute Delayed Neutron Emissions from the Irradiation of ^{235}U

Hundreds of data sets have been collected for the delayed neutron production resultant from the irradiation of ^{235}U under a variety of irradiation times, fissile content and neutron flux. Figure A-4 is a representative example of the comparison between experimental measurements for the irradiation of ^{235}U, and MCNP6 predictions using both CINDER and ACE *dnb* options. As previously mentioned, the *wgt* option of the *sdef* card was applied to reproduce the experimentally measured thermal neutron flux. ACE model delayed neutron predictions were systematically less than observed count rates for count times up to 3 *min*. The temporal behavior of ACE and experimental results was consistent and the slight variations in magnitude can be attributed the previously mentioned

uncertainties in DNC system efficiency. A comparison of CINDER MCNP6 output and experimentation shows a slight overestimation of delayed neutron production and a deviation in the die-away behavior at count times greater than 100 *s*. A direct comparison of ACE and CINDER indicates ACE was a more successful predictor of measured delayed neutron temporal behavior.

Table A-1: Example Delayed Neutron Emissions for ACE and CINDER Models

	ACE	CINDER
dnb option	-1001	-101
Total Prompt Neutrons	1.1e7	1.1e7
Total Delayed Neutrons	7.3e4	8.7e4

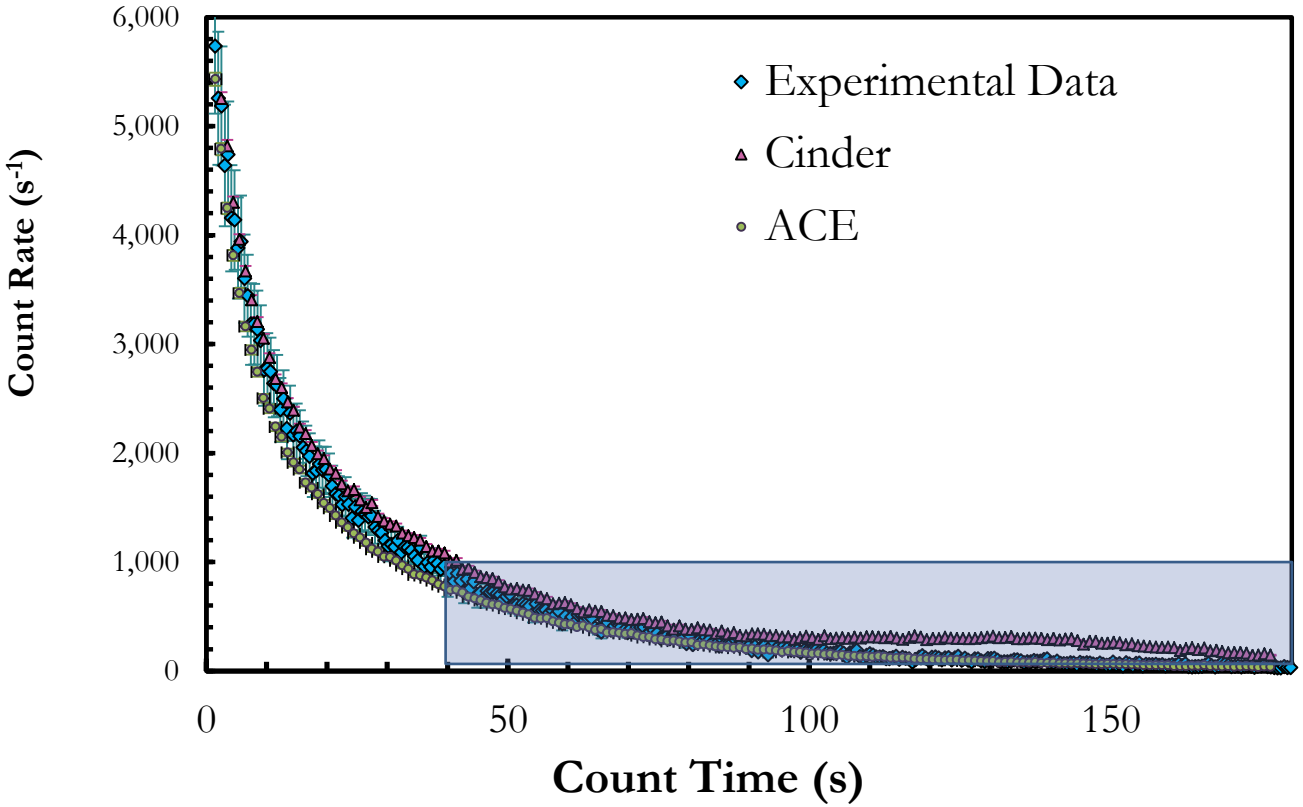

Figure A-4: Delayed Neutron Temporal Behaviour: Experimental and MCNP6 Absolute Comparisons of Fission of ^{235}U.

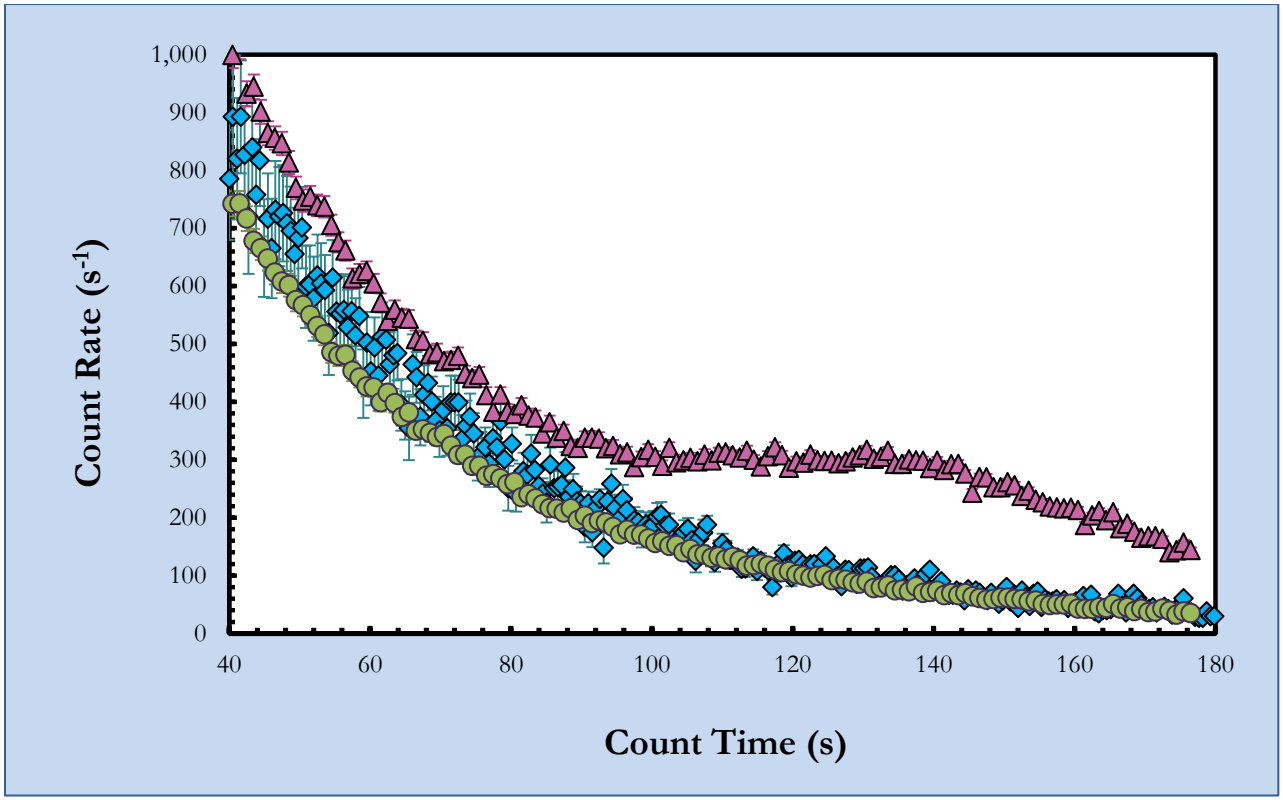

Figure A-5 Delayed Neutron Temporal Behaviour: Experimental and MCNP6 Absolute Comparisons of Fission of ^{235}U.

A.4 Future Work

Further experimentation and MCNP6 comparisons will include the analysis of ^{239}Pu, ^{233}U, and mixtures of the fissile isotopes ^{233}U, ^{235}U and ^{239}Pu. Proposed upgrades to DNC system hardware aim to both reduce uncertainties in delay time and shorten this delay time by decreasing the transfer time between the irradiation site and counter and by initiating counting more rapidly. These changes will also allow the examination of the delayed neutron die-away after shorter delays. MCNP6 model development will continue to explore available options pertaining specifically to the modeling of detector physics and delayed neutron production.

A.5 Acknowledgements

The authors would like to thank the staff of the SLOWPOKE-2 Facility at the Royal Military College of Canada for assisting in the experimentation for this paper. Also, the authors acknowledge the Advanced Simulation and Computing program at Los Alamos National Laboratory, the Director General of Nuclear Safety and Royal Military College of Canada for providing funding for this project.

-This page is intentionally left blank-

Appendix B

Fission Product γ-ray Measurements of ^{235}U and MCNP6 Predictions

M.T. Andrews[1], E.C. Corcoran[1], D.G. Kelly[1], J.T. Goorley[2]

[1]Royal Military College of Canada,
P.O. Box 17000 Stn Forces, Kingston, ON K7K 7B4

[2]Monte Carlo Codes, MS: A143
Los Alamos National Laboratory, Los Alamos, NM 87545.[xxi]

[xxi] M.T. Andrews, E.C. Corcoran, D.G. Kelly, J.T. Goorley, "Fission Product γ-ray Measurements of ^{235}U and MCNP6 Predictions" *Transactions of the American Nuclear Society*, 109 (2013).

B.1 Introduction

The delayed neutron (DN) counting system at the Royal Military College of Canada (RMCC) has been recently upgraded to include the capability to additionally measure delayed gammas (DGs) emitted from special nuclear materials. This summary describes an initial comparison of DG measurements from irradiated natural uranium to MCNP6 (Durkee *et al*., 2012) predictions.

B.2 Description of Actual Work

B.2.1 A Description of the Experiment

The Delayed Neutron and Gamma Counting (DNGC) system utilizes the flux of a SLOWPOKE-2 reactor to induce fission in samples containing uranium and plutonium. Samples in the present experiments contained 0.3 *mg* of natural uranium and were prepared as acidified aqueous solutions from certified reference standards (CRM 4321C, NIST, Gaithersburg, MD) before being sealed in polyethylene vials (LA Packaging, Yorba Linda, CA). These samples were irradiated and then pneumatically transferred to the counting arrangement that simultaneously recorded the DGs and DNs emitted via fission product decay, as is depicted in Figure B-1.

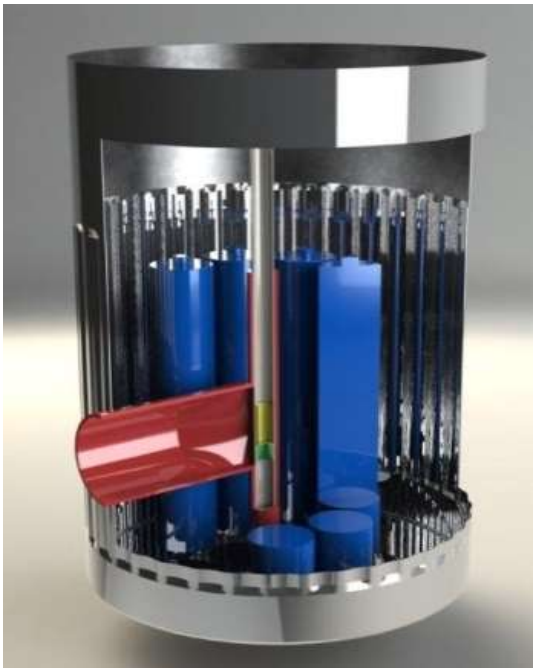

Figure B-1: A Schematic of the DNGC System

The counting system consists of six ^{3}He detectors (RSP4-1613-202, GE Energy, Twinsburg, OH) imbedded in neutron moderating paraffin. Gamma rays are recorded by a High Purity Germanium (HPGe) detector (GMX-18190, SH-GMX CFG: S/N 26-N1476A). The detector is able to slide in and out of the lead mold (Figure B-1) to modify geometric efficiency and detector dead-time. Lead shielding is extensively used in the system; to reduce environment background at the HPGe detector's crystal and to reduce γ background in the ^{3}He detectors. The fissile content was isolated from the detectors by the sample vial and polyethylene tubing.

A custom LabVIEW™ program has been written, which records the energy spectra of the delayed gammas and neutrons for predefined time intervals. For example, the measurements discussed here were performed as follows: 60 *s* irradiation of the sample, followed by 35 *s* decay before 565 *s* of counting. The cumulative counts for the entire energy spectra were recorded every ~2 *s* for both neutrons and gammas. Neutron measurements had been previously simulated in MCNP6 (Andrews *et al*., 2014b), their comparison is outside the scope of this summary.

B.2.2 The MCNP6 Model

MCNP6beta3 is the newest public release of the Monte Carlo code developed by Los Alamos National Laboratory. A description of the delayed particle features of MCNP6 can be found in (Durkee *et al*., 2012). The DG=lines activation control option was used to sample DGs. Modeling the entire process (from irradiation, DG production, to the detection of photons) was computationally expensive. Thus two MCNP6 input decks were created to decrease relative errors in the output and speed up computations.

The first input deck modeled the irradiation of the uranium content and the resulting DG emissions. The fixed source option produced thermal neutrons, which irradiated a small amount of aqueous uranium content for 60 *s*. As this work is preliminary the magnitude of the flux within the SLOWPOKE-2 was not reproduced. Another modeled deviation from physical experiments was a ~1500x increase in fissile mass in order to improve the relative error of the DG emissions. Surface current (F1) tallies recorded the relative energy distributions of gammas emitted from the solution with chosen energy and time bins corresponding to the experiments conducted at the RMCC. The output corresponding to 565 *s* of counting after a 60 *s* irradiation and 35 *s* decay was used to define the source in the second MCNP input deck.

The second simulation deck reproduced the counting geometry and conditions. The geometry of the DNGC system was modeled in MCNP using the dimensions measured during the system upgrade in 2012. The output from the previous simulation was used for source definition and placed inside the polyethylene vial. A Pulse Height (F8) tally was placed inside the germanium crystal, which recorded photon energy depositions in energy bins once again corresponding to measured bins. The measured energy resolution of the detector was reproduced with a Gaussian Energy Broadening (GEB) modifier, which defined the full width at half max (FWHM) values as a function of energy. The output of the F8 tally was then compared to measurements. At this time, the focus was on overall trends and the comparison of the individual DG peak intensities from measurements and simulations, no attempt to reproduce magnitudes has been made.

B.3 Results

Both the measurement and simulations were read by a Matlab™ script, which corrected for dead time effects in the former. This script also contained an algorithm provided by Matlab Central that was modified to identify peaks in a

user-defined energy range. A Savitzky-Golay filter (Savitzky and Golay, 1964) was applied to smooth the measured data in order to increase the effectiveness of peak identification. Uncertainties in the measurements were propagated by assuming an uncertainty associated (σ_c) with each count, *C*, as:

$$\sigma_C = \sqrt{C}$$

This error propagation did not account for uncertainties introduced via dead time corrections, spectra filtering, decay and count timings and sample concentrations, and is therefore an underestimation of the true uncertainty.

Once measurements had been corrected for dead time and experimental peaks were found, the analysis program identified peaks predicted by MCNP6. These MCNP peaks were then compared to measurements and if peak energies were within 0.8 *keV* of one another that pair was selected for comparison. The comparison was completed by calculating the area under each peak and subtracting background contributions to the spectra. For this preliminary comparison, the 25 most prominent measured peaks were selected for comparison to MCNP6 simulations. As there was no attempt to reproduce the absolute magnitude of gammas recorded, measurements and simulation peaks were all normalized to a total net area (of all 25 peaks) of 1, which allowed for the comparison of relative peak intensities.

(Beddingfield and Cecil, 1998) identified > 800 *keV* fission product gammas as important energies when examining unidentified fissile material and their measurements have been previously compared to MCNP simulations (Durkee *et al*., 2009). These energies were therefore originally selected for comparison in this work. The signal to noise ratio in measurements for many peaks > 1.1 *MeV* was less than 2:1 so they were omitted from this analysis. The lower range of analysis was extended down to 685 *keV* to include multiple $^{132/132m}$Sb decay energies for reasons that will be discussed later in this section.

Figure B-2 shows measurements, MCNP6, and relative intensity comparisons of fission product gamma-ray spectra produced from 685 – 1100 *keV*. Analysis of measurements identified 56 peaks that are marked in Figure B-2, of which 49 were predicted by MCNP6 simulations. The 25 most intense measured peaks were all predicted by MCNP6 and are also shown on both the measured and simulated spectra. The relative intensities of these peaks are displayed at the bottom of Figure B-2.

Overall, the relative intensities of the peaks were comparable in simulations and experiments with several notable exceptions. When the original range of analysis from 800 – 1100 *keV* was used a $^{132/132m}$Sb peak energy emerged

as a prominent outlier. The range of analysis was therefore extended down to 685 *keV* to include another prominent $^{132/132m}$Sb decay at 697 *keV*. MCNP6 over predicts the intensities of both observed $^{132/132m}$Sb peaks by a factor of 1.5 and 1.4 at the energies of 697 and 974 *keV*, respectively. The observed over-prediction of $^{132/132m}$Sb by MCNP appears to concur with comparisons of highly enriched uranium metal measurements and MCNPX performed by Durkee *et al*. 2009.

Energy intensities corresponding to the decay of $^{90/90m}$Rb were significantly higher in measurements than simulations. The possibility of non-^{235}U fission contributions to measured $^{90/90m}$Rb counts was ruled out via the comparison of several experimental gamma counts, Figure B-3. In each case the vial was irradiated for 60 *s*, allowed to decay for 10 *s* and counted for 170 *s*. In these comparisons the relative contributions of the irradiated empty vials, HNO_3 solutions and ^{238}U content were ascertained and none were found to produce a noticeable 832 or 1061 *keV* peak.

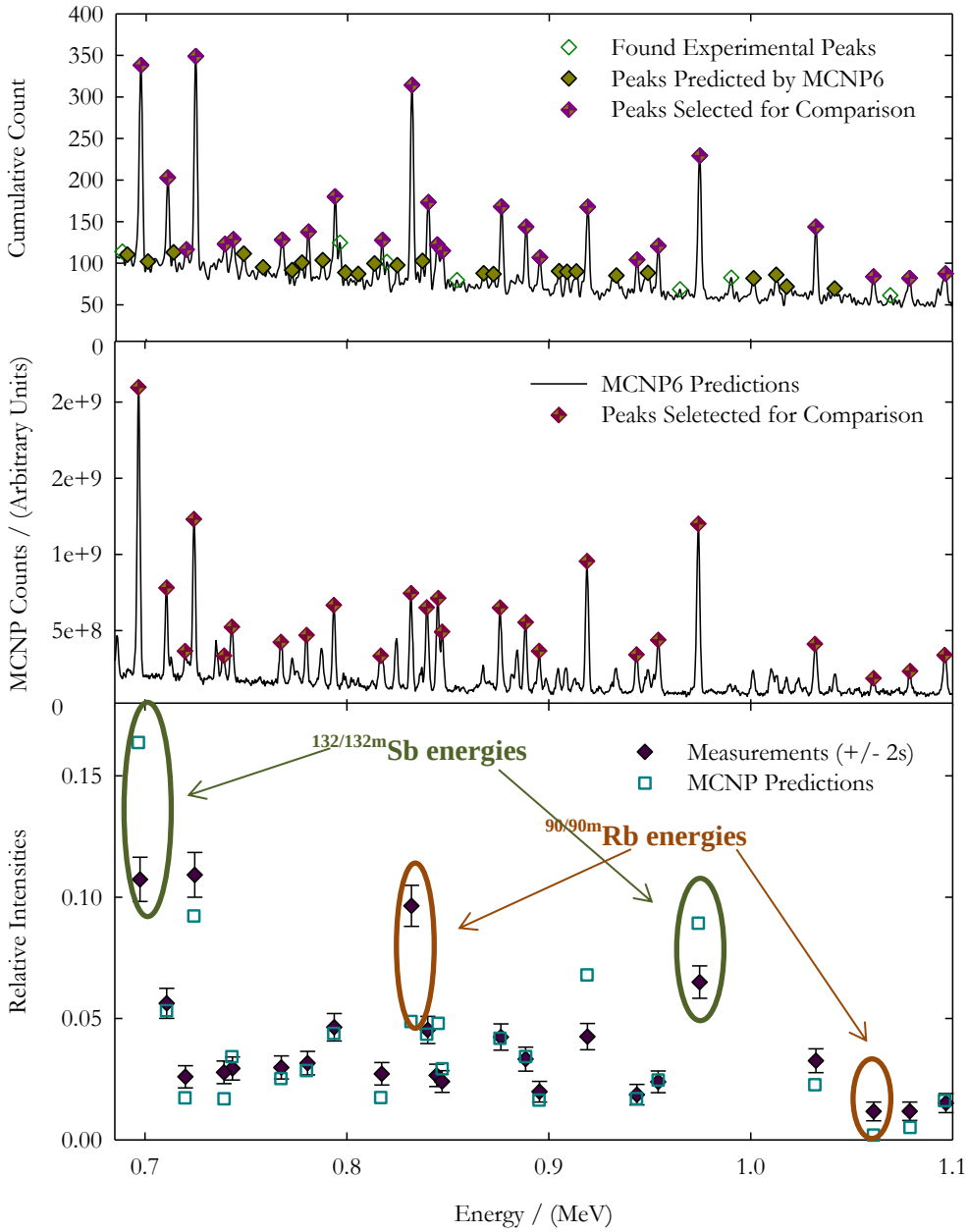

Figure B-2: Measured and MCNP6 Simulated Delayed Gamma Counting Comparisons

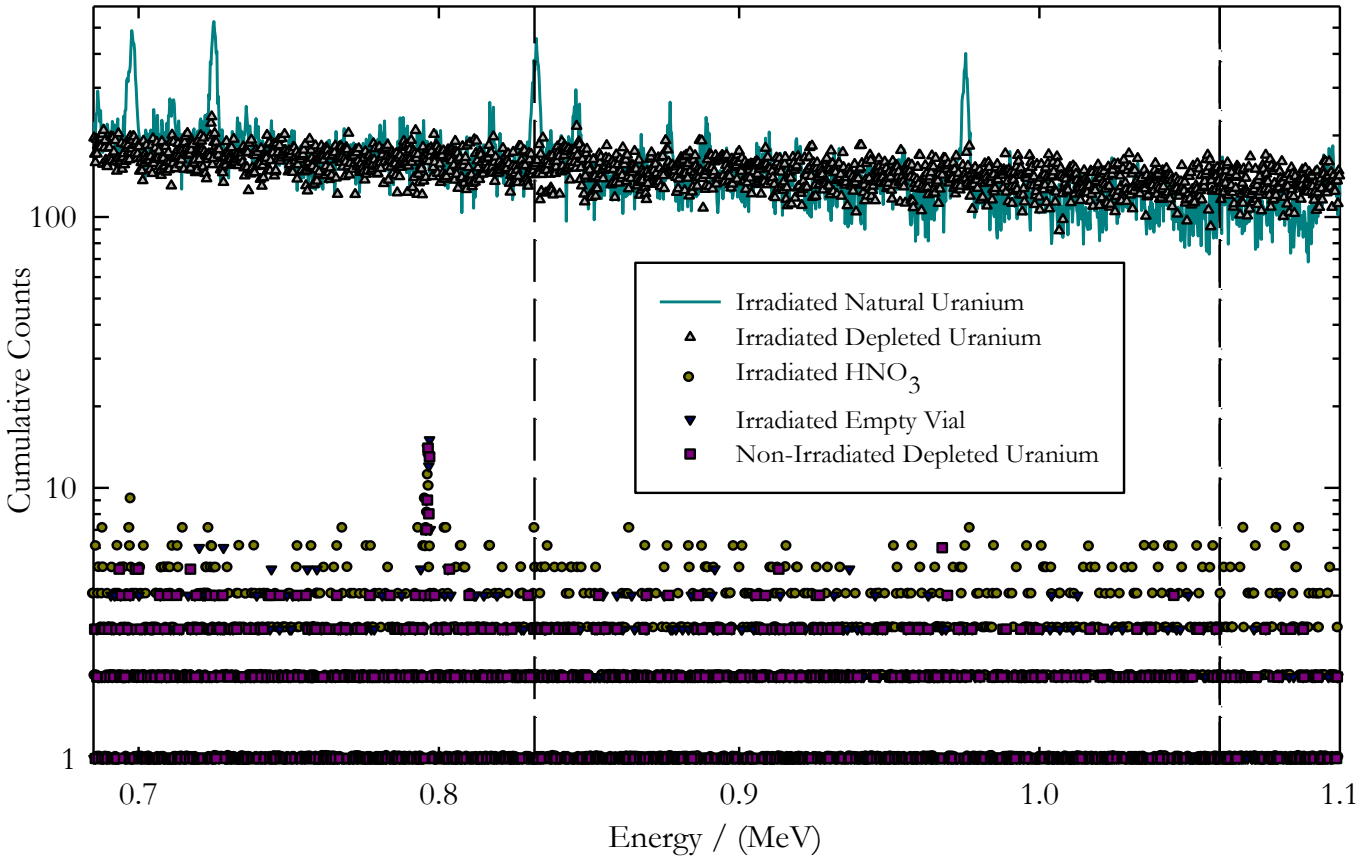

Figure B-3: – Relative count contributions from delayed & natural uranium, empty vials and HNO_3 solutions.

B.4 Conclusions & Future Work

Preliminary comparisons of the measured gamma ray spectra of ^{235}U fission products at RMCC and MCNP6 predictions have been completed. In the range of 0.685 – 1.1 *MeV* MCNP6 predicted the presence of the majority of prominent measured peaks. The relative intensities of the 25 most prominent peaks were in general agreement with several notable discrepancies, notably $^{90/90m}Rb$ and $^{132/132m}Sb$. Future work will include ^{233}U and ^{239}Pu measurements, varied irradiation, decay and count times and their simulation in MCNP6. A comparison of peak growth with respect to count time will also be included in future efforts.

B.5 Acknowledgements

Funding was provided by the Advanced Simulation and Computing program at LANL, the Director General of Environment & Nuclear Safety and NSERC. The work of Kathy Nielsen, Dave Ferguson, Clarence McEwen, and John Shaw is much appreciated.

-This page is intentionally left blank-

Appendix C

Updated Delayed Neutron Counting Test Suite Comparisons from RMCC for MCNP6 Version 1 Release

M.T. Andrews[1,2], T.L. Beames-Canivet[1], D.G. Kelly[1], E.C. Corcoran, J.T. Goorley[2]

[1]Royal Military College of Canada,
P.O. Box 17000 Stn. Forces, Kingston, ON K7K 7B4

[2]Monte Carlo Codes, MS: A143
Los Alamos National Laboratory, Los Alamos, NM 87545.[xxii]

[xxii] **M.T. Andrews,** T.L. Beames-Canivet, D.G. Kelly, E.C. Corcoran, J.T. Goorley, "Updated Delayed Neutron Counting Test Suite Comparisons from RMCC for MCNP6 Version 1 Release" *Los Alamos National Laboratory Report* LA-UR-14-25702 (2014).

C.1 Introduction

This brief report describes significantly updated versions of several delayed neutron files contained within the version 1 release of MCNP6. MCNP6.1 simulations recreate the irradiation of milligram quantities of special nuclear materials (SNMs) in aqueous solutions for 60 *s*. Delayed neutron (DN) magnitudes and temporal behaviors are recorded with F1 tallies and compared to measurements at the Royal Military College of Canada. These comparisons are described in detail in(Andrews *et al*., 2014b). The three different DN options currently available in MCNP6v1(DN=model, DN=library and DN=both) were tested, for ^{233}U, ^{235}U (contained in Nat. U), and ^{239}Pu emissions up to 3 minutes after the elapse of irradiation. Also included in this report is a comparison of measurements with a modified MCNP6 executable containing an updated time-bin structure for DN=model option emissions.

C.2 Experimentation

Solutions containing ^{233}U, ^{239}Pu and natural uranium were prepared from certified reference material standards and further diluted with nitric acid and distilled water. Samples were placed in polyethylene vials before pneumatic transport to an inner SLOWPOKE-2 research reactor irradiation site where they were exposed to a predominately thermal neutron flux for 60 *s*. After irradiation the samples were sent to an array of ^{3}He detectors which recorded the DN emissions as a function of count time for up to 3 minutes. Further details regarding the delayed neutron counting system and these measurements can be found in (Andrews *et al*., 2014b; Sellers *et al*., 2012a). Experimental data has been corrected for dead time effects and neutron background contributions (Sellers *et al*., 2013). **Measurements have been normalized by fissile mass [*g*] and detection efficiency (33 %) to obtain DN emission rate, *Q(t)* [$s^{-1}g^{-1}$].** Each isotope (^{233}U, ^{235}U, and ^{239}Pu) was irradiated and counted in triplicate; the provided measurements represent their average *Q(t)*. Plots with error bars included represent the 95 % confidence interval on measurements.

C.3 MCNP Simulations

Atomic Energy of Canada Limited has provided a MCNP input deck containing LEU SLOWPOKE-2 dimension and material specifications, the contents of which are detailed in (Nguyen *et al*., 2012). This input deck was modified to include a polyethylene vial within an inner irradiation site to determine a higher fidelity neutron flux spectrum. This flux was recreated within the vial solution of a second

input deck, which includes the irradiation of a fissile solution for 60 *s* and the recording of subsequent DN emissions from the vial. The DN emission rate, *Q(t)* [$s^{-1}g^{-1}$], for each MCNP6v1 simulation was compared to the normalized measurements described in the previous section. The time-bin structure for the former was updated in a modified MCNP6 executable, MCNP6_dbf.exe[xxiii]; its comparison is also presented.

C.4 Comparisons

C.4.1 MCNP6v1 DN=model. Library, and both comparisons

Measurements are now compared as DN emission rates, *Q(t)* [$g^{-1}s^{-1}$]. Figure C-1 compares the measurements of DN emissions for ^{233}U, and MCNP6v1 simulations using the three DN emission options. The DN=both option is omitted in subsequent comparisons because it is indistinguishable from the DN=library option. Figure C-2- Figure C-7 compare the DN emission rate for ^{233}U, ^{235}U (in Nat. U), and ^{239}Pu, using the DN=model and DN=library options in MCNP6v1.

C.4.2 MCNP6v1 with Delayed Bin Fix

Using the DN=model option in SNM simulations with MCNP6v1 resulted in a deviation from the measurements at approximately 100 *s*. This anomaly is eliminated by using MCNP6v1 with the delayed bin fix (DBF), as shown in Figure C-2 - C-7. Figure C-8 - Figure C-10compare the DN emission rates for ^{233}U, ^{235}U (in Nat. U), and ^{239}Pu, using MCNP6_dbf.exe for the DN=model option and MCNP6v1 for the DN=library option.

C.5 Summary

DN emissions from ^{233}U, ^{235}U, and ^{239}Pu were compared to MCNP6v1 simulations using the DN=model, both, and library options. Previously noted time-dependent anomalies resultant from the use of the DN model option were noted and resolved with a modified MCNP6 executable containing an updated time-bin structure for DN emissions. Overall the model option (when used with the modified executable) yields the best agreement when compared to measurements from RMCC. Future work could include comparisons of measurements to MCNP simulations using MCNP6 1.1 Beta, which includes an option in the DBCN card for a more refined time-bin structure for delayed particle emissions (Weldon *et al*., 2014).

[xxiii] The MCNP6_dbf.exe was provided by M. James.

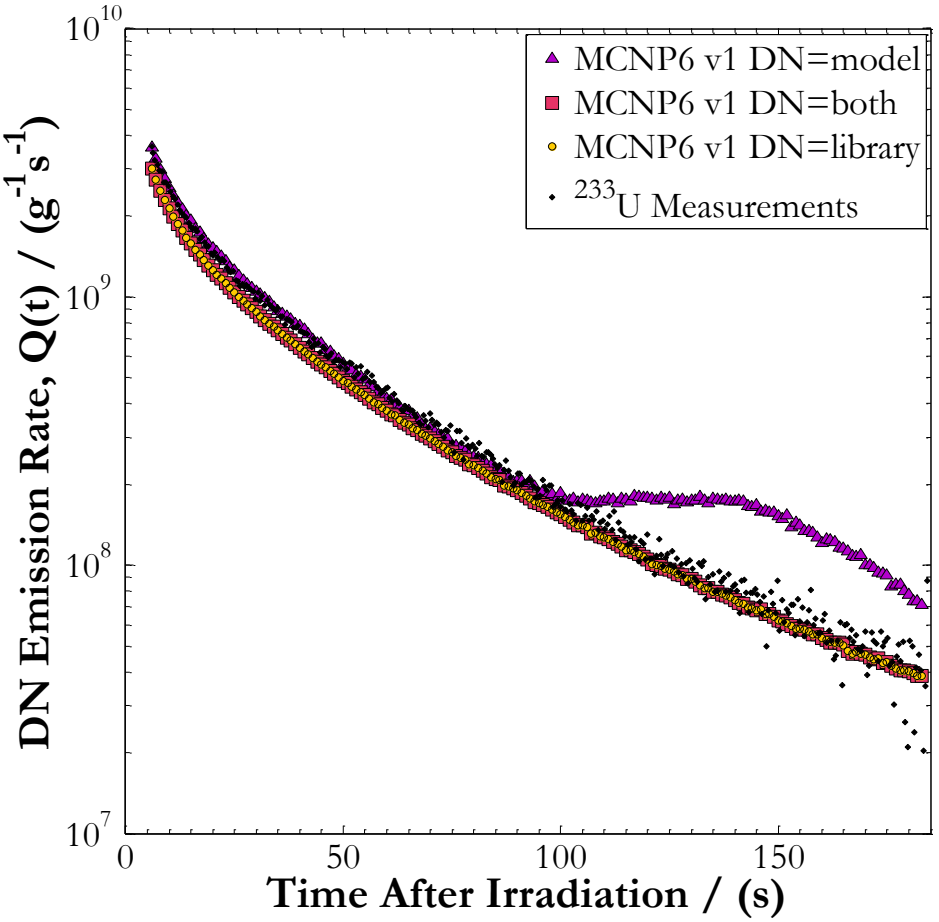

Figure C-1: Delayed neutron emission rates from ^{233}U measurements, and three DN options in MCNP6v1 simulations.

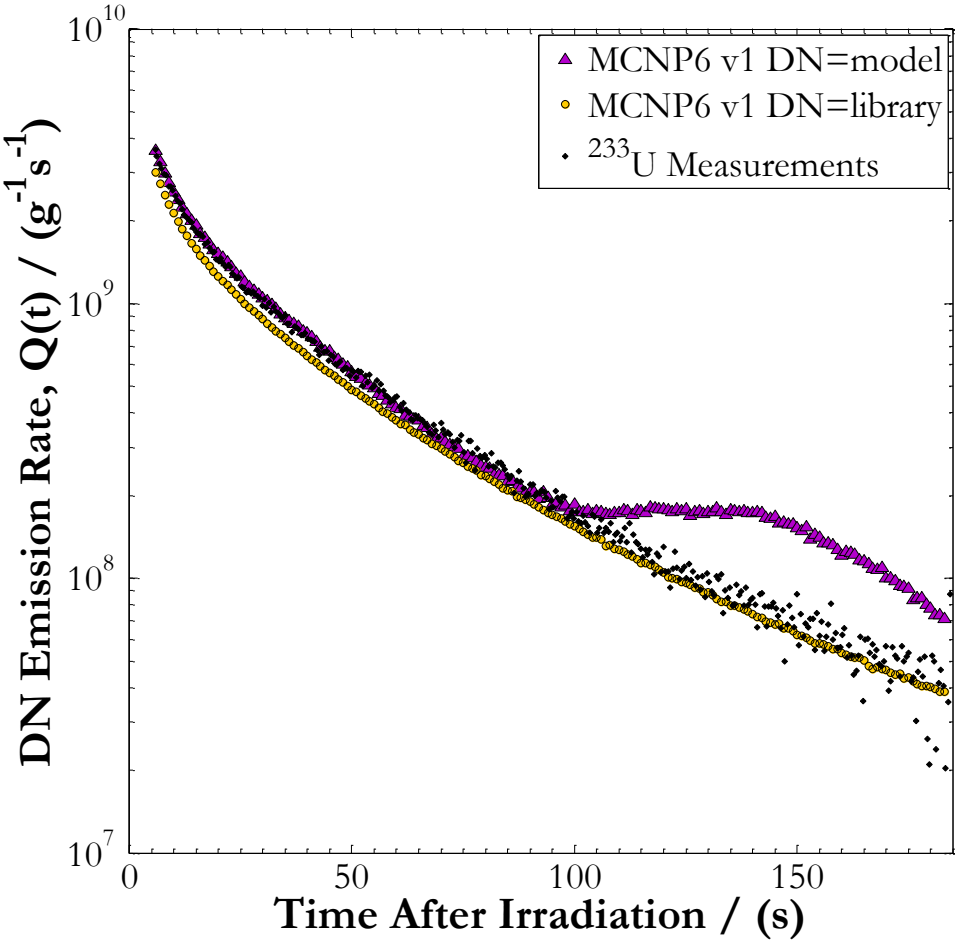

Figure C-2: Delayed neutron emission rates from ^{233}U measurements, model and library DN options in MCNP6v1 simulations.

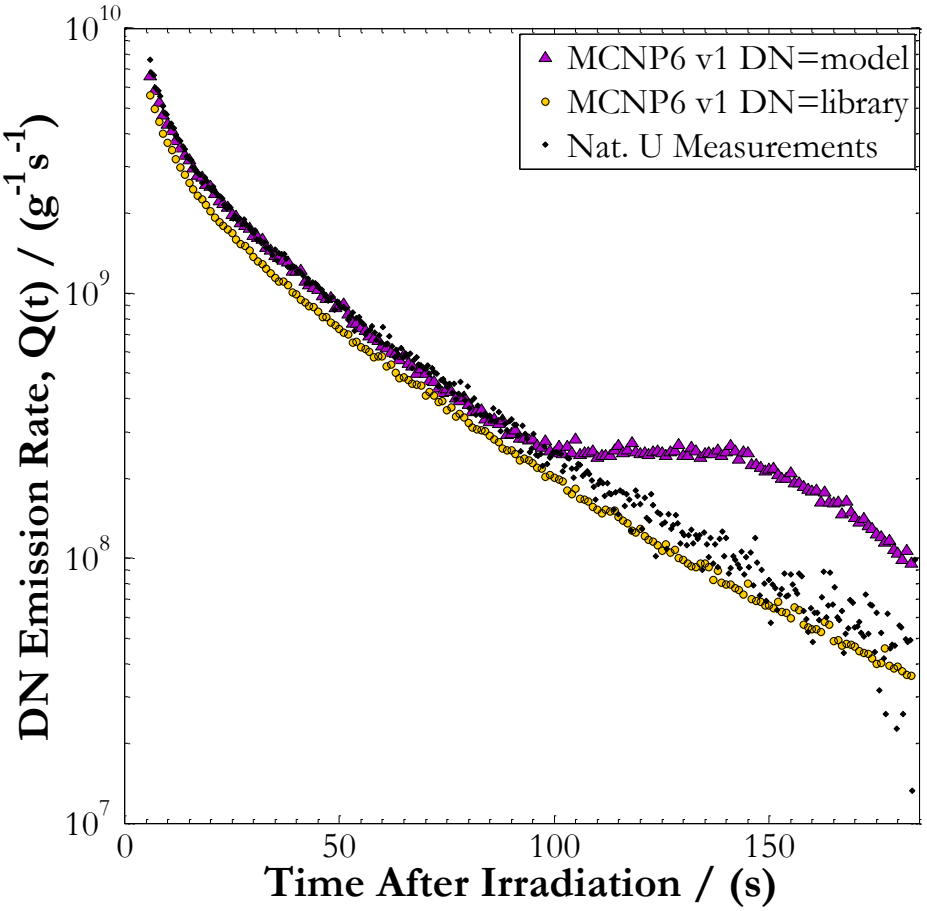

Figure C-3: Delayed neutron emission rates from Nat. U measurements, model and library DN options in MCNP6v1 simulations.

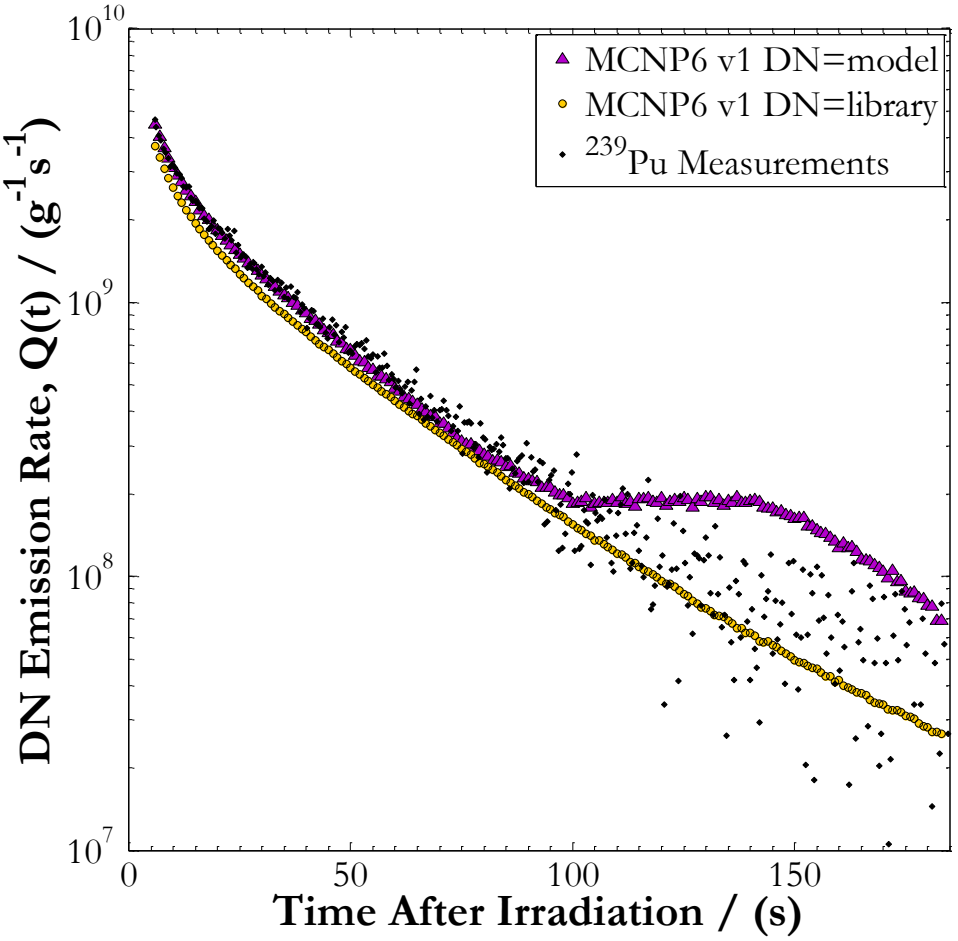

Figure C-4: Delayed neutron emission rates from ^{239}Pu measurements, model and library DN options in MCNP6v1 simulations.

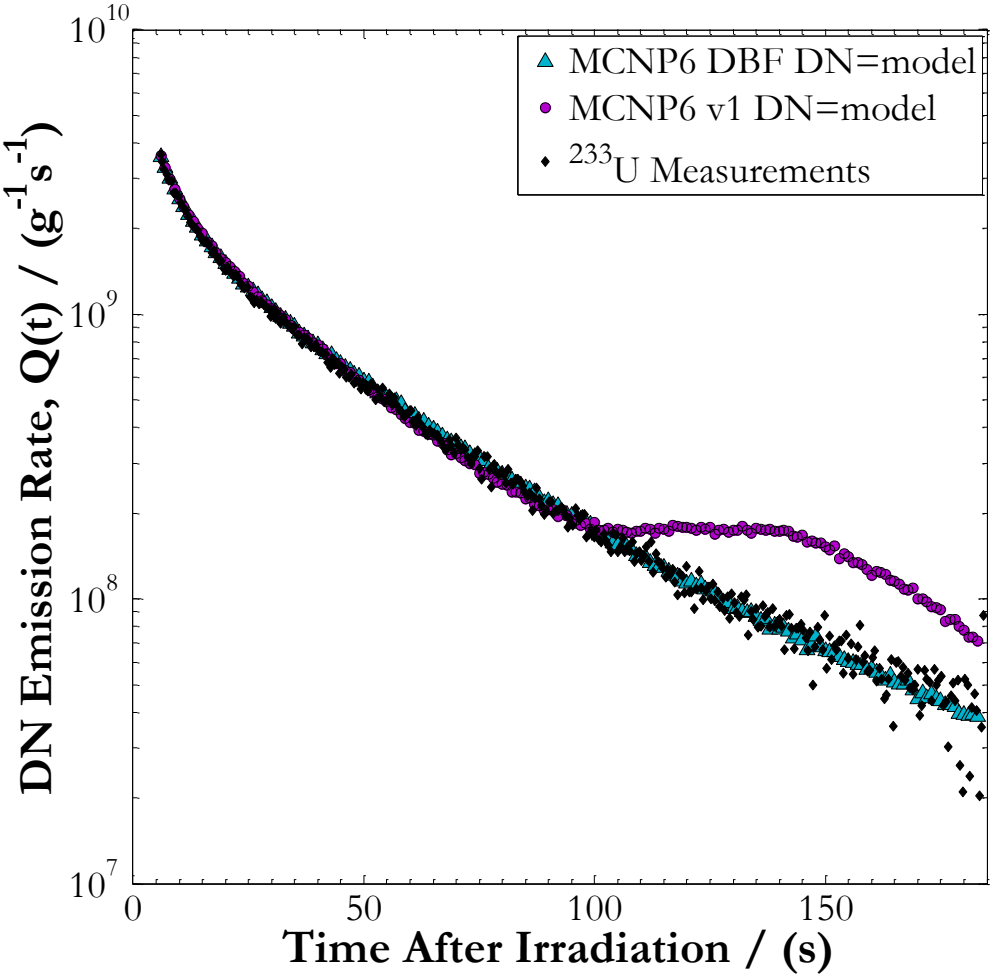

Figure C-5: Delayed neutron emission rates from ^{223}U measurements, DN=model simulations with MCNP6v1 and a modified MCNP6 executable with a delayed bin fix (DBF).

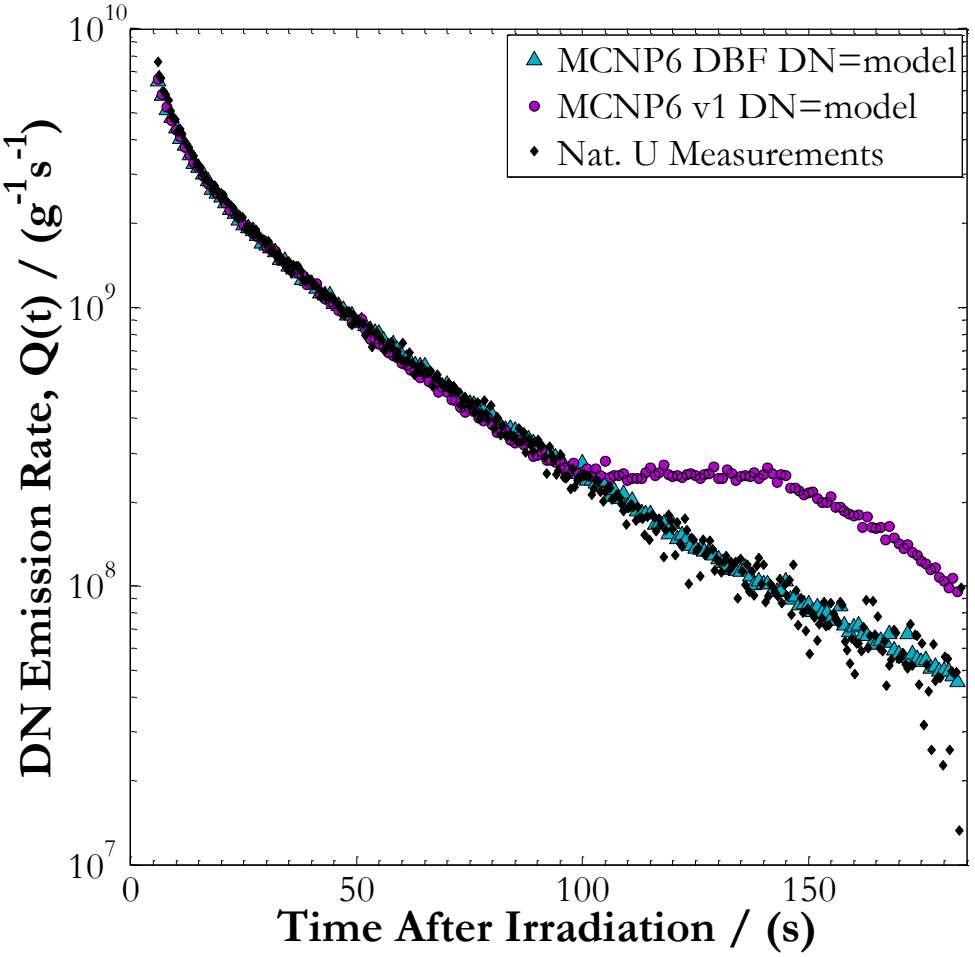

Figure C-6: Delayed neutron emission rates from nat. U measurements, DN=model simulations with MCNP6v1 and a modified MCNP6 executable with a delayed bin fix (DBF).

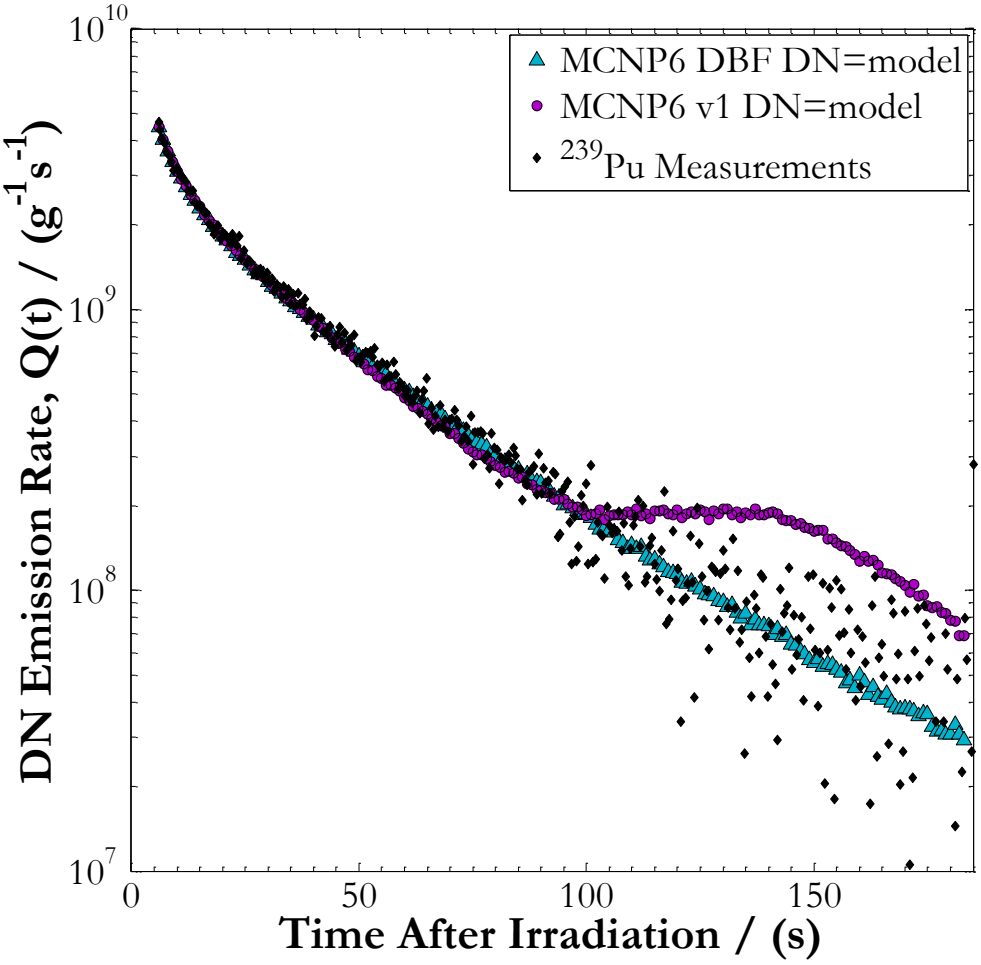

Figure C-7: Delayed neutron emission rates from ^{239}Pu measurements, DN=model simulations with MCNP6v1 and a modified MCNP6 executable with a delayed bin fix (DBF).

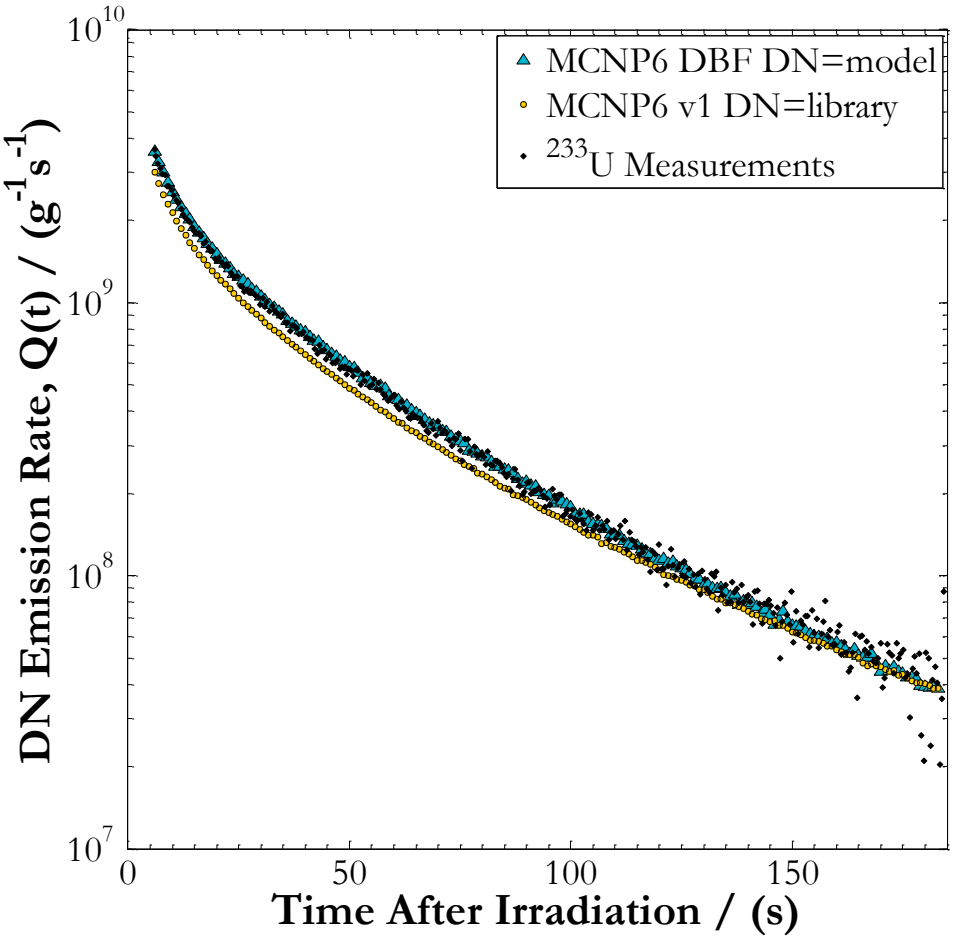

Figure C-8: A comparison of delayed neutron emission rates from ^{223}U measurements, MCNP6v1 with DN=library and a modified MCNP6 executable with a delayed bin fix (DBF) and DN=model option selected.

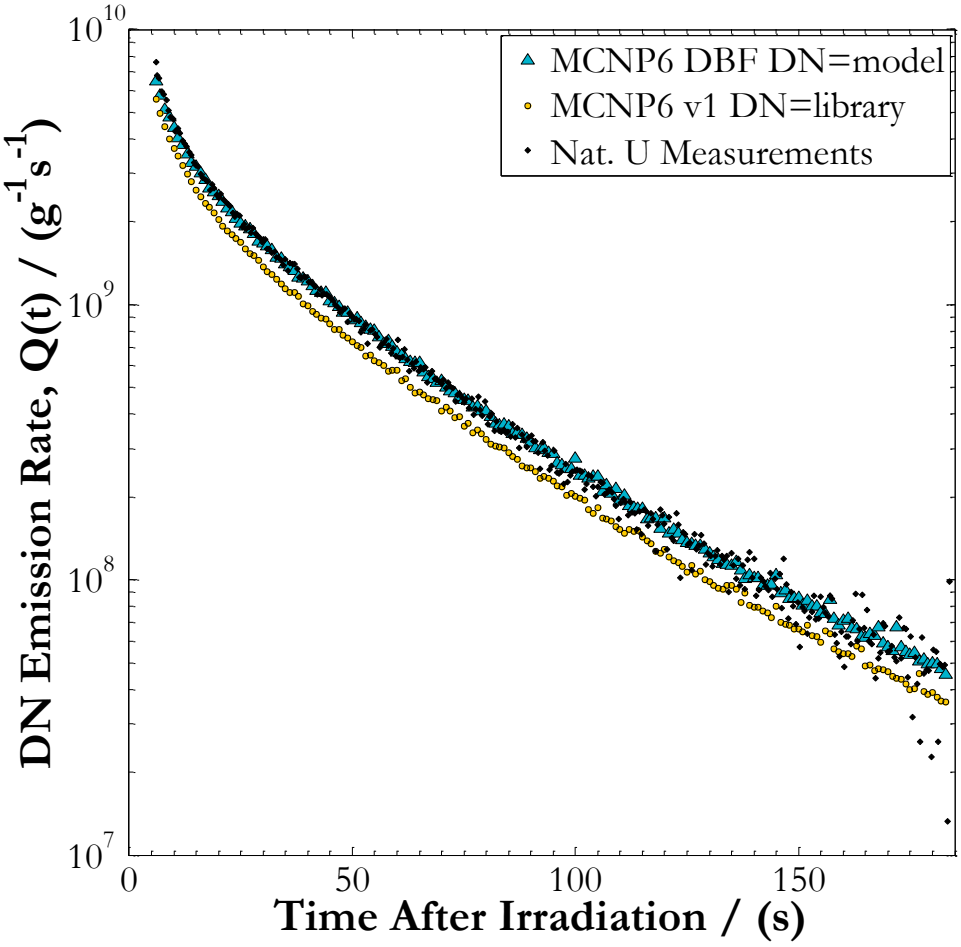

Figure C-9: A comparison of delayed neutron emission rates from nat. U measurements, MCNP6v1 with DN=library and a modified MCNP6 executable with a delayed bin fix (DBF) and DN=model option selected.

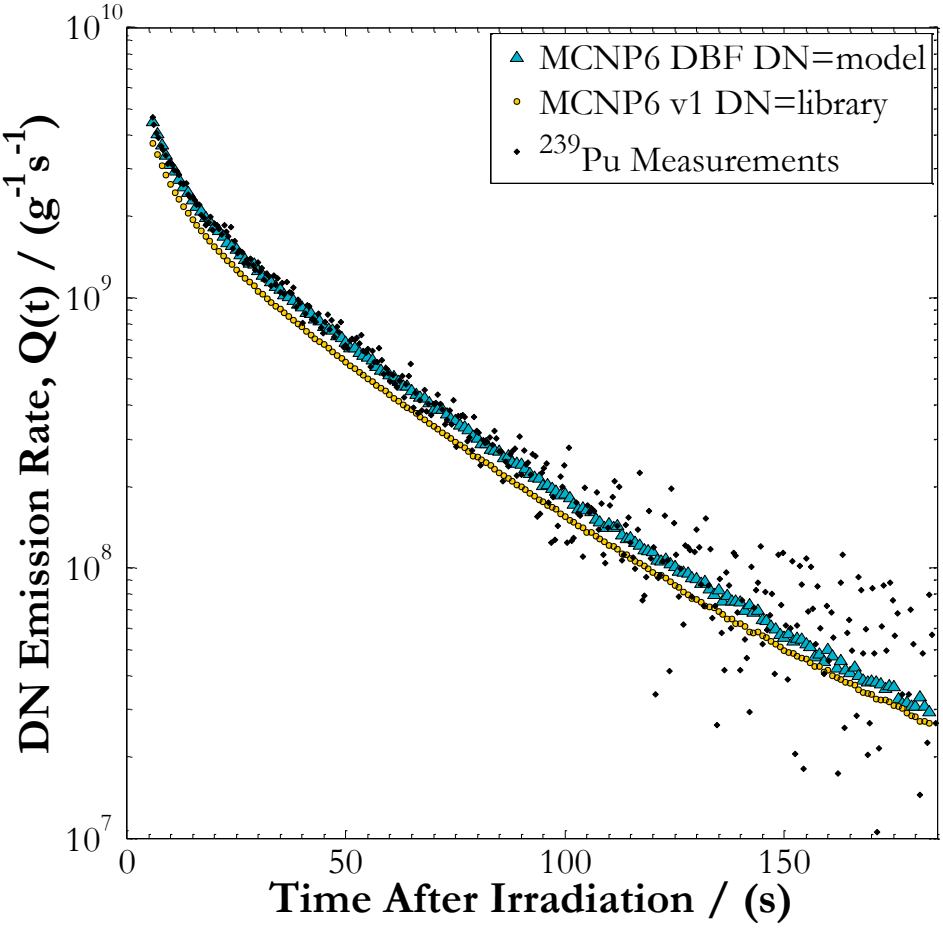

Figure C-10: A comparison of delayed neutron emission rates from ^{239}Pu measurements, MCNP6v1 with DN=library and a modified MCNP6 executable with a delayed bin fix (DBF) and DN=model option selected.

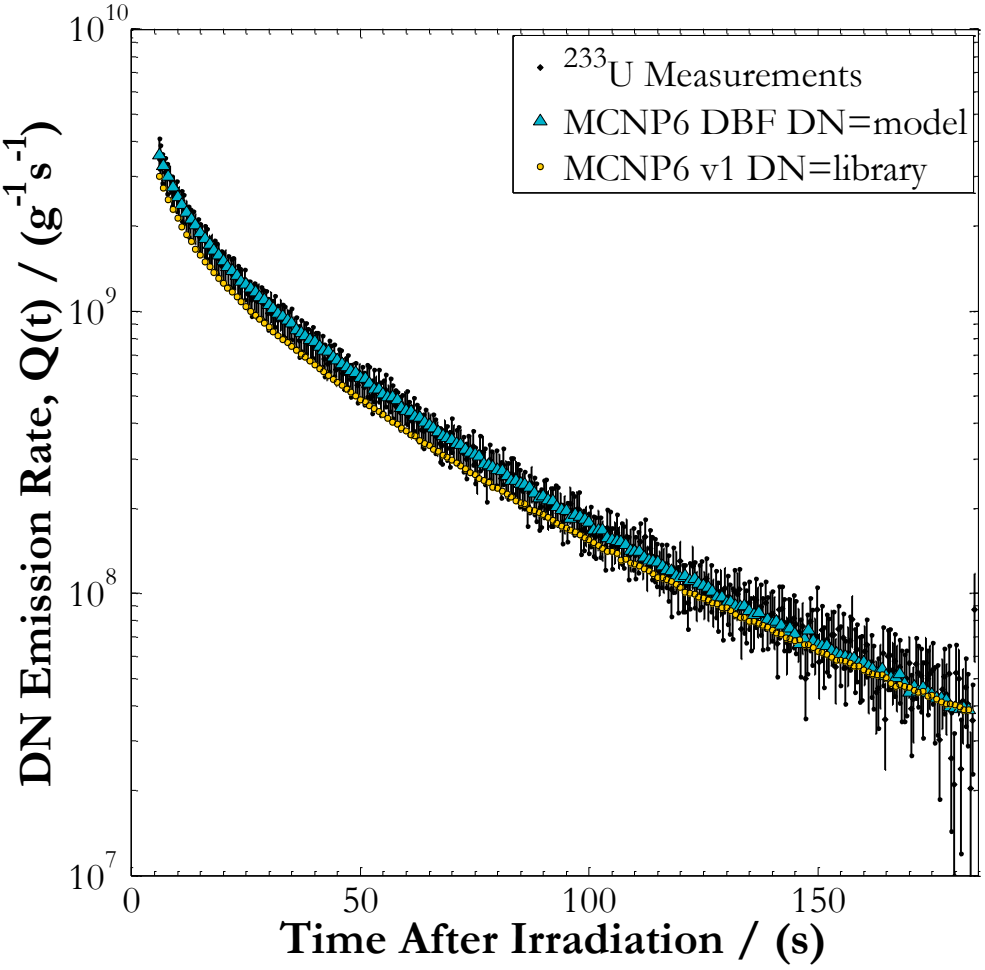

Figure C-11: Delayed neutron emission rates from ^{233}U measurements, MCNP6v1 with DN=library, and a modified MCNP6 executable with a delayed bin fix (DBF) with DN=model simulations. Error bars represent 95 % confidence intervals.

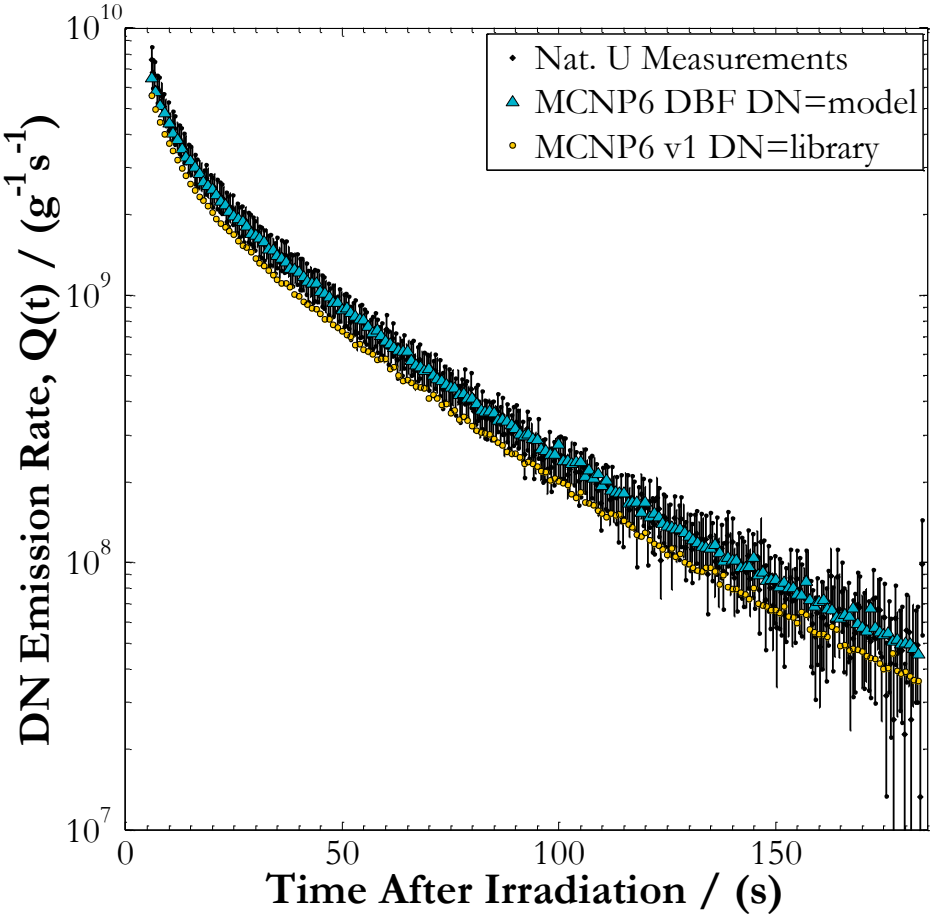

Figure C-12: Delayed neutron emission rates from natural U measurements, MCNP6v1 with DN=library, and a modified MCNP6 executable with a delayed bin fix (DBF) with DN=model simulations. Error bars represent 95 % confidence intervals.

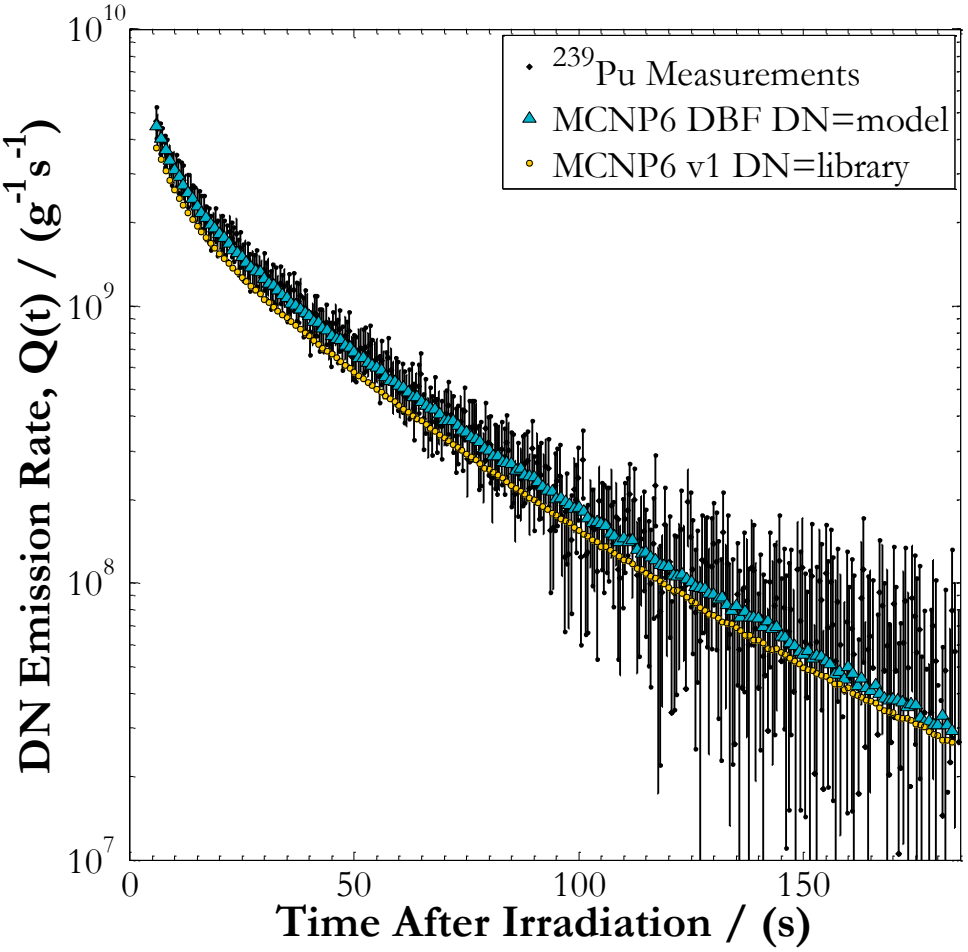

Figure C-13: Delayed neutron emission rates from ^{239}Pu measurements, MCNP6v1 with DN=library, and a modified MCNP6 executable with a delayed bin fix (DBF) with DN=model simulations. Error bars represent 95 % confidence intervals.

Example of an Input Deck

```
Modeling Delayed Neutron Emissions in RMCC's DNC System
c
c ----------------------------GEOMETRY-----------------------------------
c
  27  5000   -0.9977    -509   $ top smaller vial solution
      imp:n=1
c
  30     0              509   $ geometry void
      imp:n=0
c

c ----------------------SURFACE CARDS-------------------------------------------------------
c
 509       rcc 0 0 17.3            0 0 1.38       0.4826   $ top small vial solution
c

c --------------------------MATERIAL AND SOURCE CARDS-------------------------------------
c
mode  n
c
 ACT
      DN=both   $ change between DN=model, DN=both and DN=library
      DNBIas=10   $ biases the # of DNs produced
c
c ------------------------------MATERIAL DEFINITIONS-----------------------------------
c
m5000
       94239      -2.14e-3   $ 94239 for Pu239, 92233 for U233, 92235 for U235
       1001       -0.10531
       8016       -0.87777
       7014       -0.01478
mt5000  lwtr.10t
c
c -------------------------SOURCE DEFINITION---------------------------------------------
c
sdef pos=0 0 18.0 par=n cel=27
    Rad=D2 Ext=D3 AXS 0 1 0
c To be used when reproducing flux magnitude
    erg=d4 tme=d1   wgt=1.92e14   $ accounts for flux and mass norms
c
c                    Irradiation Time (shakes)
si1 H 0 60e8
sp1 D 0 1
c
si2 H 0 0.4826
sp2 -21 1
si3 -0.7 0.7
c                   Particle Time, Weight and Energy Cut-Offs
cut:n 243e8 j 0 0
c
```

```
F1:n (509.1 509.2 509.3)
T1: 63e8 179i 243e8
c
F44:n 27   $ checking the flux distribution
E44: 0.625e-6 0.5 10
T44: 1e8 243e8
c
c si4 & sp4 reproduce the 69 energy group neutron flux of the SLOWPOKE-2 (omitted from report).
```

Appendix D

Further Derivation of the Delayed Neutron Counting Equation

This derivation follows that by (Binney and Scherpelz, 1978). If the source of counts is delayed neutrons, the total emission, *s* from t_1 [*s*], to final count t_2 [*s*] can be described as:

$$s = \int_{t_1}^{t_2} A(t)dt \qquad \text{D-1}$$

Where *A(t)* is the activity of delayed neutrons [s^{-1}], which have been conveniently organized into *k* groups such that:

$$A(t) = \sum_{i=1}^{k} A_{o_i} e^{-\lambda_i t} \qquad \text{D-2}$$

The initial activity, A_o [s^{-1}] of a particular delayed neutron group *i* is dependent on the number of fissile atoms and the flux it is exposed to, and duration of irradiation, t_{irr} [*s*], it is given by Eq. (D-3):

$$A_{o_i} = \frac{\beta_i v N_A \sigma_f \Phi m}{MM}(1 - e^{-\lambda_i t_{irr}}) \qquad \text{D-3}$$

Where *MM* is the molar mass of the sample [$g\ mol^{-1}$], *m* the fissile mass present [g], and N_A Avogadro's number [mol^{-1}]. Substituting equations. (D-2) and (D-3) into (D-1) gives:

$$s = \int_{t_1}^{t_2} \sum_{i=1}^{k} A_{o_i} e^{-\lambda_i t}\, dt \qquad \text{D-4}$$

$$s = \int_{t_1}^{t_2} \sum_{i=1}^{k} \frac{\beta_i v N_A \sigma_f \Phi m}{MM}(1 - e^{-\lambda_i t_{irr}}) e^{-\lambda_i t}\, dt \qquad \text{D-5}$$

$$s = \sum_{i=1}^{k} \frac{\beta_i v N_A \sigma_f \Phi m}{MM} (1 - e^{-\lambda_i t_{irr}}) - \frac{1}{\lambda_i} e^{-\lambda_i t} \Big|_{t_1}^{t_2} \quad \text{D-6}$$

$$s = \sum_{i=1}^{k} \frac{\beta_i v N_A \sigma_f \Phi m}{MM} (1 - e^{-\lambda_i t_{irr}}) (-\frac{1}{\lambda_i}) (e^{-\lambda_i t_2} - e^{-\lambda_i t_1}) \quad \text{D-7}$$

$$s = \sum_{i=1}^{k} \frac{\beta_i v N_A \sigma_f \Phi m}{MM} (1 - e^{-\lambda_i t_{irr}}) (\frac{1}{\lambda_i}) (e^{-\lambda_i t_1} - e^{-\lambda_i t_2}) \quad \text{D-8}$$

Defining count time, $\Delta t = t_2 - t_1$, therefore $t_2 = \Delta t + t_1$

$$s = \sum_{i=1}^{k} \frac{\beta_i v N_A \sigma_f \Phi m}{MM} (1 - e^{-\lambda_i t_{irr}}) (\frac{1}{\lambda_i}) (e^{-\lambda_i t_1} - e^{-\lambda_i (\Delta t + t_1)}) \quad \text{D-9}$$

$$s = \sum_{i=1}^{k} \frac{\beta_i v N_A \sigma_f \Phi m}{MM} (1 - e^{-\lambda_i t_{irr}}) (\frac{1}{\lambda_i}) (e^{-\lambda_i t_1}) (1 - e^{-\lambda_i (\Delta t)}) \quad \text{D-10}$$

Where

$$s = \sum_{i=1}^{k} \frac{\beta_i v N_A \sigma_f \Phi m}{MM} (1 - e^{-\lambda_i t_{irr}}) (\frac{1}{\lambda_i}) (e^{-\lambda_i t_d}) (1 - e^{-\lambda_i t_c}) \quad \text{D-11}$$

$$s = \frac{v N_A \sigma_f \Phi m}{MM} \sum_{i=1}^{k} \frac{\beta_i}{\lambda_i} (1 - e^{-\lambda_i t_{irr}}) (1 - e^{-\lambda_i t_c}) (e^{-\lambda_i t_d}) \quad \text{D-12}$$

The count rate S(t) at time t_c is the derivative of Eq. (D-5), its substitution into Eq. (D-10) yields the familiar equation found in delayed neutron counting papers:

$$S(t) = \frac{ds}{dt} \quad \text{D-13}$$

$$S(t) = \frac{d}{dt} \frac{v N_A \sigma_f \Phi m}{MM} \sum_{i=1}^{k} \frac{\beta_i}{\lambda_i} (1 - e^{-\lambda_i t_{irr}}) (1 - e^{-\lambda_i t}) (e^{-\lambda_i t_d}) \quad \text{D-14}$$

$$S(t) = \frac{v N_A \sigma_f \Phi m}{MM} \sum_{i=1}^{k} \beta_i (1 - e^{-\lambda_i t_{irr}}) (e^{-\lambda_i t}) (e^{-\lambda_i t_d}) \quad \text{D-15}$$

$$C(t) = \varepsilon M_L S(t) + \mathrm{B(t)} \quad \text{D-16}$$

$$C(t) = \frac{\varepsilon v N_A \sigma_f \Phi m}{MM} \sum_{i=1}^{k} \beta_i \left(1 - e^{-\lambda_i t_o}\right) \left(e^{-\lambda_i t_c}\right) \left(e^{-\lambda_i t_d}\right) + B(t) \quad \text{D-17}$$

Appendix E

Additional MCNP6 Input Decks and Descriptions

E.1 Overview

MCNP input deck examples are provided which detail geometries and materials used throughout the simulation progress.

E.2 The SLOWPOKE-2 Reactor Model

The SLOWPOKE-2 MCNP model used was provided by Atomic Energy of Canada Limited. It is considered confidential as it contains SLOWPOKE-2 dimensions and materials properties in great detail, therefore it is not provided in this thesis. Nguyen *et al*., 2012 contains a description of the model.

E.3 Detection Geometries

E.3.1 The Delayed Neutron Counting System

```
c
c ----------------------------GEOMETRY-------------------------------------
c
c PRESSURIZED HELIUM-3 DETECTORS
c
c   Detector 1
  1       1000     -0.000517         -201 601                      $Fill Gas
           imp:n=1 imp:h=1 imp:t=1
c
  2       2000    -7.92               201 -101                     $S.S Container
          imp:n=1 imp:h=1 imp:t=1
c
c   Detector 2
  3       1000     -0.000517         -202 602
           imp:n=1 imp:h=1 imp:t=1
c
  4        2000    -7.92               202 -102
          imp:n=1 imp:h=1 imp:t=1
c
c   Detector 3
  5       1000     -0.000517         -203 603
          imp:n=1 imp:h=1 imp:t=1
c
```

```
  6       2000    -7.92               203 -103
          imp:n=1 imp:h=1 imp:t=1
c
c  Detector 4
  7       1000     -0.000517        -204 604
           imp:n=1 imp:h=1 imp:t=1
c
  8       2000    -7.92               204 -104
          imp:n=1 imp:h=1 imp:t=1
c
c  Detector 5
  9       1000     -0.000517        -205 605
     imp:n=1 imp:h=1 imp:t=1
c
  10      2000    -7.92               205 -105
          imp:n=1 imp:h=1 imp:t=1
c
c  Detector 6
  11      1000     -0.000517        -206 606
           imp:n=1 imp:h=1 imp:t=1
c
  12      2000    -7.92               206 -106
          imp:n=1 imp:h=1 imp:t=1
c
c ACTIVE FILL AREA OF DETECTORS
c
  13      1000     -0.000517        -601
          imp:n=1 imp:h=1 imp:t=1
c
  14      1000     -0.000517        -602
          imp:n=1 imp:h=1 imp:t=1
c
  15      1000     -0.000517        -603
           imp:n=1 imp:h=1 imp:t=1
c
  16      1000     -0.000517         -604
           imp:n=1 imp:h=1 imp:t=1
c
  17      1000     -0.000517        -605
          imp:n=1 imp:h=1 imp:t=1
c
  18      1000     -0.000517        -606
          imp:n=1 imp:h=1 imp:t=1
```

```
c
c COUNTER ARRANGEMENT
c
  19     2000     -7.92              -901  902 904                    $S.S. Container
         imp:n=1 imp:h=1 imp:t=1
c
  20     6000     -0.93    -902 -901 904 101 102
                           103  104 105 106 801             $paraffin moderator
         imp:n=1 imp:h=1 imp:t=1
c
  21     3000    -0.0013 -903  901 902 801 101
                          102  103 105 106 803
                          904  104                      $air surrounding apparatus
         imp:n=1 imp:h=1 imp:t=1
c
c POLYETHYLENE SAMPLE HOLDER
c
  22     4000   -0.94    -801 802 -903 992  507           $PE outer tubing
         imp:n=1 imp:h=1 imp:t=1
c
  23     3000   -0.0013    -802 -903 507 508 509           $PE inner tubing bottom
         imp:n=1 imp:h=1 imp:t=1
c
  24     3000   -0.0013    -992 -903 507 508 509 802       $Pe inner tubing upper
         imp:n=1 imp:h=1 imp:t=1
c
  25     4000   -0.94     -507 508 509 510 992 802         $large vial
        imp:n=1 imp:h=1 imp:t=1
c
  26     3000   -0.0013    -508                      $bottom smaller vial
         imp:n=1 imp:h=1 imp:t=1
c
c The contents of this vial changed through the thesis work
         27       0          -509                      $top smaller vial solution
         imp:n=1 imp:h=1 imp:t=1
c
  28     7000   -0.689     -803                      $wooden stand
         imp:n=1 imp:h=1 imp:t=1
c
  29     3000   -0.0013    -510
     imp:n=1 imp:h=1 imp:t=1
c
  30    0                  903                      $geometry void
```

```
      imp:n=0 imp:h=0 imp:t=0
c
  31  6000    -0.93         -904 101 102 103 104 105
                             106 801       $paraffin between sample & detectors
      imp:n=1 imp:h=1 imp:t=1
c

c ----------------------SURFACE CARDS-----------------------------------------------------
c
c These surfaces are used for active part inside detectors
c
  601      rcc 4 6.928 2.4939              0 0 31.115    2.45 $active area
  602      rcc 8 0 2.4939                  0 0 31.115    2.45
  603      rcc 4 -6.928 2.4939             0 0 31.115    2.45
  604      rcc -4 -6.928 2.4939            0 0 31.115    2.45
  605      rcc -8 0 2.4939                 0 0 31.115    2.45
  606      rcc -4 6.928 2.4939             0 0 31.115    2.45
c
  101      rcc 4 6.928 0.5          0 0 36.195    2.54    $detector outsides
  102      rcc 8 0 0.5              0 0 36.195    2.54
  103      rcc 4 -6.928 0.5         0 0 36.195    2.54
  104      rcc -4 -6.928 0.5        0 0 36.195    2.54
  105      rcc -8 0 0.5             0 0 36.195    2.54
  106      rcc -4 6.928 0.5         0 0 36.195    2.54
c
c Inside the Detectors
c
  201      rcc 4 6.928 0.5889              0 0 36.0172   2.4511   $detector fill
  202      rcc 8 0 0.5889                  0 0 36.0172   2.4511
  203      rcc 4 -6.928 0.5889             0 0 36.0172   2.4511
  204      rcc -4 -6.928 0.5889            0 0 36.0172   2.4511
  205      rcc -8 0 0.5889                 0 0 36.0172   2.4511
  206      rcc -4 6.928 0.5889             0 0 36.0172   2.4511
c
c Detector Tops
c
  507      rcc 0 0 14.7        0 0 5.72      0.8509   $large vial outer
  508      rcc 0 0 15.1        0 0 2.20      0.4826   $bottom small vial
  509      rcc 0 0 17.3        0 0 1.38      0.4826   $top small vial solution
  510      rcc 0 0 18.7        0 0 0.82      0.4826   $air in the top vial
c
c Container & Paraffin
c
```

```
 901      rcc 0 0 0          0 0 34      15     $container outside
 902      rcc 0 0 0.5        0 0 33.5    14.5   $paraffin outside
 903      rcc 0 0 -10        0 0 64      20     $air around container
 904      rcc 0 0 0.5        0 0 33.5    4      $paraffin for vr purposes
c
c Sample Tubing
c
 801      rcc 0 0 0.5      0  0 43       1.3    $PE tubing outer diameter
 802       rcc 0 0 0.5       0 0 14.2     0.8509  $PE tubing inner diameter (bottom)
 992      rcc 0 0 20.42    0 0 23.08     0.8509  $PE inner (upper)
c
c Wooden stand on which the apparatus sits
c
 803      rcc 0 0 -5         0  0 4.9      18     $wooden stand
c
c --------------------------End of DNC Geometry Cards--------------------------
```

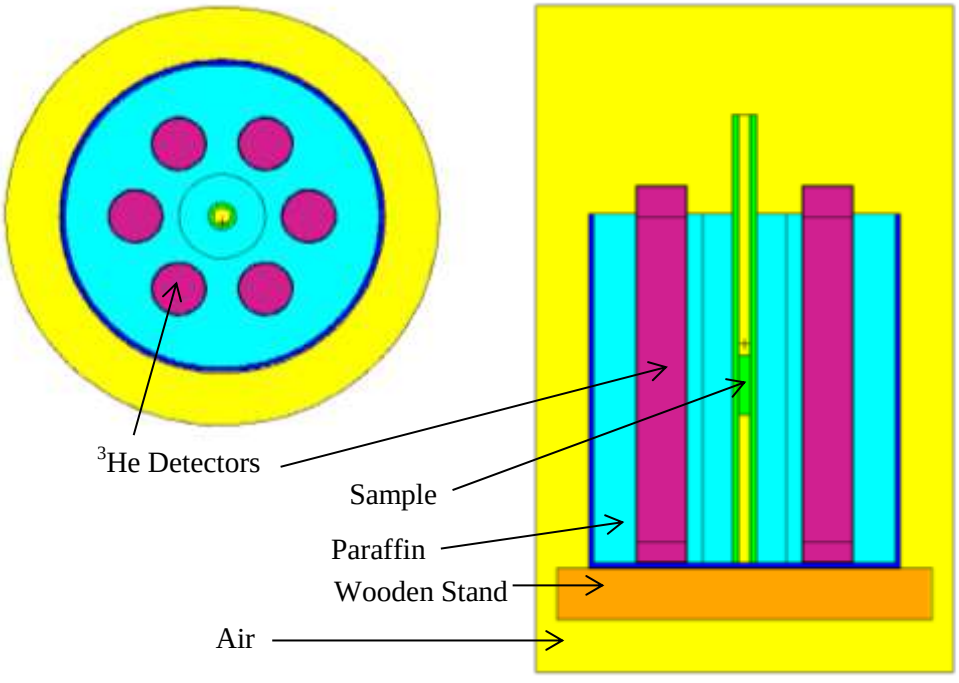

Figure E-1: MCNP MCPLOT of Delayed Neutron Counting System Geometry

E.3.2 The Delayed Neutron & Gamma Counting System

```
c
c ----------------------------GEOMETRY-------------------------------------
c PRESSURIZED HELIUM-3 DETECTORS
c
c   Detector 1
  1       7000    -5.11e-4          -201  601                 $Fill Gas
          imp:p=1
  2       8000    -7.92e+0          201 -101                  $S.S Container
          imp:p=1
c
c   Detector 2
  3       7000    -5.11e-4          -202  602
          imp:p=1
  4       8000    -7.92e+0          202 -102
          imp:p=1
c
c   Detector 3
  5       7000    -5.11e-4          -203  603
          imp:p=1
  6       8000    -7.92e+0          203 -103
          imp:p=1
c
c   Detector 4
  7       7000   -5.11e-4           -204  604
          imp:p=1
  8       8000   -7.92e+0           204 -104
          imp:p=1
c
c   Detector 5
  9       7000   -5.11e-4           -205  605
          imp:p=1
  10      8000  -7.92e+0            205 -105
          imp:p=1
c
c   Detector 6
  11  7000        -5.11e-4          -206  606
     imp:p=1
  12  8000        -7.92e+0          206 -106
     imp:p=1
c
```

```
c ACTIVE FILL AREA OF DETECTORS
c
  13  7000        -0.000511        -601
      imp:p=1
  14  7000        -0.000511        -602
      imp:p=1
  15  7000        -0.000511        -603
      imp:p=1
  16  7000        -0.000511        -604
      imp:p=1
  17  7000        -0.000511        -605
      imp:p=1
  18  7000        -0.000511        -606
      imp:p=1
c
c COUNTER ARRANGEMENT
c
  19  2000             -7.92    -901  902  905  303  302  307 410     $S.S. Container
      imp:p=1
c
  20  5000             -0.93        -902  101  106 -306  318        $paraffin -y direction
      imp:p=1
c
  21  5000             -0.93        -902  308 -318  319  302        $paraffin -y direction
      imp:p=1
c
  22  5000             -0.93        -902 -306  101 -319             $paraffin -y direction
      imp:p=1
c
  23  5000             -0.93        -902  102  103  104  105
                                    106  306  307                   $paraffin +y direction
      imp:p=1
c
  24  5000             -0.93        -902 -308  307 -306  316
                                      319 -318  101  106            $paraffin -y direction
      imp:p=1
c
  25  5000             -0.93        -902 -308  307 -306 -317
                                    106  319 -318  101  106        $paraffin -y direction
      imp:p=1
c
  26  3000             -0.0013      -903  901 803  302 413  303          $air
      imp:p=1
```

```
c
  27  8000          -11.35       -901 -905  902  801  303  302
                                 307 410                $lead shielding within container
      imp:p=1
c
c
c POLYETHYLENE SAMPLE HOLDER
c
  28  1001                -0.94              -801 802 -903 992
                                             507 -902 101              $PE outer tubing
      imp:p=1
c
  29  4000                -11.35             -307 801 -903 -901
                                             -902  101 316 -306 $lead tubing
      imp:p=1
c
  30  4000                -11.35             -307 801 -903 -901 -902
                                             101 -317 -306 $lead tubing
      imp:p=1
c
  31  4000                -11.35              306 -307 801 -902
                                             $right side of lead tubing
      imp:p=1
c
  32  3000                -0.0013            -802 -903 507 508 509
                                             $PE inner tubing bottom
      imp:p=1
c
  33  3000                -0.0013            -992 -903 507 508 509 802
                                             $Pe inner tubing upper
      imp:p=1
c
  34  1001                 -0.94              -507 508 509  510 992 802
                                             $large vial
      imp:p=1
c
  35  3000                 -0.94              -508    $bottom smaller vial
      imp:p=1
c
  36  3000                 -0.0013            -509
      imp:p=1                                          $top smaller vial solution
c
c
```

```
  37  2001              -0.689          -803 410                    $wooden stand
      imp:p=1
c
  38  3000              -0.0013         -510                    $air in the top vial
      imp:p=1
c
  39  4000              -11.35          -302 303 -903  410      $lead cylinder
      imp:p=1
c
  40  3000              -0.0013         -303 -302 307  410 413   $air
      imp:p=1
c
  41  4000              -11.35           -308 -311 -310 313 -314 315
                                       -306 410       $lead
      imp:p=1
c
  42  4000              -11.35          -308 -311 312 -310 -314 315
                                       -306 410        $lead
      imp:p=1
c
  43  3000               -0.0013        -308 -312 -313 307
                                       -314 315 -306 410 406          $air
      imp:p=1
c
  44  3000              -0.0013         -309 -307 801 507 508 -313
                                       -312 -314 315 41               $air
      imp:p=1
c
  45  4000             -11.35       -307 801 314 -306 -316   410          $lead
      imp:p=1
c
  46  4000             -11.35       -307 801 -315 -306 317    410          $lead
      imp:p=1
c
  47  4000             -11.35        314 -316 -308 307 -311 -310
                                       -306 -308  410                 $lead
      imp:p=1
c
  48  4000             -11.35        -315 317 -308 307 -311 -310 -306 -308  410
      imp:p=1
c
  49  5000             -0.93        -306 311 319 101 -316 317
      imp:p=1
```

```
c
  50  5000              -0.93             -306 310 -318 106 -316 317      $paraffin
      imp:p=1
  111     0                               903                              $void
       imp:p=0
c   112  3000             -0.0013           -411 410    $air surrounding HPGe
c        imp:p=1
  113  2000              -5.36             405 406 (-407:-404)       $tally GE
       imp:p=1
   114     0                              (-405:-406)       $hole inside detector
       imp:p=1
   115     0                              -409 404 407 405 406    $vacuum
        imp:p=1
   116  1000              -2.98             -410 409                  $insulator shield
       imp:p=1
   117     0                              -411 410 412 409 $end cap to crys gap
       imp:p=1
   118  9000              -1.84             -412                      $be window
       imp:p=1
   119  1000              -2.98             -413 411 412 410 409    $end cap wall
       imp:p=1

c ----------------------SURFACE CARDS-----------------------------------------
c These surfaces are used for the active part of the He-3 Detectors
c
  601       rcc -8.3149 -3.4415 2.4939      0 0 31.115     2.451     $active area
  602       rcc -8.3149 +3.4415 2.4939      0 0 31.115     2.451
  603       rcc -3.4415 +8.3149 2.4939      0 0 31.115     2.451
  604       rcc +3.4415 +8.3149 2.4939      0 0 31.115     2.451
  605       rcc +8.3149 +3.4415 2.4939      0 0 31.115     2.451
  606       rcc +8.3149 -3.4415 2.4939      0 0 31.115     2.451
c
  101       rcc -8.3149 -3.4415 0.5         0 0 36.195     2.54      $detector outsides
  102       rcc -8.3149 +3.4415 0.5         0 0 36.195     2.54
  103       rcc -3.4415 +8.3149 0.5         0 0 36.195     2.54
  104       rcc +3.4415 +8.3149 0.5         0 0 36.195     2.54
  105       rcc +8.3149 +3.4415 0.5         0 0 36.195     2.54
  106       rcc +8.3149 -3.4415 0.5         0 0 36.195     2.54
c
c Inside the Detectors
c
  201       rcc -8.3149 -3.4415 0.5889      0 0 36.0172    2.4511    $detector fill
  202       rcc -8.3149 +3.4415 0.5889      0 0 36.0172    2.4511
```

```
 203     rcc -3.4415 +8.3149 0.5889     0 0 36.0172    2.4511
 204     rcc +3.4415 +8.3149 0.5889     0 0 36.0172    2.4511
 205     rcc +8.3149 +3.4415 0.5889     0 0 36.0172    2.4511
 206     rcc +8.3149 -3.4415 0.5889     0 0 36.0172    2.4511
c
c Vial Positioning
c
 507     rcc 0 0 14.7          0 0 5.72      0.8509   $large vial outer
 508     rcc 0 0 15.1          0 0 2.20      0.4826   $bottom small vial
 509     rcc 0 0 17.3          0 0 1.38      0.4826   $top small vial solution
 510     rcc 0 0 18.7          0 0 0.82      0.4826   $air in the top vial
c
c
c Container & Paraffin
c
 901     rcc 0 0.79 0          0 0 59        22.1     $container outside
 902     rcc 0 0.79 0.5        0 0 43        21.1     $paraffin outside
 903     rcc 0 0.79 -30        0 0 100       40       $air around container
 905     rcc 0 0.79 0.5        0 0 43        21.6     $lead around paraffin
c
c Sample Tubing
C
 801     rcc 0 0 0.5           0 0 43.0      1.3      $PE tubing outer diameter
 802     rcc 0 0 0.5           0 0 14.2      0.8509   $PE tubing inner diameter
(bottom)
 992     rcc 0 0 20.42         0 0 22.58     0.8509   $PE inner (upper)
c
 803     rcc 0 0.79 -5         0  0 4.9     23         $wooden stand
c
c Lead Lining Containing the Gamma Spectrometer
 302     rcc  0 -8.31 17.56    0.0 -15.31 0    5.5     $outer area of cylinder
 303     rcc  0 0 17.56        0.0 -23.62 0    5       $inner area of cylinder
 306     py   0                                       $plane used to define lead cone
 307     rcc  0 0 0.5          0.0  0.00 43     1.8       $lead surrounding the
PE tubing
 310     p    5.5 -8.31 23.06     1.8  0.00 23.06        5.5 -8.31 12.06
 311     p   -5.5 -8.31 23.06    -1.8  0.00 23.06       -5.5 -8.31 12.06
 312     p   -5 -8.31 23.06      -1.3  0.00 23.06       -5.0 -8.31 12.06
 313     p    5 -8.31 23.06       1.3  0.00 23.06        5.0 -8.31 12.06
 308     p   -5 -8.31 23.06       5.0 -8.31 23.06        5.0 -8.31 12.06
 309     rcc  0 -8.31 17.56       0.0  8.31 0            5.5
 314     pz                                             22.56
 315     pz                                             12.56
```

```
 316      pz   23.06
 317      pz   12.06
 318      px   5.5
 319      px  -5.5
c
 404      rcc 0 -16.11 17.56      0 -3.58 0        2.2      $ge de
 405      rcc 0 -19.70 17.56      0 3.115 0        0.475    $hole
 406        s   0 -16.585 17.56   0.475            $rounded part of hole
 407      ell  0 -16.11 17.56     0 0.8 0   -2.2   $detec. end radius
 408       px -15.31
 409      rcc 0 -15.31 17.56      0 -9.08 0        2.2      $vacuum
 410      rcc 0 -15.31 17.56      0 -9.4 0         2.336    $Al mount cup
 411      rcc 0 -15.005 17.56     0 -9.43 0        2.636    $gap to crystal
 412      rcc 0 -14.955 17.56     0 -0.05 0        2.336
 413      rcc 0 -14.955 17.56     0 -10 0          3.475
c -------------------------End of DNGC Geometry Cards-------------------------
```

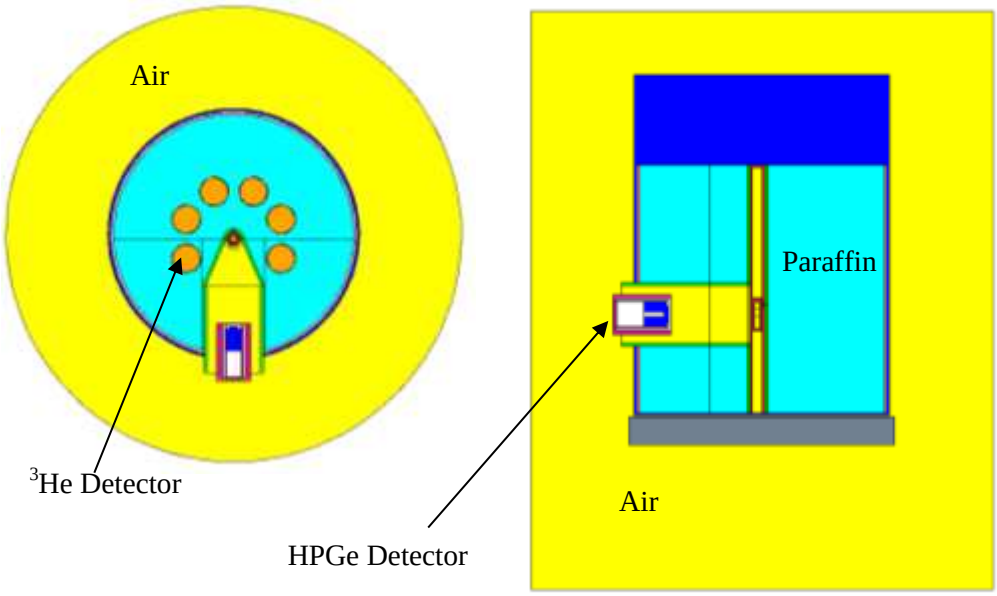

Figure E-2: MCNP MCPlot of the Delayed Neutron and Gamma Counting System

E.4 Materials

```
c HELIUM-3 GAS
m1000          2003.70c          1
c
c STEEL, STAINLESS 304
m2000          24050.70c         -0.00793
               24052.70c         -0.159032
               24053.70c         -0.018378
               24054.70c         -0.004661
               25055.70c         -0.02
               26054.70c         -0.039605
               26056.70c         -0.638496
               26057.70c         -0.01488
               26058.70c         -0.002019
               28058.70c         -0.064024
               28060.70c         -0.025321
               28061.70c         -0.001115
               28062.70c         -0.003599
               28064.70c         -0.000942
c
c AIR AT SEA LEVEL
m3000          7014.70c          -0.755636   $Air at sea level
               8016.70c          -0.231475
               18036.70c         -3.9e-5
               18038.70c          -8e-6
               18040.70c         -0.012842
c
c POLYETHYLENE
m4000          1001.70c           -0.143716
               6000.70c           -0.856284
mt4000         poly.10t
c
c U238 DISSOLVED IN HNO3/H20
m5000
               92238.70c         -2.94e-4
               1001.70c          -0.10531
               8016.70c          -0.87777
               7014.70c          -0.01478
mt5000         lwtr.10t
c
```

```
c PARAFFIN
m6000       1001.70c        -0.148605
            6000.70c        -0.851395
mt6000      poly.10t
c
c WOODEN STAND
m7000       1001.70c        -0.057889   $wooden stand
            6000.70c        -0.482667
             8016.70c       -0.459440
c
c BERYLLLIUM
m9000       4009            -1
c
c GERMANIUM
m2000       32073           0.073
            32070           0.2123
            32072           0.2766
            32074           0.3592
            32076           0.0744
```

-This page is intentionally left blank-

Madison Andrews (née Sellers)

1-574 Princess Street
Kingston, Ontario
Tel: +1 613.876.3459 madi.andrews16@gmail.com

Education

Ph.D. **Nuclear Engineering**
January 2012 – January 2015 **Royal Military College of Canada**
Dissertation: Delayed Neutron & Gamma Measurements of Special Nuclear Materials, their Monte Carlo Simulations, and Applications.
Advisors: Dr. David Kelly, Dr. Emily Corcoran

M.A.Sc. **Nuclear Engineering**
September 2009 – June 2011 **Royal Military College of Canada**

B.Sc.Eng. **Engineering Physics**
September 2005 – June 2009 **Queen's University**

Experience

Graduate Student **Nuclear Engineering Group**
September 2009 – January 2015 **Royal Military College of Canada**

Assisted in the supervision of three 4th year theses (Queen's University) and projects (RMCC). Two undergraduate students were supervised throughout their internship in 2014. Reviewed conference and journal submissions.

Graduate Research Assistant **X Computational Physics**
July 2011- August 2014 **Los Alamos National Laboratory**

Interned with the Monte Carlo Codes & Radiation Transport Application Group (XCP-3). Collaborated on the production of a delayed particle test suite for distribution with MCNP6. Internships completed in the summers of 2011, 2012, fall 2013, and summer 2014.
Mentor: Dr. Tim Goorley

Research Assistant — **Analytical Sciences Group**
May 2008 – September 2008 — **Royal Military College of Canada**
May 2009 – August 2009

Awards & Honors

Director's Postdoctoral Fellowship (2015)
Los Alamos National Laboratory sponsored postdoctoral fellowship.

Governor General's Gold Medal Nominee (2015)
These medals are considered the most prestigious award for a graduate student in Canada. Nomination requires a dissertation and student to be considered in the top 5 % of nominating university. (Decision due in 2015).

R. E. Jervis Award (2014)
Distributed by the Canadian Nuclear Society, the R.E. Jervis award recognizes excellence in research and overall academic achievement by a graduate student in nuclear engineering.

Outstanding Technical Paper, 2nd place overall (2014)
Radiation Protection and Shielding Division of the American Nuclear Society.

Best Student Paper & Presentation Award (2014)
Radiation Protection and Shielding Division of the American Nuclear Society.

Canada Graduate Scholarship (2013)
Award sponsored by the Canadian Nuclear Safety Commission and distributed by the Natural Science and Engineering Research Council of Canada. Total value for three years: $105,000.

Young Scientist Finalist (2012)
NuMat 2012 Conference, October 22 – 25, 2012. Osaka, Japan.

Young Scientist and Student Competitive Award (2011)
Modern Trends in Activation Analysis, March 13-18, 2011. College Station, TX.

Best MASc Student Paper & Presentation (2010)
Canadian Nuclear Society Conference, Montreal, QC, May 2010

Undergraduate Science Research Award (2009)
Natural Science and Engineering Research Council of Canada sponsorship of a 16 week undergraduate internship at the Royal Military College of Canada. Total value $4,500.

Publications

Peer Reviewed - Journal Publications

6. **M.T. Andrews**, J.T. Goorley, E.C. Corcoran, D.G. Kelly, "MCNP6 Simulations of Gamma Line Emissions from Fission Products and their Comparisons to Plutonium and Uranium Measurements" *Progress in Nuclear Engineering,* **79** (2015) pp. 87-95.

5. **M.T. Andrews**, E.C. Corcoran, J.T. Goorley, D.G. Kelly, "A System for the Measurement of Delayed Neutrons and Gammas from Special Nuclear Materials" *Journal of Radioanalytical and Nuclear Chemistry, in press* (2015) DOI:10.1007/s10967-014-3786-6.

4. **M.T. Andrews**, J.T. Goorley, E.C. Corcoran, D.G. Kelly, "Modeling the Detection of Delayed Neutron Signatures in MCNP6 and Comparison with Measurements of ^{233}U, ^{235}U and ^{239}Pu" *Journal of Nuclear Technology,* 187 3 (2014) pp. 235-242.

3. M.J. Roeterink, D.G. Kelly, E.G. Dickson, **M.T. Andrews**, E.C. Corcoran, "Analysis and Monte Carlo Modelling of Radio-Opaque Personal Protective Fabrics" *Journal of Radioanalytical and Nuclear Chemistry,* 300 3 (2014) pp. 1031-1039.

2. **M.T. Sellers**, E.C. Corcoran, D.G. Kelly, "The Analysis and Attribution of the Time Dependent Neutron Background Resultant from Sample Irradiation in a SLOWPOKE-2 Reactor" *Journal of Radioanalytical and Nuclear Chemistry,* 295 2 (2013) pp.1221-1228.

1. **M.T. Sellers**, D.G. Kelly, E.C. Corcoran, "An Automated Delayed Neutron Counting System for Mass Determinations of Special Nuclear Materials" *Journal of Radioanalytical and Nuclear Chemistry,* 291 2 (2012) pp. 281 – 285.

Peer Reviewed – Conference Proceedings * *indicates presenting author.*

13. P. Hungler, **M.T. Andrews**, D.G. Kelly, K.S. Nielsen**,** "The SLOWPOKE-2 Nuclear Reactor at the Royal Military College of Canada: Applications for the Canadian Armed Forces" Canadian Nuclear Bulletin, 35 1 (2014) pp. 19-22.

12. **M.T. Andrews***, T.L. Beames-Canivet, R.S. Elliot, D.G. Kelly, E.C. Corcoran, "Use of a SLOWPOKE-2 Reactor for Nuclear Forensics Applications" 3rd International Meeting on Small Reactors, Ottawa, Ontario, November 5 – 7, 2014.

11. P.C. Hungler*, **M.T. Andrews**, R.D. Weir, K.S. Nielsen, P.K. Chan, L.G.I. Bennett "Enhancements to the SLOWPOKE-2 Research Reactor at the Royal Military College of Canada" 3rd International Meeting on Small Reactors, Ottawa, Ontario, November 5 – 7 2014.

10. **M.T. Andrews***, D.G. Kelly, E.C. Corcoran, J.T. Goorley "Uranium and Plutonium Fission Product Gamma Intensity Measurements and MCNP6 Simulations" American Nuclear Society Transactions, 110 (2014) pp. 490-493.

9. **M.T. Andrews***, D.G. Kelly, E.C. Corcoran "Delayed Particles from Special Nuclear Materials and their Nuclear Forensics Applications" 19th Pacific Basin Nuclear Conference Proceedings, Vancouver, British Columbia, August 24-28 2014.

8. **M.T. Andrews**[*], J.T. Goorley, E.C. Corcoran, D.G. Kelly, "Fission Product γ-ray Measurements of ^{235}U and MCNP6 Predictions" American Nuclear Society Transactions, 109 (2013) pp. 995-998.

7. **M.T. Sellers**[*], E.C. Corcoran, D.G. Kelly "An Introduction to the Delayed Neutron and Gamma Counting System at the Royal Military College of Canada" Canadian Nuclear Society Student Conference, Toronto, ON, June 2013.

6. **M.T. Sellers**[*], E.C. Corcoran, D.G. Kelly, "Simultaneous ^{233}U and ^{235}U Characterization through the Assay of Delayed Neutron Temporal Behaviour" Advances in Reactor Physics Radiation Applications, Nuclear Safeguards Session, Knoxville, TN, April 2012.

5. **M.T. Sellers**[*], E.C. Corcoran, D.G. Kelly "Nuclear Forensics Applications of Delayed Neutron Counting" Canadian Nuclear Society Student Conference, Saskatoon, SK, June 2012.

4. C. French[*], P.K. Chan, S. Paquette, J. Morelli, **M.T. Sellers**, "Improving the useful life of a 37-element fuel bundle" Canadian Nuclear Society Student Conference, Saskatoon, SK, June 2012.

3. **M.T. Sellers**[*], J.T. Goorley, E.C. Corcoran, D.G. Kelly, "A Preliminary Comparison of MCNP6 Delayed Neutron Emission from ^{235}U and Experimental Measurements" American Nuclear Society Transactions, 106 1 (2012) pp. 813-816.

2. **M.T. Sellers**[*], E.C. Corcoran, D.G. Kelly, "An Examination of the Time-Dependent Background Counts in the Delayed Neutron Counting System at the Royal Military College of Canada" Canadian Nuclear Society Conference, Niagara, ON, June 2011.

1. **M.T. Sellers**[*], E.C. Corcoran, D.G. Kelly, "An Automated Delayed Neutron Counting System for the Mass Determination of Fissile Isotopes in Special Nuclear Materials at the Royal Military College of Canada" Canadian Nuclear Society Student Conference, Montreal, QC, May 2010.

Non – Peer Reviewed Technical Reports

6. R. Rogge, **M. Andrews**, D.G. Kelly, "In-Beam Delayed Neutron Measurements for Fissile/Fissionable Material Identification: RMC Detector Test" Canadian Nuclear Laboratories Report (2015).

5. **M.T. Andrews**, T.L. Beames-Canivet, D.G. Kelly, E.C. Corcoran, J.T. Goorley, "MCNP6.1.1 Beta Test Suite Comparisons to Delayed Neutron Measurements of ^{233}U, ^{235}U, and ^{239}Pu at the Royal Military College of Canada" Los Alamos National Laboratory Report, (2014) LA-UR-14-26521.

4. **M.T. Andrews**, T.L. Beames-Canivet, D.G. Kelly, E.C. Corcoran, J.T. Goorley, "Updated Delayed Neutron Counting Test Suite Comparisons from RMCC and MCNP6 version 1" Los Alamos National Laboratory Report, (2014), LA-UR-14-25702.

3. **M.T. Andrews**, J.T. Goorley, E.C. Corcoran, D.G. Kelly "Changes to Delayed Neutron Measurements at RMCC and their corresponding MCNP6 Simulations" Los Alamos National Laboratory Report, (2013), LA-UR-13-29472.

2. **M.T. Sellers**, J.T. Goorley, D.G. Kelly, E.C. Corcoran "Helium-3 Detector Response in MCNP6 and Comparison to Measurements" Los Alamos National Laboratory Report, (2012), LA-UR-12-25291.

1. **M.T. Sellers**, L.G.I. Bennett, D.G. Kelly "A Study of the Transportation of Radioactive Material by the Department of National Defense" Canadian Department of National Defense Private Document, (2008).

Invited Presentations

1. **M.T. Andrews** "Delayed Neutron & Gamma Measurements of Special Nuclear Materials" Canadian Nuclear Safety Commission (CNSC), Ottawa, ON, February 3, 2015.

Contributed Talks & Presentations

Oral Presentations

7. **M.T. Andrews*** "The Royal Military College of Canada's Delayed Neutron and Gamma Counting System" Canada Nuclear Laboratory – RMCC Meeting on Nuclear Forensics Collaboration, Kingston, ON, November 2014.
6. **M.T. Andrews***, E.C. Corcoran, D.G. Kelly, J.T. Goorley "Delayed Neutron and Gamma measurements from Special Nuclear Materials at the Royal Military College of Canada" Fission Experiments and Theoretical Advances, Santa Fe, NM, USA, September 8 – 12 2014.

5. **M.T. Andrews***, J.T. Goorley, E.C. Corcoran, D.G. Kelly "Gamma Ray Measurements and their Simulations in MCNP6" X Computational Physics, Monte Carlo Codes & Radiation Transport Applications, Los Alamos National Laboratory, Los Alamos, NM, USA, December 2013.

4. **M.T. Sellers***, J.T. Goorley, E.C. Corcoran, D.G. Kelly "Delayed Gamma & Neutron Emissions from Special Nuclear Materials: Measurements and MCNP6 Modeling" X Computational Physics, Monte Carlo Codes, Los Alamos National Laboratory, Los Alamos, NM, USA, October 2012.

3. **M.T. Sellers***, J.T. Goorley, E.C. Corcoran, D.G. Kelly "Delayed Particle Measurements from Fissile Isotopes and MCNP6 Modeling: Previous, Current and Planned Work" X Computational Physics, Monte Carlo Codes, Los Alamos National Laboratory, Los Alamos, NM, USA, August 2012.

2. **M.T. Sellers***, J.T. Goorley, E.C. Corcoran, D.G. Kelly "MCNP6 Delayed Neutron Emission Validation with Experimental Measurements" X Computational Physics, Monte Carlo Codes, Los Alamos National Laboratory, Los Alamos, NM, USA, October 2011.

1. D.G. Kelly*, E.C. Corcoran, **M.T. Sellers***, "Nuclear Forensics at the Royal Military College of Canada" Defence Research & Development Canada – RMCC Meeting on Nuclear Forensics, Kingston, ON, June 2011.

Poster Presentations

8. R.S. Elliot, T.L. Beames-Canivet*, **M.T. Andrews,** D.G. Kelly, E.C. Corcoran, "Delayed Neutron and Delayed Gamma Ray Spectrometry for Special Nuclear Material Identification" 50th Annual Canadian Undergraduate Physics Conference, Kingston, ON, October 2014.

7. **M.T. Andrews*,** D.G. Kelly, E.C. Corcoran, J.T. Goorley "Delayed Particles from Special Nuclear Materials and their Nuclear Forensics Applications" Canadian Nuclear Society Student Conference, Vancouver, BC, August 2014.

6. T.L. Beames-Canivet*, R.S. Elliot, **M.T. Andrews,** D.G. Kelly, E.C. Corcoran, "Preparations for RMCC's Participation in the Nuclear Forensics International Technical Working Group's 4th Collaborative Materials Exercise" Canadian Nuclear Society Student Conference, Vancouver, BC, August 2014.

5. **M.T. Andrews*,** D.G. Kelly, E.C. Corcoran "Special Nuclear Material Characterization via Delayed Neutron and Gamma Temporal Signatures" Student showcase in the ANS Topical Meeting on Nuclear Nonproliferation, Washington, D.C., November 2013.

4. **M.T. Sellers***, D.G. Kelly, E.C. Corcoran "Special Nuclear Materials Analysis & MCNP6 Delayed Particle Modelling for Nuclear Forensics Applications" 2013 CANDU Owner's Group – Canadian Nuclear Safety Commission Meeting, Ottawa, ON, May 2013.

3. **M.T. Sellers***, D.G. Kelly, E.C. Corcoran, J.T. Goorley "A Comparison of MCNP6 Delayed Neutron Emission from ^{233}U, ^{235}U and ^{239}Pu and Experimental Measurements" Presented at:
    - 2013 Nuclear Data Conference, New York, NY, March 2013.
    - University Network of Excellence in Nuclear Engineering Workshop, Mississauga, December 2011, December 2012.

2. **M.T. Sellers***, D.G. Kelly, E.C. Corcoran, "Post Irradiation Examination of Delayed Neutron Signatures from Special Nuclear Materials" *Numat 2012*, Osaka Japan, October 21 – 26, 2012.

1. **M.T. Sellers***, D.G. Kelly, E.C. Corcoran, "An Automated Delayed Neutron Counting System for the Analysis of Special Nuclear Materials". This poster was presented at:
    - Modern Trends in Activation Analysis, TX, March 2011.
    - SLOWPOKE-2 25th Anniversary at the Royal Military College of Canada, Kingston, ON, June 2010.

Relevant Activities

Reviewing Activities

- Currently serving on the 2015 Canadian Nuclear Society Conference Reviewing Committee
- 19th Pacific Basin Nuclear Conference (2014) (1 paper reviewed)
- 38th Annual Canadian Nuclear Society Student Conference (2014) (4 papers reviewed)
- Journal of Radioanalytical and Nuclear Chemistry (2013) (1 paper reviewed)

Professional Memberships

- Canadian Nuclear Society (2010 – present)
- American Nuclear Society (2012 – present)
- Institute of Nuclear Materials Management (2014 – present)

Additional Training

- ZED-2 Physics School, Canada's Nuclear Laboratory, December 2011.
- MCNP5/MCNPX Training, Los Alamos National Laboratory, October 2010.
- LabVIEW Core I & II, National Instruments, March 2010.
- Radiation Safety Training, Royal Military College of Canada, May 2009.

Volunteering

- Pacific Basin Nuclear Conference Volunteer, August 2014.
- Canadian Nuclear Society Conference Volunteer, 2011 – 2013.
- Department Civilian Graduate Student Representative, Sept 2012 – Sept 2013.
- Science Rendezvous Volunteer, Queen's University, May 2012.
- CANDU Fuel Conference Student Volunteer, 2010.
- SLOWPOKE-2 Reactor 25th Anniversary Meeting, Student Volunteer, June 2010.